Peder Aursand

# Numerical solution of the dynamics of director fields in nematic liquid crystals

Doctoral thesis
for the degree of PhD

Trondheim, June 2015

Norwegian University of Science and Technology
Faculty of Information Technology, Mathematics and Electrical Engineering
Department of Mathematical Sciences

NTNU
Innovation and Creativity

**NTNU**

Norwegian University of Science and Technology

Doctoral thesis
for the degree of PhD

Faculty of Information Technology, Mathematics and Electrical Engineering
Department of Mathematical Sciences



ISBN (printed version)
ISBN (electronic version)
ISSN 1503-8181

Doctoral theses at NTNU,

Printed by NTNU-trykk

# Abstract

Since their discovery in the late 1800s, liquid crystals have become an important part of the technology of the modern world. As a consequence the study of anisotropic liquids in general, and liquid crystals in particular, has grown into a large interdisciplinary field involving physics, mathematics, chemistry and biology to name a few.

In a series of papers we consider numerical solution of the evolution of the director, a vector valued field giving the local average orientation of the long axis of molecules in nematic liquid crystals. The flow field is assumed to be stationary throughout this work. We consider both the free elastic dynamics of the director as well as the case with applied electric fields on a finite domain.

We study the dynamics of the 1D Fréedericksz transition, where an applied electric field forces reorientation in the director field. The director is assumed strongly anchored and the boundaries. Herein, we study the role of inertia and dissipation on the time evolution of the director field during the reorientation. In particular, we show through simulations that inertia will introduce standing waves that might effect transition time of the reorientation, but only for very small time scales or extremely high molecular inertia.

The Fréedericksz transition is also numerically studied with weak boundary anchoring. For this problem it has been shown analytically that there exists a hierarchy of meta-stable equilibrium configurations. This is in sharp contrast to the strongly anchored case, where the equilibrium is globally well defined. We derive an implicit numerical scheme for this problem and show the well-posedness of the discrete equation system. The method can be used for the fully nonlinear model with coupled electric field. Through simulations we show that the director can transition into different meta-stable

states given different small perturbations to the initial data.

The numerical solution of variational wave equations describing the elastic dynamics of nematic liquid crystals is considered in both 1D and 2D. Using energy respecting Runge–Kutta Discontinuous Galerkin methods we show that numerical solutions that either conserve or dissipate a discrete version of the energy can be obtained by efficient time marching. The dissipative scheme uses a dissipative up-winding at the cell interfaces combined with a shock-capturing method.

Finally, we consider the application of nonintrusive sampling methods for uncertainty quantification for the elastic problem with uncertain Frank constants. The multi-level Monte Carlo (MLMC) method has been successfully applied to systems of hyperbolic conservation laws, but its applicability to other nonlinear problems is unclear. We show that MLMC is 5-10 times more efficient in approximating the mean compared to regular Monte Carlo sampling, when applied to variational wave equations in both 1D and 2D.

# Preface

This dissertation is the culmination of three years of research as a PhD student at the Department of Mathematical Sciences at the Norwegian University of Science and Technology, Trondheim. As a former graduate student in physics, the transition to mathematics has been both challenging and rewarding. Having to educate myself on the mathematics of partial differential equations has required patience and perseverance both from myself and from my advisors and collaborators. The content of this thesis reflects both my diverse background as well as the journey I have taken into mathematics over the last few years. The theory of liquid crystals was largely unknown to me when I started my thesis work. During my research I have come to appreciate the vast volume of ideas and results that make up this truly interdisciplinary field.

For me the lessons learned from my PhD work have not all been of a scientific nature. I have been lucky to have thesis advisors that gave me a tremendous amount of freedom to pursue topics I found interesting. With this freedom comes the often underestimated challenge of planning and sustaining long-term research. Through this often painful process I have learned a lot about myself, what motivates me and how best to translate motivation into results. These are lessons I will undoubtedly carry with me into the future.

I am extraordinarily grateful to my advisors, Professor Helge Holden and Professor Nils Henrik Risebro, for taking me on as a PhD student. They have always had an open office door for me no matter how small the issue or how busy their schedule was. Not only have they patiently offered their vast expertise to help me in my research, but they have also encouraged and supported me in visiting other institutions and attending international conferences and workshops. The collaborations that followed have proved

essential in my work.

The research making up this thesis would not have been possible without my many collaborators. I am grateful to my fellow PhD students Johanna Ridder and Franziska Weber at the University of Oslo for hosting me for numerous research stays and for the fruitful cooperation that followed. I greatly enjoyed working with Dr. Ujjwal Koley at TIFR Centre for Applicable Mathematics in applying numerical DG methods to liquid crystals. While at a research stay at ETH, Dr. Jonas Šukys helped introduce me to uncertainty quantification for hyperbolic PDEs. In a hectic semester, with his help, I was able to apply some of these techniques to liquid crystals.

I am indebted to Professor Siddhartha Mishra both for patiently introducing me to several of the topics that make up this thesis and for graciously hosting me at his group at ETH in Zürich. Being embedded among the brilliant students and staff at the Seminar for Applied Mathematics at ETH gave me a significant personal and professional motivation boost. The research of Professor Mishra speaks for itself, and I remain deeply impressed by the work he and his students have done, and are continuing to do, in the field of numerical solution to hyperbolic PDEs.

The advice of senior staff and former students can only go so far in preparing you for the isolation and loneliness involved in pursuing a PhD degree. Through these years I have shared an office with my fellow PhD students Anders Nordli and Erik Makino Bakken. While I have not worked directly with them, the comradery of someone who shares the frustrations of PhD work cannot be overestimated.

Lastly, I want to thank my family for supporting me through my entire life, allowing me to develop a scientific mindset, and being there for me when I needed it. My fiancée deserves my deepest gratitude for all of her support and encouragement, and for tolerating my often frustrating work hours. Also, her diligent proofreading helped make this dissertation easier to read.

*Peder Aursand*
Trondheim, June 2015

# Contents

# Part I

# Introduction

Chapter 1

# Introduction to liquid crystals

The classical view in the physical sciences describes three basic states of matter: gas, liquid and solid. By varying pressure and temperature, a phase transition can be induced between any of these. However, it turns out that this picture is not entirely accurate for all substances. Certain organic compounds have intermediate phases, often referred to as mesophases, with properties in between those of a liquid and those of a solid. Consequently, a substance in any of these phases is called a liquid crystal.

The essential features of liquid crystals can be understood by considering which aspects of liquids and solids they inherit. In general, the solid state is characterized by strongly bound atoms in a rigid configuration. The geometry can be completely irregular, like in the case of glass, or in the form of an ordered lattice as is the case for diamonds and metals. The latter case is often referred to as a crystalline configuration and involves ordering in both the position and orientation of the constituent molecules. On the other hand, the identifying property of a liquid is that its molecules are free to flow. Here no correlation exists between the position of the center of gravity of different molecules, apart from the average particle density.

As its name suggests, a liquid crystal flows like a liquid while inheriting some crystalline properties of the solid phase. In practice, the type of ordering in liquid crystals can vary greatly, depending on the geometric and physical properties of their molecules. For something to be defined as a liquid crystal, it has to exhibit fluid-like properties in at least one spatial dimension while having some crystalline anisotropy on the molecular level [13].

The liquid crystal literature is extensive, owing to many decades of experimental and theoretical interdisciplinary research. An exhaustive liter-

ature survey will not be given here, but a few essential sources should be mentioned. The books of Collings [11, 10] serve as excellent introductions to this vast topic both from a historical and a technical perspective. Kelker's survey [34] gives a comprehensive and detailed account of the history of liquid crystals. De Gennes and Prost [13] have written what has become a classical reference on the physics and modeling of liquid crystals. Other excellent sources include the books of Chandrasekhar [9] and Blinov [3]. The book of Virga [58] is a rigorous account of the mathematical framework of modern liquid crystal theory. Stewart's recent book [56] is an accessible and comprehensive introduction to the mathematical modeling of liquid crystals.

## 1.1 A brief history of liquid crystals

Liquid crystals were observed by several scientists in the mid to late nineteenth century. However, the discovery of liquid crystals is usually attributed to the Austrian botanist Friedrich Reinitzer in 1881 [10]. While studying the role of cholesterol derivatives in plants, Reinitzer described a substance he was studying as having *two* melting points. While heating a sample of solid cholesteryl benzoate he noticed that at 145.5 °C it melts into a cloudy liquid. When raising the temperature further he noticed a second phase transition occurring at 178.5 °C, leaving the sample as a clear liquid.

Two decades after his initial discovery, Reinitzer mentioned his observations in a letter to the German physicist Otto Lehmann. This initial correspondence proved very fruitful, and it prompted the systematic study of liquid crystals by Lehmann using precise instruments for studying materials using polarized light. It is Lehmann that eventually coined the term "liquid crystal" ("Flüssige Krystalle" in German).

Today we know that the substance studied by Reinitzer, cholesteryl benzoate, belongs to an important sub-group of liquid crystals called *cholesteric* (or chiral) liquid crystals. Lehmann continued his work on liquid crystals and eventually experimented on what is now known as nematic liquid crystals, a class of particular importance in modern applications. It would take decades for Lehmann's ideas about liquid crystals to become part of the mainstream theory. Meanwhile, several established scientists would oppose the concept of a fourth state of matter and offer alternative explanations for Reinitzer and Lehmann's observations.

From the beginning of the 20th century, Daniel Vörlander's group at the University of Halle continued the experimentation on liquid crystals. Together with his coworkers Vörlander was able to put out an enormous volume of results. They were able to identify essential features of materials

that have a liquid crystal phase and synthesized a large number of the liquid crystals known today.

The 1930s saw the first major developments in the theoretical work on liquid crystals. In particular, the Swedish physicist Carl Wilhelm Oseen [51] developed a continuum theory for the elastic properties of nematic liquid crystals. This enabled the mathematical modeling of the ordering in liquid crystals for the first time, which in turn made theoretical explanations for experimental observations possible. In the same period, Zocher [65] pioneered the theoretical research into the interaction between nematic liquid crystals and electromagnetic fields. This would later pave the way for applications in liquid crystal displays.

In the time following the Second World War, the group of the British chemist George William Gray worked on synthesizing a large number of liquid crystals. Gray went on to publish one of the classic texts in the understanding of which substances will exhibit a liquid crystal state [25].

Oseen's pioneering work on elasticity in nematics was continued in the 1950s by the British physicist Frederick Charles Frank [19]. Today the Oseen–Frank elastic continuum theory is a cornerstone in the theoretical description of nematic liquid crystal.

In 1962 scientists of the Radio Corporation of America labs demonstrated for the first time that the optical properties of a liquid crystal layer can be manipulated by applying an electric field. This discovery laid the groundwork for the first liquid crystal display (LCD), arguably the most important application of liquid crystals in the modern world. Applications in consumer devices such as LCDs prompted research into substances that remain in the liquid crystal mesophase at room temperatures. MBBA and 5CB are examples of liquid crystals that are stable at room temperatures; they were both synthesized during this era because of their specific temperature profile.

In 1991, the crucial role of liquid crystal theory and the theory of complex fluids was recognized by the Nobel prize in physics being awarded to Pierre-Gilles de Gennes. The prize was awarded in part for de Gennes' major contribution to the general continuum theory for nematic liquid crystals, the Landau–de Gennes theory [45, 13].

## 1.2 The nematic mesophase

One of the most studied liquid crystal mesophases is the nematic phase. Usually, nematic liquid crystals consist of elongated organic molecules. Because of the geometry, the long axis of neighboring molecules will tend to

align. This causes macroscopic order in the molecular orientation, as illustrated in Figure 1.1, while the centers of mass as free to flow like a liquid.

Figure 1.1: Illustration of the orientational ordering in nematic liquid crystals. The elongated molecules tend to align their long axes while flowing like a liquid.

The origin of the word nematic is the Greek word for thread. This comes from the thread-like patterns (discliniations) often observed in nematic liquid crystals. Disclinations can be seen as singularities in the director field, the average local orientation of the long axes.

The first nematic liquid crystal, p-azoxyanisole (PAA), was synthesized in the late 1800s by Gattermann and Ritschke [22]. PAA is in the nematic phase between 118 °C and 136 °C and was one of the liquid crystals extensively studied by Lehmann in his early work.

One of the most important applications of nematics is in display devices. This has prompted a great interest in liquid crystals that have a stable nematic phase at room temperature. First synthezised by Kelker and Scheurle [35], the liquid crystal 4-methoxybenzylidene-4-butylabiline (MBAA) was the first discovered liquid crystal with a nematic phase a room temperature. The liquid crystal 4-pentyl-4-cyanobiphenyl (5CB) was designed specifically for use in liquid crystal display devices and is in the nematic state for temperatures from 18 °C to 35 °C. Shown in Figure 1.2, the long axis of 5CB is about 20 Å and the short axis about 5 Å.

## 1.3 The cholesteric mesophase

In the cholesteric phase, the geometry of the molecules causes a helical configuration of the long axes. In the ground state, the director (average orientation of the long axis) will twist around a common axis. The characteristic length scale of the twist (the pitch) is usually orders of magnitude

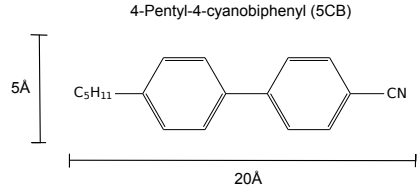


Figure 1.2: Schematic representation of the nematic liquid crystal 4-pentyl-4-cyanobiphenyl (designated 5CB).

larger than the size of the molecules.

Cholesteric liquid crystals were the first liquid crystals to be discovered by Reinitzer in the late 1800s. The name has a historic origin; even though cholesterol itself is not a cholesteric liquid crystal, many cholesterol derivatives are. The inaccuracy of this naming convention has caused many to refer to this as the *chiral* phase.

## 1.4 The smectic mesophase

In the smectic liquid crystal phase, the molecules form *layers*. Within the layers, the molecules behave much like in nematic liquid crystals, having a preferred orientation among a common local director. Smectic liquid crystals is an example of a liquid with both positional and orientational molecular ordering. There is positional ordering along the direction perpendicular to the layer planes, while inside the layers the molecules are free to flow like a liquid.

As illustrated in Figure 1.3, it is common to denote different types of smectic liquid crystals depending on how the molecules are oriented within the layers. In particular, if the average molecular orientation is orthogonal to the layer plane it is defined as a smectic A type material. If the orientation is at an angle compared to the normal, we refer to it as a smectic C liquid crystal.

It should be noted that different types of mesophases can in some cases be observed in the same material. An often-seen picture is the following: at low temperatures a material will be solid. When the sample is heated up it will undergo a phase transition into the smectic liquid crystal phase. When it is heated further, it then transitions into the nematic phase. Lastly, at high temperatures, the liquid crystal will be in an isotropic liquid state with no positional or orientation ordering.

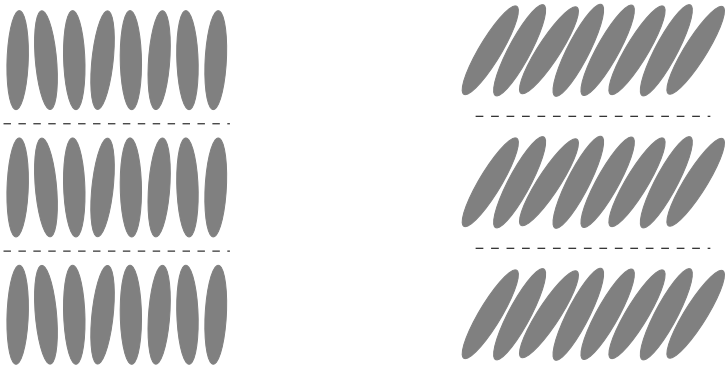

(a) Smectic A (b) Smectic C

Figure 1.3: Illustration of the smectic mesophase. For the smectic A phase (left) the molecules align in layers with the orientation normal to the layer interface. In the smectic C phase (right) the average orientation is tilted.

## 1.5 Application: Display devices

One of the best known applications of liquid crystals is in display devices. Since the discovery of the basic technology in the 1960s and the commercialization in the 1990s, liquid crystal displays (LCDs) have since surpassed the traditional cathode ray tube (CRT) technology for the use in televisions. Benefits of LCDs include low power consumption, compact design and safe disposal. This has helped make LCDs omnipresent in the modern world and they can be found in everything from computer monitors to cell phones and calculators.

An LCD screen is composed of a matrix of pixels. Many different variations on this technology exist, but the basic principle behind a single pixel in an LCD is illustrated in Figure 1.4. A liquid crystal cell is placed between two glass plates fitted with electrodes. The liquid crystal used has a natural twist in the molecular ordering. Furthermore, the glass substrate is designed so that the molecular orientation near the back plate is vertical, and the length of the cell is designed specifically to allow the molecules to twist 90 °C before hitting the front plate. A vertical polarizer is placed in the back of the cell and a horizontal polarizer is placed in the front.

In its *ON* state there is no voltage applied to the electrodes and the configuration is a shown in the top part of Figure 1.4. Unpolarized light

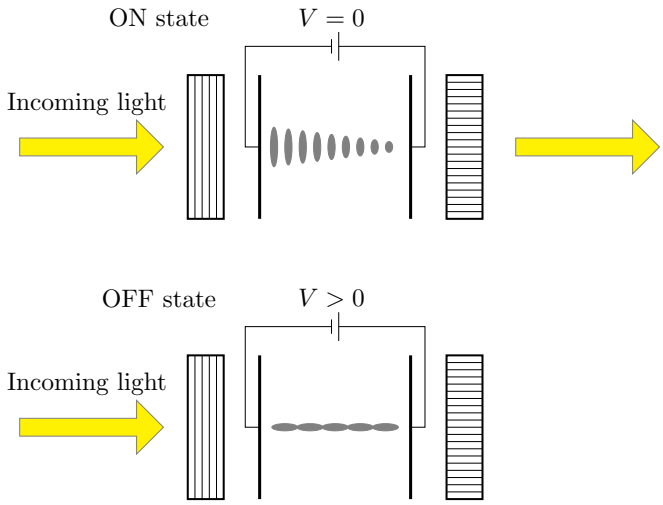


Figure 1.4: Schematic illustration of a TFT LCD display. A liquid crystal cell with twisted molecular orientation is placed between crossed polarizers. The polarization of the light is twisted by the liquid crystal, allowing it to pass through the second polarizer. A voltage difference can be applied to the cell in order to straighten out the orientation of the molecules, thus stopping light from passing through.

enters from the back and gets vertically polarized before entering the liquid crystal. The twist of the molecular orientation acts to twist the polarization of the light by 90 °C over the length of the cell. The light then passes through the horizontal polarizer in the front and goes on to hit the front of the display.

In the *OFF* state a voltage difference is applied over the electrodes. This induces an electric field in the cell which, because of the dielectric anisotropy of the molecules, will induce a torque favoring the alignment along a common axis. For sufficiently high voltages these torques will overcome the natural twist in the liquid crystal, as shown in the bottom part of Figure 1.4. In this case the light will remain vertically polarized when passing through the liquid crystal and will be stopped by the horizontal polarizer.

Chapter 2

# Static continuum theory for director fields in nematics

In an ideal nematic liquid crystal, all molecules will be aligned along a common direction enforced by bounding surfaces or external fields. However, in many practical situations there will be a competition between different external influences on the liquid crystal cell, potentially leading to nontrivial configurations. In addition, thermal excitations means that individual molecules will not be perfectly aligned, which introduces the concept of different *degrees* of orientation.

Since the typical correlation length in nematic liquid crystals is of the order of µm while the molecular size is measured in nm, a continuum description is often adopted. Herein, the orientational state of a nematic liquid crystal can be represented by two objects, as illustrated in Figure 2.1: the first one is the *director field*, a vector $\boldsymbol{n}(\boldsymbol{r})$ of unit length, giving the average molecular orientation in some small ball $\mathcal{B}$. The second is the *order parameter* $S(\boldsymbol{r})$ giving the local degree of orientation, often given in terms of the second Legendre polynomial as

$$S = \langle P_2(\cos(\theta)) \rangle = \left\langle \frac{3\cos^2(\theta) - 1}{2} \right\rangle. \tag{2.1}$$

Here the brackets indicate the weighted average

$$\langle g(\theta) \rangle = \int_{\mathcal{B}} g(\theta) f(\theta) \, \mathrm{d}V, \tag{2.2}$$

where $f(\theta)$ is the statistical distribution of the molecular angles $\theta$. Special cases of the order parameters are:

- S = 1: Perfect alignment along the director
- S = 0: No orientation (isotropic)
- S = -1/2: Perfect alignment orthogonal to the director

The order parameter can be defined in terms of higher order Legendre polynomials in cases where the higher accuracy is needed.

It should be noted that the picture above only applies to uniaxial nematics. Certain nematic liquid crystals are *biaxial*, i.e. consisting of molecules having a shape that must be described by two anisotropic axes. The most general continuum theory for nematics thus requires two vector valued quantities $\boldsymbol{n}_1$ and $\boldsymbol{n}_2$, as well as two scalar order parameters $S_1$ and $S_2$ [45]. The common general framework for describing nematic liquid crystals is the so-called Landau–de Gennes theory. Herein, the continuum state is given by the tensor

$$\boldsymbol{Q} = S_1(\boldsymbol{n}_1 \otimes \boldsymbol{n}_1) + S_2(\boldsymbol{n}_2 \otimes \boldsymbol{n}_2) - \frac{1}{3}\boldsymbol{I}(S_1 + S_2).$$

The tensor $\boldsymbol{Q}$ is symmetric and has, due to the last term, trace zero. $\boldsymbol{Q}$-tensor theory has been widely successful in part for its ability to describe defects and phase transitions in nematics. It should also be mentioned that MacMillan [41] in his thesis developed a similar theory for biaxial nematics. However, this topic is outside the scope of this text as we will focus on models for uniaxial molecules.

The degree of which the Oseen–Frank picture can be seen as is a special case of the more general Landau–de Gennes theory is a nontrivial issue that has received some attention lately [42]. In some simplified geometries, the equilibrium solutions of the two models coincide. However, counterexamples can be constructed for which this is not the case [1]. This is due to the fact that the director picture does not implicitly respect the physical symmetry of the states $\boldsymbol{n}$ and $-\boldsymbol{n}$ being equivalent.

A common simplifying assumption in the modeling of nematic liquid crystals is to assert a constant order parameter $S$. Indeed, this is the paradigm that will be considered presently. It should be mentioned that theory exists including effects of variable degree of molecular orientation. The modeling of elastics given variable orientation was introduced by Ericksen [17] in 1991 as a proposed tool for describing defects in nematics (often referred to as disclinations). For a detailed account of the theory of nematics of variable orientation, Virga's book [58] is an excellent starting point.

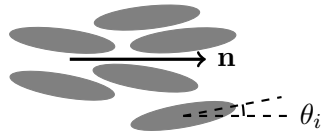


Figure 2.1: The continuum description of a uniaxial nematic liquid crystal involves a director field $\boldsymbol{n}$ and a local degree of orientation along this direction, given by a scalar $S = \langle P_2(\cos(\theta))\rangle$.

## 2.1 The Oseen–Frank elastic energy

In a nematic liquid crystal, inter-molecular forces will favor the alignment of the director field along a common direction. The free energy $\mathcal{W}_{\mathrm{OF}}$ (per volume) associated with distortions from a constant alignment is given by the Oseen–Frank functional. It is based on the following constraints:

- $\mathcal{W}_{\mathrm{OF}}$ should vanish for undistorted director fields ($\nabla \boldsymbol{n} = 0$)
- Since the states $\boldsymbol{n}$ and $-\boldsymbol{n}$ are physically indistinguishable, the energy must be an even function of $\boldsymbol{n}$
- Rotationally invariance prohibits terms linear in $\nabla \boldsymbol{n}$
- Assuming moderate distortions, only terms of order $(\nabla \boldsymbol{n})^2$ are included.

The derivation of the general form of the free energy $\mathcal{W}_{\mathrm{OF}}(\boldsymbol{n}, \nabla \boldsymbol{n})$ satisfying the constraints above is a cumbersome exercise which is omitted from this text. An interested reader is referred to the book of de Gennes [13, Ch. 3] for a detailed discussion. The final form of the Oseen–Frank energy, given by

$$\mathcal{W}_{\mathrm{OF}}(\boldsymbol{n}, \nabla \boldsymbol{n}) = \frac{1}{2}\alpha_1 |\boldsymbol{n} \times (\nabla \times \boldsymbol{n})|^2 + \frac{1}{2}\alpha_2 (\nabla \cdot \boldsymbol{n})^2 + \frac{1}{2}\alpha_3 (\boldsymbol{n} \cdot (\nabla \times \boldsymbol{n}))^2 + \frac{1}{2}(\alpha_2 + \alpha_4)\nabla \cdot ((\nabla \boldsymbol{n})\boldsymbol{n} - (\nabla \cdot \boldsymbol{n})\boldsymbol{n}), \quad (2.3)$$

is a result of decades of discussions dating back to the early work by Oseen [51] and Zocher [65] and later modifications by Frank [19]. The material constants $\alpha_1$, $\alpha_2$ and $\alpha_3$ correspond to the three basic types of elastic distortions of the director field, bend, splay and twist, respectively, as illustrated in Figure 2.2. Finding stable equilibrium configurations with respect to this

energy has been a key topic in the static continuum theory of nematics. The existence and partial regularity of minimizers to the Oseen–Frank energy functional (2.3) was established by Hardt et al. [27] in their now classic paper.


Figure 2.2: The three basic types of distortions that go into the Oseen–Frank elastic energy (2.3).

The last term of (2.3) is a saddle-splay term and is in the form of a pure divergence. Therefore, by using the divergence theorem, it can be written as a surface integral. This term will not contribute to the static theory when using fixed (anchored) director fields at the boundaries. Also, the term will vanish identically in certain commonly studied cases. One example is the bend-splay geometry in 1D,

$$\boldsymbol{n}(x) = (\cos(\psi(x)), \sin(\psi(x)), 0). \tag{2.4}$$

As a result of this, the term is often ignored in the literature. Indeed, this will also be the case for the remainder of this text.

A common additional assumption seen in the literature is the *one-constant approximation*

$$\alpha_1 = \alpha_2 = \alpha_3 = \alpha_4. \tag{2.5}$$

The assertion of equality of the different elastic constants is made purely out of mathematical convenience. For common nematic liquid crystals the values of these material constants can differ significantly, as seen in Table 2.1. However, the simplified form of (2.3) resulting from the one-constant approximation can significantly ease the analysis of nematics. Therefore, (2.5) is almost ubiquitous in the theoretical analysis of nematics.

| | Elastic constants ($10^{-12}$ N) | | |
|---|---|---|---|
| | MBBA (25 °C) [26] | 5CB (26 °C) [14] | PAA (122 °C) [40] |
| $\alpha_1$ | 6.0 | 6.2 | 6.9 |
| $\alpha_2$ | 3.8 | 3.9 | 3.8 |
| $\alpha_3$ | 7.5 | 8.2 | 11.9 |

Table 2.1: Experimentally measured values for the elastic constants appearing in the Oseen–Frank energy (2.3) representing bend ($\alpha_1$), splay ($\alpha_2$) and twist ($\alpha_3$).

## 2.2 Electric fields

The interaction between electromagnetic fields and the director field has historically been central both in the experimental study of nematic liquid crystals as well as in applications. In general, applying an electric field to a liquid crystal sample will produce temporary dipoles moments. The size of these will, because of the anisotropic nature of the molecules, depend on the orientation of the director field.

The polarization $\boldsymbol{P}$ (electric dipole moment per unit volume) is in a dielectric proportional with the electric field $\boldsymbol{E}$ and given by

$$\boldsymbol{P} = \varepsilon_0 \boldsymbol{\chi} \boldsymbol{E},$$

where $\varepsilon_0 \approx 8.854 \times 10^{-12}\,\mathrm{F\,m^{-1}}$ is the permittivity of free space. Nematic liquid crystals are anisotropic, so the constant of proportionality is a susceptibility tensor and the polarization will in general not be parallel to the applied field. In a coordinate system defined by the director, i.e. by letting $\boldsymbol{n} = (1, 0, 0)$, we can write (for uniaxial nematics)

$$\boldsymbol{\chi}_{\mathrm{E}} = \begin{pmatrix} \chi_{\mathrm{E},\parallel} & 0 & 0 \\ 0 & \chi_{\mathrm{E},\perp} & 0 \\ 0 & 0 & \chi_{\mathrm{E},\perp} \end{pmatrix},$$

where $\chi_{\mathrm{E},\parallel}$ and $\chi_{\mathrm{E},\perp}$ are the electric susceptibilities parallel and perpendicular to the long axis of the molecules, respectively.

The electric displacement $\boldsymbol{D}$ is defined as

$$\boldsymbol{D} = \varepsilon_0 \boldsymbol{E} + \boldsymbol{P}. \tag{2.6}$$

In the case of linear polarization, it is common to combine the terms of the displacement into

$$\boldsymbol{D} = \varepsilon_0 \boldsymbol{\varepsilon} \boldsymbol{E} \tag{2.7}$$

using the dielectric tensor

$$\boldsymbol{\varepsilon} = \begin{pmatrix} \varepsilon_{\parallel} & 0 & 0 \\ 0 & \varepsilon_{\perp} & 0 \\ 0 & 0 & \varepsilon_{\perp} \end{pmatrix} = \begin{pmatrix} 1+\chi_{\mathrm{E},\parallel} & 0 & 0 \\ 0 & 1+\chi_{\mathrm{E},\perp} & 0 \\ 0 & 0 & 1+\chi_{\mathrm{E},\perp} \end{pmatrix}, \tag{2.8}$$

where $\varepsilon_{\parallel}$ and $\varepsilon_{\perp}$ are the relative (dimensionless) electric susceptibilities parallel and perpendicular to molecular long axis, respectively. In terms of the relative susceptibilities, we can write (2.7) in the form

$$\boldsymbol{D} = \varepsilon_0 \varepsilon_{\perp} \boldsymbol{E} + \varepsilon_0 \varepsilon_a (\boldsymbol{n} \cdot \boldsymbol{E}) \boldsymbol{n}, \tag{2.9}$$

where $\varepsilon_a = \varepsilon_{\parallel} - \varepsilon_{\perp}$ is the dielectric anisotropy. The displacement can always be described locally in this way by choosing the appropriate coordinate system, hence the form (2.9) is the general form most commonly used in modeling.

The bulk energy density associated with the electric field is given by

$$\mathcal{W}_{\mathrm{E}} = -\frac{1}{2} \boldsymbol{D} \cdot \boldsymbol{E} = -\frac{1}{2} \varepsilon_0 \left( \varepsilon_{\perp} |\boldsymbol{E}|^2 + \varepsilon_a (\boldsymbol{n} \cdot \boldsymbol{E})^2 \right). \tag{2.10}$$

The negative sign in (2.10) can be a source of confusion for readers used to the standard energy density of dielectrics used in electrostatics. The reason for this is that (2.10) comes from considering the energy required to maintain a constant voltage difference across the liquid crystal. For a more detailed derivation an interested reader can turn to Collings and Hird's excellent book [11, Ch. 10].

The first (isotropic) term on the right hand side of (2.10) does not depend on the director configuration if the electric field is assumed constant. In this case the isotropic term will not affect the equilibrium equation for the director field and is often ignored in the literature. In the current work, both terms in the electric energy are kept both for completeness and due to the fact that the electric field will be coupled to the director through Maxwell's equations.

Some basic quantitative features of the model are immediately apparent from (2.10), see Figure 2.3. In particular, for $\varepsilon_a > 0$, the alignment of the director field along the electric field ($\boldsymbol{n} \cdot \boldsymbol{E} = 1$) is energetically favored. Conversely, a negative electric anisotropy will cause alignment perpendicular to the electric field. The dielectric constants for some common nematic liquid crystals can be found in Table 2.2.

Electric fields are known to couple strongly with the director field in a nematic liquid crystal. In general, the configuration of an electric field in

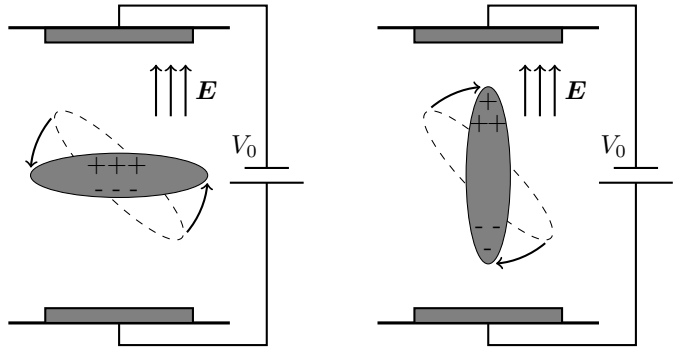


Figure 2.3: Illustration of the orientation of liquid crystal molecules under the influence of an electric field. The orientation of the long axis will be perpendicular or parallel to the applied field, depending on the sign of the dielectric anisotropy.

| | Dielectric constants (dimensionless) | | |
|---|---|---|---|
| | MBBA (25 °C) [55] | 5CB (26 °C) [40] | PAA (122 °C) [55] |
| $\varepsilon_\parallel$ | 4.7 | 18.5 | 5.538 |
| $\varepsilon_\perp$ | 5.4 | 7 | 5.705 |
| $\varepsilon_a$ | -0.7 | 11.5 | -0.167 |

Table 2.2: Experimentally measured values for the dielectric constants appearing in the dielectric tensor (2.8) for some common liquid crystals.

the presence of a dielectric is given Maxwell's equations. In the absence of free charge they are given by

$$\nabla \cdot \boldsymbol{D} = 0 \qquad \text{and} \qquad \nabla \times \boldsymbol{E} = 0. \tag{2.11}$$

The equations (2.11) must be solved together with the equilibrium equations for the director field to give the correct configuration. However, in many simplified settings the assumption is made that $\varepsilon_a \ll 1$ allowing for the solution of Maxwell's equation in a vacuum. In this case, the electric field $\boldsymbol{E}$ is treated as a constant in the nematic energy (2.10).

## 2.3 Magnetic fields

The theory on applied magnetic fields in nematics is similar to that for electric fields described in Section 2.2. An external magnetic field $\boldsymbol{H}$ will induce a magnetic moment $\boldsymbol{M}$ (per unit volume) given as

$$\boldsymbol{M} = \boldsymbol{\chi}_{\mathrm{M}} \boldsymbol{H}. \tag{2.12}$$

Like for electric fields, the magnetization will depend on the orientation of the director field $\boldsymbol{n}$. In the coordinate system of the director, the magnetic susceptibility tensor $\boldsymbol{\chi}_{\mathrm{M}}$ can be written as

$$\boldsymbol{\chi}_{\mathrm{M}} = \begin{pmatrix} \chi_{\mathrm{M},\parallel} & 0 & 0 \\ 0 & \chi_{\mathrm{M},\perp} & 0 \\ 0 & 0 & \chi_{\mathrm{M},\perp} \end{pmatrix},$$

for uniaxial nematics. In the above, $\chi_{\mathrm{M},\parallel}$ and $\chi_{\mathrm{M},\perp}$ are the magnetic susceptibilities parallel and perpendicular to the molecular long axis, respectively. A straightforward calculation then allows for the magnetization $\boldsymbol{M}$ to be divided into an isotropic and an anisotropic term, written as

$$\boldsymbol{M} = \chi_{\mathrm{M},\perp} \boldsymbol{H} + \chi_{M,a} (\boldsymbol{n} \cdot \boldsymbol{H}) \boldsymbol{n}, \tag{2.13}$$

where $\chi_{\mathrm{M},a} = \chi_{\mathrm{M},\parallel} - \chi_{\mathrm{M},\perp}]$.

The magnetic *induction* $\boldsymbol{B}$ in the presence of magnetization is defined as

$$\boldsymbol{B} = \mu_0 (\boldsymbol{H} + \boldsymbol{M}),$$

where $\mu_0 = 4\pi \times 10^{-7}\,\mathrm{H\,m^{-1}}$ is the vacuum permeability. By inserting for the magnetization (2.13), and introducing the quantities

$$\mu_{\parallel} = 1 + \chi_{\mathrm{M},\parallel}, \qquad \mu_{\perp} = 1 + \chi_{\mathrm{M},\perp} \tag{2.14}$$

we obtain

$$\boldsymbol{B} = \mu_0\mu_\perp \boldsymbol{H} + \mu_0\mu_a(\boldsymbol{n}\cdot\boldsymbol{H})\boldsymbol{n}, \tag{2.15}$$

where $\mu_a = \mu_\parallel - \mu_\perp$.

The bulk magnetic energy density is, analogously as in Section 2.2, given by

$$\mathcal{W}_{\mathrm{M}} = -\frac{1}{2}\boldsymbol{B}\cdot\boldsymbol{H} = -\frac{1}{2}\mu_0\mu_\perp|\boldsymbol{H}|^2 - \frac{1}{2}\mu_0\mu_a(\boldsymbol{n}\cdot\boldsymbol{H})^2. \tag{2.16}$$

Comparing (2.16) to (2.10) reveals a striking resemblance in the theoretical treatment of electric and magnetic fields. Also in this case it is common to disregard the term in (2.16) that is independent of $\boldsymbol{n}$, as it does not influence the equilibrium configuration of the director. However, it might be kept in cases where the total energy dependence on the applied electric field is of interest. A simple inspection of (2.16) reveals that for $\mu_a > 0$, the alignment of the director along the magnetic field is energetically preferred. Conversely, for negative magnetic anisotropy, the orthogonal configuration is preferred.

The configuration of a magnetic field is in general given by Maxwell's equations, similarly to the situation for electric fields. However, unlike electric fields, magnetic fields are known to be virtually unaffected by the presence of a liquid crystal [56]. Therefore, it is usually seen as sufficient to consider the vacuum equations

$$\nabla\cdot\boldsymbol{H} = 0 \qquad \text{and} \qquad \nabla\times\boldsymbol{H} = 0.$$

The solution of these will in many simple geometries be a constant magnetic field.

## 2.4 Weak and strong boundary anchoring

Surface effects are essential in the understanding of the basic physics of nematics as well as in applications such as optical devices. The bounding plates in a liquid crystal cell can be treated chemically or mechanically in such a way that a specific molecular orientation is energetically preferred near the boundary. In the modeling, the simplifying assumption is often made that the director is fixed *a priori* to some set value at the boundary. This is often referred to as *strong* anchoring.

In most optical liquid crystal devices the surface anchoring is sufficiently strong so that the assumption of a fixed director at the boundary is appropriate [8]. However, in cases with e.g. strong applied fields the electromagnetic torques might be able to compete with, or even overcome, the boundary

anchoring. Rapini and Papoular [53] are credited with being the first to introduce a *weak* anchoring in the modeling of nematic liquid crystals. They proposed adding a penalty term to the free energy in the form

$$\mathcal{W}_B = -\frac{1}{2}w(\boldsymbol{n}\cdot\boldsymbol{n}_A)^2, \tag{2.17}$$

where $\boldsymbol{n}_A$ is some preferred orientation at the boundary and $w$ is the anchoring strength. Rapini and Papoular's form (2.17) has since been widely used in modeling and its validity indicated by experiments [46].

## 2.5 Equilibrium equations

Given the free energy associated with elastic, electric, magnetic and boundary effects, the static equilibrium configuration for the director field can be obtained using the calculus of variations. Variational techniques have been central in the theoretical treatment of liquid liquid crystals, and a vast and comprehensive literature exists, including advanced topics such as defects and variable domains. Herein, a good starting point is Virga's book [58], which gives a rigorous and in-depth account of variational theories applied to liquid crystals. In this section the discussion is limited to a brief summary of the principles needed in the scope of this thesis.

Consider a liquid crystal on a regular domain $\Omega$ with boundary denoted by $\partial\Omega$. Summarizing the results from the preceding sections, we can write the total free energy as the functional

$$W[\boldsymbol{n}] = \int_\Omega (\mathcal{W}_{\mathrm{OF}} + \mathcal{W}_{\mathrm{E}} + \mathcal{W}_{\mathrm{M}})\,\mathrm{d}\boldsymbol{x} + \int_{\partial\Omega}\mathcal{W}_B\,\mathrm{d}S. \tag{2.18}$$

For strong anchoring the boundary energy can be set to zero and replaced by an a priori assumption $\boldsymbol{n} = \boldsymbol{n}_0$ on $\partial\Omega$.

Following the principles of classical mechanics, we look for an equilibrium solution for the director field $\boldsymbol{n}$ by looking for stationary points of the energy (2.18) [58]. This is done by considering variations of the director configurations in the form

$$\boldsymbol{n}_\epsilon = \boldsymbol{n} + \epsilon\boldsymbol{u} \tag{2.19}$$

for some smooth vector $\boldsymbol{u}$ and some small $\epsilon \in [-\epsilon_0, \epsilon_0]$. For strong anchoring, $\boldsymbol{u}$ is chosen in such a way that $\boldsymbol{n}_\epsilon$ fulfills that boundary condition for any $\epsilon$. For a given $\boldsymbol{u}$, $\boldsymbol{n}_\epsilon$ then gives a path of configurations parameterized by $\epsilon$.

We say that a solution $\boldsymbol{n}$ is a stationary (equilibrium) configuration with regard to the energy (2.18) if the first variation vanishes for all $\boldsymbol{u}$, i.e.

$$\frac{\partial}{\partial\epsilon}W[\boldsymbol{n}+\epsilon\boldsymbol{u}]\Big|_{\epsilon=0} = 0. \tag{2.20}$$

We note that given strong anchoring, any term in the bulk energy density that can be written in the form of a pure divergence will not affect the equilibrium solution. An example of such a term is the saddle-splay term in the Oseen–Frank energy (2.3). Such a term is often referred to as a *null Lagrangian*.

Chapter 3

# The Fréedericksz transition

The interaction between electromagnetic fields and the director field is an essential part of liquid crystal theory and a key component in applications. Herein, the Fréedericksz transition is the classical example. In its simplest form, it can be seen as a competition between elastic torques resisting distortions in the director and dielectric torques aligning the director with the electric field, see Figure 3.1. Consider a one-dimensional liquid crystal cell of finite length with strong anchoring at the boundary fixing the director parallel to the surfaces. A voltage difference is applied across the cell, resulting in a torque aligning the director with the electric field in the bulk of the liquid crystal. For low applied voltages, and hence low electric fields, the homogeneous unperturbed state remains a stable configuration. However, when the electric field exceeds a specific threshold, $E > E_{\mathrm{F}}$, there is an abrupt reconfiguration.

The Fréedericksz transition can be observed experimentally due to the optical birefringence of liquid crystals. This was first done in 1927 by Fréedericksz[1] [20] by using applied magnetic fields. In particular, he observed an inverse relationship between the critical field strength and the sample thickness. Soon after, Zocher [65] was able to formulate a theory for the transition which predicted the same behavior.

The Fréedericksz transition is omnipresent in the liquid crystal literature. It is a simple example which illustrates essential features of the interaction between a liquid crystal and an external field. At the same time, the mechanism of the abrupt transition is precisely what allows for switch-on and switch-off in display devices. Also, the phenomenon allows for the ex-

[1] The brilliant Russian physicist Vsevolod Fréedericksz' last name is also often written Frederiks.

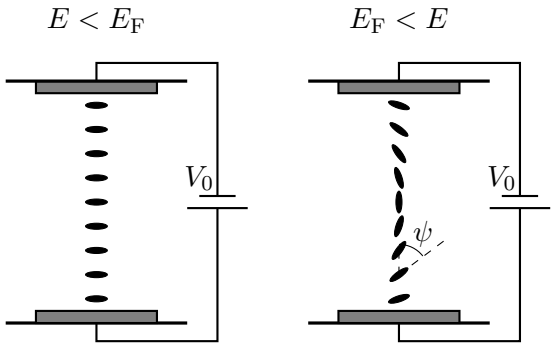


Figure 3.1: Illustration of the Fréedericksz transition. Left: For a low electric field the anchoring forces dominate and the director field is in a homogeneous ($\psi = \pi/2$) configuration. Right: For electric fields above the Fréedericksz threshold but below the saturation threshold there is a competition between electric and anchoring forces leading to a nontrivial configuration.

perimental determination of certain material constants, since they directly influence the value of the critical field.

## 3.1 The bend-splay geometry in 1D

In the following we consider a liquid crystal cell in one spatial dimension of length $L$. For simplicity, we will focus the discussion of the Fréedericksz transition on the bend-splay geometry, i.e. we consider the director

$$\boldsymbol{n}(x) = (\cos(\psi(x)), \sin(\psi(x)), 0), \tag{3.1}$$

where $\psi(x)$ is the angle between the director and the $x$-axis. We assume the director is strongly anchored at the boundary with $\psi(0) = \psi(L) = \pi/2$.

In the bend-splay geometry the elastic energy, obtained by integrating the Oseen–Frank energy density (2.3) over the domain, becomes

$$W_{\mathrm{OF}}[\psi] = \frac{1}{2}\int_0^L c^2(\psi)\psi_x^2 \,\mathrm{d}x, \tag{3.2}$$

where we have introduced the function

$$c(\psi) = \sqrt{\alpha_1 \cos^2(\psi) + \alpha_2 \sin^2(\psi)}. \tag{3.3}$$

As the name suggests, in the bend-splay geometry the contribution from the twist term is absent from the elastic energy.

We assume that the applied electric field $E$ is constant through the bulk of the cell. The electric contribution to the bulk energy is then obtained from the integral of the energy density (2.10) over the cell, yielding

$$W_{\mathrm{E}}[\psi] = -\frac{1}{2}\varepsilon_0 E^2 \int_0^L \left(\varepsilon_\perp + \varepsilon_a \cos^2(\psi)\right) \mathrm{d}x. \tag{3.4}$$

The equilibrium configuration $\psi(x)$ is then given as a minimizer of the energy functional

$$W[\psi] = \frac{1}{2}\int_0^L \left(c^2(\psi)\psi_x^2 - \varepsilon_0 E^2 \left(\varepsilon_\perp + \varepsilon_a \cos^2(\psi)\right)\right) \mathrm{d}x, \tag{3.5}$$

under the constraint of the strong anchoring boundary condition.

The calculus of variations can be used to derive an equation for the director configuration. Looking for stationary points in the energy (3.5), we calculate

$$\begin{aligned}
\frac{\partial}{\partial\epsilon}\Big|_{\epsilon=0} W[\psi+\epsilon\phi] &= \frac{\partial}{\partial\epsilon}\Big|_{\epsilon=0} \frac{1}{2}\int_0^L \big(c^2(\psi+\epsilon\phi)(\psi_x+\epsilon\phi_x)^2 \\
&\qquad - \varepsilon_0 E^2 \left(\varepsilon_\perp + \varepsilon_a \cos^2(\psi+\epsilon\phi)\right)\big) \,\mathrm{d}x \\
&= \frac{1}{2}\int_0^L \big(2c(\psi+\epsilon\phi)c'(\psi+\epsilon\phi)(\psi_x+\epsilon\phi)^2\phi \\
&\qquad + 2c^2(\psi+\epsilon\phi)(\psi_x+\epsilon\phi_x)\phi_x \\
&\qquad + \varepsilon_0\varepsilon_a E^2 \sin(2(\psi+\epsilon\phi))\phi\big) \,\mathrm{d}x\Big|_{\epsilon=0} \\
&= \frac{1}{2}\int_0^L \big(-2c(\psi)(c(\psi)\psi_x)_x + \varepsilon_0\varepsilon_a E^2 \sin(2\psi)\big)\phi \,\mathrm{d}x = 0,
\end{aligned} \tag{3.6}$$

where we have used integration by parts and the strong anchoring at the boundary. If (3.6) is to hold for all $\phi$, the director angle needs to satisfy

$$c(\psi)\left(c(\psi)\psi_x\right)_x - \frac{1}{2}\varepsilon_0\varepsilon_a E^2 \sin(2\psi) = 0, \qquad x \in (0, L). \tag{3.7}$$

A dimensionless version of (3.7) can be derived by introducing the *extrapolation length*

$$\xi = \frac{1}{E}\sqrt{\frac{\alpha_1}{\varepsilon_0\varepsilon_a}}$$

as well as the dimensionless quantities $h = L/\xi$ and

$$\tilde{c}(\psi) = \frac{1}{\sqrt{\alpha_1}} c(\psi) = \sqrt{\cos^2(\psi) + \frac{\alpha_2}{\alpha_1} \sin^2(\psi)}.$$

The equilibrium equation (3.7) can then be written in the form

$$\tilde{c}(\psi) \left(\tilde{c}(\psi)\psi_X\right)_X - \frac{1}{2} h^2 \sin(2\psi) = 0, \qquad X \in (0,1), \tag{3.8}$$

where $X = x/L$ is the unit-scaled length.

## 3.2 Critical threshold for transition

The threshold for which the transition occurs can be approximated using linear analysis. We introduce $\theta = \pi/2 - \psi$ and linearize the energy (3.5) around $\theta = 0$ to obtain

$$\overline{W} = \int_0^L \left(\alpha_2 \theta_x^2 - \varepsilon_0 \varepsilon_a E^2 \theta^2\right) \mathrm{d}x, \tag{3.9}$$

where constant terms have been ignored. Now, following the approach of de Gennes [13, Ch. 3], we consider strongly anchored perturbations in the form of the Fourier series

$$\theta(x) = \sum_k \delta_k \sin\left(\frac{k\pi x}{L}\right). \tag{3.10}$$

By inserting (3.10) into (3.9) and integrating over the length of the domain, we arrive at

$$\overline{W} = \frac{1}{2} \sum_k \delta_k \left(\alpha_2 \frac{\pi^2}{2L} - \frac{\varepsilon_0 \varepsilon_a}{2k} E^2 L\right). \tag{3.11}$$

For the unperturbed state to remain stable, the change in energy associated with the modes (3.10) must be positive. We can therefore conclude that for

$$\alpha_2 \frac{\pi^2}{2L} > \frac{\varepsilon_0 \varepsilon_a}{2} E^2 L \tag{3.12}$$

the homogeneous state is linearly stable. Hence, the critical threshold for the Fréedericksz transition is approximated as

$$E_{\mathrm{F}} = \frac{\pi}{L} \left(\frac{\alpha_2}{\varepsilon_0 \varepsilon_a}\right)^{\frac{1}{2}}. \tag{3.13}$$

Note the inverse relationship between the critical field strength and the cell length $L$, as originally observed by Fréedericksz. In terms of the dimensionless parameter $h$ we obtain the critical value

$$h_{\mathrm{F}} = \sqrt{\frac{\alpha_1}{\alpha_2}}\pi. \tag{3.14}$$

The nature of this abrupt transition is illustrated in Figure 3.2. Using the one-constant approximation, equation (3.8) was solved numerically for different values of $h$. Indeed, for $h < h_{\mathrm{F}} = \pi$, the solution is a homogeneous ($\psi = \pi/2$) director configuration. When the field strength $h$ is increased beyond the Fréedericksz threshold $h_{\mathrm{F}}$ the solution becomes a nontrivial symmetric profile with $\pi/2 \leq \psi \leq \pi$.

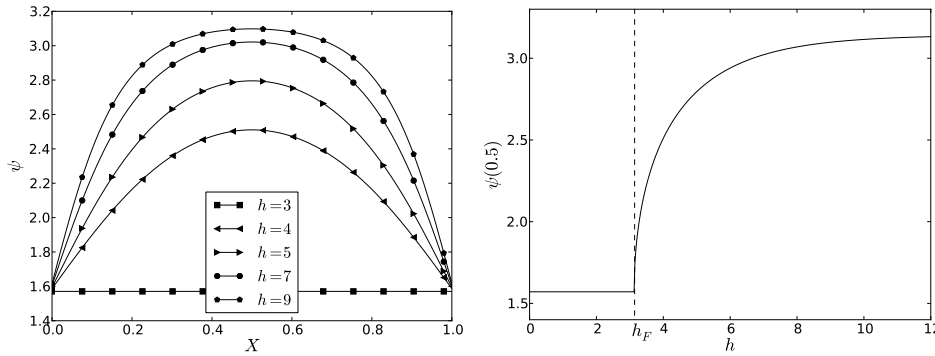


Figure 3.2: Solutions of (3.8) using $\alpha_2/\alpha_1 = 1$, illustrating the Fréedericksz transition with strong anchoring. For $h < h_{\mathrm{F}} = \pi$ the equilibrium solution is a constant state $\psi = \pi/2$. When $h > h_{\mathrm{F}}$ there is an abrupt reorientation into a nontrivial even-symmetric state.

## 3.3 Weak anchoring

Introducing weak boundary anchoring, as described in Section 2.4, will significantly affect the modeling of the Fréedericksz transition. Crucially, having a finite energy penalty for deviations from the preferred direction allows for the electric torques to overcome the anchoring torques. Therefore, in the *weak* Fréedericksz transition, there are two critical points when changing the electric field strength, as illustrated in Figure 3.3. For sufficiently low applied fields, similar as in the standard case, the stable configuration is an unperturbed homogeneous state with the director aligned with the easy direction at the boundary. When the field is increased beyond the Fréedericksz

threshold, the equilibrium configuration represents a nontrivial balance between the different torques involved. If the field is increased further, it will eventually reach the *saturation* threshold. Here, electric torques are large enough to overcome the boundary anchoring, and the stable configuration is homeotropic.

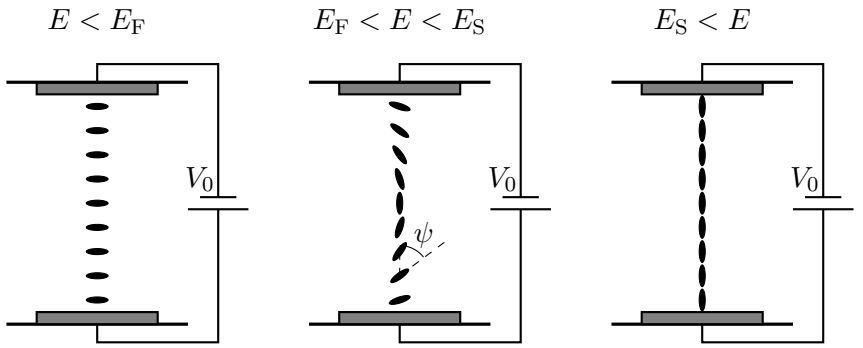


Figure 3.3: Illustration of the weak Fréedericksz transition. Left: For a low electric field the anchoring forces dominate and the director field is in a homogeneous ($\psi = \pi/2$) configuration. Middle: For electric fields above the Fréedericksz threshold but below the saturation threshold there is a competition between electric and anchoring forces leading to a nontrivial configuration. Right: For strong electric fields (over the saturation threshold) the electric forces overcome the anchoring and the configuration is homeotropic ($\psi = 0$).

Adding boundary energy terms, the total energy for the weak Fréedericksz cell in the bend-splay geometry becomes

$$W[\psi] = \frac{1}{2}\int_0^L \left(c^2(\psi)\psi_x^2 - \varepsilon_0 E^2\left(\varepsilon_\perp + \varepsilon_a \cos^2(\psi)\right)\right) \mathrm{d}x + \frac{w}{2}\cos^2(\psi)\left(|_{x=0} + |_{x=L}\right), \quad (3.15)$$

where $w$ is the anchoring strength. Using the same technique as before, we look for equilibrium solutions of (3.15). Calculating the variation, this time

with smooth test functions $\phi$ that are nonzero at the boundaries, we obtain

$$\begin{aligned}\frac{\partial}{\partial\epsilon}\Big|_{\epsilon=0} W[\psi+\epsilon\phi] &= \frac{\partial}{\partial\epsilon}\Big|_{\epsilon=0}\frac{1}{2}\int_0^L \big(c^2(\psi+\epsilon\phi)(\psi_x+\epsilon\phi_x)^2 \\ &\qquad - \varepsilon_0 E^2\left(\varepsilon_\perp + \varepsilon_a\cos^2(\psi+\epsilon\phi)\right)\big)\,\mathrm{d}x \\ &\qquad + \frac{w}{2}\cos^2(\psi+\epsilon\phi)\left(|_{x=0}+|_{x=L}\right) \\ &= \frac{1}{2}\int_0^L \big(2c(\psi+\epsilon\phi)c'(\psi+\epsilon\phi)(\psi_x+\epsilon\phi)^2\phi \\ &\qquad + 2c^2(\psi+\epsilon\phi)(\psi_x+\epsilon\phi_x)\phi_x \\ &\qquad + \varepsilon_0\varepsilon_a E^2\sin(2(\psi+\epsilon\phi))\phi\big)\,\mathrm{d}x\Big|_{\epsilon=0} \\ &\qquad - \frac{w}{2}\sin\left(2(\psi+\epsilon\phi)\right)\phi\left(|_{x=0}+|_{x=L}\right)\Big|_{\epsilon=0} \\ &= \frac{1}{2}\int_0^L \big(-2c(\psi)(c(\psi)\psi_x)_x + \varepsilon_0\varepsilon_a E^2\sin(2\psi)\big)\phi\,\mathrm{d}x \\ &\qquad + \Big(c^2(\psi(L))\psi_x(L) - \frac{w}{2}\sin(2\psi(L))\Big)\phi(L) \\ &\qquad + \Big(-c^2(\psi(0))\psi_x(0) - \frac{w}{2}\sin(2\psi(0))\Big)\phi(0) = 0.\end{aligned} \tag{3.16}$$

If (3.16) is to hold for all test functions $\phi$, the director angle must satisfy the equation

$$c(\psi)\left(c(\psi)\psi_x\right)_x - \frac{1}{2}\varepsilon_0\varepsilon_a E^2\sin(2\psi) = 0, \qquad x\in(0,L), \tag{3.17}$$

with boundary conditions

$$\psi_x + \frac{1}{2}\frac{w}{c^2(\psi)}\sin(2\psi) = 0, \qquad x = 0, \tag{3.18a}$$

$$\psi_x - \frac{1}{2}\frac{w}{c^2(\psi)}\sin(2\psi) = 0, \qquad x = L. \tag{3.18b}$$

We can derive a dimensionless version of this model. By introducing the *extrapolation length*

$$\ell = \frac{\alpha_1}{w}$$

and the number $\beta = \frac{L}{\ell}$, we can rewrite the equations (3.17)–(3.18) in the form

$$\tilde{c}(\psi)(\tilde{c}(\psi)\psi_X)_X - \frac{1}{2}h^2\sin(2\psi) = 0, \qquad X\in(0,1)\,, \tag{3.19}$$

with boundary conditions

$$\psi_X + \frac{1}{2}\frac{\beta}{\tilde{c}^2(\psi)}\sin(2\psi) = 0, \qquad X = 0, \tag{3.20a}$$

$$\psi_X - \frac{1}{2}\frac{\beta}{\tilde{c}^2(\psi)}\sin(2\psi) = 0, \qquad X = 1. \tag{3.20b}$$

The critical transition thresholds for the electric field strength will depend on the anchoring [58, Ch. 5]. As before, the critical field for the Fréedericksz transition can be analyzed by introducing $\theta = \pi/2 - \psi$ and linearizing the energy (3.15) around $\theta = 0$. In terms of the dimensionless parameters $h$ and $\beta$ we obtain

$$\overline{W}[\theta] = \int_0^1 \left(\frac{\alpha_2}{\alpha_1}\theta_X^2 - h^2\theta^2\right) \mathrm{d}X + \frac{\beta}{2}\theta^2\left(\big|_{X=0} + \big|_{X=1}\right), \tag{3.21}$$

where constant terms have been ignored. The Euler–Lagrange equation corresponding to the energy (3.21) is

$$\theta_{XX} + \frac{\alpha_1}{\alpha_2}h^2\theta = 0, \qquad X \in (0,1), \tag{3.22}$$

with boundary conditions

$$\theta_X + \frac{\alpha_1}{\alpha_2}\beta\theta = 0, \qquad X = \{0,1\}. \tag{3.23}$$

An even (w.r.t. the cell centre) solution to (3.22) is given by

$$\theta(X) = \theta_0 \cos\left(\sqrt{\frac{\alpha_1}{\alpha_2}}h\left(X - \frac{1}{2}\right)\right). \tag{3.24}$$

By inserting (3.24) into the boundary equation (3.23) we obtain the constraint

$$h = \sqrt{\frac{\alpha_1}{\alpha_2}}\beta\cot\left(\sqrt{\frac{\alpha_1}{\alpha_2}}\frac{h}{2}\right). \tag{3.25}$$

We refer to the *smallest* $h$ that satisfies (3.25) as the Fréedericksz threshold $h_{\mathrm{F}}$.

Similarly, the saturation threshold $h_{\mathrm{S}}$ can be obtained by linearizing the energy around $\psi = 0$. Here we obtain

$$\overline{W}[\psi] = \int_0^1 \left(\psi_X^2 + h^2\psi^2\right) \mathrm{d}X - \frac{\beta}{2}\psi^2\left(\big|_{X=0} + \big|_{X=1}\right), \tag{3.26}$$

with the corresponding equilibrium equation

$$\psi_{XX} - h^2\psi = 0, \qquad X \in (0,1), \tag{3.27}$$

with boundary equation

$$\psi_X - \beta\psi = 0, \qquad X = \{0,1\}. \tag{3.28}$$

An even solution to the bulk equation (3.27) is given by

$$\psi(X) = \psi_0 \cosh\left(h\left(X - \frac{1}{2}\right)\right). \tag{3.29}$$

As before, we insert the solution (3.29) into the boundary equation (3.28) to obtain the saturation threshold [47, 58, 48]

$$h_{\mathrm{S}} = \beta \coth\left(\frac{h_{\mathrm{S}}}{2}\right).$$

Figure 3.4 shows both critical fields for the weak Fréedericksz transition for different values of the anchoring strengths $\beta$. Note that in the strongly anchored limit $\beta \to \infty$ the critical field $h_{\mathrm{F}} = \pi\sqrt{\alpha_1/\alpha_2}$ is recovered.

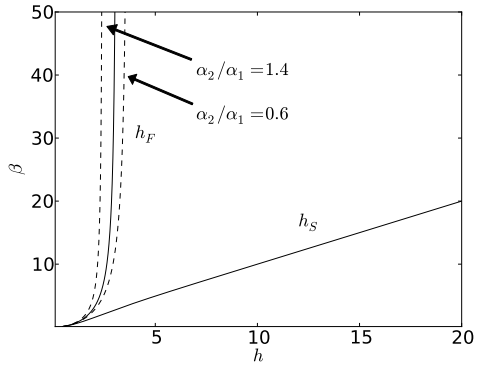


Figure 3.4: The Fréedericksz threshold $h_{\mathrm{F}}$ and the saturation threshold $h_{\mathrm{S}}$ for the weakly anchored case. The Fréedericksz threshold is shown for the one-constant approximation ($\alpha_2/\alpha_1 = 1$) and $\alpha_2/\alpha_1 = 1 \pm 0.4$.

The question of well-posedness for the weak Fréedericksz transition is more complicated than in the case for strong anchoring. Only recently, Costa et al. [12] were able to prove the long conjectured existence of a unique solution $\psi \in [0, \pi/2]$ to the boundary value problem (3.19)–(3.20), where

the one-constant approximation was assumed. However, in a recent experimental work by Kumar and coworkers [37], director states of odd parity with regard to the cell center were observed. This interesting result prompted a theoretical investigation by Bevilacqua and Napoli [2] where the uniqueness of equilibrium states was investigated on the full interval $\psi \in [0, \pi]$. By calculating exact solutions in terms of Jacobi elliptic functions, a technique dating back to the classic work of Nehring [48], they were able to show the existence of a hierarchy of stable excited director states. These states come in addition to the even symmetric ground states described by the classic theory. Moreover, the energy difference between the ground state and the first excited state is relatively small for certain $h$ and $\beta$. This indicates that odd configurations might play an important role in the weak Fréedericksz transition. This issue will be explored numerically in Paper B.

Chapter 4

# The dynamic problem in the bend-splay geometry

So far we have only considered static equilibrium solutions for the director configuration. In what follows, we will apply similar energy variational principles to formulate a *dynamic* theory. We will restrict ourselves to the bend-splay geometry, as described in Section 3.1. Specifically, we assume a director field in the form

$$\boldsymbol{n}(\boldsymbol{r},t) = (\cos(\psi(\boldsymbol{r},t)), \sin(\psi(\boldsymbol{r},t), 0), \tag{4.1}$$

where $\psi(\boldsymbol{r},t)$ denotes the angle between the first coordinate axis and the director. In this case, the twist term of the Oseen–Frank elastic energy (2.3) will vanish identically.

The classic macroscopic description of the dynamic flow of liquid crystals was developed by Ericksen [15, 16] in the early 1960s and later completed by Leslie [38, 39] and Parodi [52]. In their full form, the Leslie–Ericksen equations are a set of balance laws and constitutive relations for mass and momentum, involving both the fluid flow and the director field. Starting with the experimental verifications by Fishers and Fredrickson [18], this model has since been firmly established as the accepted theory for liquid crystal flow.

In this work we will assume a stationary flow field and focus on the dynamics of the director. This warrants a simpler approach than the framework of Leslie and Ericksen. Using principles of classical mechanics, we use an energy variational approach to derive the governing equations for the director angle $\psi$. The relationship between the governing equations derived by

this method and Leslie–Ericksen theory will be briefly discussed in Section 4.3

## 4.1 The dynamic energy balance

In order to formulate a dynamic theory, the energy equation (2.18) must be appended with the effect of inertia and dissipation. If the liquid crystal is assumed to consist of rigid rods, the kinetic energy density associated with rotational moment of inertia is given by

$$\mathcal{K} = \frac{1}{2}\sigma|\boldsymbol{n}_t|^2 = \frac{1}{2}\sigma\psi_t^2, \tag{4.2}$$

where $\sigma > 0$ is an inertial material constant. As an example, for the nematic liquid crystal MBAA, experiments indicate $\sigma \sim 10^{-13}\,\mathrm{kg\,m^{-1}}$ [21].

Liquid crystals are in general viscous, resulting in a loss of macroscopic energy (entropy production) due to shear stresses, similar to what is seen in isotropic fluids. However, in the case of liquid crystals the viscous stresses will in general depend on the relative orientation of the director field. In addition, as discussed by e.g. de Gennes [13], there is entropy production as a result of the rotation of the optical axis of the molecules relative to the surrounding fluid. Under the present assumption of a stationary flow field, only the latter effect comes into play. As explained by e.g. Stewart [56], this dissipation per volume is proportional with the square of the rate of change of the director, which under the assumption (4.1) is given by

$$\mathcal{D} = \frac{1}{2}\kappa|\boldsymbol{n}_t|^2 = \frac{1}{2}\kappa\psi_t^2, \tag{4.3}$$

where $\kappa > 0$ is a viscosity coefficient. The material constant $\kappa$ can be experimentally determined, and has been measured to be $\kappa = 0.1093\,\mathrm{Pa\,s}$ at $T = 25\,^\circ\mathrm{C}$ for MBAA and $\kappa = 0.0777\,\mathrm{Pa\,s}$ at $T = 26\,^\circ\mathrm{C}$ for 5CB [36].

The full energy balance for the director field can now be assembled. By including the contributions from the elasticity, electric fields, magnetic fields and boundary anchoring discussed in Chapter 2, we assert the energy balance equation

$$\frac{\mathrm{d}}{\mathrm{d}t}\left(\int_\Omega \left(\frac{1}{2}\sigma|\boldsymbol{n}_t|^2 + \mathcal{W}_{\mathrm{OF}} + \mathcal{W}_{\mathrm{E}} + \mathcal{W}_{\mathrm{M}}\right)\mathrm{d}\boldsymbol{x} + \int_{\partial\Omega}\mathcal{W}_B\,\mathrm{d}S\right) = -\frac{1}{2}\kappa\int_\Omega |\boldsymbol{n}_t|^2\,\mathrm{d}\boldsymbol{x}. \tag{4.4}$$

For typical nematic liquid crystals, dissipative effects will dominate over inertial forces. It is for this reason the inertial energy is often ignored all together when modeling nematics [21, 57]. However, as was noted early by Leslie [39], the effect of molecular rotational inertia might influence the dynamics when the director is subject to large accelerations. Speaking in general terms, dissipation is a long-time effect while inertia is more important on smaller time scales. This suggests that the inclusion of inertia might be warranted for example in the modeling of liquid crystals under high-frequency mechanical oscillations [59] and liquid crystal acoustics [33]. Also, as discussed by Yun [60], the effect is also measurable when a liquid crystal is under the influence of a quickly oscillating electromagnetic field. In the present discussion we will keep both the effect of inertial and dissipation in the energy balance for completeness. Paper A will be devoted to an in-depth numerical analysis of the influence of these on the dynamics of the Fréedericksz transition.

## 4.2 Variational principles

Variational principles are a cornerstone of the classic static theory of nematic liquid crystals [58]. Similar techniques can be applied to obtain governing equations for the evolution of the director field, given the energy balance equation (4.4).

Hamilton's principle of classical mechanics describes the motion of a *conservative* system [24]. Let the system be described by $n$ generalized coordinates $q_1, \cdots, q_n$ with a Lagrangian

$$L = L(q_1, \cdots, q_n, q_{1,t}, \cdots, q_{n,t}, t)$$

depending explicitly only on the coordinates $q_i$, their time derivatives $q_{i,t}$ and time $t$. Hamilton's principle states that the evolution of the system between times $t_0$ and $t_1$ is given by the path in configuration space for which the time integral of the Lagrangian is stationary. Specifically, the mechanical system follows the path where

$$\delta \int_{t_0}^{t_1} L(q_1, \cdots, q_n, q_{1,t}, \cdots, q_{n,t}, t)\,\mathrm{d}t = 0, \tag{4.5}$$

where $\delta$ denotes the first variation.

**Example 1 (Variational wave equation)** *As an example we can consider the evolution of a fully elastic (conservative) nematic liquid crystal on*

*an infinite domain. Further, we disregard any coupling with electromagnetic fields. Here, the degrees of freedom are the components of the director field* $\boldsymbol{n}$ *and the Lagrangian is given by*

$$L = \int_{\mathbb{R}^3} \left( \frac{1}{2}\sigma |\boldsymbol{n}_t|^2 - \mathcal{W}_{OF}(\boldsymbol{n}, \nabla \boldsymbol{n}) \right) \mathrm{d}\boldsymbol{x}.$$

*Using variations of the director field in the form*

$$\boldsymbol{n}_\epsilon = \boldsymbol{n} + \epsilon \boldsymbol{u},$$

*where* $\boldsymbol{u}$ *decays at infinity, we obtain*

$$\begin{aligned}
\delta \int_{t_0}^{t_1} L \,\mathrm{d}t &= \frac{\partial}{\partial \epsilon}\Big|_{\epsilon=0} \int_{t_0}^{t_1} \int_{\mathbb{R}^3} \Bigg( \frac{1}{2}\sigma \left(\boldsymbol{n}_t + \epsilon \boldsymbol{u}_t\right) \cdot \left(\boldsymbol{n}_t + \epsilon \boldsymbol{u}_t\right) \\
&\qquad\qquad - \mathcal{W}_{OF}(\boldsymbol{n} + \epsilon \boldsymbol{u}, \nabla \boldsymbol{n} + \epsilon \nabla \boldsymbol{u}) \Bigg) \mathrm{d}\boldsymbol{x}\, \mathrm{d}t \\
&= \int_{t_0}^{t_1} \int_{\mathbb{R}^3} \left( \sigma \left(\boldsymbol{n}_t + \epsilon \boldsymbol{u}_t\right) \boldsymbol{u}_t - \frac{\partial \mathcal{W}_{OF}}{\partial \boldsymbol{n}} \boldsymbol{u} - \frac{\partial \mathcal{W}_{OF}}{\partial \nabla \boldsymbol{n}} \nabla \boldsymbol{u} \right) \mathrm{d}\boldsymbol{x}\, \mathrm{d}t \Big|_{\epsilon=0} \\
&= \int_{t_0}^{t_1} \int_{\mathbb{R}^3} \left( -\sigma \boldsymbol{n}_{tt} - \frac{\partial \mathcal{W}_{OF}}{\partial \boldsymbol{n}} + \nabla \cdot \frac{\partial \mathcal{W}_{OF}}{\partial \nabla \boldsymbol{n}} \right) \boldsymbol{u}\, \mathrm{d}\boldsymbol{x}\, \mathrm{d}t = 0.
\end{aligned} \tag{4.6}$$

*In the above, we used integration by parts together with the decaying director at infinity to obtain the last equality. If* (4.6) *is to hold for* any $\boldsymbol{u}$*, the variational wave equation*

$$\sigma \boldsymbol{n}_{tt} + \frac{\partial \mathcal{W}_{OF}}{\partial \boldsymbol{n}} - \nabla \cdot \frac{\partial \mathcal{W}_{OF}}{\partial \nabla \boldsymbol{n}} = 0 \tag{4.7}$$

*must be satisfied in the whole domain. The equation* (4.7) *in the bend-splay geometry will be discussed in the 1D and 2D case in Sections 4.4 and 4.5, respectively.*

Hamilton's principle as described above gives the equations of motion for a conservative system. In order to obtain evolution equations satisfying the energy law (4.4) for $\kappa > 0$, a different approach has to be adopted. The question of how to describe nonequilibrium dynamics of mechanical systems is indeed an old one, and remains to some extent an active field of research to this date. Here we consider a *dissipative* variational formulation based on the principle of maximum entropy production. This approach can be

traced back to Onsager's early work on nonequilibrium dynamics [49, 50], and comes in many different forms depending on the particular field in question. Martyushev and Seleznev [43] gives an excellent review of the use of this technique in the physical sciences. Maximov [44] shows how the Lagrangian can be modified to account for the dissipation, allowing for a similar formalism as in the conservative case. A common approach, which we will use in this work, involves adding a "dissipative" force to the balance equation given by the least action principle. This method has been used by Hyon et al. [32] to described the dissipative dynamics of complex fluids, and can be broken down into three steps:

1. Hamilton's principle (4.5) is used to calculate the sum $f_c$ of the *conservative* forces

2. The "dissipative" forces $f_d$ are given by the variation

$$\delta \int_{t_0}^{t_1} \int_{\mathbb{R}^3} \mathcal{D} \, \mathrm{d}\boldsymbol{x} \, \mathrm{d}t = 0$$

3. The evolution equation given by the force balance

$$f_c = f_d$$

   will then satisfy the dissipative energy law.

## 4.3 Relationship to the classic Leslie–Ericksen theory

It is instructive to look at the relationship between the comprehensive Leslie–Ericksen theory and the simplified mechanical principles used in this text. Indeed, for consistency, the latter should follow from the former. The classic Leslie–Ericksen equations for the dynamic incompressible flow a nematic liquid crystals with constant density $\rho$ are [56]:

**Conservation of mass**

$$\nabla \cdot \boldsymbol{u} = 0 \tag{4.8}$$

**Conservation of linear momentum**

$$\rho \dot{\boldsymbol{u}} + \sigma \ddot{\boldsymbol{n}} \cdot \nabla \boldsymbol{n} = \rho \boldsymbol{F} + \boldsymbol{G} \cdot \nabla \boldsymbol{n} + \nabla \cdot \boldsymbol{\tau} \tag{4.9}$$

**Conservation of angular momentum**

$$\sigma\ddot{\boldsymbol{n}} + \lambda\boldsymbol{n} = \boldsymbol{G} + \tilde{\boldsymbol{g}} - \frac{\partial \mathcal{W}_{\mathrm{OF}}}{\partial \boldsymbol{n}} + \nabla \cdot \frac{\partial \mathcal{W}_{\mathrm{OF}}}{\partial \nabla \boldsymbol{n}} \tag{4.10}$$

Here a dot denotes the usual material derivative

$$\dot{\boldsymbol{w}} := \boldsymbol{w}_t + \boldsymbol{u} \cdot \nabla \boldsymbol{w}.$$

In the above, we have the following variables and parameters:

- $\boldsymbol{u} \in \mathbb{R}^3$: Velocity field of the liquid crystal flow
- $\boldsymbol{F} \in \mathbb{R}^3$: Vector of external body forces
- $\boldsymbol{G} \in \mathbb{R}^3$: Vector of generalized body forces
- $\lambda$: Lagrange multiplier corresponding to the constraint $|\boldsymbol{n}| = 1$
- $\boldsymbol{\tau} = -p\boldsymbol{I} - \rho\frac{\partial \mathcal{W}_{\mathrm{OF}}}{\partial \nabla \boldsymbol{n}}\nabla \boldsymbol{n} + \tilde{\boldsymbol{\tau}}$: Stress tensor
- $p$: Pressure of the liquid
- $\tilde{\boldsymbol{\tau}} \in \mathbb{R}^3 \times \mathbb{R}^3$: Viscous stress tensor

In order to define the viscous stress tensor $\tilde{\boldsymbol{t}}$ and the vector $\tilde{\boldsymbol{g}}$, we introduce the rate of strain tensor and the vorticity tensor, given by

$$\boldsymbol{A} = \frac{1}{2}\left(\nabla \boldsymbol{u} + (\nabla \boldsymbol{u})^{\intercal}\right) \qquad \text{and} \qquad \Omega = \frac{1}{2}\left(\nabla \boldsymbol{u} - (\nabla \boldsymbol{u})^{\intercal}\right),$$

respectively. Using these we define the *co-rotational time flux*

$$\boldsymbol{N} = \dot{\boldsymbol{n}} - \Omega \boldsymbol{n},$$

observing that the constraint $\boldsymbol{n} \cdot \boldsymbol{n} = 0$ implies $\boldsymbol{n} \cdot \boldsymbol{N} = 0$. In terms of these quantities, the viscous stress tensor is given by [56, Eq. (4.121)]

$$\begin{aligned}\tilde{\boldsymbol{\tau}} = \mu_1 \left(\boldsymbol{n}^{\intercal}\boldsymbol{A}\boldsymbol{n}\right) \boldsymbol{n} \otimes \boldsymbol{n} + \mu_2 \boldsymbol{N} \otimes \boldsymbol{n} + \mu_3 \boldsymbol{n} \otimes \boldsymbol{N} + \mu_4 \boldsymbol{A} \\ + \mu_5 \boldsymbol{A}\,\boldsymbol{n} \otimes \boldsymbol{n} + \mu_6\, \boldsymbol{n} \otimes \boldsymbol{A}\,\boldsymbol{n},\end{aligned} \tag{4.11}$$

where $\mu_i$, $i \in 1, \cdots, 6$, are viscosity constants. There are several constraints on the constants $\mu_i$, including

$$\gamma_1 := \mu_3 - \mu_2 \geq 0$$

due to the positivity of the dissipation function [56, Eqs. (4.91)–(4.95)]. In addition Parodi [52] derived

$$\gamma_2 := \mu_3 + \mu_2 = \mu_6 - \mu_5$$

from Onsager's reciprocity relations. The vector $\tilde{\boldsymbol{g}}$ is given by [56, Eq. (4.122)]

$$\tilde{\boldsymbol{g}} = -\gamma_1 \boldsymbol{N} - \gamma_2 \boldsymbol{A}\boldsymbol{n}.$$

In order to verify the consistency with Hamilton's principle, we now make the same assumptions as in Example 1 on page 35. Specifically we disregard flow ($\boldsymbol{u} = 0$), assume no external forces acting on the liquid crystal ($\boldsymbol{F} = 0$, $\boldsymbol{G} = 0$), and assume vanishing viscosity

$$\mu_i = 0, \qquad i = 1, \cdots, 6.$$

The mass conservation (4.8) is then trivially satisfied, while the equations for linear and angular momentum become

$$\sigma \boldsymbol{n}_{tt} \cdot \nabla \boldsymbol{n} + \nabla \cdot \left( p\boldsymbol{I} + \rho \frac{\partial \mathcal{W}_{\mathrm{OF}}}{\partial \nabla \boldsymbol{n}} \nabla \boldsymbol{n} \right) = 0 \tag{4.12}$$

and

$$\sigma \boldsymbol{n}_{tt} + \lambda \boldsymbol{n} + \frac{\partial \mathcal{W}_{\mathrm{OF}}}{\partial \boldsymbol{n}} - \nabla \cdot \frac{\partial \mathcal{W}_{\mathrm{OF}}}{\partial \nabla \boldsymbol{n}} = 0, \tag{4.13}$$

respectively. Note that when disregarding flow, material derivatives turn into regular partial derivatives. We see that apart from the term with the Lagrange multiplier, which can usually be eliminated by adding or subtracting the components of the equation, the simplified equation (4.13) is precisely the variational wave equation (4.7) obtained through Hamilton's principle.

If we keep the assumption above, but also allow for nonzero viscosity, the vector $\tilde{\boldsymbol{g}}$ comes into play. The equation for the balance of angular momentum (4.10) is in this case given by

$$\sigma \boldsymbol{n}_{tt} + \lambda \boldsymbol{n} + \frac{\partial \mathcal{W}_{\mathrm{OF}}}{\partial \boldsymbol{n}} - \nabla \cdot \frac{\partial \mathcal{W}_{\mathrm{OF}}}{\partial \nabla \boldsymbol{n}} = -\gamma_1 \boldsymbol{n}_t. \tag{4.14}$$

Again, a short calculation reveals that the extra term is precisely what is given when applying the dissipative variational principle described in Section 4.2. If $\kappa = \gamma_1$ in (4.3) then

$$\frac{\partial}{\partial \epsilon}\Big|_{\epsilon=0} \int_{t_0}^{t_1} \int_{\mathbb{R}^3} \frac{1}{2} \gamma_1 |\boldsymbol{n}_t + \epsilon \boldsymbol{u}_t|^2 \,\mathrm{d}\boldsymbol{x}\,\mathrm{d}t = \int_{t_0}^{t_1} \int_{\mathbb{R}^3} \gamma_1 \boldsymbol{n}_t \boldsymbol{u}_t \,\mathrm{d}\boldsymbol{x}\,\mathrm{d}t, \tag{4.15}$$

which gives the "dissipative force"

$$f_d = \gamma_1 \boldsymbol{n}_t.$$

## 4.4 The 1D variational wave equation

A simplified model for the elastic dynamics in the bend-spay geometry can be derived by making the following assumptions:

1. The director angle only depends on $x$ and $t$:

$$\psi(\boldsymbol{r}, t) = \psi(x, t)$$

2. There is no energy dissipation:

$$\kappa = 0$$

3. The domain is infinite:

$$\Omega = \mathbb{R}$$

In this case the action is

$$S[\psi] = \frac{1}{2} \int_{t_0}^{t_1} \int_{\mathbb{R}} \left( \sigma \psi_t^2 - c^2(\psi) \psi_x^2 \right) \mathrm{d}x \, \mathrm{d}t, \tag{4.16}$$

where again $c(\psi)$ is given by (3.3) on page 24. Looking for stationary solutions w.r.t. the action, using compactly supported $\phi$, we obtain

$$\begin{aligned} \frac{\partial}{\partial \epsilon}\Big|_{\epsilon=0} S[\psi + \epsilon\phi] &= \int_{t_0}^{t_1} \int_{\mathbb{R}} \Big( \sigma(\psi_t + \epsilon\phi_t)\phi_t - c^2(\psi + \epsilon\phi)(\psi_x + \epsilon\phi_x)\phi_x \\ &\qquad - c(\psi + \epsilon\phi)c'(\psi + \epsilon\phi)(\psi_x + \epsilon\phi_x)\phi \Big) \mathrm{d}x \, \mathrm{d}t \Big|_{\epsilon=0} \\ &= \int_{t_0}^{t_1} \int_{\mathbb{R}} \Big( \sigma\psi_t\phi_t - c^2(\psi)\psi_x\phi_x - c(\psi)c'(\psi)\psi_x\phi \Big) \mathrm{d}x \, \mathrm{d}t \\ &= \int_{t_0}^{t_1} \int_{\mathbb{R}} \Big( -\sigma\psi_{tt} + c^2(\psi)\psi_{xx} + c(\psi)c'(\psi)\psi_x^2 \Big) \phi \, \mathrm{d}x \, \mathrm{d}t = 0. \end{aligned} \tag{4.17}$$

If (4.17) is to hold for all $\phi$ then the director field must satisfy the variational wave equation

$$\sigma\psi_{tt} - c(\psi) \left( c(\psi)\psi_x \right)_x = 0. \tag{4.18}$$

By multiplying (4.18) with $\psi_t$ and integrating in space, we can easily verify that sufficiently smooth solutions of (4.18) satisfy

$$\frac{\mathrm{d}}{\mathrm{d}t} \left( \int_{\mathbb{R}} (\sigma\psi_t^2 + c^2(\psi)\psi_x^2) \mathrm{d}x \right) = 0. \tag{4.19}$$

Since it was first introduced by Hunter and Saxton [54, 30], the Cauchy problem (obtained by setting $\sigma = 1$ in (4.18))

$$\psi_{tt} - c(\psi)\left(c(\psi)\psi_x\right)_x = 0, \qquad (x,t) \in \mathbb{R} \times [0,T), \tag{4.20a}$$

$$\psi(x,0) = \psi_0(x), \qquad x \in \mathbb{R}, \tag{4.20b}$$

$$\psi_t(x,0) = \psi_1(x), \qquad x \in \mathbb{R}, \tag{4.20c}$$

has been the subject of much study, due to its interesting mathematical properties. It has been long established that solutions of (4.20) might exhibit blow up in finite time [23], which means one has to consider solutions in the weak sense:

**Definition 1** *Set* $\Pi_T = \mathbb{R} \times (0,T)$. *A function*

$$\psi(t,x) \in L^\infty\left([0,T]; W^{1,p}(\mathbb{R})\right) \cap C(\Pi_T), \psi_t \in L^\infty\left([0,T]; L^p(\mathbb{R})\right),$$

*for all* $p \in [1, 3+q]$, *where* $q$ *is some positive constant, is a weak solution of the initial value problem* (4.20) *if it satisfies:*

1. *For all test functions* $\varphi \in \mathcal{D}(\mathbb{R} \times [0,T))$

$$\int\int_{\Pi_T} \left(\psi_t\varphi_t - c^2(\psi)\psi_x\varphi_x - c(\psi)c'(\psi)(\psi_x)^2\varphi\right)\, dx\, dt = 0.$$

2. $\psi(\cdot,t) \to \psi_0$ *in* $C\left([0,T]; L^2(\mathbb{R})\right)$ *as* $t \to 0^+$.

3. $\psi_t(\cdot,t) \to \psi_1$ *as a distribution in* $\Pi_T$ *when* $t \to 0^+$.

A key property of the variational wave equation (4.20) is the existence of different classes of weak solutions. In particular, one can show the existence of both *conservative* and *dissipative* weak solutions with respect to the energy

$$\mathcal{E}(t) = \int_{\mathbb{R}} \left(\psi_t^2 + c^2(\psi)\psi_x^2\right) \mathrm{d}x. \tag{4.21}$$

A conservative solution means in this case a solution for which the energy (4.21) stays constant for almost every time $t \in \mathbb{R}^+$. This ambiguity of weak solutions is similar to the situation for the related Hunter–Saxton equation [31] and Camassa–Holm equation [5, 6], and it makes the question of well-posedness of the initial value problem particularly delicate.

There is a significant volume of research in the literature on weak solutions to the Cauchy problem (4.20). Herein, the papers by Zhang and Zheng [61, 62, 63, 64], Bressan and Zheng [7] and Holden and Raynaud [29] should

all be mentioned. In [64], the authors show existence of a global weak solution using the method of Young measures for initial data $\psi_0 \in H^1(\mathbb{R})$ and $\psi_1 \in L^2(\mathbb{R})$. The function $c(\psi)$ is assumed to be smooth, bounded, positive with derivative that is nonnegative and strictly positive on the initial data $\psi_0$. This means that the analysis in [61, 62, 63, 64] does not directly apply to the case where $c(\psi)$ is given by (3.3) on page 24.

A different approach was taken by Bressan and Zheng [7]. Here, they rewrote the equation a set of variables for which the singularities disappeared. They show that for $\psi_0$ absolutely continuous with $(\psi_0)_x, \psi_1 \in L^2(\mathbb{R})$, the Cauchy problem (4.20) allows a global weak solution with the following properties: the solution $\psi$ is locally Lipschitz continuous and the map $t \to \psi(t, \cdot)$ is continuously differentiable with values in $L^p_{\text{loc}}(\mathbb{R})$ for $1 \leq p < 2$.

Holden and Raynaud [29] prove the existence of a global semigroup for conservative solutions of (4.20), allowing for concentration of energy density on sets of zero measure. Furthermore they also allow for initial data $\psi_0, \psi_1$ that contain measures. The proof involves constructing the solution by introducing new variables related to the characteristics, leading to a characterization of singularities in the energy density. They also prove that energy can only focus on a set of times of zero measure or at points where $c'(\psi)$ vanishes.

The uniqueness of weak solutions within the two different classes of solutions has also proved challenging. In their recent paper, Bressan et al. [4] were able to prove uniqueness of *conservative* solutions for a general set of initial data $\psi_0 \in H^1(\mathbb{R})$ and $\psi_1 \in L^2(\mathbb{R})$. The uniqueness of dissipative weak solutions to (4.20) remains an open problem.

It is common to study (4.20) by rewriting it as a system of first-order equations. By introducing the Riemann invariants

$$R = \psi_t + c(\psi)\psi_x \qquad \text{and} \qquad S = \psi_t - c(\psi)\psi_x,$$

we obtain

$$R_t - c(\psi)R_x = \frac{c'(\psi)}{4c(\psi)}\left(R^2 - S^2\right), \tag{4.22a}$$

$$S_t + c(\psi)S_x = -\frac{c'(\psi)}{4c(\psi)}\left(R^2 - S^2\right). \tag{4.22b}$$

The equations (4.22) are similar to a system of conservation laws, but with nonlinear source terms. Where the singularities of conservation laws (shocks) comes from the crossing of characteristics, the blow-up mechanism in (4.22) can be traced to its source terms. As discussed in detail

by Glassey [23], one can have initial data for which the quadratic term on the right hand side of (4.22a) causes $R$ to blow up before $c'(\psi)$ changes sign, as long as $S$ remains small. The same argument can be made when interchanging the roles of $R$ and $S$.

The system (4.22) is not a conservation law, and it can not be cast in a conservative form. However, it can be written as

$$R_t - (c(\psi)R)_x = -\frac{c_x(\psi)}{2}\left(R - S\right), \tag{4.23a}$$

$$S_t + (c(\psi)S)_x = -\frac{c_x(\psi)}{2}\left(R - S\right), \tag{4.23b}$$

with a left-hand side like that of a conservation law. It is straightforward to show that the a priori energy principle from which the variational wave equation (4.20) was derived is inherited by the systems (4.22) and (4.23). By multiplying (4.23a) by $R$ and (4.23b) by $S$ and adding them together we obtain the conservation law

$$\left(\frac{1}{2}\left(R^2 + S^2\right)\right)_t - \left(\frac{1}{2}c(\psi)\left(R^2 - S^2\right)\right)_x = 0. \tag{4.24}$$

If both functions $R$ and $S$ decay at infinity, the equation (4.24) can be integrated in space to give

$$\frac{\mathrm{d}}{\mathrm{d}t}\left(\frac{1}{2}\int_{\mathbb{R}}\left(R^2 + S^2\right)\mathrm{d}x\right) = 0. \tag{4.25}$$

The numerical study of the initial-value problem (4.20) has so far not received much attention. Glassey et al. [23] presented some numerical simulations using a simple dissipative scheme in order to emphasize some aspects of their analysis. A convergent dissipative finite difference scheme was developed by Holden et al. [28]. Also, in their recent work, Holden and Raynaud [29] derived a numerical scheme giving a *conservative* solution. This scheme does however not involve time marching, and it requires the solution to be calculated in all of space-time.

## 4.5 The 2D variational wave equation

We can derive a model for the elastic dynamics in the bend-splay geometry in two spatial dimensions in a similar way as in Section 4.4. Spesifically, the following assumptions are made:

1. The director angle only depends on $x$, $y$ and $t$:

$$\psi(\boldsymbol{r}, t) = \psi(x, y, t)$$

2. There is no energy dissipation:

$$\kappa = 0$$

3. The domain is infinite:

$$\Omega = \mathbb{R}$$

Under the assumptions above, the Oseen–Frank energy density (2.3) takes the form

$$\mathcal{W}(\psi, \psi_x, \psi_y) = \frac{1}{2}c^2(\psi)\psi_x^2 + \frac{1}{2}b^2(\psi)\psi_y^2 + a(\psi)\psi_x\psi_y,$$

which gives the action

$$S[\psi] = \frac{1}{2}\int_{t_0}^{t_1}\int_{\mathbb{R}^2}\left(\sigma\psi_{tt}^2 - c^2(\psi)\psi_x^2 - b^2(\psi)\psi_y^2 - 2a(\psi)\psi_x\psi_y\right)\mathrm{d}x\,\mathrm{d}y\,\mathrm{d}t.$$

In the above, we have introduced the shorthands

$$\begin{aligned} a(\psi) &= \frac{\alpha_1 - \alpha_2}{2}\sin(2\psi), \\ b(\psi) &= \sqrt{\alpha_1\sin^2(\psi) + \alpha_2\cos^2(\psi)}, \end{aligned}$$

in addition to (3.3) on page 24.

As before, the evolution equation of the conservative system is obtained by finding a stationary solution w.r.t. the action. For the first variation we

obtain

$$\begin{aligned}\frac{\partial}{\partial\epsilon}\Big|_{\epsilon=0} S[\psi+\epsilon\phi] = \int_{t_0}^{t_1}\int_{\mathbb{R}^2}\Big(&\sigma(\psi_t+\epsilon\phi_t)\phi_t - c^2(\psi+\epsilon\phi)(\psi_x+\epsilon\phi_x)\phi_x\\ &- c(\psi+\epsilon\phi)c'(\psi+\epsilon\phi)(\psi_x+\epsilon\phi_x)^2\phi\\ &- b^2(\psi+\epsilon\phi)(\psi_y+\epsilon\phi_y)\phi_y\\ &- b(\psi+\epsilon\phi)b'(\psi+\epsilon\phi)(\psi_y+\epsilon\phi_y)^2\phi\\ &- a'(\psi+\epsilon\phi)\psi_x\psi_y\phi - a(\psi+\epsilon\phi)(\psi_y+\epsilon\phi_y)\phi_x\\ &- a(\psi+\epsilon\phi)(\psi_x+\epsilon\phi_x)\phi_y\Big)\mathrm{d}x\,\mathrm{d}y\,\mathrm{d}t\Big|_{\epsilon=0}\\ = \int_{t_0}^{t_1}\int_{\mathbb{R}^2}\Big(&\sigma\psi_t\phi_t\phi_t - c^2(\psi)\psi_x\phi_x - c(\psi)c'(\psi)\psi_x^2\phi\\ &- b^2(\psi)\psi_y\phi_y - b(\psi)b'(\psi)\psi_y^2\phi\\ &- a'(\psi)\psi_x\psi_y\phi - a(\psi)\psi_y\phi_x\\ &- a(\psi)\psi_x\phi_y\Big)\mathrm{d}x\,\mathrm{d}y\,\mathrm{d}t\Big|_{\epsilon=0} = 0.\end{aligned}$$

By assuming compactly supported test functions $\phi$ we can use integration by parts to arrive at

$$\begin{aligned}\int_{t_0}^{t_1}\int_{\mathbb{R}^2}\Big(&-\sigma\psi_{tt} + c(\psi)\left(c(\psi)\psi_x\right)_x + b(\psi)\left(b(\psi)\psi_y\right)_y\\ &+ a'(\psi)\psi_x\psi_y + 2a(\psi)\psi_{xy}\Big)\phi\,\mathrm{d}x\,\mathrm{d}y\,\mathrm{d}t = 0.\end{aligned} \tag{4.26}$$

If (4.26) is to hold for any $\phi$, the director angle must satisfy the equation

$$\sigma\psi_{tt} - c(\psi)\left(c(\psi)\psi_x\right)_x - b(\psi)\left(b(\psi)\psi_y\right)_y - a'(\psi)\psi_x\psi_y - 2a(\psi)\psi_{xy} = 0 \tag{4.27}$$

for $(x,y)\in\mathbb{R}^2$ and $t\in\mathbb{R}^+$.

The Cauchy problem (obtained from the scaling $\sigma = 1$ in (4.27))

$$\psi_{tt} - c(\psi)\left(c(\psi)\psi_x\right)_x - b(\psi)\left(b(\psi)\psi_y\right)_y - a'(\psi)\psi_x\psi_y - 2a(\psi)\psi_{xy} = 0,$$

$$(x,y,t)\in\mathbb{R}^2\times[0,T), \tag{4.28a}$$

$$\psi(x,y,0) = \psi_0(x,y), \qquad (x,y)\in\mathbb{R}^2, \tag{4.28b}$$

$$\psi_t(x,y,0) = \psi_1(x,y), \qquad (x,y)\in\mathbb{R}^2, \tag{4.28c}$$

is far less studied than its one-dimensional counterpart (4.20). However, it is clear that there is a close relationship between the models. Indeed, (4.20) can be easily recovered from (4.28) for functions $\psi(x,y,t) = \psi(x,t)$.

By introducing the matrix

$$T(\psi) = \begin{pmatrix} \sqrt{\alpha_1}\cos(\psi) & \sqrt{\alpha_1}\sin(\psi) \\ -\sqrt{\alpha_2}\sin(\psi) & \sqrt{\alpha_2}\cos(\psi) \end{pmatrix},$$

we can write the equation (4.28a) in the more aesthetic form

$$\psi_{tt} - (T(\psi)\nabla)\cdot(T(\psi)\nabla\psi) = 0. \tag{4.29}$$

It is tempting to attempt to rewrite (4.28) in terms of Riemann invariants, similarly as was done for (4.20). However, introducing the variables

$$\begin{aligned} P &= \psi_t + c(\psi)\psi_x, \qquad & Q &= \psi_t - c(\psi)\psi_x, \\ R &= \psi_t + b(\psi)\psi_t, \qquad & S &= \psi_t - b(\psi)\psi_y, \end{aligned}$$

will *not* give a system of linearly independent equations. An alternative formulation can be obtained by introducing the quantities

$$\begin{aligned} p &= \psi_t, \\ v &= \cos(\psi)\psi_x + \sin(\psi)\psi_y, \\ w &= \sin(\psi)\psi_x - \cos(\psi)\psi_y. \end{aligned}$$

Then, for smooth solutions, we see that

$$\begin{aligned} v_t &= \cos(\psi)\psi_{xt} - \sin(\psi)\psi_t\psi_x + \sin(\psi)\psi_{yt} + \cos(\psi)\psi_t\psi_y \\ &= (\cos(\psi)\psi_t)_x - \psi_t(\cos(\psi))_x + (\sin(\psi)\psi_t)_y - \psi_t(\sin(\psi))_y \\ &\qquad - \psi_t\big(\sin(\psi)\psi_x - \cos(\psi)\psi_y\big), \end{aligned}$$

and

$$\begin{aligned} w_t &= \sin(\psi)\psi_{xt} + \cos(\psi)\psi_t\psi_x - \cos(\psi)\psi_{yt} + \sin(\psi)\psi_t\psi_y \\ &= (\sin(\psi)\psi_t)_x - \psi_t(\sin(\psi))_x - (\cos(\psi)\psi_t)_y + \psi_t(\cos(\psi))_y \\ &\qquad + \psi_t\left(\cos(\psi)\psi_x + \sin(\psi)\psi_y\right). \end{aligned}$$

Moreover, a straightforward calculation using equation (4.28a) reveals that

$$\begin{aligned} p_t - (\alpha_1 - \alpha_2)\big(&\cos(\psi)\sin(\psi)\psi_x^2 - \cos^2(\psi)\psi_x\psi_y + \sin^2(\psi)\psi_x\psi_y \\ &- \cos(\psi)\sin(\psi)\psi_y^2\big) \\ = {}& \alpha_1\left(\cos(\psi)(\cos(\psi)\psi_x + \sin(\psi)\psi_y)\right)_x \\ &+ \alpha_1\left(\sin(\psi)(\cos(\psi)\psi_x + \sin(\psi)\psi_y)\right)_y \\ &+ \alpha_2\left(\sin(\psi)(\sin(\psi)\psi_x - \cos(\psi)\psi_y)\right)_x \\ &- \alpha_2\left(\cos(\psi)(\sin(\psi)\psi_x - \cos(\psi)\psi_y)\right)_y. \end{aligned}$$

Hence, for smooth solutions, equation (4.28a) is equivalent to the system

$$\begin{aligned} p_t - \alpha_1(f(\psi)v)_x - \alpha_1(g(\psi)v)_y - \alpha_2(g(\psi)w)_x + \alpha_2(f(\psi)w)_y \\ - \alpha_1 vw + \alpha_2 vw = 0, \end{aligned} \tag{4.30a}$$

$$v_t - (f(\psi)p)_x + pf(\psi)_x - (g(\psi)p)_y + pg(\psi)_y + pw = 0, \tag{4.30b}$$

$$w_t - (g(\psi)p)_x + pg(\psi)_x + (f(\psi)p)_y - pf(\psi)_y - pv = 0, \tag{4.30c}$$

$$\psi_t = p, \tag{4.30d}$$

where $f(\psi) = \cos(\psi)$, and $g(\psi) = \sin(\psi)$.

Similarly as for the 1D variational wave equation, the energy principle for which the model was derived is inherited by the system (4.30). Indeed, a straightforward calculation reveals that any smooth solution of (4.30) satisfies the conservation law

$$\begin{aligned} \left(p^2 + \alpha_1\, v^2 + \alpha_2\, w^2\right)_t + 2\left(\alpha_1\, p\, f(u)\, v + \alpha_2\, p\, g(u)\, w\right)_x \\ + 2\left(\alpha_1\, p\, g(u)\, v - \alpha_2\, p\, f(u)\, w\right)_y = 0. \end{aligned} \tag{4.31}$$

Consequently, if the functions $p$, $v$ and $w$ all decay at infinity, we can integrate (4.31) in space to obtain

$$\frac{\mathrm{d}}{\mathrm{d}t}\left(\int_{\mathbb{R}^2} \left(p^2 + \alpha_1\, v^2 + \alpha_2\, w^2\right)\, \mathrm{d}x\, \mathrm{d}y\right) = 0.$$

## 4.6 The Fréedericksz cell with strong anchoring

In the derivation of the models considered in Sections 4.4 and 4.5 an infinite domain was assumed. Arguably, the evolution of director fields on a finite domain while under the influence of electromagnetic fields is of great practical interest. As discussed in Chapter 3, the Fréedericksz transition is closely related to the fundamental mechanism behind switch-on and switch-of in a pixel of a liquid crystal display.

Using the same principles as in the preceding sections, we venture to derive a simple model for the director on a finite domain under the influence of an electric field. To that end, we make the following assumptions:

1. The director angle only depends on $x$ and $t$:

$$\psi(\boldsymbol{r}, t) = \psi(x, t)$$

2. The liquid crystal is restricted to a finite domain:

$$\Omega = [0, L]$$

3. An applied voltage difference $V_0$ leads to an electric field

$$\boldsymbol{E} = E(x,t)\hat{\boldsymbol{x}}$$

which is assumed to only have a component in the $x$-direction.

4. The director is assumed to be strongly anchored at the boundaries:

$$\psi(0,t) = \psi(L,t) = \frac{\pi}{2}$$

We include both the effects of inertia and dissipation, hence the evolution equation is obtained by applying the dissipative variational principle as described in Section 4.2.

First, we consider the balance of conservative forces. It is convenient to denote the electric field as the gradient of a scalar electric potential, i.e.

$$E = -U_x.$$

Due to Gauss' law, the potential must satisfy

$$\left(d(\psi)U_x\right)_x = 0, \tag{4.32}$$

where we have introduced the shorthand

$$d(\psi) = \varepsilon_0\left(\varepsilon_\perp + \varepsilon_a\cos^2(\psi)\right).$$

Using the electric free energy density (2.10) on page 16, the action is in this case

$$S[\psi] = \frac{1}{2}\int_{t_0}^{t_1}\int_0^L \left(\sigma\psi_t^2 - c^2(\psi)\psi_x^2 - \frac{1}{2}d(\psi)U_x^2\right)\mathrm{d}x\,\mathrm{d}t. \tag{4.33}$$

By considering variations $\phi$ that are zero at the boundary (due to strong

anchoring) we obtain

$$\begin{aligned}\frac{\partial}{\partial\epsilon}\Big|_{\epsilon=0} S[\psi+\epsilon\phi] &= \int_{t_0}^{t_1}\int_0^L \Big(\sigma(\psi_t+\epsilon\phi_t)\phi_t - c^2(\psi+\epsilon\phi)(\psi_x+\epsilon\phi_x)\phi_x \\ &\qquad - c(\psi+\epsilon\phi)c'(\psi+\epsilon\phi)(\psi_x+\epsilon\phi_x)\phi \\ &\qquad\qquad + \frac{1}{2}d'(\psi+\epsilon\phi)U_x^2\phi\Big)\,\mathrm{d}x\,\mathrm{d}t\Big|_{\epsilon=0} \\ &= \int_{t_0}^{t_1}\int_0^L \Big(\sigma\psi_t\phi_t - c^2(\psi)\psi_x\phi_x - c(\psi)c'(\psi)\psi_x\phi \\ &\qquad\qquad + \frac{1}{2}d'(\psi)U_x^2\phi\Big)\,\mathrm{d}x\,\mathrm{d}t \\ &= \int_{t_0}^{t_1}\int_0^L \Big(-\sigma\psi_{tt} + c(\psi)(c(\psi)\psi_x)_x + \frac{1}{2}d'(\psi)U_x^2\Big)\phi\,\mathrm{d}x\,\mathrm{d}t \\ &= 0.\end{aligned} \tag{4.34}$$

If this is to hold for any strongly anchored $\phi$, the conservative force balance becomes

$$f_c = -\sigma\psi_{tt} + c(\psi)(c(\psi)\psi_x)_x + \frac{1}{2}d'(\psi)U_x. \tag{4.35}$$

The bulk energy dissipation is assumed to take the form

$$D = \frac{1}{2}\kappa\int_0^L \psi_t^2\,\mathrm{d}x. \tag{4.36}$$

The "dissipative" force can then be calculated similarly as in (4.15) on page 39 and is given by

$$f_d = \kappa\phi_t. \tag{4.37}$$

Following the principle of maximum dissipation we assemble conservative and dissipative forces to arrive at the evolution equation

$$\sigma\psi_{tt}+\kappa\psi_t - c(\psi)(c(\psi)\psi_x)_x - \frac{1}{2}d'(\psi)U_x = 0, \qquad (x,t)\in(0,L)\times\mathbb{R}^+. \tag{4.38}$$

Under the present simplifying assumptions, Gauss' law can be solved for the electric potential given a director configuration $\psi(x)$. By integrating the equation (4.32) we obtain

$$U(x)[\psi] = \int_0^x \frac{C}{d(\psi(\xi))}\,\mathrm{d}\xi + U(0)\,, \qquad C = \left(\int_0^L \frac{1}{d(\psi(\xi))}\,\mathrm{d}\xi\right)^{-1} U(L)\,, \tag{4.39}$$

for $x\in(0,L)$ with boundary conditions $U(0)=0$ and $U(L)=V_0$, where $V_0$ is the applied voltage.

The numerical solution of this model will be the topic of Paper A.

## 4.7 The Fréedericksz cell with weak anchoring

In Section 3.3 we discussed issues related to the existence of excited director states for the Fréedericksz transition with weak anchoring. This situation makes the study of the dynamics of the problem of particular interest. To this end, the basic 1D Fréedericksz cell discussed in Section 4.6 can be extended to take into account weak anchoring. Specifically, we make the following assumptions:

1. The director angle only depends on $x$ and $t$:

$$\psi(\boldsymbol{r}, t) = \psi(x, t)$$

2. The liquid crystal is restricted to a finite domain:

$$\Omega = [0, L]$$

3. An applied voltage difference $V_0$ leads to an electric field

$$\boldsymbol{E} = E(x, t)\hat{\boldsymbol{x}}$$

   which is assumed to only have a component in the $x$-direction.

4. The director is assumed to be weakly anchored with a surface energy in the form of (2.17) on page 20 with $\boldsymbol{n}_A = (0, 1, 0)$

The model assumptions are the same as for the system considered in Section 4.6 except for the treatment of the boundaries. Here, the strong anchoring condition $\psi(0) = \psi(L) = \pi/2$ is replaced by a boundary energy term [53] in the form

$$W_{\mathrm{B}} = \frac{1}{2} w \cos^2(\psi) \left( \Big|_{x=0} + \Big|_{x=L} \right). \tag{4.40}$$

From (4.40) one can easily deduce that for $w > 0$ the alignment $\psi = \pi/2$ will be energetically favored at the cell boundary. Conversely, for $w < 0$, the alignment $\psi = 0$ is favored.

The energy balance equation for the weak Fréedericksz cell then takes the form

$$\frac{\mathrm{d}}{\mathrm{d}t}\Big( \frac{1}{2} \int_0^L \left( \sigma \psi_t^2 + c^2(\psi)\psi_x^2 - d(\psi) U_x^2 \right) \mathrm{d}x + \frac{1}{2} w \cos^2(\psi) \left( |_{x=0} + |_{x=L} \right) \Big) = -\frac{1}{2} \kappa \int_0^L \psi_t^2 \, \mathrm{d}x. \tag{4.41}$$

As before we calculate the conservative dynamics via the first variation of the Lagrangian. In this case the variation $\phi$ is not zero at the boundaries, and we obtain

$$\begin{aligned}
\frac{\partial}{\partial\epsilon}\Big|_{\epsilon=0} S[\psi+\epsilon\phi] &= \int_{t_0}^{t_1}\int_0^L \Big(\sigma(\psi_t+\epsilon\phi_t)\phi_t - c^2(\psi+\epsilon\phi)(\psi_x+\epsilon\phi_x)\phi_x \\
&\quad - c(\psi+\epsilon\phi)c'(\psi+\epsilon\phi)(\psi_x+\epsilon\phi_x)\phi \\
&\quad + \frac{1}{2}d'(\psi+\epsilon\phi)U_x^2\phi\Big)\,\mathrm{d}x\,\mathrm{d}t\Big|_{\epsilon=0} \\
&\quad + \frac{1}{2}w\sin\left(2(\psi+\epsilon\phi)\right)\phi\left(|_{x=0}+|_{x=L}\right)\Big|_{\epsilon=0} \\
&= \int_{t_0}^{t_1}\int_0^L \Big(\sigma\psi_t\phi_t - c^2(\psi)\psi_x\phi_x - c(\psi)c'(\psi)\psi_x\phi \\
&\quad + \frac{1}{2}d'(\psi)U_x^2\phi\Big)\,\mathrm{d}x\,\mathrm{d}t \\
&\quad + \int_{t_0}^{t_1}\frac{1}{2}w\sin\left(2\psi\right)\phi\left(|_{x=0}+|_{x=L}\right)\mathrm{d}t \\
&= \int_{t_0}^{t_1}\int_0^L \Big(-\sigma\psi_{tt} + c(\psi)(c(\psi)\psi_x)_x + \frac{1}{2}d'(\psi)U_x^2\Big)\phi\,\mathrm{d}x\,\mathrm{d}t \\
&\quad + \int_{t_0}^{t_1} c^2(\psi)\psi_x\phi\left(|_{x=0}-|_{x=L}\right)\,\mathrm{d}t \\
&\quad + \int_{t_0}^{t_1}\frac{1}{2}w\sin\left(2\psi\right)\phi\left(|_{x=0}+|_{x=L}\right)\,\mathrm{d}t \\
&= 0.
\end{aligned} \tag{4.42}$$

If (4.42) is to hold for any $\phi$, the director field must (in the conservative case) satisfy the equations

$$\sigma\psi_{tt} - c(\psi)(c(\psi)\psi_x)_x - \frac{1}{2}d'(\psi)E^2 = 0, \qquad (x,t)\in(0,L)\times\mathbb{R}^+,$$

with boundary conditions

$$c^2(\psi)\psi_x + \frac{w}{2}\sin(2\psi) = 0, \quad x=0, \tag{4.43a}$$

$$c^2(\psi)\psi_x - \frac{w}{2}\sin(2\psi) = 0, \quad x=L. \tag{4.43b}$$

The dissipation is assumed to be in the same form as in Section 4.6, and can be included using the principle of maximum dissipation. This gives the full bulk equation

$$\sigma\psi_{tt}+\kappa\psi_t - c(\psi)(c(\psi)\psi_x)_x - \frac{1}{2}d'(\psi)E^2 = 0, \qquad (x,t)\in(0,L)\times\mathbb{R}^+. \tag{4.44}$$

The electric field can also be calculated in the same way as in the previous section. Summarizing, the weak Fréedericksz cell under the present assumptions is governed by the bulk equation (4.44) with boundary conditions (4.43), where the electric potential $U$ is given by (4.39).

# Bibliography


[1] J. M. Ball and A. Zarnescu. Orientability and energy minimization in liquid crystal models. *Archive for Rational Mechanics and Analysis*, 202(2):493–535, 2011.

[2] G. Bevilacqua and G. Napoli. Parity of the weak Fréedericksz transition. *The European Physics Journal E*, 35(12):1–5, 2012.

[3] L. M. Blinov. *Electro-optical and magneto-optical properties of liquid crystals.* John Wiley & Sons, Inc., New York, 1983.

[4] A. Bressan, G. Chen, and Q. Zhang. Unique conservative solutions to a variational wave equation. Preprint, 2015.

[5] A. Bressan and A. Constantin. Global conservative solutions of the Camassa–Holm equation. *Archive for Rational Mechanics and Analysis*, 183(2):215–239, 2007.

[6] A. Bressan and A. Constantin. Global dissipative solutions of the Camassa–Holm equation. *Analysis and Applications*, 5(01):1–27, 2007.

[7] A. Bressan and Y. Zheng. Conservative solutions to a nonlinear variational wave equation. *Communications in Mathematical Physics*, 266(2):471–497, 2006.

[8] G. P. Bryan-Brown, E. L. Wood, and I. C. Sage. Weak surface anchoring of liquid crystals. *Nature*, 399(6734):338–340, 1999.

[9] S. Chandrasekhar. *Liquid crystals.* Cambridge University Press, Cambridge, 2 edition, 1992.

[10] P. J. Collings. *Liquid crystals: nature's delicate phase of matter*. Princeton University Press, Princeton, 2002.

[11] P. J. Collings and M. Hird. *Introduction to liquid crystals: chemistry and physics*. Taylor & Francis, London, 1997.

[12] F. P. da Costa, M. Grinfeld, N. J. Mottram, and J. T. Pinto. Uniqueness in the Fréedericksz transition with weak anchoring. *Journal of Differential Equations*, 246(7):2590–2600, 2009.

[13] P. G. de Gennes and J. Prost. *The Physics of Liquld Crystals*. Clarendon Press, Oxford, 1993.

[14] W. H. de Jeu. *Physical properties of liquid crystalline materials*, volume 1. Gordon and Beach, New York, 1980.

[15] J. L. Ericksen. Conservation laws for liquid crystals. *Transactions of of The Society of Rheology*, 5(1):23–34, 1961.

[16] J. L. Ericksen. Hydrostatic theory of liquid crystals. *Archive for Rational Mechanics and Analysis*, 9(1):371–378, 1962.

[17] J. L. Ericksen. Liquid crystals with variable degree of orientation. *Archive for Rational Mechanics and Analysis*, 113:97–120, 1991.

[18] J. Fishers and A. G. Fredrickson. Interfacial effects on the viscosity of a nematic mesophase. *Molecular Crystals and Liquid Crystals*, 8(1):267–284, 1969.

[19] F. C. Frank. I. liquid crystals. on the theory of liquid crystals. *Discussions of the Faraday Society*, 25:19–28, 1958.

[20] V. Fredericksz and A. Repiewa. Theoretisches und experimentelles zur frage nach der natur der anisotropen flssigkeiten. *Zeitschrift fr Physik*, 42(7):532–.546, 1927.

[21] X. Gang, S. Chang-Qing, and L. Lei. Perturbed solutions in nematic liquid crystals under time-dependent shear. *Physical Review A*, 36(1):277–284, 1987.

[22] L. Gattermann and A. Ritschke. Über azoxyphenoläther. *Berichte der Deutschen Chemischen Gesellschaft*, 23:1738–1750, 1890.

[23] R. T. Glassey, J. K. Hunter, and Y. Zheng. Singularities of a variational wave equation. *Journal of Differential Equations*, 129(1):49–78, 1996.

[24] H. Goldstein. *Classical mechanics*. Pearson Education India, 1957.

[25] G. W. Gray. *Molecular structure and the properties of liquid crystals*. Academic press, London, 1962.

[26] I. Haller. Elastic constants of the nematic liquid crystalline phase of p-methoxybenzylidene-p-n-butylaniline (mbba). *Journal of Chemical Physics*, 57(4):1400–1405, 1972.

[27] R. Hardt, D. Kinderlehrer, and F.-H. Lin. Existence and partial regularity of static liquid crystal configurations. *Communications in Mathematical Physics*, 105(4):547–570, 1986.

[28] H. Holden, K. H. Karlsen, and N. H. Risebro. A convergent finite-difference method for a nonlinear variational wave equation. *IMA Journal of Numerical Analysis*, 29(3):539–572, 2009.

[29] H. Holden and X. Raynaud. Global semigroup of conservative solutions of the nonlinear variational wave equation. *Archive for Rational Mechanics and Analysis*, 201(3):871–964, 2011.

[30] J. K. Hunter and R. Saxton. Dynamics of director fields. *SIAM Journal on Applied Mathematics*, 51(6):1498–1521, 1991.

[31] J. K. Hunter and Y. Zheng. On a nonlinear hyperbolic variational equation: I. Global existence of weak solutions. *Archive for Rational Mechanics and Analysis*, 129(4):305–353, 1995.

[32] Y. Hyon, D. Y. Kwak, and C. Liu. Energetic variational approach in complex fluids: Maximum dissipation principle. *Discrete and Continuous Dynamical Systems*, 26:1291–1304, 2010.

[33] O. A. Kapustina. Liquid crystal acoustics: A modern view of the problem. *Crystallography Reports*, 49(4):680–692, 2004.

[34] H. Kelker. History of liquid crystals. *Molecular Crystals and Liquid Crystals*, 21(1-2):1–48, 1973.

[35] H. Kelker and B. Scheurle. A liquid-crystalline (nematic) phase with a particularly low solidification point. *Angewandte Chemie International Edition in English*, 8(11):884–885, 1969.

[36] H. Kneppe, F. Schneider, and N. K. Sharma. Rotational viscosity $\gamma_1$ of nematic liquid crystals. *Journal of Chemical Physics*, 77(6):3203–3208, 1982.

[37] T. A. Kumar, P. Sathyanarayana, V. S. S. Sastry, H. Takezoe, N. V. Madhusudana, and S. Dhara. Temperature-and electric-field-induced inverse Fréedericksz transition in a nematogen with weak surface anchoring. *Physical Review E*, 82(1):011701, 2010.

[38] F. M. Leslie. Some constitutive equations for liquid crystals. *Archive for Rational Mechanics and Analysis*, 28(4):265–283, 1968.

[39] F. M. Leslie. Theory of flow phenomena in liquid crystals. *Advances in Liquid Crystals*, 4:1–81, 1979.

[40] G. R. Luckhurst, D. A. Dunmur, and A. Fukuda. *Physical properties of liquid crystals: nematics*. IET, London, 2001.

[41] E. H. MacMillan. *A theory of anisotropic fluids*. PhD thesis, University of Minnesota, 1987.

[42] A. Majumdar and A. Zarnescu. Landau–de gennes theory of nematic liquid crystals: the oseen–frank limit and beyond. *Archive for Rational Mechanics and Analysis*, 196(1):227–280, 2010.

[43] L. M. Martyushev and V. D. Seleznev. Maximum entropy production principle in physics, chemistry and biology. *Physics reports*, 426(1):1–45, 2006.

[44] G. A. Maximov. Generalized variational principle for dissipative continuum mechanics. In *Mechanics of Generalized Continua*, volume 21 of *Advances in Mechanics and Mathematics*, pages 297–305. Springer New York, 2010.

[45] N. J. Mottram and C. Newton. Introduction to q-tensor theory. university of strathclyde, department of mathematics. Technical report, Research Report, 10, 2004.

[46] S. Naemura. Measurement of anisotropic interfacial interactions between a nematic liquid crystal and various substrates. *Applied Physics Letters*, 33(1):1–3, 1978.

[47] G. Napoli. Weak anchoring effects in electrically driven Fréedericksz transitions. *Journal of Physics A: Mathematical and General*, 39(1):11, 2006.

[48] J. Nehring, A. R. Kmetz, and T. J. Scheffer. Analysis of weak-boundary-coupling effects in liquid-crystal displays. *Journal of Applied Physics*, 47(3):850–857, 2008.

[49] L. Onsager. Reciprocal relations in irreversible processes. i. *Physical Review*, 37(4):405–426, 1931.

[50] L. Onsager. Reciprocal relations in irreversible processes. ii. *Physical Review*, 38(12):2265–2279, 1931.

[51] C. W. Oseen. The theory of liquid crystals. *Transactions of the Faraday Society*, 29(140):883–899, 1933.

[52] O. Parodi. Stress tensor for a nematic liquid crystal. *Journal de physique*, 31(7):581–584, 1970.

[53] A. Rapini and M. Papoular. Distorsion d'une lamelle nématique sous champ magnétique conditions d'ancrage aux parois. *Journal de Physique. Colloques*, 30(C4):C4–54, 1969.

[54] R. A. Saxton. Dynamic instability of the liquid crystal director. In W. B. Lindquist, editor, *Contemporary Mathematics*, volume 100 of *Current Progress in Hyperbolic Systems, Providence, RI, USA, 1989.*, pages 325–330, 1989.

[55] M. J. Stephen and J. P. Straley. Physics of liquid crystals. *Reviews of Modern Physics*, 46(4):617, 1974.

[56] I. W. Stewart. *The static and dynamic continuum theory of liquid crystals: a mathematical introduction.* Taylor & Francis, London, 2004.

[57] C. Z. van Doorn. Dynamic behavior of twisted nematic liquidcrystal layers in switched fields. *Journal of Applied Physics*, 46:3738–3745, 1975.

[58] E. G. Virga. *Variational theories for liquid crystals*, volume 8. Chapman & Hall, London, 1994.

[59] V. A. Vladimirov and M. Y. Zhukov. Vibrational Fréedericksz transition in liquid crystals. *Physical Review E*, 76:031706, 2007.

[60] C. K. Yun. Inertial coefficient of liquid crystals: A proposal for its measurements. *Physical Review A*, 45(2):119–120, 1973.

[61] P. Zhang and Y. Zheng. On oscillations of an asymptotic equation of a nonlinear variational wave equation. *Asymptotic Analysis*, 18(3):307–327, 1998.

[62] P. Zhang and Y. Zheng. Singular and rarefactive solutions to a nonlinear variational wave equation. *Chinese Annals of Mathematics*, 22(02):159–170, 2001.

[63] P. Zhang and Y. Zheng. Weak solutions to a nonlinear variational wave equation. *Archive for Rational Mechanics and Analysis*, 166(4):303–319, 2003.

[64] P. Zhang and Y. Zheng. Weak solutions to a nonlinear variational wave equation with general data. In *Annales de l'Institut Henri Poincare (C) Non Linear Analysis*, volume 22, pages 207–226. Elsevier, 2005.

[65] H. Zocher. The effect of a magnetic field on the nematic state. *Transactions of the Faraday Society*, 29:945–957, 1933.

# Part II

# Research articles

# Paper A

**The role of inertia and dissipation in the dynamics of the director for a nematic liquid crystal coupled with an electric field**

Peder Aursand and Johanna Ridder

Published in Communications in Computational Physics.

## Preface

The idea for this study came from a wish to understand the quantitative and qualitative differences between the variational wave equation (no dissipation) and the dissipative evolution equations (without inertia) more used in modeling. By deriving a model including both inertia and dissipation we were able to numerically study the transition between the two extremes for a basic Fréedericksz transition.

This was a joint work with my good friend and fellow PhD student Johanna Ridder at the University of Oslo. Together we developed and implemented an object-oriented MATLAB code able to solve the general director equation together with Maxwell's equations for the electric field. Personally, the work on this paper gave me a lot of intuition and physical understanding of the qualitative aspects of these models.

Commun. Comput. Phys.
doi: 10.4208/cicp.220414.231214a

Vol. **18**, No. 1, pp. 147-166
July 2015

# The Role of Inertia and Dissipation in the Dynamics of the Director for a Nematic Liquid Crystal Coupled with an Electric Field

Peder Aursand[1,*] and Johanna Ridder[2]

[1] *Department of Mathematical Sciences, Norwegian University of Science and Technology, NO–7491 Trondheim, Norway.*
[2] *Department of Mathematics, University of Oslo, P.O.Box NO-1053, Blindern, Oslo-0316, Norway.*

Communicated by Pingwen Zhang

Received 22 April 2014; Accepted (in revised version) 23 December 2014

**Abstract.** We consider the dynamics of the director in a nematic liquid crystal when under the influence of an applied electric field. Using an energy variational approach we derive a dynamic model for the director including both dissipative and inertial forces.

A numerical scheme for the model is proposed by extending a scheme for a related variational wave equation. Numerical experiments are performed studying the realignment of the director field when applying a voltage difference over the liquid crystal cell. In particular, we study how the relative strength of dissipative versus inertial forces influence the time scales of the transition between the initial configuration and the electrostatic equilibrium state.

**AMS subject classifications**: 76A15, 82D30, 65M06

**Key words**: Nematic liquid crystals, Fréedericksz transition, dynamics of director fields.

## 1 Introduction

Liquid crystal refers to a state of matter that exhibits free flow similarly to a liquid, but with certain crystalline properties commonly associated with solids. In the nematic liquid crystal state, the long axis of the constituent molecules tend to align. This results in long-range orientational order with no long-range correlation of the centre-of-mass. In the classical continuum theory, the configuration of a nematic liquid crystal is described by a velocity field and a director field.

*Corresponding author. *Email addresses:* peder.aursand@math.ntnu.no (P. Aursand), johanrid@math.uio.no (J. Ridder)

 

The behaviour of a finite sample of a liquid crystal under the influence of an electric field is of particular importance. When applying an electric field there is a competition between the boundary energy and the elastic and electrostatic forces. In the *Fréedericksz* transition, the liquid crystal cell will realign when the applied field (electric or magnetic) is above a certain critical threshold. These kinds of switching-phenomena under applied fields are of great importance because of the application to Liquid Crystal Displays (LCDs).

In this paper we will focus on the director field and use numerical experiments to simulate its dynamics under the influence of an electric field. In particular, we aim to quantify the influence of the inertia term in comparison with the dissipation term on the dynamics of the director when the electric field is switched on. The present model is derived from the Oseen-Frank elastic energy, the electric energy, and a dissipation function by the least action principle and the principle of maximum dissipation. The resulting equation can be seen as a special case of the classical Ericksen-Leslie dynamic equations. More precisely, for a planar director field $\psi$ and an electric potential $U$ depending only on one space variable $x$ and time, we will derive the equation

$$\sigma\psi_{tt}+\kappa\psi_t-c(\psi)(c(\psi)\psi_x)_x-\frac{1}{2}d'(\psi)U_x^2=0, \tag{1.1}$$

where

$$c(\psi)=\sqrt{\alpha\cos^2(\psi)+\beta\sin^2(\psi)}, \quad d(\psi)=\varepsilon_0(\varepsilon_\perp+\varepsilon_a\cos^2(\psi)),$$

and $\sigma$ is an inertial constant, $\kappa$ is a dissipation coefficient, $\alpha$ and $\beta$ are the bend and splay elastic constants, $\varepsilon_0$ is the vacuum permittivity, and $\varepsilon_\perp$ and $\varepsilon_a$ are dielectric constants.

The current model is closely related to the variational wave equation

$$\psi_{tt}-c(\psi)(c(\psi)\psi_x)_x=0. \tag{1.2}$$

This equation was first introduced by Saxton [24], and has since been subject to a considerable amount of research, see, e.g., [8, 10–12]. In the current context, (1.2) can be seen as a special case of (1.1) when there is neither an electric field nor dissipation. Also, Chen and Zheng [2] investigated the equations without electric field that include both inertia and dissipation.

Disregarding inertial terms is almost ubiquitous in the modeling of nematic liquid crystals, and herein lies the main interest of the present paper. The behavior of nematics under an electric field has been studied extensively during the last decades [3–6, 23, 25]. However, to the authors' knowledge, analytical and numerical investigations have mostly been conducted for the static equations to find equilibrium solutions or for the parabolic equations where the inertia of the director is neglected. As discussed by Gang et al. [7] and van Doorn [26], in many cases there are good physical reasons why inertial terms are neglected. However, it was early noted by Leslie [19] that the rotational kinetic energy might play a role when the director is subjected to large accelerations. More

recently, its relevance has been argued specifically in the modeling of liquid crystals under mechanical vibrations [27], acoustics [20], and, more generally, for liquid crystals with large moment of inertia that are subject to high-frequency excitation [1]. In general, inertial effects become more significant for problems of certain geometrical scalings, e.g., for very small time scales. The main purpose of this paper is to study a model which includes both inertial and dissipative terms. Moreover, we will not restrict ourselves to the one-constant approximation, which is commonly used in the literature as a simplification. Through numerical experiments using a non-dimensional form of the equations, we wish to study the transition from the viscosity-dominated regime to the inertia-dominated regime.

The basic equation derived in this work can also be derived from the general theory of anisotropic fluids, see, e.g., the fundamental work of McMillan [21]. The novel contribution of this paper lies first and foremost in the systematic numerical study of the qualitative and quantitative influence of inertia in these models for a standard test case. To do this we arguably push some physical parameters beyond the scope of present day liquid crystal devices (e.g. sub-nanosecond time scales), as was also done in the related work by Lenzi and Barbero [18].

To keep the focus on the influence of the inertia and dissipative term on the dynamics of the director field, we have restricted ourselves to a simplified setting. In the general case, the coupling between velocity and director field can lead to complicated effects, but for simplicity we will in this work assume that the velocity field is zero. In the case of the splay Fréedericksz transition this means that we neglect the so called backflow and kickback effects, which can be physically reasonable under some circumstances [25]. Furthermore, we restrict our study to a director and an electric field that vary only in one space dimension, $x$, and assume that the director lies in the $x-y$ plane, while the electric field only has a component in $x$ direction. This last assumption also implies that Maxwell's equations, which govern the electric field, reduce to the stationary equations. In other words, the electric field is assumed to be in constant electrostatic equilibrium with the changing director field.

The outline of the paper is as follows. In Section 2 we will present the derivation of our model using the least action principle and the maximum dissipation principle with the Oseen-Frank energy, the electric energy and Maxwell's equations, and a dissipation function as starting point. We will also derive a non-dimensional form of the equations, which we will be more convenient in the numerical experiments. Section 3 contains a suggested numerical method which can be used for the model. The scheme is adapted from a numerical method used for the nonlinear variational wave equation (1.2). In Section 4 we present results of numerical experiments of the Fréedericksz transition from a homogeneous initial state when applying an electric field. The observed time scales of the transition are compared to a linear analysis. Furthermore, in Section 5, we perform similar numerical experiments on a transition in a pi-cell when applying an electric field.

150 P. Aursand and J. Ridder / Commun. Comput. Phys., **18** (2015), pp. 147-166

## 2 The model

### 2.1 The general approach

We will derive the model for the director field of a nematic liquid crystal using the least action principle for the conservative part of the equation and the maximum dissipation principle that allows us to include the effect of dissipation. To do this, we need to determine the free energy of the liquid crystal, which is the sum of the kinetic energy, the Oseen-Frank elastic energy, and the electric energy.

In the following, $\mathbf{n}(x,t)$ denotes the director field of the liquid crystals. Note that at any point in time and space, $\mathbf{n}$ has unit length, i.e., $\mathbf{n}\cdot\mathbf{n}=1$. For simplicity, we will assume that the liquid crystal does not flow, i.e., the fluid velocity is zero. The kinetic energy for the director is then given by

$$K=\frac{1}{2}\sigma|\mathbf{n}_t|^2, \tag{2.1}$$

where $\sigma$ denotes an inertial constant. A typical value for $\sigma$ is $\sim 10^{-13}\mathrm{kgm}^{-1}$ (for the nematic MBBA [7]). The Oseen-Frank elastic energy, which describes the tendency of the directors to align parallel, is

$$W_{OF}=\frac{1}{2}\alpha|\mathbf{n}\times(\nabla\times\mathbf{n})|^2+\frac{1}{2}\beta(\nabla\cdot\mathbf{n})^2+\frac{1}{2}\gamma(\mathbf{n}\cdot(\nabla\times\mathbf{n}))^2, \tag{2.2}$$

where $\alpha$, $\beta$, and $\gamma$ are the Frank elastic constants for bend, splay, and twist, typical values being $8.2\times10^{-12}$N, $6.2\times10^{-12}$N, and $3.9\times10^{-12}$N, respectively (for 5CB [25]). The contribution to the total energy density from the electric field is given by

$$W_{el}=-\frac{1}{2}\mathbf{D}\cdot\mathbf{E}, \tag{2.3}$$

where $\mathbf{E}$ is the electric field and $\mathbf{D}$ is the electric displacement. For a uniaxial nematic, if we consider only dielectric contributions to the polarization, $\mathbf{D}$ is related to $\mathbf{E}$ through

$$\mathbf{D}=\varepsilon_0(\varepsilon_\perp\mathbf{E}+\varepsilon_a(\mathbf{n}\cdot\mathbf{E})\mathbf{n}), \tag{2.4}$$

where $\varepsilon_0=8.854\times10^{-12}\mathrm{Fm}^{-1}$ is the permittivity in free space, $\varepsilon_\perp$ is the relative permittivity perpendicular to the director ($\varepsilon_\perp=7$ for 5CB [25]) and $\varepsilon_a$ is the dielectric anisotropy ($\varepsilon_a=11.5$ for 5CB [25]). The electric displacement is also subject to Gauss' law, which reads (in the absence of free charges)

$$\nabla\cdot\mathbf{D}=0. \tag{2.5}$$

Altogether, the total free energy is

$$\mathcal{E}=\int\left(K(\mathbf{n}_t)+W_{OF}(\mathbf{n},\nabla\mathbf{n})+W_{el}(\mathbf{n})\right)\mathrm{d}x,$$

with the corresponding Lagrangian $\mathcal{L}=K(\mathbf{n}_t)-W_{OF}(\mathbf{n},\nabla\mathbf{n})-W_{el}(\mathbf{n})$. The conservative system would then be described by the Euler-Lagrange equation

$$\frac{\mathrm{d}}{\mathrm{d}t}\left(\frac{\partial\mathcal{L}}{\partial\mathbf{n}_t}\right)+\frac{\mathrm{d}}{\mathrm{d}x}\left(\frac{\partial\mathcal{L}}{\partial\mathbf{n}_x}\right)+\frac{\mathrm{d}}{\mathrm{d}y}\left(\frac{\partial\mathcal{L}}{\partial\mathbf{n}_y}\right)+\frac{\mathrm{d}}{\mathrm{d}z}\left(\frac{\partial\mathcal{L}}{\partial\mathbf{n}_z}\right)-\frac{\partial\mathcal{L}}{\partial\mathbf{n}}=0,$$

which is derived from the least action principle for the action functional $\mathcal{A}=\int L\mathrm{d}x$. For dissipative systems we can write the energy law

$$\frac{\mathrm{d}}{\mathrm{d}t}\left(\int\left(K(\mathbf{n}_t)+W_{OF}(\mathbf{n},\nabla\mathbf{n})+W_{el}(\mathbf{n})\right)\mathrm{d}x\right)=-\int\mathcal{D}(\mathbf{n}_t)\mathrm{d}x \tag{2.6}$$

for some non-negative dissipation function $\mathcal{D}(\mathbf{n}_t)$. To obtain the evolution equation corresponding to (2.6), it is common practice [13, 16, 22, 28] to apply Onsager's maximum dissipation principle to incorporate it in the Euler-Lagrange equation by

$$\frac{\mathrm{d}}{\mathrm{d}t}\left(\frac{\partial\mathcal{L}}{\partial\mathbf{n}_t}\right)+\frac{\mathrm{d}}{\mathrm{d}x}\left(\frac{\partial\mathcal{L}}{\partial\mathbf{n}_x}\right)+\frac{\mathrm{d}}{\mathrm{d}y}\left(\frac{\partial\mathcal{L}}{\partial\mathbf{n}_y}\right)+\frac{\mathrm{d}}{\mathrm{d}z}\left(\frac{\partial\mathcal{L}}{\partial\mathbf{n}_z}\right)-\frac{\partial\mathcal{L}}{\partial\mathbf{n}}=-\frac{\partial\mathcal{D}}{\partial\mathbf{n}_t}.$$

In the present case the dissipation function, as given, e.g., in [25], is

$$\mathcal{D}=\frac{1}{2}\kappa|\mathbf{n}_t|^2, \tag{2.7}$$

where $\kappa>0$ is a viscosity coefficient (for MBBA, $\kappa=0.0777\,\mathrm{Pa\,s}$, [25]).

### 2.2 The one-dimensional case

For the experiments in this paper, we restrict ourselves to the one-dimensional case, i.e., we assume that both the director field and the electric field depend only on the $x$-coordinate and time. Furthermore, we will assume that the electric field can be written as the gradient of a scalar potential and hence only has a component in the $x$-direction. This simplifies the equations considerably, but still allows us to model physically interesting phenomena, like the Fréedericksz transition. More precisely, we consider a liquid crystal cell that only differs in $x$ dimension on an interval $[0,L]$ and assume that the director field is strongly anchored at the boundary, i.e., we have Dirichlet boundary conditions $\mathbf{n}(0,t)=\mathbf{n}_0$ and $\mathbf{n}(L,t)=\mathbf{n}_L$. We assume further that the director lies in the $xy$ plane and thus can be described by an angle $\psi(x,t)$ through

$$\mathbf{n}(x,t)=(\cos(\psi(x,t)),\sin(\psi(x,t)),0).$$

Expressed in terms of $\psi$, the kinetic energy (2.1) and the Oseen-Frank energy (2.2) then become

$$K=\frac{1}{2}\sigma\psi_t^2,\quad W_{OF}=\frac{1}{2}c^2(\psi)\psi_x^2,$$

where

$$c(\psi)=\sqrt{\alpha\cos^2(\psi)+\beta\sin^2(\psi)}.$$

We write $\mathbf{E}$ as the gradient of an electric potential $U$, i.e.,

$$\mathbf{E}(x,t)=(E(x,t),0,0)=-\nabla U(x,t)=(U(x,t)_x,0,0),$$

with boundary conditions $U(0,t)=0$ and $U(L,t)=V_0>0$, corresponding to the applied voltage. The electric displacement (2.4) is then given by

$$\mathbf{D}(x,t)=\Big(-d(\psi)U_x,\frac{1}{2}d'(\psi)U_x,0\Big),$$

where $d(\psi)=\varepsilon_0(\varepsilon_\perp+\varepsilon_a\cos^2(\psi))$. The electric energy (2.3), written in terms of $\psi$, becomes

$$W_{el}=-\frac{1}{2}d(\psi)U_x^2.$$

In addition, due to Gauss' law (2.5), the electric potential must satisfy

$$(d(\psi)U_x)_x=0, \tag{2.8}$$

which implies

$$U(x)=\int_0^x\frac{C}{d(\psi(\xi))}\mathrm{d}\xi+U(0),\quad\text{where}\quad C=\left(\int_0^L\frac{1}{d(\psi(\xi))}\mathrm{d}\xi\right)^{-1}U(L). \tag{2.9}$$

Finally, insert the Lagrangian,

$$\mathcal{L}(\psi_t,\psi_x,\psi)=K-W_{OF}-W_{el}=\frac{1}{2}\left(\sigma\psi_t^2-c^2(\psi)\psi_x^2+d(\psi)U_x^2\right),$$

and the dissipation function (2.7),

$$\mathcal{D}(\psi_t)=\frac{1}{2}\kappa\psi_t^2,$$

into the modified Euler-Lagrange equation for the dissipative system,

$$\frac{\mathrm{d}}{\mathrm{d}t}\left(\frac{\partial\mathcal{L}}{\partial\psi_t}\right)+\frac{\mathrm{d}}{\mathrm{d}x}\left(\frac{\partial\mathcal{L}}{\partial\psi_x}\right)-\frac{\partial\mathcal{L}}{\partial\psi}=-\frac{\partial\mathcal{D}}{\partial\psi_t},$$

to arrive at the equation for the director field,

$$\sigma\psi_{tt}+\kappa\psi_t-c(\psi)(c(\psi)\psi_x)_x-\frac{1}{2}d'(\psi)U_x^2=0. \tag{2.10}$$

Note that in the derivation we followed common practice and neglected the dependency of $U$ on $\psi$.

### 2.3 The nondimensional form

To quantify the impact of the inertial constant in comparison with the dissipation constant, we derive a nondimensional version of Eq. (2.10). As scaling parameters, we use the interval length $L$, the electric potential at the boundary, $V_0$, and some fixed time scale $\tau$, which results in the dimensionless length $X=x/L$, electric potential $u=U/V_0$, and time $T=t/\tau$. Furthermore, define

$$\tilde{c}(\psi)=\sqrt{\cos^2(\psi)+\frac{\beta}{\alpha}\sin^2(\psi)},\quad \tilde{d}(\psi)=1+\frac{\varepsilon_a}{\varepsilon_\perp}\cos^2(\psi)$$

and the parameters

$$\tilde{\kappa}=\frac{\kappa\tau}{\sigma},\quad \tilde{\lambda}=\frac{\tau}{L}\left(\frac{\alpha}{\sigma}\right)^{1/2},\quad \tilde{\varepsilon}=\frac{1}{2}\frac{\tau^2}{L^2}\frac{\varepsilon_0\varepsilon_\perp}{\sigma}V_0^2.$$

Then, Eq. (2.10) is equivalent to

$$\psi_{TT}+\tilde{\kappa}\psi_T-\tilde{\lambda}^2\tilde{c}(\psi)(\tilde{c}(\psi)\psi_X)_X-\tilde{\varepsilon}\tilde{d}'(\psi)(u_X)^2=0. \tag{2.11}$$

Similarly, (2.8) and (2.9) become

$$(\tilde{d}(\psi)u_X)_X=0,\quad \text{i.e.,}\quad u(X)=\left(\int_{[0,1]}\frac{1}{\tilde{d}(\psi(\xi))}\mathrm{d}\xi\right)^{-1}\int_0^X\frac{1}{\tilde{d}(\psi(\xi))}\mathrm{d}\xi. \tag{2.12}$$

If $\sigma\sim10^{-13}\mathrm{kgm}^{-1}$ and $\kappa\sim10^{-1}\mathrm{Pas}$, as it is the case for example for MBBA or 5CB, then $\tilde{\kappa}\sim1$ for $\tau\sim10^{-12}$s, i.e., for very small time scales. For materials with larger moment of inertia, the time scale corresponding to $\tilde{\kappa}\sim1$ increases.

### 2.4 The inertialess model

In many physical situations it is argued that the inertia is negligible, i.e., $\sigma\approx0$ and $\tilde{\kappa},\tilde{\lambda},\tilde{\varepsilon}\gg1$. Then the term $\psi_{TT}$ in the above equations vanishes and (2.11) reduces to

$$\tilde{\kappa}\psi_T-\tilde{\lambda}^2\tilde{c}(\psi)(\tilde{c}(\psi)\psi_X)_X-\tilde{\varepsilon}\tilde{d}'(\psi)(u_X)^2=0, \tag{2.13}$$

which is the model that is widely applied in the literature and that we will use to compare our numerical results.

## 3 Numerical scheme

We proceed to derive a numerical scheme for solving the non-dimensional equations (2.11)-(2.12). Introducing the auxiliary variables $v=\psi_T$ and $w=\tilde{\lambda}\tilde{c}(\psi)\psi_X$, we can rewrite (2.11)

as a system of first-order equations,

$$v_T+\tilde{\kappa}v-\tilde{\lambda}(\tilde{c}(\psi)w)_X=-\tilde{\lambda}\tilde{c}(\psi)_X w-\tilde{\varepsilon}\tilde{d}'(\psi)(u_X)^2, \tag{3.1a}$$

$$w_T-\tilde{\lambda}(\tilde{c}(\psi)v)_X=0, \tag{3.1b}$$

$$\psi_T=v, \tag{3.1c}$$

which we want to solve for $X\in[0,1]$, $T>0$, and some given initial data $\psi_0(X)$. As a basic first-order scheme, we adapt a semi-discrete energy preserving method presented by Koley et al. [15]. This scheme was developed for the variational wave equation

$$\psi_{tt}-c(\psi)(c(\psi)\psi_x)_x=0, \tag{3.2}$$

but it extends straightforwardly to the present case with an electric field and dissipation term.

Let $\Delta X=1/N$ for some positive integer $N$ and denote any grid function $f_j(T)=f(j\Delta X,T)$. Furthermore, we introduce the shorthands

$$\bar{a}_{j+1/2}=\frac{a_{j+1}+a_j}{2}$$

and the interface jump

$$[\![a]\!]_{j+1/2}=a_{j+1}-a_j.$$

Now let $u_{X,j}$ be the discrete electric field given by

$$u_{X,j}=\left(\sum_{i=0}^{N}\frac{1}{\tilde{d}(\psi_i)}\right)^{-1}\sum_{i=0}^{j}\frac{1}{\tilde{d}(\psi_i)}. \tag{3.3}$$

The evolution of the semi-discrete approximations $v_j$, $w_j$ and $\psi_j$ is then given by the scheme

$$\begin{aligned}(v_j)_T+\tilde{\kappa}v_j-\frac{\tilde{\lambda}}{\Delta X}\left(\overline{\tilde{c}}_{j+1/2}\overline{w}_{j+1/2}-\overline{\tilde{c}}_{j-1/2}\overline{w}_{j-1/2}\right)&\\ =-\frac{\tilde{\lambda}}{2\Delta X}\left([\![\tilde{c}]\!]_{j+1/2}\overline{w}_{j+1/2}+[\![\tilde{c}]\!]_{j-1/2}\overline{w}_{j-1/2}\right)+\tilde{\varepsilon}\tilde{d}'(\psi_j)\left(u_{X,j}\right)^2,&\end{aligned} \tag{3.4}$$

$$(w_j)_T-\frac{1}{\Delta X}\left(\overline{\tilde{c}v}_{j+1/2}-\overline{\tilde{c}v}_{j-1/2}\right)=0, \tag{3.5}$$

and

$$(\psi_j)_T=v_j. \tag{3.6}$$

For the temporal integration, we let

$$\Delta T=\frac{\Delta X}{\tilde{\lambda}\left(1+\frac{\beta}{\alpha}\right)} \tag{3.7}$$

and denote $T^n=n\Delta T$ and a fully discrete grid function as $f_j^n=f_j(n\Delta T)$. The semi-discrete form $(u_j)_T=g(u)$ is integrated using the third-order SSP Runge-Kutta scheme [9]

$$\begin{aligned}
u^* &= u_j^n+\Delta T g(u^n),\\
u^{**} &= \frac{3}{4}u_j^n+\frac{1}{4}u^*+\frac{1}{4}\Delta T g(u^*),\\
u_j^{n+1} &= \frac{1}{3}u_j^n+\frac{2}{3}u^{**}+\frac{2}{3}\Delta T g(u^{**}).
\end{aligned}$$

## 4 Fréedericksz transition from homogeneous initial state

Consider a liquid crystal cell initially in a near homogeneous state. When a sufficiently large electric field is applied, the Fréedericksz transition changes the director configuration corresponding to a new electrostatic equilibrium. We venture to use the current model to study the dynamics of this transition in the case of significant inertial forces. To be precise, we consider the initial-boundary problem

$$\begin{cases}
\psi_{TT}+\tilde{\kappa}\psi_T-\tilde{\lambda}^2\tilde{c}(\psi)\big(\tilde{c}(\psi)\psi_X\big)_X-\tilde{\varepsilon}\tilde{d}'(\psi)u_X^2=0, & (X,T)\in[0,1]\times[0,\infty),\\
u_X=\frac{1}{\tilde{d}(\psi)}\left(\int_{[0,1]}\frac{1}{\tilde{d}(\psi)}\mathrm{d}\xi\right)^{-1}, & \\
\psi(X,0)=\frac{\pi}{2}+\delta\sin(\pi X), & X\in[0,1],\\
\psi_T(X,0)=0, & X\in[0,1],\\
\psi(0,T)=\psi(1,T)=\frac{\pi}{2}, & T\in[0,\infty).
\end{cases} \tag{4.1}$$

### 4.1 Linear analysis for the dissipation-dominated case

Following the procedure from [25], we analyze the Fréedericksz transition dynamics in the dissipation-dominated case. Also, for the present analysis, we make the one-constant approximation ($\alpha=\beta$). Disregarding the inertial term in (2.11), we consider the following simplified form of (2.13),

$$\tilde{\kappa}\psi_T=\tilde{\lambda}^2\psi_{XX}+\tilde{\varepsilon}\tilde{d}'(\psi)(u_X)^2, \tag{4.2}$$

$$\big(\tilde{d}(\psi)u_X\big)_X=0 \tag{4.3}$$

for the initial data

$$\psi(X,0)=\psi_0(X),\quad \left|\psi_0(X)-\frac{\pi}{2}\right|\ll 1 \tag{4.4}$$

and boundary conditions

$$\psi(0,T)=\psi_0(1,T)=\frac{\pi}{2},\quad u(0,T)=0,\quad u(1,T)=0. \tag{4.5}$$

By introducing $\theta=\psi-\pi/2$ we can linearize (4.2) around $\theta=0$ to obtain

$$\tilde{\kappa}\theta_T=\tilde{\lambda}^2\theta_{XX}+2\tilde{\varepsilon}\frac{\varepsilon_a}{\varepsilon_\perp}(u_X)^2\theta, \tag{4.6}$$

$$u_{XX}=0. \tag{4.7}$$

Notice that in this case (4.7) simply implies $u_X=1$. Furthermore, we can introduce

$$\eta=\frac{\tilde{\lambda}^2}{\tilde{\kappa}}T \quad \text{and} \quad c=2\frac{\tilde{\varepsilon}}{\tilde{\lambda}^2}\frac{\varepsilon_a}{\varepsilon_\perp} \tag{4.8}$$

as well as the transformation

$$\theta(X,\eta)=\Theta(X,\eta)\exp(c\eta) \tag{4.9}$$

in order to write (4.6) as

$$\Theta_\eta=\Theta_{XX}. \tag{4.10}$$

By standard techniques, the solution to (4.10) can be written in the form

$$\Theta(X,\eta)=\sum_{n=1}^{\infty}A_n\sin(n\pi X)\exp\left(-(n\pi)^2\eta\right) \tag{4.11}$$

which gives the solution

$$\theta(X,T)=\sum_{n=1}^{\infty}A_n\sin(n\pi X)\exp\left(-\frac{T}{\tau_n}\right), \tag{4.12}$$

with

$$\tau_n=\frac{\tilde{\kappa}}{2\frac{\varepsilon_a}{\varepsilon_\perp}\tilde{\varepsilon}_c\left(n^2-\frac{\tilde{\varepsilon}}{\tilde{\varepsilon}_c}\right)}, \tag{4.13}$$

where we have introduced the critical non-dimensional electric field

$$\tilde{\varepsilon}_c:=\frac{1}{2}\frac{\varepsilon_\perp}{\varepsilon_a}\pi^2\tilde{\lambda}^2. \tag{4.14}$$

From (4.12) we see that all Fourier modes decay exponentially if $\tilde{\varepsilon}<\tilde{\varepsilon}_c$. For $\tilde{\varepsilon}>\tilde{\varepsilon}_c$ the initial state is not linearly stable and we get the onset of the Fréedericksz transition. For a near-critical electric field $\tilde{\varepsilon}>\tilde{\varepsilon}_c$, it is then natural to define the switch-on time as [25]

$$\tau_{\text{on}}=:-\tau_1=\frac{\tilde{\kappa}}{2\frac{\varepsilon_a}{\varepsilon_\perp}\tilde{\varepsilon}_c\left(\frac{\tilde{\varepsilon}}{\tilde{\varepsilon}_c}-1\right)}. \tag{4.15}$$

### 4.2 Numerical experiments

We wish to numerically study the evolution of the numerical solution compared to the stationary solution for different values of the parameters involved. To this end, we define the following: Let $\psi_{\text{eq}}(X)$ be the stationary solution of (4.1). Given a solution $\psi(X,T)$, we define the normalized distance function

$$d_2(T) := \frac{\|\psi(\cdot,T)-\psi_{\text{eq}}(\cdot)\|_{L^2}}{\|\psi(\cdot,0)-\psi_{\text{eq}}(\cdot)\|_{L^2}}. \tag{4.16}$$

Numerical experiments were performed demonstrating how the dynamics of the Fréedericksz transition depends on the relationship between rotational inertia and the dissipation. We set $\delta = 0.01$ and the physical parameters $\beta/\alpha = 0.756$ and $\varepsilon_a/\varepsilon_\perp = 1.643$, consistent with the liquid crystal 5CB [25]. Moreover, we let $\tilde{\lambda}=1$ and $\tilde{\varepsilon}=100$, thereby ensuring that we are well above the critical electric field $\tilde{\varepsilon}_c \approx 3$ for the onset of the Fréedericksz transition. The problem (4.1) was solved numerically using the finite-difference scheme (3.4)-(3.6) with $N=100$. Figs. 1, 2 and 3 show the numerical solution and distance (4.16) for $\tilde{\kappa} = 1$, 5 and 10, respectively. The results show that the presence of inertial forces causes standing waves to occur in the director field. For $\tilde{\kappa}=1$ these are of a significant magnitude and cause the distance $d_2(T)$ to oscillate around zero. For stronger dissipation the standing waves are suppressed and the Fréedericksz transition is more monotone.

In light of the standing waves seen in Figs. 1, 2 and 3, we wish to determine the influence of these oscillations on the transition time from the initial state to the electrostatic equilibrium state. To that end, we in addition to (4.16) define the alternative distance function

$$e_2(T) := \frac{\|\psi(\cdot,T)-\psi(\cdot,0)\|_{L^2}}{\|\psi(\cdot,0)-\psi_{\text{eq}}(\cdot)\|_{L^2}}. \tag{4.17}$$

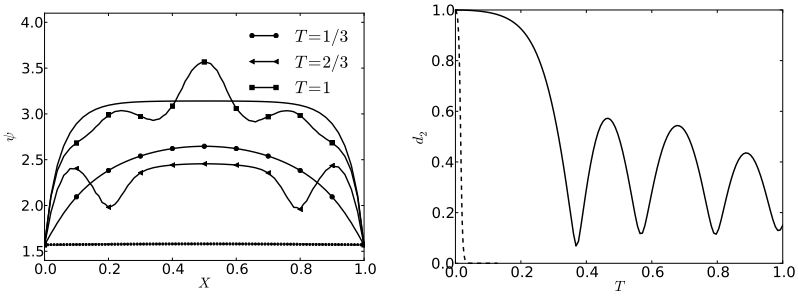


(a) $\psi$ at different times (b) Distance from equilibrium (4.16)

Figure 1: The numerical solution of the homogeneous switch-on case (4.1) using $\tilde{\kappa}=1$. Left: $\psi$ at different times. The solid line is the stationary solution and the dotted line the initial data. Right: The evolution of the distance from equilibrium (4.16). The dashed line is the corresponding solution from the inertialess model (2.13).

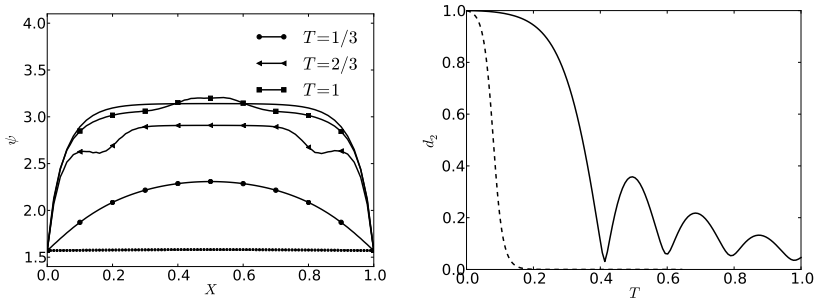


(a) $\psi$ at different times (b) Distance from equilibrium (4.16)

Figure 2: The numerical solution of the homogeneous switch-on case (4.1) using $\tilde{\kappa}=5$. Left: $\psi$ at different times. The solid line is the stationary solution and the dotted line the initial data. Right: The evolution of the distance from equilibrium (4.16). The dashed line is the corresponding solution from the inertialess model (2.13).

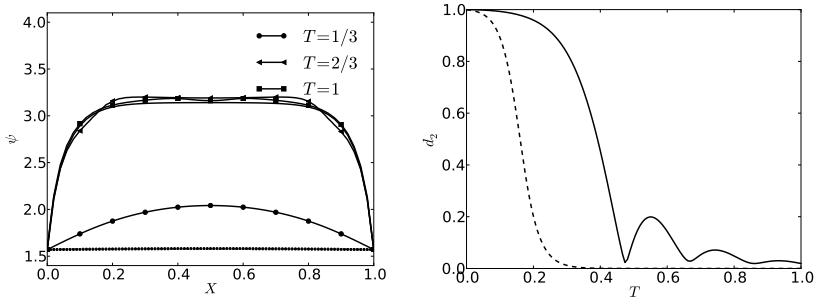


(a) $\psi$ at different times (b) Distance from equilibrium (4.16)

Figure 3: The numerical solution of the homogeneous switch-on case (4.1) using $\tilde{\kappa}=10$. Left: $\psi$ at different times. The solid line is the stationary solution and the dotted line the initial data. Right: The evolution of the distance from equilibrium (4.16). The dashed line is the corresponding solution from the inertialess model (2.13).

While (4.16) is a normalized distance to the equilibrium, the function (4.17) gives the corresponding distance to the initial state. Using these we can now define the *switch-on time*

$$T_* := \sup\{T : e_2(T) < \mathrm{e}^{-1}\} \tag{4.18}$$

and the *relaxation time*

$$T^* := \sup\{T : d_2(T) > \mathrm{e}^{-1}\}. \tag{4.19}$$

Fig. 4 shows the switch-on and relaxation time using the definitions above. As before, the numerical solutions were obtained using $N=100$ with $\tilde{\lambda}=1$. We set the physical

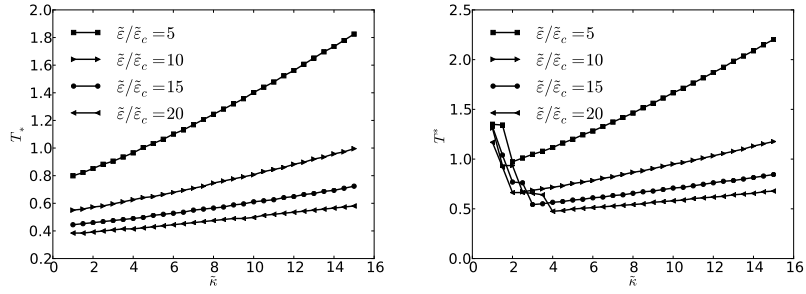


(a) Switch-on time (b) Relaxation time

Figure 4: Transition times for $\tilde{\lambda}=1$ as a function of $\tilde{\kappa}$ for different values of the scaled non-dimensional electric field.

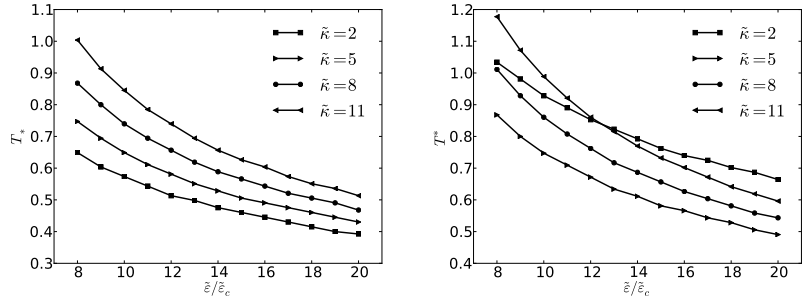


(a) Switch-on time (b) Relaxation time

Figure 5: Transition times for $\tilde{\lambda}=1$ as a function of $\tilde{\varepsilon}/\tilde{\varepsilon}_c$ for different values of the non-dimensional dissipation constant.

parameters to $\beta/\alpha=0.756$ and $\varepsilon_a/\varepsilon_\perp=1.643$. For large values of $\tilde{\kappa}$ the transition times are close to linear, a result that agrees with the characteristic time scale (4.15) from the linear analysis. However, when the inertial terms become significant, the standing waves cause and increase in the relaxation time. This effect does not influence the switch-on time.

Fig. 5 shows the switch-on and relaxation time as a function of the scaled non-dimensional electric field. Here, the linear analysis predicts an inverse relationship (4.15). Indeed, the results indicate that this is also the case for the full transition. However, also in this case the standing waves for low $\tilde{\kappa}$ increase the relaxation time, as shown in Fig. 5(b).

Fig. 7 shows the switch-on time (4.18) and the relaxation time (4.19) for the current model compared to the inertialess model (2.13) over a wide range of $\tilde{\kappa}$. As expected, the

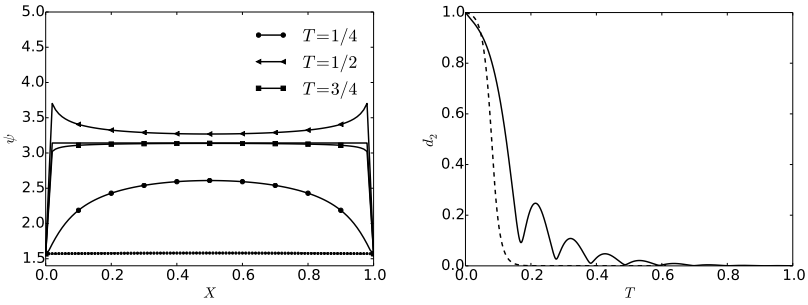


(a) $\psi$ at different times

(b) Distance from equilibrium (4.16)

Figure 6: The numerical solution of the homogeneous switch-on case (4.1) for physical values of the inertia and dissipation coefficient. Left: $\psi$ at different times. The solid line is the stationary solution and the dotted line the initial data. Right: The evolution of the distance from equilibrium (4.16). The dashed line is the corresponding solution from the inertialess model (2.13).

models seem to agree in the dissipation dominated limit $\tilde{\kappa} \to \infty$. However, a significant difference in transition times becomes apparent when $\tilde{\kappa}$ approaches $\sim$10 from above. Values for the viscous constant $\kappa$ are usually reported in the order of $10^{-1}$Pas [25]. Quoted values for the rotational inertia varies from $10^{-11}$–$10^{-16}$kgm$^{-1}$ [7, 29]. Even with the highest reported values for the molecular inertia, $\tilde{\kappa} \sim 10$ still requires time scales in the nano-second range. This is outside the physical domain of most current liquid crystal devices and experiments—the effect of inertia is here rightfully ignored.

We note that, under extreme conditions and within small time scales, inertial effects can become significant in the dynamics of the Fréedericksz transition. To illustrate this, we consider the Fréedericksz transition in the liquid crystal 5CB (with the physical parameters as before according to [25] and an estimated rotational inertia of $\sigma$=$10^{-13}$kgm$^{-1}$) under the influence of a strong electric field ($U_L$=$5.00\times10^4$V). As length scale and thickness of the liquid crystal sample we choose as before $L = 10^{-6}$m, and as the time scale we let $\tau = 2\times10^{-11}$s. This gives the non-dimensional parameters $\tilde{\kappa} = 15.5$, $\tilde{\lambda} = 1.8\times10^{-4}$, and $\tilde{\varepsilon} = 3.1\times10^2$. The plots in Fig. 6 as well as the resulting switch-on time $T_* = 0.1040$ (0.0715 without inertia) and relaxation time $T^* = 0.1375$ (0.0865 without inertia) show the qualitative and quantitative effect of including inertia in this case.

Two other experiments where inertia becomes significant were suggested by Yun [29]. In the first one, the liquid crystal is subjected to a rapidly rotating magnetic field that is turned off abruptly. In the second one, the magnetic field is assumed to oscillate, leading to oscillations also in the director field with amplitude and phase lag depending on the inertia.

Finally we note that, because of the small time scales involved, the inclusion of inertia might also be warranted in, e.g., models for liquid crystal systems under high-frequency

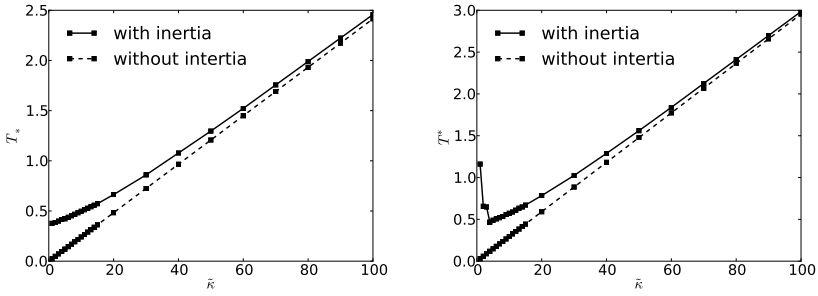


(a) Switch-on time (b) Relaxation time

Figure 7: Transition times for the inertialess model (2.13) compared to the current model for $\tilde{\lambda}=1$ and $\tilde{\varepsilon}/\tilde{\varepsilon}_c=20$.

mechanical vibrations [27], liquid crystal acoustics [14] and studies of the light-induced Freedericksz transition [17].

## 5 The pi-cell

We now consider the transition from a stationary non-trivial initial state when applying an electric field. More precisely, we consider the initial-boundary problem

$$\begin{cases} \psi_{TT}+\tilde{\kappa}\psi_T-\tilde{\lambda}^2\tilde{c}(\psi)\left(\tilde{c}(\psi)\psi_X\right)_X-\tilde{\varepsilon}\tilde{d}'(\psi)u_X^2=0, & (X,T)\in[0,1]\times[0,\infty), \\ u_X=\frac{1}{\tilde{d}(\psi)}\left(\int_{[0,1]}\frac{1}{\tilde{d}(\psi)}\mathrm{d}\xi\right)^{-1}, & \\ \left(\tilde{c}(\psi)\psi_X\right)_X=0, & X\in[0,1],\ T=0, \\ \psi(0,T)=-\frac{\pi}{2}+\psi_{bc}, & T\in[0,\infty), \\ \psi(1,T)=\frac{\pi}{2}-\psi_{bc}, & T\in[0,\infty). \end{cases} \tag{5.1}$$

This experiment was studied by Mottram and Newton [23] in the stationary case using the one-constant approximation ($\alpha=\beta$) and by ignoring the inertial term. Note that in that case the equilibrium solution of (5.1) without electric field is a linear profile, while for the present nonlinear model it is nontrivial.

As before, we perform numerical experiments in order to study the dynamics of the transition occurring when applying an electric potential over the liquid crystal cell. For the initial data we follow Mottram and Newton [23] and use the equilibrium solution for the equation without electric field. In the nonlinear case $\alpha\neq\beta$ this solution is calculated numerically beforehand. For the boundary condition we define the parameter $\psi_{bc}=\pi/30$. Furthermore, we let $\tilde{\lambda}=1$ and set the non-dimensional electric field to $\tilde{\varepsilon}=100$.

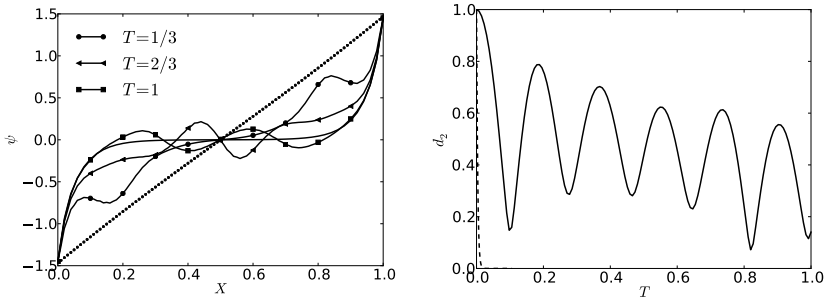


(a) $\psi$ at different times (b) Distance from equilibrium (4.16)

Figure 8: The numerical solution of the Pi-cell initial value problem (5.1) using $\tilde{\kappa}=1$. Left: $\psi$ at different times. The solid line is the stationary solution and the dotted line the initial data. Right: The evolution of the distance from equilibrium (4.16). The dashed line is the corresponding solution from the inertialess model (2.13).

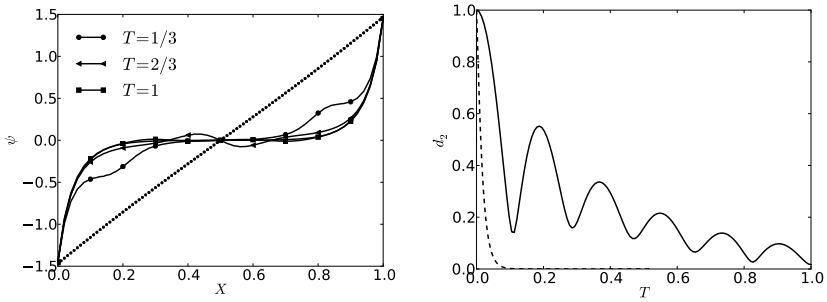


(a) $\psi$ at different times (b) Distance from equilibrium (4.16)

Figure 9: The numerical solution of the Pi-cell initial value problem (5.1) using $\tilde{\kappa}=5$. Left: $\psi$ at different times. The solid line is the stationary solution and the dotted line the initial data. Right: The evolution of the distance from equilibrium (4.16). The dashed line is the corresponding solution from the inertialess model (2.13).

Figs. 8, 9 and 10 show the numerical solution and the distance (4.16) for $\tilde{\kappa}=1$, 5 and 10, respectively. The physical parameters were $\beta/\alpha=0.756$ and $\varepsilon_a/\varepsilon_\perp=1.643$, consistent with the liquid crystal 5CB [25]. The results all agree with the qualitative behavior that was observed for the homogeneous switch-on case. When dissipative forces are weak (compared to inertial forces) the initial part of the transition happens faster, but standing waves slow down the final relaxation towards equilibrium.

Similarly as in previous section, we now look at the transition times (4.18) and (4.19) under variations of the electric field and rate of dissipation. Fig. 11 shows the switch-on

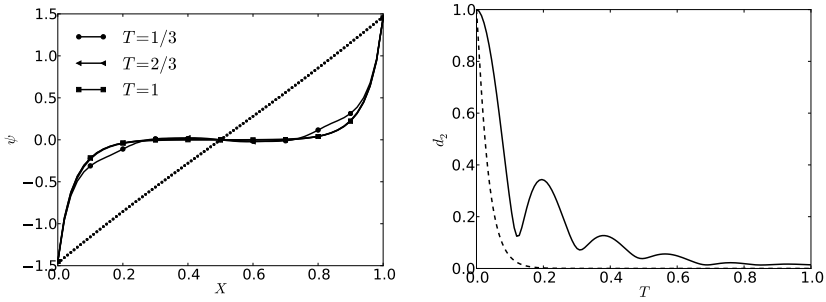


(a) $\psi$ at different times (b) Distance from equilibrium (4.16)

Figure 10: The numerical solution of the Pi-cell initial value problem (5.1) using $\tilde{\kappa}=10$. Left: $\psi$ at different times. The solid line is the stationary solution and the dotted line the initial data. Right: The evolution of the distance from equilibrium (4.16). The dashed line is the corresponding solution from the inertialess model (2.13).

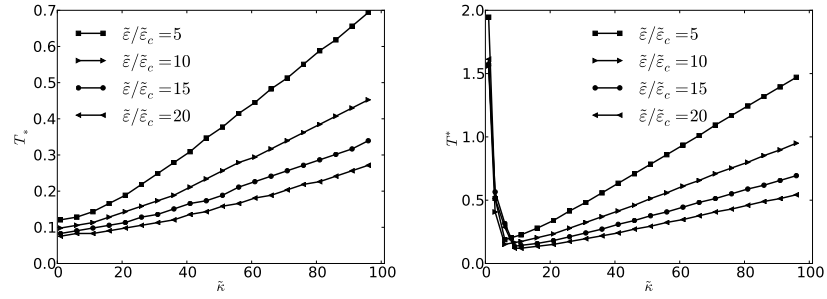


(a) Switch-on time (b) Relaxation time

Figure 11: Transition times for the Pi-cell initial value problem (5.1) using $\tilde{\lambda}=1$, $\beta/\alpha=0.756$ and $\varepsilon_a/\varepsilon_\perp=1.643$.

and relaxation time as a function of the non-dimensional dissipation $\tilde{\kappa}$. The numerical solutions were obtained using $N=100$ with $\tilde{\lambda}=1$ with physical parameters to $\beta/\alpha=0.756$ and $\varepsilon_a/\varepsilon_\perp=1.643$. We note that also for the Pi-cell we have that the transition times are close to linear for large values of $\tilde{\kappa}$. Furthermore, when the $\tilde{\kappa}$ approaches 5 from above we observe an increase in the relaxation time due to the formation of standing waves.

Fig. 12 shows the switch-on and relaxation time as a function of the scaled non-dimensional electric field. Also here, the results agree (for large $\tilde{\kappa}$) with the inverse relationship (4.15) predicted by the linear analysis. However, also in this case we observe an increase in the relaxation time, shown in Fig. 12(b).

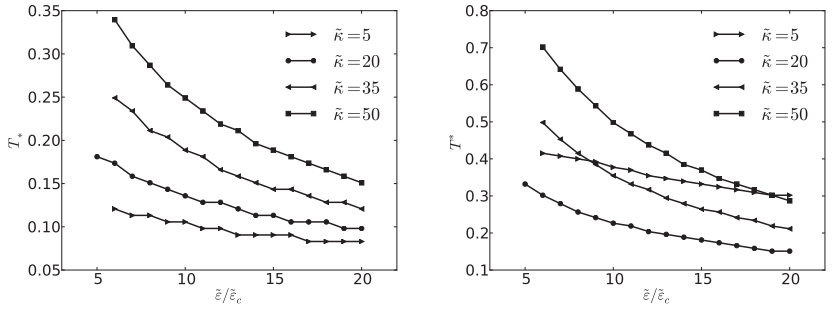


(a) Switch-on time (b) Relaxation time

Figure 12: Transition times for the Pi-cell initial value problem (5.1) using $\tilde{\lambda}=1$, $\beta/\alpha=0.756$ and $\varepsilon_a/\varepsilon_\perp=1.643$.

## 6 Summary

We have derived a model for the dynamics of the director of a nematic liquid crystal under the influence of an electric field using an energy variational approach. Contrary to most of the literature, we have included both inertial forces and dissipation in our model. The model is coupled with the stationary Maxwell's equation for the electric field.

A semi-discrete numerical scheme has been proposed for solving the model. The method is an adaptation of a previously proposed scheme for a related variational wave equation modeling liquid crystals.

Numerical experiments have been performed demonstrating the influence of the relative strength between dissipative and inertial forces on two well-known cases from the literature. Both cases involve the reorientation of director field on a finite domain when applying an electric voltage. We observe that for moderate dissipation the transition times are proportional to the dissipation constant. However, when the scaling of the problem is such that the inertial term becomes dominant, this behavior breaks down as standing waves slow down or prevent the relaxation to electrostatic equilibrium.

## Acknowledgments

The work of Peder Aursand and Johanna Ridder has been funded by the Research Council of Norway (project numbers 213638 and 214495, respectively).

The authors are grateful to Professor Nils Henrik Risebro and Professor Helge Holden for useful advice in the course of the preparation of this manuscript.

**References**


[1] Giuseppe Alì and John K. Hunter. Orientation waves in a director field with rotational inertia. Kinet. Relat. Models, 2(1):1–37, 2009.

[2] G. Chen and Y. Zheng. Singularity and existence to a wave system of nematic liquid crystals. J. Math. Anal. Appl., 398(1):170–188, 2013.

[3] P. G. De Gennes and J. Prost. The Physics of Liquld Crystals. Clarendon Press, Oxford, 1993.

[4] H. J. Deuling. Deformation of nematic liquid crystals in an electric field. Molecular Crystals and Liquid Crystals, 19(2):123–131, 1972.

[5] H. J. Deuling. Deformation pattern of twisted nematic liquid crystal layers in an electric field. Mol. Cryst. Liq. Cryst., 27(1-2):81–93, 1974.

[6] B. J. Frisken and P. Palffy-Muhoray. Electric-field-induced twist and bend Freedericksz transitions in nematic liquid crystals. Phys. Rev. A, 39(3):1513, 1989.

[7] X. Gang, S. Chang-Qing, and L. Lei. Perturbed solutions in nematic liquid crystals under time-dependent shear. Phys. Rev. A, 36(1):277–284, 1987.

[8] R.T. Glassey, J.K. Hunter, and Y. Zheng. Singularities of a variational wave equation. J. Diff. Eq., 129(1):49–78, 1996.

[9] S. Gottlieb, C.W. Shu, and E. Tadmor. Strong stability-preserving high-order time discretization methods. SIAM Rev., 43(1):89–112, 2001.

[10] H. Holden, K.H. Karlsen, and N.H. Risebro. A convergent finite-difference method for a nonlinear variational wave equation. IMA J. Numer. Anal., 29(3):539–572, 2009.

[11] H. Holden and X. Raynaud. Global semigroup of conservative solutions of the nonlinear variational wave equation. Arch. Rat. Mech. Anal., 201(3):871–964, 2011.

[12] J. K. Hunter and R. Saxton. Dynamics of director fields. SIAM J. Appl. Math., 51(6):1498–1521, 1991.

[13] Y. Hyon, D. Y. Kwak, and C. Liu. Energetic variational approach in complex fluids: Maximum dissipation principle. Disc. Cont. Dyn. Sys., 26:1291–1304, 2010.

[14] O.A. Kapustina. Liquid crystal acoustics: A modern view of the problem. Crystallogr. Rep., 49(4):680–692, 2004.

[15] U. Koley, S. Mishra, N. H. Risebro, and F. Weber. Robust finite difference schemes for a nonlinear variational wave equation modeling liquid crystals. ArXiv e-prints, 2013.

[16] L. D. Landau and E. M. Lifshitz. Statistical physics, volume 5. Pergamon Press, 1969.

[17] M. F. Ledney and O. S. Tarnavskyy. Influence of the anchoring energy on hysteresis at the Freedericksz transition in confined light beams in a nematic cell. Liq. Cryst., 39(12):1482–1490, 2012.

[18] E. K. Lenzi and G. Barbero. Relaxation of the nematic deformation when the distorting field is removed. Phys. Rev. E, 81:021703, 2010.

[19] F. M. Leslie. Theory of flow phenomena in liquid crystals. Adv. Liq. Cryst., 4:1–81, 1979.

[20] V. B. Lisin and A. I. Potapov. Nonlinear interactions between acoustic and orientation waves in liquid crystals. Radiophysics and Quantum Electronics, 38(1–2):98–101, 1995.

[21] E. H. MacMillan. A theory of anisotropic fluids. PhD thesis, University of Minnesota, 1987.

[22] G. A. Maximov. Generalized variational principle for dissipative continuum mechanics. In Mechanics of Generalized Continua, volume 21 of Advances in Mechanics and Mathematics, pages 297–305. Springer New York, 2010.

[23] N. J. Mottram and C. J. P. Newton. Handbook of Visual Display Technology: Liquid crystal theorey and modelling. Springer-Verlag, Berlin, 2012.

[24] R. A. Saxton. Dynamic instability of the liquid crystal director. In W. B. Lindquist, editor,

Contemporary Mathematics, volume 100 of Current Progress in Hyperbolic Systems, Providence, RI, USA, 1989., pages 325–330, 1989.

[25] I. W. Stewart. The static and dynamic continuum theory of liquid crystals: a mathematical introduction. CRC Press, 2004.

[26] C. Z. van Doorn. Dynamic behavior of twisted nematic liquidcrystal layers in switched fields. J. Appl. Phys., 46:3738–3745, 1975.

[27] V. A. Vladimirov and M. Y. Zhukov. Vibrational Freedericksz transition in liquid crystals. Phys. Rev. E, 76:031706, 2007.

[28] Q. A. Wang and R. Wang. Is it possible to formulate least action principle for dissipative systems? ArXiv e-prints, 2012.

[29] C. K. Yun. Inertial coefficient of liquid crystals: A proposal for its measurements. Phys. Rev. A, 45(2):119–120, 1973.

# Paper B

**On the dynamics of the weak Fréedericksz transition for nematic liquid crystals**

Peder Aursand, Gaetano Napoli and Johanna Ridder

Submitted for publication.

## Preface

The origin of this work is a personal communication between Johanna Ridder, Gaetano Napoli and myself regarding Paper A. Professor Napoli is an expert on weak anchoring effects in the Fréedericksz transition and expressed interest in the dynamics of this problem. In the work that followed, we were able to numerically show how introducing weak boundaries make the dynamic problem ill-posed, since several stable equilibriums exist.

Together with Johanna, and following the advice of professor Napoli, we extended the code from Paper A in order to account for weak boundary conditions. A big part of this work was figuring out a stable and efficient numerical scheme that was able to handle a large range of electric fields and boundary strengths. Then, having a robust code, we could go on to systematically study how the different aspects of the static theory manifest in the dynamic problem.

# ON THE DYNAMICS OF THE WEAK FRÉEDERICKSZ TRANSITION FOR NEMATIC LIQUID CRYSTALS

P. AURSAND, G. NAPOLI, AND J. RIDDER

Abstract. We consider the dynamics of the director in a nematic liquid crystal cell with an applied electric field. The bend-splay geometry is assumed, and the director is weakly anchored at the boundary. For this setting, excited equilibrium states of odd parity have been observed experimentally by Kumar et al. (2010) and investigated analytically by Bevilacqua and Napoli (2012), but the dynamics of the transition between them has so far not been the subject of much study.

An implicit finite difference method is derived for studying the time-evolution of the director field under varying voltages and anchoring strengths. The scheme solves the general nonlinear equations, i.e., it does not assert the one-constant approximation, and allows coupling with Gauss' law for the electric field. Through numerical simulation of basic transition experiments, we show how excited states of odd parity can manifest, also in the general nonlinear case.

## 1. Introduction

1.1. **Background.** Nematic liquid crystals usually consist of rod-shaped organic molecules for which it is energetically favorable for neighboring molecules to align. This causes macroscopic correlation in the orientation of their long axis, while the molecules themselves are free to flow like a liquid. Nematic liquid crystals have seen widespread use in display devices, due to the optical birefringence associated with the anisotropy of the molecules. Since the orientation of the long axis can be manipulated by applied electromagnetic fields, polarized light can be either stopped by or let through a liquid crystal cell, depending on the applied voltage difference.

Under the assumption of constant degree of orientation, the state of a nematic liquid crystal is often represented in terms of two linearly independent vector fields: the velocity field giving the flow and the

*Date*: June 21, 2015.

*Key words and phrases.* Nematic liquid crystals; Fréedericksz transition; Weak anchoring.

director field giving the local average molecular orientation. In this work we will assume a steady flow field and focus on the dynamics of the director. This implies disregarding phenomena such a back-flow, which can be important in the rheology of liquid crystals [5]. Furthermore, we will restrict our discussion to a one-dimensional liquid crystal cell on $x \in [0, L]$ in the bend-splay geometry. Specifically, we assume the director $\mathbf{n}$ is fixed to the $x - y$ plane, i.e.,

$$\mathbf{n}(x,t) = (\cos(\psi(x,t)), \sin(\psi(x,t)), 0), \tag{1}$$

where $\psi$ is the angle between the $x$-axis and the director. Herein, we will consider numerical solutions to the initial-value problem

$$q\psi_T - \tilde{c}(\psi)(\tilde{c}(\psi)\psi_X)_X + \frac{1}{2}h^2 \sin(2\psi)\tilde{E}^2 = 0, \qquad (X,T) \in (0,1) \times \mathbb{R}^+, \tag{2a}$$

$$\psi(X,0) = \psi_0(X), \qquad X \in (0,1), \tag{2b}$$

with boundary conditions

$$\psi_X + \frac{1}{2}\frac{\beta}{\tilde{c}^2(\psi)} \sin(2\psi) = 0, \quad X = 0, \tag{3a}$$

$$\psi_X - \frac{1}{2}\frac{\beta}{\tilde{c}^2(\psi)} \sin(2\psi) = 0, \quad X = 1. \tag{3b}$$

In the above, the dimensionless constants $q$, $h$ and $\beta$ represent dissipation, field strength and anchoring strength, respectively, and

$$\tilde{c}(\psi) = \sqrt{\cos^2(\psi) + \frac{\alpha_2}{\alpha_1}\sin^2(\psi)}.$$

The classical example of interaction between the director field and an external electric or magnetic field is the Fréedericksz transition. In its most basic form, it can be described as a competition between elastic torques resisting distortions in the director field, and electromagnetic torques aligning molecules along a preferred direction: Consider e.g. a liquid crystal cell where the the easy direction at the surfaces is fixed at $\psi = \pi/2$. The equilibrium configuration is then a homogeneous director field. An electric field is applied twisting the director towards the angle $\pi$. When the applied field is below some critical value, $E < E_{\mathrm{F}}$, elastic forces dominate and the constant director state $\psi = \pi/2$ is stable. However, when the field is sufficiently strong, $E > E_{\mathrm{F}}$, the equilibrium state becomes a nontrivial configuration where $\pi/2 < \psi \leq \pi$ in the interior of the domain. This sudden realignment is what is often referred to as the Fréedericksz transition.

Usually, the surfaces of liquid crystals are designed in such a way that the director remains strongly anchored at normal operating voltages in display devices [3]. However, it has been theorized that having more weakly anchored director fields at the surfaces could allow for lower operating voltages and quicker response times [10]. In the modeling, this can be introduced by applying *weak* boundary conditions, i.e., introducing an energy penalty for deviations from the anchoring angle [11]. As shown in Figure 1, in the weak Fréedericksz transition there are *two* critical points. The first one, as in the classic case, represents electric forces overcoming the elastic. The second, the *saturation* threshold, is reached when the electric torque is strong enough to overcome the boundary anchoring. Here, the stable configuration is

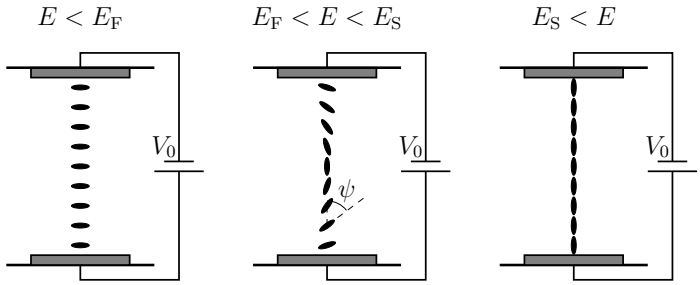


FIGURE 1. Illustration of the weak Fréedericksz transition. Left: For a low electric field the anchoring forces dominate and the director field is in a homogeneous ($\psi = \pi/2$) configuration. Middle: For electric fields above the Fréedericksz threshold but below the saturation threshold there is a competition between electric and anchoring forces leading to a nontrivial configuration. Right: For strong electric fields (over the saturation threshold) the electric forces overcome the anchoring and the configuration is homeotropic ($\psi = 0$).

a constant homeotropic ($\psi = \pi$) state.

Since it was proposed by Rapini and Papoular [11], the weak Fréedericksz transition has been an important part of the liquid crystal literature [5, 13, 12]. In their recent paper, Costa et al. [4] were able to prove a uniqueness property for stationary solutions of the weak Fréedericksz transition. Specifically, they showed that for any given values of the

applied field, field susceptibility, elastic constants and anchoring energy, there exists a unique solution $\psi(x) \in [0, \pi/2]$ of the equations describing the force balance of the director field.

However, in their recent work, Kumar et al. [7] observed experimentally director states that break the even symmetry around the center of the cell. This discovery led Bevilacqua and Napoli [2] to investigate the uniqueness of minimizers of the free energy on the full interval $\psi \in [0, \pi]$. Specifically, they studied the model

$$\psi_{XX} - \frac{1}{2}h^2 \sin(2\psi) = 0, \qquad X \in (0, 1), \tag{4}$$

with boundary conditions

$$\psi_X + \frac{1}{2}\beta \sin(2\psi) = 0, \quad X = 0, \tag{5a}$$

$$\psi_X - \frac{1}{2}\beta \sin(2\psi) = 0, \quad X = 1, \tag{5b}$$

where $h$ is the dimensionless field and $\beta$ is the dimensionless anchoring strength. By using direct methods and calculating exact solutions, they showed that there exists a hierarchy of excited states satisfying the stationary equations (4)–(5). Moreover, these solutions were shown to be of different parities.

The nonuniqueness of stationary solutions for the weak Fréedericksz transition makes the dynamics of the problem particularly interesting, and herein lies the main purpose of this paper. Given a constant electric field ($\tilde{E} = 1$) and the one-constant approximation ($\alpha_1 = \alpha_2$), the model (2)–(3) reduces to that of Bevilacqua and Napoli (4)–(5). However, it is not clear how the existence of excited stationary director states will effect the dynamics of the Fréedericksz transition. We aim to derive a robust and efficient numerical scheme for (2)–(3), and use this to study the evolution of the director field. Specifically, we wish to address two questions:

(1) How will excited equilibrium states manifest in the basic Fréedericksz transition experiment?
(2) Will relaxing the one-constant approximation and coupling with a nonconstant electric field influence the experiment?

To the best of our knowledge, this work is the first attempt to numerically study the dynamic transition to excited director states in the Fréedericksz transition with weak anchoring.

This paper is organized as follows: In Section 2 we use an energy variational approach to derive the basic nondimensional model under

consideration (2)–(3). Different simplifications with regard to the electric field and elasticity will be also be discussed. Section 3 concerns an implicit numerical time-stepping scheme for solving the governing equations. Herein, we show the well-posedness of the nonlinear implicit equations of the discrete problem. In Section 4 we perform numerical experiments addressing the questions posed above. In particular, we will show that excited director states can be observed in numerical experiments.

## 2. Variational derivation of the dynamic model

The governing equations for the director field will be derived by assering an energy law for the system. The time evolution of the director field is then given by a dissipative variational principle.

2.1. **The full model.** Under the assumption that $\mathbf{n}$ is given by (1), the governing equations for the director field will be derived using the different contributions to the energy with an action principle. Expressed in terms of $\psi$, the bulk kinetic energy can be written as

$$W_{\mathrm{K}} = \frac{1}{2}\int_0^L \sigma\psi_t^2 \,\mathrm{d}x,$$

where $\sigma$ is an inertial constant. A typical value for $\sigma$ is $\sim 10^{-13}\,\mathrm{kg\,m^{-1}}$ (for the nematic MBBA [6]).

The elasticity of the liquid crystal will resist distortions in the director field. The standard model for the elasticity in nematics is given by the Oseen–Frank free energy density

$$\mathcal{W}_{OF}(\mathbf{n},\nabla\mathbf{n}) = \frac{1}{2}\alpha_1|\mathbf{n}\times(\nabla\times\mathbf{n})|^2 + \frac{1}{2}\alpha_2(\nabla\cdot\mathbf{n})^2 + \frac{1}{2}\alpha_3(\mathbf{n}\cdot(\nabla\times\mathbf{n}))^2\,. \quad (6)$$

The energy (6) is the most general form which is both quadratic in $\nabla\mathbf{n}$ and invariant with respect to the transformation $\mathbf{n}\to-\mathbf{n}$. The constants $\alpha_1$, $\alpha_2$ and $\alpha_3$ represents bend, splay and twist distortions, respectively. For the typical liquid crystal 5CB, values have been measured to $\alpha_1 = 8.2\times10^{-12}\,\mathrm{N}$, $\alpha_2 = 6.2\times10^{-12}\,\mathrm{N}$, and $\alpha_3 = 3.9\times10^{-12}\,\mathrm{N}$. Given the director field (1), the elastic bulk energy takes the form

$$W_{\mathrm{OF}} = \frac{1}{2}\int_0^L c^2(\psi)\psi_x^2 \,\mathrm{d}x$$

with

$$c(\psi) = \sqrt{\alpha_1\cos^2(\psi) + \alpha_2\sin^2(\psi))}\,.$$

The anisotropic nature of the molecules will cause the electric displacement in the liquid crystal to depend on the director field. In what

follows, we will assume that the contribution to the displacement is purely dielectric and given by

$$\mathbf{D} = \varepsilon_0(\varepsilon_\perp \mathbf{E} + \varepsilon_a(\mathbf{n}\cdot\mathbf{E})\mathbf{n}), \tag{7}$$

where $\varepsilon_0 = 8.854 \times 10^{-12}\,\mathrm{F\,m^{-1}}$ is the permittivity in free space, $\varepsilon_\perp$ is the relative permittivity perpendicular to the director ($\varepsilon_\perp = 7$ for 5CB [12]) and $\varepsilon_a$ is the dielectric anisotropy ($\varepsilon_a = 11.5$ for 5CB [12]). The contribution to the bulk energy from the electric field is then

$$W_{\mathrm{E}} = -\frac{1}{2}\int_0^L \mathbf{E}\cdot\mathbf{D}\,\mathrm{d}x = -\frac{1}{2}\int_0^L d(\psi)E^2\,\mathrm{d}x, \tag{8}$$

where

$$d(\psi) = \varepsilon_0(\varepsilon_\perp + \varepsilon_a\cos^2(\psi)).$$

We assume that the surfaces at each end of the cell has been treated in such a way that a particular director orientation is energetically preferred. To achieve this, we apply an anchoring potential, and let

$$W_{\mathrm{B}} = \frac{1}{2}w\cos^2(\psi), \quad x = 0, L \tag{9}$$

for some constant $w$ representing the anchoring strength. We note that for this choice the parallel (homogeneous) alignment will be energetically preferred at the boundary for $w > 0$ and, conversely, the homeotropic for $w < 0$.

The energy dissipation rate is assumed to be of the form

$$D = \frac{1}{2}\kappa\int_0^L \psi_t^2\,\mathrm{d}x, \tag{10}$$

where $\kappa$ is a dissipation constant. For the liquid crystal MBBA, $\kappa = 0.0777\,\mathrm{Pa\,s}$, [12].

Taking into account elastic, electric and boundary energies, the total energy balance takes the form

$$\frac{\mathrm{d}}{\mathrm{d}t}\Big(\frac{1}{2}\int_0^L \big(\sigma\psi_t^2 + c^2(\psi)\psi_x^2 - d(\psi)E^2\big)\mathrm{d}x + \frac{1}{2}w\cos^2(\psi)\,(|_{x=0}+|_{x=L})\Big) = -\frac{1}{2}\kappa\int_0^L \psi_t^2\,\mathrm{d}x. \tag{11}$$

Following the approach from [1], we can use the dissipative principle of least action to derive the evolution equation

$$\sigma\psi_{tt} + \kappa\psi_t - c(\psi)(c(\psi)\psi_x)_x - \frac{1}{2}d'(\psi)E^2 = 0, \qquad (x,t)\in(0,L)\times\mathbb{R}^+, \tag{12}$$

with boundary conditions

$$c^2(\psi)\psi_x + \frac{w}{2}\sin(2\psi) = 0, \quad x = 0, \tag{13a}$$

$$c^2(\psi)\psi_x - \frac{w}{2}\sin(2\psi) = 0, \quad x = L. \tag{13b}$$

In the rest of this paper, we will follow common practice and assume that the inertial term can be neglected in favor of dissipative forces, i.e. $\sigma = 0$.

In general, the electric field will depend on the director configuration through Gauss' law. Under the assumptions above, we can write the field $E = -U_x$, and the equation to be solved is

$$\left(d(\psi)U_x\right)_x = 0\,,$$

with boundary conditions $U(0) = 0$ and $U(L) = V_0$. Hence, for a given director configuration, $U_x$ can be determined by

$$U_x(x) = \frac{1}{d(\psi(x))}\Big(\int_0^L \frac{1}{d(\psi(x'))}\,\mathrm{d}x'\Big)^{-1} V_0\,. \tag{14}$$

In the interest of deriving a dimensionless version of the model (12)–(13), we introduce the scalings $X = x/L$, $T = t/\tau$ and $u = U/V_0$. Here, $\tau$ is some characteristic time scale for the dynamics of the system. Furthermore, we follow Bevilacqua and Napoli [2] and introduce the *extrapolation length*

$$\ell = \frac{\alpha_1}{w}$$

and the *electric coherence length*

$$\xi = \frac{L}{V_0}\sqrt{\frac{\alpha_1}{\varepsilon_0\varepsilon_a}}$$

Moreover, we define the nondimensional quantities

$$\tilde{c}(\psi) = \sqrt{\cos^2(\psi) + \frac{\alpha_2}{\alpha_1}\sin^2(\psi)}, \quad h = \frac{L}{\xi}, \quad \beta = \frac{L}{\ell} \quad \text{and} \quad q = \frac{L^2\kappa}{\alpha_1\tau}.$$

Using the numbers defined above, we can write (12) in the equivalent form

$$q\psi_T - \tilde{c}(\psi)(\tilde{c}(\psi)\psi_X)_X + \frac{1}{2}h^2\sin(2\psi)u_X^2 = 0, \qquad (X,T) \in (0,1)\times\mathbb{R}^+\,, \tag{15}$$

and for the boundary conditions (13),

$$\psi_X + \frac{1}{2}\frac{\beta}{\tilde{c}^2(\psi)}\sin(2\psi) = 0, \quad X = 0, \tag{16a}$$

$$\psi_X - \frac{1}{2}\frac{\beta}{\tilde{c}^2(\psi)}\sin(2\psi) = 0, \quad X = 1. \tag{16b}$$

2.2. **Constant electric field approximation.** The assumption that the electric field remains constant, i.e., is unaffected by the state of the director field, can be introduced by removing the coupling with Gauss' law. The nondimensional electric field is then given by $u_X = 1$, and we can replace (15) with

$$q\psi_T - \tilde{c}(\psi)(\tilde{c}(\psi)\psi_X)_X + \frac{1}{2}h^2\sin(2\psi) = 0, \qquad (X,T) \in (0,1)\times\mathbb{R}^+, \tag{17}$$

endowed with the boundary condition (16).

2.3. **One-constant approximation.** A common simplification made in the literature is the so-called one-constant approximation $\alpha_1 = \alpha_2 = \alpha_3$. Under this assumption we have $\tilde{c}(\psi) = 1$, and the nondimensional problem can be written as

$$q\psi_T - \psi_{XX} + \frac{1}{2}h^2\sin(2\psi) = 0, \qquad (X,T) \in (0,1)\times\mathbb{R}^+, \tag{18}$$

with boundary conditions

$$\psi_X + \frac{1}{2}\beta\sin(2\psi) = 0, \quad X = 0, \tag{19a}$$

$$\psi_X - \frac{1}{2}\beta\sin(2\psi) = 0, \quad X = 1. \tag{19b}$$

**Remark 2.1.** *A simple transformation $X \to X - 1/2$ and $\psi \to \pi/2 - \psi$ reveals that the stationary version of* (18)–(19) *is equivalent to the problem studied by Bevilacqua and Napoli [2].*

## 3. The numerical method

To define the numerical scheme, divide the interval $[0,1]$ into $N$ cells of length $\Delta X$ and choose a time step $\Delta T$. This gives grid points

$$(X_i, T^n) = (i\Delta X, n\Delta T),$$

where $i = 0,\dots,N$ and $n \in \mathbb{N}$. The numerical method defined below will calculate values $\psi_i^n$ that approximate the exact solution $\psi$ on these grid points.

The discretization defined below is based on central differences. However, derivatives in space must be handled with care to accommodate the fact that the director describes the orientation of symmetric molecules, i.e., $\mathbf{n} = -\mathbf{n}$. For example, $\psi_0^n = 0$ and $\psi_1^n = \frac{\pi}{2}$ describe physically the same situation as $\psi_0^n = 0$ and $\psi_1^n = \frac{3\pi}{2}$, and should thus give rise to the same elastic energy. Hence, the straightforward discretization $D_X\psi^n_{i+\frac{1}{2}} = \frac{1}{\Delta X}(\psi^n_{i+1} - \psi^n_i)$ is adjusted to

$$\begin{aligned}
&D_X\psi^n_{i+\frac{1}{2}} \cdot \Delta X \\
&= p_{[-\frac{\pi}{2},\frac{\pi}{2})}(\psi^n_{i+1} - \psi^n_i) \\
&:= \begin{cases} (\psi^n_{i+1} - \psi^n_i) \bmod \pi & \text{if } ((\psi^n_{i+1} - \psi^n_i) \bmod \pi) \in [0, \frac{\pi}{2}), \\ ((\psi^n_{i+1} - \psi^n_i) \bmod \pi) - \pi & \text{otherwise,} \end{cases}
\end{aligned}$$

which guarantees $D_X\psi^n_{i+\frac{1}{2}} \cdot \Delta X \in [-\frac{\pi}{2}, \frac{\pi}{2})$. For the discretization in time such an adjustment is not necessary, because $|\psi_i^{n+1} - \psi_i^n| < \pi/2$ for sufficiently small time steps.

For better readability, define the averages

$$\psi_i^{n+\frac{1}{2}} = \frac{1}{2}(\psi_i^n + \psi_i^{n+1}), \qquad \sin(2\psi_i)^{n+\frac{1}{2}} = \frac{1}{2}\left(\sin(2\psi_i^n) + \sin(2\psi_i^{n+1})\right),$$
$$c_i^{n+\frac{1}{2}} = \frac{1}{2}\left(\tilde{c}(\psi_i^n) + \tilde{c}(\psi_i^{n+1})\right), \qquad c_{i+\frac{1}{2}}^{n+\frac{1}{2}} = \frac{1}{2}\left(c_i^{n+\frac{1}{2}} + c_{i+1}^{n+\frac{1}{2}}\right),$$

and the difference operators

$$D_T\psi_i^{n+\frac{1}{2}} = \frac{1}{\Delta T}(\psi_i^{n+1} - \psi_i^n), \quad D_X\psi_{i+\frac{1}{2}}^{n+\frac{1}{2}} = \frac{1}{\Delta X}p_{[-\frac{\pi}{2},\frac{\pi}{2})}(\psi_{i+1}^{n+\frac{1}{2}} - \psi_i^{n+\frac{1}{2}}),$$

and accordingly,

$$D_X(c\, D_X\psi)_i^{n+\frac{1}{2}} = \frac{1}{\Delta X}\left(c_{i+\frac{1}{2}}^{n+\frac{1}{2}}(D_X\psi)_{i+\frac{1}{2}}^{n+\frac{1}{2}} - c_{i-\frac{1}{2}}^{n+\frac{1}{2}}(D_X\psi)_{i-\frac{1}{2}}^{n+\frac{1}{2}}\right).$$

The following implicit finite difference scheme discretizes the nonlinear model with constant electric field (17) and weak anchroing boundary conditions (16).

**Definition 1** (The numerical method)**.** *Let some initial data $\psi_i^0$, $i = 0, \ldots, N$ be given. For each time step $n = 1, 2, 3, \ldots$, define $\psi_1^{n+1}, \ldots, \psi_{N-1}^{n+1}$ by*

$$qD_T\psi_i^{n+\frac{1}{2}} - c_i^{n+\frac{1}{2}}D_X(c\, D_X\psi)_i^{n+\frac{1}{2}} + \frac{1}{2}h^2\sin(2\psi_i)^{n+\frac{1}{2}} = 0, \qquad (20)$$

*and* $\psi_0^{n+1}$, $\psi_N^{n+1}$ *by*

$$D_X\psi_{\frac{1}{2}}^{n+\frac{1}{2}} + \frac{\beta}{2c_{\frac{1}{2}}^{n+\frac{1}{2}}c_0^{n+\frac{1}{2}}}\sin(2\psi_0^{n+\frac{1}{2}}) = 0\,, \tag{21a}$$

$$D_X\psi_{N-\frac{1}{2}}^{n+\frac{1}{2}} - \frac{\beta}{2c_{N-\frac{1}{2}}^{n+\frac{1}{2}}c_N^{n+\frac{1}{2}}}\sin(2\psi_N^{n+\frac{1}{2}}) = 0\,. \tag{21b}$$

A corresponding discrete version of the energy (11) is given by

$$\begin{aligned} E^n = \frac{\Delta X}{2}\left(\sum_{i=1}^{N-1}\left(c_{i+\frac{1}{2}}^n\right)^2\left(D_X\psi_{i+\frac{1}{2}}^n\right)^2 - h^2\left(\frac{\varepsilon_\perp}{\varepsilon_a} + \cos^2(\psi_i^n)\right)\right) \\ + \frac{\beta}{2}\Big(\cos^2(\psi_0^n) + \cos^2(\psi_N^n)\Big). \end{aligned} \tag{22}$$

In the following we will show that the implicit equations that define the scheme have a unique solution. Furthermore, we will prove that scheme conserves approximately a discrete energy and converges to the exact solution as $\Delta X$ and $\Delta T$ go to zero.

3.1. **Well-definedness of the scheme.** For fixed $\psi_i^n$, $i = 0, \dots, N$, equations (20)–(21) can be written in the fixed point form

$$(\psi_0^{n+1}, \dots, \psi_N^{n+1}) = \mathcal{F}(\psi_0^{n+1}, \dots, \psi_N^{n+1})\,,$$

where $\mathcal{F}$ is given by

$$\begin{aligned} (\mathcal{F}(\psi_0^{n+1}, \dots, \psi_N^{n+1}))_i = \psi_i^n + \frac{\Delta T}{q}c_i^{n+\frac{1}{2}}D_X(c\,D_X\psi)_i^{n+\frac{1}{2}} \\ - \frac{\Delta T}{2q}h^2\sin(2\psi_i)^{n+\frac{1}{2}}\,, \end{aligned} \tag{23a}$$

for $i = 1, \dots, N-1$, and, for $\Delta X$ sufficiently small,

$$(\mathcal{F}(\psi_0^{n+1}, \dots, \psi_N^{n+1}))_0 = -\psi_0^n + 2\psi_1^{n+\frac{1}{2}} + \frac{\beta\Delta X}{c_{\frac{1}{2}}^{n+\frac{1}{2}}c_0^{n+\frac{1}{2}}}\sin(2\psi_0^{n+\frac{1}{2}})\,, \tag{23b}$$

$$(\mathcal{F}(\psi_0^{n+1}, \dots, \psi_N^{n+1}))_N = -\psi_N^n + 2\psi_{N-1}^{n+\frac{1}{2}} + \frac{\beta\Delta X}{c_{N-\frac{1}{2}}^{n+\frac{1}{2}}c_N^{n+\frac{1}{2}}}\sin(2\psi_N^{n+\frac{1}{2}})\,. \tag{23c}$$

Hence, (20)–(21) have a solution if $\mathcal{F}$ is a contraction.

To show this, first define the constants

$$|\widetilde{c}(\psi)| = \sqrt{\cos^2(\psi) + \frac{\alpha_2}{\alpha_1}\sin^2(\psi)} \leq \max\left(1, \sqrt{\frac{\alpha_2}{\alpha_1}}\right) =: C_1\,,$$
$$|\widetilde{c}'(\psi)| = \frac{|\frac{\alpha_2}{\alpha_1} - 1||\sin(\psi)\cos(\psi)|}{\sqrt{\cos^2(\psi) + \frac{\alpha_2}{\alpha_1}\sin^2(\psi)}} \leq \frac{\frac{1}{2}|\frac{\alpha_2}{\alpha_1} - 1|}{\min\left(1, \sqrt{\frac{\alpha_2}{\alpha_1}}\right)} =: C_2\,,$$
$$|\widetilde{c}(\psi)| = \sqrt{\cos^2(\psi) + \frac{\alpha_2}{\alpha_1}\sin^2(\psi)} \geq \min\left(1, \sqrt{\frac{\alpha_2}{\alpha_1}}\right) =: C_3\,,$$

and note that if $\|\psi^n\|_{l^\infty} \leq K_0$, for some constant $K_0$, then

$$|\mathcal{F}(\psi^{n+1})_i| \leq K_0 + \frac{\Delta T}{q} C_1^2 \frac{1}{\Delta X^2}(2(K_0 + \|\psi^{n+1}\|_{l^\infty})) + \frac{\Delta T}{2q}h^2\,,$$

for $i = 1, \ldots, N-1$,

$$|\mathcal{F}(\psi^{n+1})_0| \leq K_0 + 2\left(\frac{1}{2}(K_0 + \mathcal{F}(\psi^{n+1})_1)\right) + \frac{\beta}{C_3^2}\Delta X\,,$$

and similarly for $|\mathcal{F}(\psi^{n+1})_N|$.

Next, choose some $K_1, K_2, K_3 > 0$ and $\Delta X$, $\Delta T$, such that

$$\Delta X \leq \frac{C_3^2}{\beta} K_1\,, \tag{24a}$$
$$\Delta T \leq \frac{2q}{h^2} K_2\,, \tag{24b}$$
$$\Delta T \leq \frac{q}{2C_1^2} \frac{K_3 \Delta X^2}{K_0 + (3K_0 + K_1 + K_2 + K_3)}\,. \tag{24c}$$

Then, for $\|\psi^{n+1}\|_{l^\infty} \leq 3K_0 + K_1 + K_2 + K_3$, we have

$$\begin{aligned}
|\mathcal{F}(\psi^{n+1})_i| &\leq K_0 + K_2 + K_3\,, \quad \text{for } i = 1, \ldots, N-1,\\
|\mathcal{F}(\psi^{n+1})_0| &\leq K_0 + 2 \cdot \frac{1}{2}(K_0 + (K_0 + K_2 + K_3)) + K_1\\
&= 3K_0 + K_1 + K_2 + K_3\,,\\
|\mathcal{F}(\psi^{n+1})_N| &\leq 3K_0 + K_1 + K_2 + K_3\,,
\end{aligned}$$

i.e., $\|\mathcal{F}(\psi^{n+1})\|_{l^\infty} \leq 3K_0 + K_1 + K_2 + K_3$.

Since $\psi$ describes the angle of the director, we can choose $K_0 = \pi$. For any $K > 3K_0$, set $K_i = K/3 - K_0$ for $i = 1, 2, 3$, and choose $\Delta T$ and $\Delta X$ according to (24). Above we have shown that $\mathcal{F}$ maps

$$B_K := \{\psi^{n+1} | \|\psi^{n+1}\|_{l^\infty} \leq K\}$$

on (a subset of) itself. The following theorem states that $\mathcal{F}$ is also a contraction on $B_K$, from which follows that $\mathcal{F}$ has a unique fix point

in $B_K$ and hence the implicit equations that define the scheme have a unique solution.

**Theorem 1.** *The function $\mathcal{F}$ defined in* (23) *is a contraction on $B_K$ with respect to the $l^\infty$-norm if $\Delta T$ and $\Delta X$ satisfy* (24) *and in addition,*

$$\Delta T \left( \frac{C_A}{\Delta X^2} + C_{B_1} \right) + \Delta X C_{B_2} < 1$$

*for $C_A$, $C_{B_1}$, $C_{B_2}$ defined by* (25) *below, depending only on $K$ and the physical constants $\alpha_1$, $\alpha_2$, $h$, $q$, and $\beta$.*

*Proof.* In the following, we will prove that for arbitrary $\psi^{n+1}$ and $\widehat{\psi}^{n+1}$,

$$\|\mathcal{F}(\widehat{\psi}^{n+1}) - \mathcal{F}(\psi^{n+1})\|_{l^\infty} \leq C \|\widehat{\psi}^{n+1} - \psi^{n+1}\|_{l^\infty} ,$$

for some $C < 1$. Note that $\psi^n$ in the definition of $\mathcal{F}$ is the same for both $\mathcal{F}(\psi^{n+1})$ and $\mathcal{F}(\widehat{\psi}^{n+1})$. For the sake of brevity, define $\widehat{c}_i^{\,n+\frac{1}{2}} = (\widetilde{c}(\psi_i^n) + \widetilde{c}(\widehat{\psi}_i^{n+1}))/2$.

For $i = 1, \ldots, N-1$,

$$\begin{aligned}
|\mathcal{F}(\widehat{\psi}^{n+1})_i - \mathcal{F}(\psi^{n+1})_i| \leq \frac{\Delta T}{q} \Big( & |\widehat{c}_i^{\,n+\frac{1}{2}} - c_i^{n+\frac{1}{2}}| |D_X(\widehat{c} D_X \widehat{\psi})_i^{n+\frac{1}{2}}| \\
& + |c_i^{n+\frac{1}{2}}| |D_X((\widehat{c} - c) D_X \widehat{\psi})_i^{n+\frac{1}{2}}| \\
& + |c_i^{n+\frac{1}{2}}| |D_X(c(D_X(\widehat{\psi} - \psi)))_i^{n+\frac{1}{2}}| \Big) \\
& + \frac{h^2 \Delta T}{2q} |\sin(2\psi_i)^{n+\frac{1}{2}} - \sin(2\widehat{\psi}_i)^{n+\frac{1}{2}}| .
\end{aligned}$$

This can be further bounded by

$$\begin{aligned}
& |\widehat{c}_i^{\,n+\frac{1}{2}} - c_i^{n+\frac{1}{2}}| |D_X(\widehat{c} D_X \widehat{\psi})_i^{n+\frac{1}{2}}| \\
& \leq \frac{1}{\Delta X} \|\widetilde{c}'\|_{l^\infty} \|\widetilde{c}\|_{l^\infty} |\widehat{\psi}_i^{n+1} - \psi_i^{n+1}| \|D_X \widehat{\psi}_{i+\frac{1}{2}}^{n+\frac{1}{2}}\|_{l^\infty} \\
& \leq \frac{1}{2\Delta X} C_1 C_2 |\widehat{\psi}_i^{n+1} - \psi_i^{n+1}| (\|D_X \widehat{\psi}_{i+\frac{1}{2}}^{n+1}\|_{l^\infty} + \|D_X \psi_{i+\frac{1}{2}}^{n}\|_{l^\infty}) \\
& \leq \frac{C_1 C_2}{\Delta X^2} (\|\widehat{\psi}^{n+1}\|_{l^\infty} + \|\psi^n\|_{l^\infty}) \|\widehat{\psi}^{n+1} - \psi^{n+1}\|_{l^\infty} ,
\end{aligned}$$

and in the same manner

$$|c_i^{n+\frac{1}{2}}||D_X((\widehat{c}-c)D_X\widehat{\psi})_i^{n+\frac{1}{2}}| \le \frac{C_1C_2}{\Delta X^2}(\|\widehat{\psi}^{n+1}\|_{l^\infty}+\|\psi^n\|_{l^\infty}) \times \|\widehat{\psi}^{n+1}-\psi^{n+1}\|_{l^\infty},$$

$$|c_i^{n+\frac{1}{2}}||D_X(c(D_X(\widehat{\psi}-\psi)))_i^{n+\frac{1}{2}}| \le \frac{2\,C_1^2}{\Delta X^2}\|\widehat{\psi}^{n+1}-\psi^{n+1}\|_{l^\infty},$$

$$|\sin(2\psi_i)^{n+\frac{1}{2}}-\sin(2\widehat{\psi}_i)^{n+\frac{1}{2}}| \le \|\widehat{\psi}^{n+1}-\psi^{n+1}\|_{l^\infty}.$$

Putting the above estimates together, we arrive at

$$|\mathcal{F}(\psi^{n+1})_i-\mathcal{F}(\widehat{\psi}^{n+1})_i| \le \left(\frac{2}{q}C_1(C_1+C_2(\|\widehat{\psi}^{n+1}\|_{l^\infty}+\|\psi^n\|_{l^\infty}))\frac{\Delta T}{\Delta X^2}+\frac{h^2}{2q}\Delta T\right)\|\widehat{\psi}^{n+1}-\psi^{n+1}\|_{l^\infty},$$

for $i=1,\dots,N-1$. For $i=0$,

$$\begin{aligned}|\mathcal{F}(\psi^{n+1})_0-\mathcal{F}(\widehat{\psi}^{n+1})_0| \le{}& |\psi_1^{n+1}-\widehat{\psi}_1^{n+1}| \\ &+\beta\Delta X\left(\left|\frac{1}{\widehat{c}_{\frac{1}{2}}^{n+\frac{1}{2}}}-\frac{1}{c_{\frac{1}{2}}^{n+\frac{1}{2}}}\right|\frac{1}{\widehat{c}_0^{n+\frac{1}{2}}}|\sin(2\widehat{\psi}_0^{n+\frac{1}{2}})|\right. \\ &\quad+\frac{1}{c_{\frac{1}{2}}^{n+\frac{1}{2}}}\left|\frac{1}{\widehat{c}_0^{n+\frac{1}{2}}}-\frac{1}{c_0^{n+\frac{1}{2}}}\right||\sin(2\widehat{\psi}_0^{n+\frac{1}{2}})| \\ &\quad\left.+\frac{1}{c_{\frac{1}{2}}^{n+\frac{1}{2}}}\frac{1}{c_0^{n+\frac{1}{2}}}\left|\sin(2\widehat{\psi}_0^{n+\frac{1}{2}})-\sin(2\psi_0^{n+\frac{1}{2}})\right|\right).\end{aligned}$$

The terms on the right-hand side can be bounded by

$$\begin{aligned}|\psi_1^{n+1}-\widehat{\psi}_1^{n+1}| &= |\mathcal{F}(\psi^{n+1})_1-\mathcal{F}(\widehat{\psi}^{n+1})_1| \\ &\le \left(\frac{2}{q}C_1(C_1+C_2(\|\widehat{\psi}^{n+1}\|_{l^\infty}+\|\psi^n\|_{l^\infty}))\frac{\Delta T}{\Delta X^2}+\frac{h^2}{2q}\Delta T\right) \\ &\quad\times\|\widehat{\psi}^{n+1}-\psi^{n+1}\|_{l^\infty},\end{aligned}$$

$$\begin{aligned}\left|\frac{1}{\widehat{c}_{\frac{1}{2}}^{n+\frac{1}{2}}}-\frac{1}{c_{\frac{1}{2}}^{n+\frac{1}{2}}}\right|\frac{1}{\widehat{c}_0^{n+\frac{1}{2}}}|\sin(2\widehat{\psi}_0^{n+\frac{1}{2}})| &= \frac{|c_{\frac{1}{2}}^{n+\frac{1}{2}}-\widehat{c}_{\frac{1}{2}}^{n+\frac{1}{2}}|}{\widehat{c}_{\frac{1}{2}}^{n+\frac{1}{2}}c_{\frac{1}{2}}^{n+\frac{1}{2}}\widehat{c}_0^{n+\frac{1}{2}}}|\sin(2\widehat{\psi}_0^{n+\frac{1}{2}})| \\ &\le \frac{C_2}{2C_3^3}\|\widehat{\psi}^{n+1}-\psi^{n+1}\|_{l^\infty},\end{aligned}$$

$$\frac{1}{c_{\frac{1}{2}}^{n+\frac{1}{2}}}\left|\frac{1}{\widehat{c}_0^{n+\frac{1}{2}}}-\frac{1}{c_0^{n+\frac{1}{2}}}\right||\sin(2\widehat{\psi}_0^{n+\frac{1}{2}})| = \frac{|c_0^{n+\frac{1}{2}}-\widehat{c}_0^{n+\frac{1}{2}}|}{c_{\frac{1}{2}}^{n+\frac{1}{2}}\widehat{c}_0^{n+\frac{1}{2}}c_0^{n+\frac{1}{2}}}|\sin(2\widehat{\psi}_0^{n+\frac{1}{2}})| \leq \frac{C_2}{2C_3^3}\|\widehat{\psi}^{n+1}-\psi^{n+1}\|_{l^\infty},$$

$$\frac{1}{c_{\frac{1}{2}}^{n+\frac{1}{2}}}\frac{1}{c_0^{n+\frac{1}{2}}}\left|\sin(2\widehat{\psi}_0^{n+\frac{1}{2}})-\sin(2\psi_0^{n+\frac{1}{2}})\right| \leq \frac{2}{C_3^2}\|\widehat{\psi}^{n+1}-\psi^{n+1}\|_{l^\infty}.$$

Hence we get the estimate

$$\begin{aligned}&|\mathcal{F}(\psi^{n+1})_0-\mathcal{F}(\widehat{\psi}^{n+1})_0|\\ &\leq\left(\frac{2}{q}C_1(C_1+C_2(\|\widehat{\psi}^{n+1}\|_{l^\infty}+\|\psi^n\|_{l^\infty}))\frac{\Delta T}{\Delta X^2}+\frac{h^2}{2q}\Delta T\right.\\ &\qquad\left.+\left(\beta\frac{C_2}{C_3^3}+\frac{2\beta}{C_3^2}\right)\Delta X\right)\|\widehat{\psi}^{n+1}-\psi^{n+1}\|_{l^\infty}.\end{aligned}$$

Analogously, one can derive a bound for $i=N$. Altogether,

$$\begin{aligned}&\|\mathcal{F}(\widehat{\psi}^{n+1})-\mathcal{F}(\psi^{n+1})\|_{l^\infty}\\ &\qquad\leq\left(C_A\frac{\Delta T}{\Delta X^2}+C_{B_1}\Delta T+C_{B_2}\Delta X\right)\|\widehat{\psi}^{n+1}-\psi^{n+1}\|_{l^\infty},\end{aligned}$$

where

$$C_A=\frac{2}{q}C_1(C_1+C_2(K+\pi)), \tag{25a}$$

$$C_{B_1}=\frac{h^2}{2q}, \tag{25b}$$

$$C_{B_2}=\beta\frac{C_2}{C_3^3}+\frac{2\beta}{C_3^2}, \tag{25c}$$

and hence, for suitable $\Delta T$ and $\Delta X$, the function $\mathcal{F}$ is a contraction. □

In practice, we solve the implicit equations (20)–(21) using a Newton-Rhapson iteration.

3.2. **Varying electric field.** The numerical method from Definition 1 can be extended to solve the full model (15)–(16). Given a numerical

solution $\psi^n = (\psi_0^n, \ldots, \psi_N^n)$ for the director field, the discrete electric field is approximated as

$$(u_{X,i})^n = \frac{1}{\Delta X} \frac{1}{\tilde{d}(\psi_i^n)} \left( \sum_{j=0}^{N} \frac{1}{\tilde{d}(\psi_j^n)} \right)^{-1}, \tag{26}$$

where $\tilde{d}(\psi)$ is the nondimensional version of $d(\psi)$,

$$\tilde{d}(\psi) = 1 + \frac{\epsilon_a}{\epsilon_\perp} \cos^2(\psi)\,.$$

By defining the shorthand notation

$$(u_{X,i}^2)^{n+\frac{1}{2}} = \frac{1}{2} \left( (u_{X,i}^n)^2 + (u_{X,i}^{n+1})^2 \right), \tag{27}$$

we can propose the following numerical scheme:

**Definition 2** (The numerical method with coupled electric field)**.** *Let some initial data $\psi_i^0$, $i = 0, \ldots, N$ be given. For each time step $n = 1, 2, 3, \ldots$, define $(u_{X,1})^n, \ldots, (u_{X,N-1})^n$ by* (26)*, $\psi_1^{n+1}, \ldots, \psi_{N-1}^{n+1}$ by*

$$qD_T\psi_i^{n+\frac{1}{2}} - c_i^{n+\frac{1}{2}} D_X(c\, D_X\psi)_i^{n+\frac{1}{2}} + \frac{1}{2}h^2 \sin(2\psi_i)^{n+\frac{1}{2}} (u_{X,i}^2)^{n+\frac{1}{2}} = 0, \tag{28}$$

*and $\psi_0^{n+1}$, $\psi_N^{n+1}$ by* (21)*.*

Again, the time stepping can be performed by solving the $2N$ nonlinear implicit equations(26), (28), and (21) for $\psi^{n+1}$ and $u_X^n$.

## 4. Numerical experiments

The purpose of this section is to perform numerical experiments on the dynamics of the weak Fréedericksz transition, using the numerical scheme described in Section 3. Two experiments will be considered, illustrated in Figure 2. Both involve studying the evolution of the director configuration when $h$ and $\beta$ are changed to cross the Fréedericksz threshold $h_{\mathrm{F}}$ and the saturation threshold $h_{\mathrm{S}}$, given implicitly by

$$h_{\mathrm{F}} = \sqrt{\frac{\alpha_1}{\alpha_2}}\beta \cot\left( \sqrt{\frac{\alpha_1}{\alpha_2}} \frac{h_{\mathrm{F}}}{2} \right) \qquad \text{and} \qquad h_{\mathrm{S}} = \beta \coth\left( \frac{h_{\mathrm{S}}}{2} \right), \tag{29}$$

respectively [9, 13].

The first experiment illustrates the classic weak Fréedericksz transition shown in Figure 1. The director state is initially homogeneous ($\psi = \pi/2$) and $h < h_{\mathrm{F}}$. The field is then increased gradually until it is above the Fréedericksz threshold, and finally above the saturation threshold.

The second experiment involves a director initially in the homeotropic ($\psi = 0$) state. First, the liquid crystal is cooled, giving an increase in

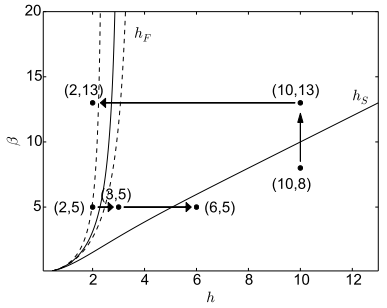


FIGURE 2. The two basic numerical experiments. Bottom: The anchoring $\beta = 5$ is kept constant while the field is increased gradually until it gets above $h_{\mathrm{F}}$, and then finally until it crossed the saturation threshold $h_{\mathrm{S}}$. Top: A cooling increases the anchoring to cross the saturation threshold, then a field reduction brings the state below $h_{\mathrm{F}}$. Dashed lines indicate the Fréedericksz threshold $h_F$ for $\alpha_2/\alpha_1 = 1 \pm 0.4$.

the anchoring strength $\beta$. Then, the field is reduced until $h < h_{\mathrm{F}}$, where the ground state is the homogeneous configuration.

A constant equilibrium state $\psi$ is a stationary solution to (2), independently of the values of $h$ and $\beta$. In order to facilitate the transition from a non-stable equilibrium state, we therefore add small stochastic perturbations to the homogeneous ($\psi = \pi/2$) and the homeotropic ($\psi = 0$) initial data in the numerical experiments. Specifically, we generate a zero-averaged fractional Brownian motion

$$\{S_n\}_{n=1}^N, \quad \sum_{n=1}^{N} S_n = 0, \quad |S_{n+1} - S_n| \leq 1, \tag{30}$$

with Hurst parameter $H = 0.9$. We then let the discrete initial data be given as

$$\psi_i^0 = \frac{\pi}{2} + \delta\, S_i + r\, \delta_S, \tag{31}$$

where $r \in [-0.5, 0.5]$ is a uniformly distributed random number and $\delta, \delta_S > 0$ are small parameters. In the following we will use $\delta = 0.01$ and $\delta_S = 0.015$.

All numerical simulations in this section are performed using $N = 100$ computational cells, if not stated otherwise. The time step is set

according to

$$\Delta T = 0.3 \frac{\Delta X}{1 + \alpha_2/\alpha_1}. \tag{32}$$

The dimensionless number $q$ is set to 1 for all experiments. For typical values of $\kappa \approx 1 \times 10^{-1}$ and $\alpha_1 \approx 1 \times 10^{-11}$, and assuming $L = 1 \times 10^{-6}\,\mathrm{m}$, this implies a characteristic time scale $\tau \approx 1 \times 10^{-2}\,\mathrm{s}$.

For the time stepping, the implicit $N$ nonlinear equations (including the boundary conditions) are solved using a standard Newton–Raphson scheme. In each time step, the configuration from the previous step is taken as an initial guess and the iteration is performed until machine precision has been reached.

4.1. **Convergence.** The convergence behavior of the implicit scheme is investigated in the following. A numerical solution was calculated for a perturbed homogeneous ($\psi = \pi/2$) initial data with $h = 4$ and $\beta = 5$ and grid size $N = N_0 = 100$. The grid was refined according to $N_k = 2^k N_0$ with $k = 0, \cdots, 4$, generating numerical solutions $\psi^{(k)}$ at $T = 1$. The error between consecutive solutions was calculated according to

$$\mathcal{E}_k = \frac{\|\psi^{(k)} - \psi^{(k-1)}\|_{L^2(0,1)}}{\|\psi^{(k-1)}\|_{L^2(0,1)}}. \tag{33}$$

In addition to the convergence of the numerical solutions, we also verify that the energy law (11) is fulfilled in the discrete sense. Specifially, we look at the residual

$$\mathrm{Res}^{n+\frac{1}{2}} = D_T E^{n+\frac{1}{2}} - \frac{1}{2} q \Delta X \sum_{i=0}^{N} D_T \psi_i^{n+\frac{1}{2}}, \tag{34}$$

where $E^{n+\frac{1}{2}} = (E^n + E^{n+1})/2$ is the discrete energy defined in (22), and calculate $\Delta T \sum_n (\mathrm{Res}^{n+\frac{1}{2}})^2$ as the grid is refined. Figure 3 shows the convergence results, and it indicates that the numerical solutions converge to second order both in the norm and in the energy balance.

4.2. **Weak Fréedericksz transition.** In order to verify the basic force balance of the weak Fréedericksz transtion shown in Figure 1, we perform the following numerical experiment: Initially, we set $h = 2$ and $\beta = 5$, consistent with a stable homogeneous ($\psi = \pi/2$) configuration. Also, for simplicity, we assume the one-constant approximation. At $T \in (0.5, 1)$ the field $h$ is increased linearly to $h = 3$, which is beyond the critical thereshold $h_{\mathrm{F}}$. The director field is then allowed to stabilize until $T = 3.5$, for which the field is again increased linearly until it reaches a value beyond the saturation threshold ($h = 6$). Figure 4 shows the evolution of both the director configuration and the

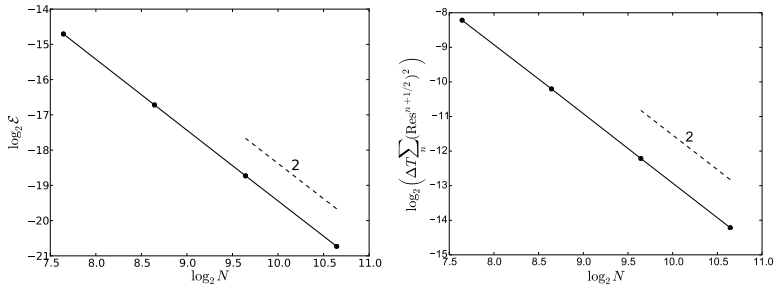


FIGURE 3. Convergence of the error under grid refinement (33) at $T = 1$ (left) and the integrated residual of the discrete energy law (34) from $T = 0$ to $T = 1$ (right). Dashed lines indicate the slope corresponding to second-order convergence.

energy. The behavior is as expected according to the classical picture of the weak Fréedericksz transition.

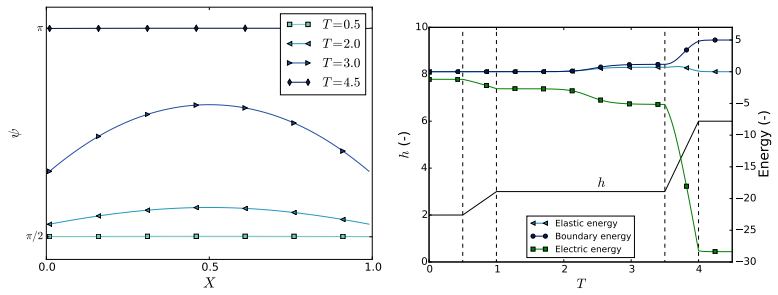


FIGURE 4. Evolution of the director field (left) and the discrete energy (22) (right) for the gradual increase of the electric field from $h = 2$ to $h = 6$. The anchoring is held constant at $\beta = 5$ and the one-constant approximation is assumed.

4.3. **Relaxing the one-constant approximation.** The basic transition experiment from Section 4.2 can also be studied numerically in the nonlinear case, i.e., by letting $\alpha_1 \neq \alpha_2$. The extrapolation length and coherence length will be defined using $\alpha_1$ as before for comparison.

Figure 5 shows a snapshot of the director configuration during the Fréedericksz transition ($T = 2$) and during the saturation ($T = 3.75$).

In the first case the influence of the nonlinearity is significant, even for modest perturbations from the one-constant approximation. For comparison, $\alpha_2/\alpha_1 \approx 0.75$ at room temperature for the liquid crystal 5CB [8]. Note that in general both the equilibrium configurations and the time evolution will be different when replacing the one-constant approximation with an $\alpha_2/\alpha_1 \neq 1$.

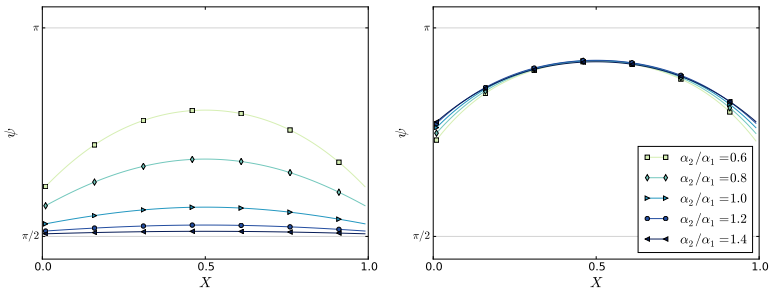


FIGURE 5. The director configuration at $T = 2$ (left) and at $T = 3.75$ (right) for the weak Fréedericksz transition experiment for different values of $\alpha_2/\alpha_1$. The electric field is assumed constant.

4.4. **Coupling with an electric field.** Using the method from Section 3.2, the weak transition experiment can also be performed with a coupled electric field. Since in this case the value of the electric field is not given a priori, the parameter $h$ must be interpreted in a slightly weaker sense. Since it is based on the applied voltage difference $V_0$, $h$ now represents represents the *average* field strength $V_0/L$, not the actual electric field $E$ since this will vary both in space and in time.

Figure 6 shows the director configuration and the electric field at $T = 2$, for different values of the relative electric anisotropy $\varepsilon_a/\varepsilon_\perp$. For simplicity, the one-constant approximation ($\alpha_1 = \alpha_2$) was used. The case $\varepsilon_a/\varepsilon_\perp = 0$ represents an uncoupled electric field, and the results indicate significant differences in the director only for large values of the electric anisotropy. As a comparison, $\varepsilon_a/\varepsilon_\perp \approx 1.64$ at room temperature for the liquid crystal 5CB [8].

Explicit general solutions for the case with a fully coupled electric field are not available. However, certain approximate solutions can be found given simplifying assumptions. In particular, Napoli [9] considers

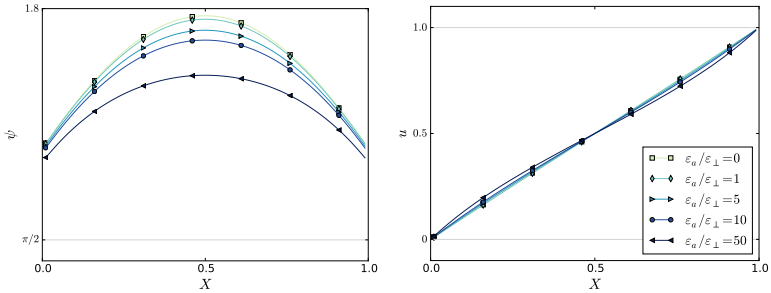


FIGURE 6. The director configuration (left) and the electric potential (right) at $T = 2$ for the weak Fréedericksz transition experiment for different values of $\varepsilon_a/\varepsilon_\perp$ using the one-constant approximation.

the fully coupled problem with an applied electric field. Using asymptotic matching, an explicit approximate solution is calculated for large voltages $V_0$ and assuming the one-constant approximation.

To compare with the approximate solution, the fully coupled problem was solved using $h = 25$ and $\beta = 30$ with the one-constant approximation. Figure 7 shows the evolution of the director configuration compared with the approximation. A small, but noticable, difference can be observed between the steady-state solution and the large-voltage approximation.

4.5. **Solutions of different parity.** In this experiment we consider a director field initially in the homeotropic state with $h = 10$ and $\beta = 8$. At $T \in [0, 0.5]$ we increase $\beta$ linearly to 13, simulating a cooling of the sample. The stronger boundary anchoring will then initiate an inverse Fréedericksz transition near the ends of the sample, giving a nontrivial even or odd symmetric state, depending on the initial perturbation. At $T \in [0.8, 1.2]$ we reduce $h$ linearly to 2, representing a gradual reduction in the electric field. Because of the reduced electric bulk energy, the new ground state will then be a homogeneous director configuration.

The results show that, depending on the initial perturbation, the final state might end up in the ground state or an excited high-energy state. Figure 8 shows that for one of the perturbations (solid lines) we first have a transition to the even symmetric ground state for $\beta = 13$ and $h = 10$ at around $T = 0.6$. When the electric field is reduced at $T = 0.8$ the director then relaxes to the homogeneous ground state. For the second random initial perturbation the cooling at $T \in [0, 0.5]$

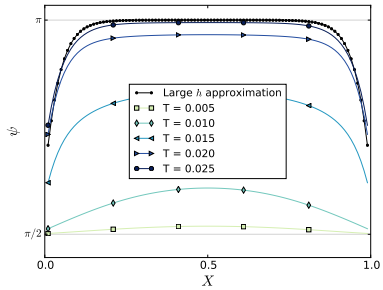


FIGURE 7. The evolution of the director configuration for the fully coupled problem using $h = 25$ and $\beta = 30$ and assuming the one-constant approximation. The initial data was a perturbed homogeneous configuration. The dotted line is the analytical approximation given by Napoli [9].

leaves the director in an excited odd symmetric state. When the field is reduced we then obtain an excited state also for $\beta = 13, h = 2$. Figure 9 shows the different contributions to the energy, for both solutions, as a function of time.

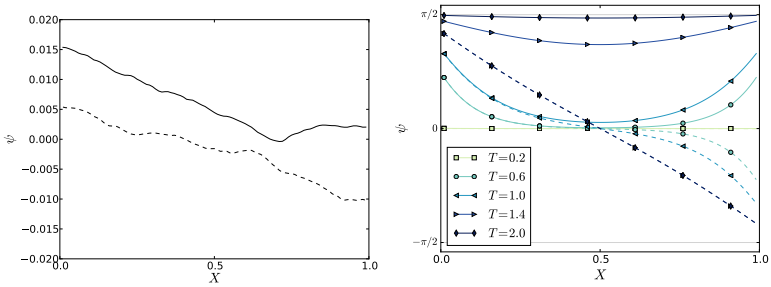


(A) Initial pertubations ($T = 0$) (B) Director evolution

FIGURE 8. The evolution of the director field for the two different initial pertubarions. The initial perturbation displayed with the solid (respectively dashed) line at the left corresponds to the evolution showed with solid (respectively dashed) lines to the right.

These results were reproduced in the nonlinear case ($\alpha_2/\alpha_1 = 0.75$) and with a coupled electric field with $\varepsilon_a/\varepsilon_\perp = 1.64$. The director

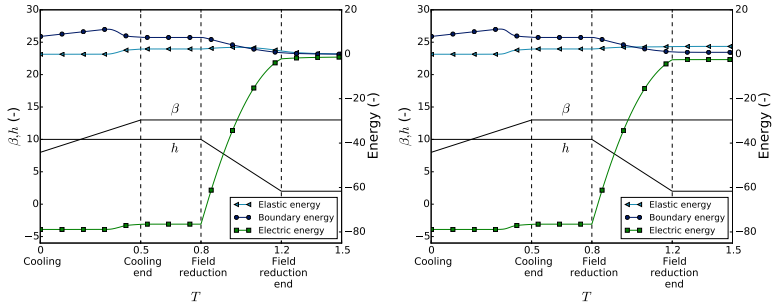


FIGURE 9. Evolution of the different terms in the discrete energy (22) as a function of time for two different realizations of the initial data.

evolution was almost indistinguishable from that seen in Figure 8, and is omitted here for brevity. These results indicate that odd director states also exist for models more general than the linear uncoupled case that was analyzed in [2].

## 5. Summary

We have studied the dynamics of the director field for the classical Fréedericksz transition in the bend-splay geometry with weak anchoring. For the dimensionless problem we have derived a simple, robust and efficient numerical method. The scheme can be used both for unequal elastic constants and with a coupled electric field. We have proved that the nonlinear discrete equations are well-posed for sufficiently small time steps.

Numerical experiments have been performed for basic transition experiments where the applied electric field and the anchoring strength are varied. Herein, the transition from a ground state to an excited (odd parity) state have been observed in a basic cooling experiment. The existence of such states has recently been shown experimentally [7] and theoretically in the stationary case [2]. However, to the best of the authors' knowledge, this is the first dynamic study of how excited (odd parity) director states manifest in the weak Fréedericksz transition.

Moreover, the sensitivity of the time evolution of the weak Fréedericksz transition with regard to common modeling assumptions has been investigated. Herein, the one-constant approximation was shown to impact the dynamics of the problem when using elastic constants comparable to those of the liquid crystal 5CB. Also, to some extent, the

problem was sensitive to the assumption of a constant electric field. However, substantial deviations when coupling with Maxwell's equations could only be observed for very high values of $\varepsilon_a/\varepsilon_\perp$.

## Acknowledgements

The work of Peder Aursand and Johanna Ridder has been funded by the Research Council of Norway (project numbers 213638 and 214495, respectively).

## References

[1] P Aursand and U. Koley. Local discontinuous Galerkin methods for a nonlinear variational wave equation modeling liquid crystals. *Preprint*, 2014.

[2] G. Bevilacqua and G. Napoli. Parity of the weak fréedericksz transition. *Eur. Phys. J. E*, 35(12):1–5, 2012.

[3] G. P. Bryan-Brown, E. L. Wood, and I. C. Sage. Weak surface anchoring of liquid crystals. *Nature*, 399(6734):338–340, 1999.

[4] F. P. da Costa, M. Grinfeld, N. J. Mottram, and J. T. Pinto. Uniqueness in the freedericksz transition with weak anchoring. *J. Diff. Eq.*, 246(7):2590–2600, 2009.

[5] P. G. De Gennes and J. Prost. *The Physics of Liquld Crystals*. Clarendon Press, Oxford, 1993.

[6] X. Gang, S. Chang-Qing, and L. Lei. Perturbed solutions in nematic liquid crystals under time-dependent shear. *Phys. Rev. A*, 36(1):277–284, 1987.

[7] T. A. Kumar, P. Sathyanarayana, V. S. S. Sastry, H. Takezoe, N. V. Madhusudana, and S. Dhara. Temperature-and electric-field-induced inverse freedericksz transition in a nematogen with weak surface anchoring. *Phys. Rev. E*, 82(1):011701, 2010.

[8] G. R. Luckhurst, D. A. Dunmur, and A. Fukuda. *Physical properties of liquid crystals: nematics*. IET, 2001.

[9] G. Napoli. Weak anchoring effects in electrically driven freedericksz transitions. *J. Phys. A Math. Gen.*, 39(1):11, 2006.

[10] J. Nehring, A. R. Kmetz, and T. J. Scheffer. Analysis of weak-boundary-coupling effects in liquid-crystal displays. *J. Appl. Phys.*, 47(3):850–857, 2008.

[11] A Rapini and M Papoular. Distorsion d'une lamelle nématique sous champ magnétique conditions d'ancrage aux parois. *J. Phys. Colloq.*, 30(C4):C4–54, 1969.

[12] I. W. Stewart. *The static and dynamic continuum theory of liquid crystals: a mathematical introduction*. CRC Press, 2004.

[13] E. G. Virga. *Variational theories for liquid crystals*, volume 8. CRC Press, 1994.

(Peder Aursand)
Department of Mathematical Sciences,
Norwegian University of Science and Technology,
NO–7491 Trondheim, Norway.
*E-mail address*: peder.aursand@math.ntnu.no

(Gaetano Napoli)
Dipartimento di Ingegneria dell´Innovazione,
Università del Salento,
via per Monteroni, 73100 Lecce, Italy
*E-mail address*: gaetano.napoli@unisalento.it

(Johanna Ridder)
Department of Mathematics,
University of Oslo,
P.O.Box NO-1053, Blindern, Oslo-0316, Norway.
*E-mail address*: johanrid@math.uio.no

# Paper C

**Local discontinuous Galerkin schemes for a nonlinear variational wave equation modeling liquid crystals**

Peder Aursand and Ujjwal Koley

Submitted for publication.

## Preface

The research that makes up this paper dates back to the earliest days of my PhD work. Looking at the mathematical issues regarding conservative and dissipative weak solutions to the 1D variational wave equation, we became interested in how to go about numerically solving these initial value problems. Specifically we asked if we could design numerical schemes that are guaranteed to either conserve or dissipate a discrete version of the energy, and if so, can we use these to numerically obtain conservative and dissipative weak solutions?

Different approaches were tested together with Dr. Koley and under the advice of Professor Siddhartha Mishra. The decision was made to look at DG methods because of their flexibility and high accuracy. The field of DG was largely unknown to me initially, and I spent a significant amount of time familiarizing myself with the formalism, notation, and techniques. Also, developing the actual object oriented DG code from the bottom up was a huge learning experience for me. In the end, the results were interesting and shows promise for the role of numerics in the investigation of these equations.

# LOCAL DISCONTINUOUS GALERKIN SCHEMES FOR A NONLINEAR VARIATIONAL WAVE EQUATION MODELING LIQUID CRYSTALS

P. AURSAND AND U. KOLEY

Abstract. We consider a nonlinear variational wave equation that models the dynamics of nematic liquid crystals. Discontinuous Galerkin schemes that either conserve or dissipate a discrete version of the energy associated with these equations are designed. Numerical experiments illustrating the stability and efficiency of the schemes are presented. An interesting feature of these schemes is their ability to approximate two distinct weak solutions of the underlying system.

## 1. Introduction

1.1. **The model.** The dynamics of liquid crystals is of utmost significance to the makers of visual displays such as LCDs. Liquid crystals are mesophases, i.e. intermediate states of matter between the liquid and the crystal phase. They exhibit characteristics of fluid flow and have optical properties typically associated with crystals. One of the most common phases in liquid crystals is the nematic phase. Nematic liquid crystals consist of strongly elongated molecules that can be considered invariant under rotation by an angle of $\pi$. The flow of a liquid crystal is commonly described by two linearly independent vector fields; one describing the fluid flow and one describing the orientation of the so-called director field that gives the orientation of the rod-like molecule. In this paper we will only consider stationary flow, and hence focus exclusively on the dynamics of the director field

$$\mathbf{n} = \mathbf{n}(\mathbf{x}, t) \in \mathcal{S}^2.$$

Given a director field $\mathbf{n}$, the well known Oseen-Frank free-energy density $\mathcal{W}$ associated with this field is given by

$$\mathcal{W}(\mathbf{n}, \nabla\mathbf{n}) = \alpha \left|\mathbf{n} \times (\nabla \times \mathbf{n})\right|^2 + \beta \left(\nabla \cdot \mathbf{n}\right)^2 + \gamma \left(\mathbf{n} \cdot (\nabla \times \mathbf{n})\right)^2. \tag{1.1}$$

The positive constants $\alpha, \beta$ and $\gamma$ are elastic constants of the liquid crystal. Note that each term on the right hand side of (1.1) arises from different types of distortions. In particular, the term $\alpha \left|\mathbf{n} \times (\nabla \times \mathbf{n})\right|^2$ corresponds to the bending of the medium, the term $\beta \left(\nabla \cdot \mathbf{n}\right)^2$ corresponds to splay, and the term $\gamma \left(\mathbf{n} \cdot (\nabla \times \mathbf{n})\right)^2$ corresponds to the twisting of the medium.

For the special case of $\alpha = \beta = \gamma$, the free-energy density (1.1) reduces to

$$\mathcal{W}(\mathbf{n}, \nabla\mathbf{n}) = \alpha \left|\nabla\mathbf{n}\right|^2,$$

*Date*: June 15, 2015.

which corresponds to the potential energy density used in harmonic maps into the sphere $\mathcal{S}^2$. The constrained elliptic system of equations for $\mathbf{n}$, derived from the potential (1.1) using a variational principle, and the parabolic flow associated with it, are widely studied, see [6, 11, 13] and references therein.

In the regime where inertial effects are dominating over viscosity, it is natural to model the propagation of orientation waves in the director field by employing the principle of least action [26], i.e.

$$\frac{\delta}{\delta \mathbf{n}} \iint \left( \mathbf{n}_t^2 - \mathcal{W}(\mathbf{n}, \nabla \mathbf{n}) \right) \, dx \, dt = 0, \qquad \mathbf{n} \cdot \mathbf{n} = 1. \tag{1.2}$$

Again, in the special case of $\alpha = \beta = \gamma$, this variational principle (1.2) yields the equation for harmonic wave maps from $(1 + 3)$-dimensional Minkowski space into the two sphere, see [9, 27, 28] and references therein.

In this paper, we will restrict ourselves to one-dimensional planar waves; the director field $\mathbf{n}$ is given by

$$\mathbf{n}(x, t) = \cos \psi(x, t) \mathbf{e}_x + \sin \psi(x, t) \mathbf{e}_y,$$

where $\mathbf{e}_x$ and $\mathbf{e}_y$ are the coordinate vectors in the $x$ and $y$ directions, respectively. That is to say the dynamics of the liquid crystal is described by some unknown function $\psi$, which represents the angle of the director field relative to the $x$-direction. In this case, the variational principle (1.2) reduces to [26, 21, 16]

$$\begin{cases} \psi_{tt} - c(\psi) \left( c(\psi) \psi_x \right)_x = 0, & (x, t) \in \Pi_T, \\ \psi(x, 0) = \psi_0(x), & x \in \mathbb{R}, \\ \psi_t(x, 0) = \psi_1(x), & x \in \mathbb{R}, \end{cases} \tag{1.3}$$

where $\Pi_T = \mathbb{R} \times [0, T]$ with fixed $T > 0$ , and the wave speed $c(\psi)$ given by

$$c^2(\psi) = \alpha \cos^2 \psi + \beta \sin^2 \psi. \tag{1.4}$$

The form (1.3) is the standard form of the nonlinear variational wave equation considered in the literature.

For the one-dimensional planar waves the energy is given by

$$\mathcal{E}(t) = \int_{\mathbb{R}} \left( \psi_t^2 + c^2(\psi) \psi_x^2 \right) \, dx. \tag{1.5}$$

A simple calculation shows that smooth solutions of the variational wave equation (1.3) satisfy

$$\frac{d\mathcal{E}(t)}{dt} = 0. \tag{1.6}$$

1.2. **Mathematical difficulties.** Despite its apparent simplicity, the mathematical analysis of (1.3) is complicated. Independently of the smoothness of the initial data, due to the nonlinear nature of the equation, singularities may form in the solution $\psi_x$. Therefore, we consider solutions in the weak sense:

**Definition 1.1.** *Set* $\Pi_T = \mathbb{R} \times (0,T)$. *A function*

$$\psi(t,x) \in L^\infty\left([0,T];W^{1,p}(\mathbb{R})\right) \cap C(\Pi_T), \psi_t \in L^\infty\left([0,T];L^p(\mathbb{R})\right),$$

*for all* $p \in [1, 3+q]$, *where* $q$ *is some positive constant, is a weak solution of the initial value problem* (1.3) *if it satisfies:*

***D**.1 For all test functions* $\varphi \in \mathcal{D}(\mathbb{R} \times [0,T))$

$$\iint_{\Pi_T} \left(\psi_t\varphi_t - c^2(\psi)\psi_x\varphi_x - c(\psi)c'(\psi)(\psi_x)^2\varphi\right)\, dx\, dt = 0. \tag{1.7}$$

***D**.2* $\psi(\cdot,t) \to u_0$ *in* $C\left([0,T];L^2(\mathbb{R})\right)$ *as* $t \to 0^+$.

***D**.3* $\psi_t(\cdot,t) \to v_0$ *as a distribution in* $\Pi_T$ *when* $t \to 0^+$.

An important aspect of the variational wave equation is that there exist both *conservative* and *dissipative* weak solutions, see e.g. [30] for a more detailed discussion. To illustrate this difference, one can consider initial data for which the solution vanishes identically at some specific (finite) time. At this point, at least two possibilities exist: to continue with the trivial zero solution, termed as the dissipative solution. Alternatively, one can show that there exists a nontrivial solution that appears as a natural continuation of the solution prior to the critical time. This solution is denoted the conservative solution as it preserves the total energy (1.5) of the system. This dichotomy makes the question of well-posedness of the initial value problem (1.3) very difficult. Additional admissibility conditions are needed to select a physically relevant solution. The specification of such admissibility criteria is still open.

Although the problem of global existence and uniqueness of solutions to the Cauchy problem of the nonlinear variational wave equation (1.3) is still open, several recent papers have explored related questions or particular cases of (1.3). It has been demonstrated in [17] that (1.3) is rich in structural phenomena associated with weak solutions. In fact, by rewriting the highest derivatives of (1.3) in conservative form

$$\psi_{tt} - \left(c^2(\psi)\psi_x\right)_x = -c(\psi)c'(\psi)\psi_x^2,$$

we see that the strong precompactness in $L^2$ of the derivatives $\{\psi_x\}$ of a sequence of approximate solutions is essential in establishing the existence of a global weak solution. However, the equation shows the phenomenon of persistence of oscillations [12] and annihilation in which a sequence of exact solutions with bounded energy can oscillate forever so that the sequence $\{\psi_x\}$ is not precompact in $L^2$. Still, the weak limit of the sequence is a weak solution.

There has been a number of papers concerning the existence of weak solutions of the Cauchy problem (1.3), starting with the papers by Zhang and Zheng [30, 31, 32, 33, 34, 35], Bressan and Zheng [7] and Holden and Raynaud [19]. In [34], the authors show existence of a global weak solution using the method of Young measures for initial data $\psi_0 \in H^1(\mathbb{R})$ and $\psi_1 \in L^2(\mathbb{R})$. The function $c(\psi)$ is assumed to be smooth, bounded, positive with derivative that is non-negative and strictly positive on the initial data $\psi_0$. This means that the analysis in [30, 31, 32, 33, 34, 35] does not directly apply to (1.3) when using the physical wave speed (1.4).

A different approach to the study of (1.3) was taken by Bressan and Zheng [7]. Here, they rewrote the equation in new variables such that the singularities disappeared. They show that for $\psi_0$ absolutely continuous with $(\psi_0)_x, \psi_1 \in L^2(\mathbb{R})$, the Cauchy problem (1.3) allows a global weak solution with the following properties: the solution $\psi$ is locally Lipschitz continuous and the map $t \to u(t, \cdot)$ is continuously differentiable with values in $L^p_{\text{loc}}(\mathbb{R})$ for $1 \leq p < 2$.

In [19], Holden and Raynaud prove the existence of a global semigroup for conservative solutions of (1.3), allowing for concentration of energy density on sets of zero measure. Furthermore they also allow for initial data $\psi_0, \psi_1$ that contain measures. The proof involves constructing the solution by introducing new variables related to the characteristics, leading to a characterization of singularities in the energy density. They also prove that energy can only focus on a set of times of zero measure or at points where $c'(\psi)$ vanishes.

1.3. **Numerical Schemes.** There are no elementary and explicit solutions available for (1.3), except for the trivial case where $c$ is constant. Consequently, robust numerical schemes for approximating the variational wave equation are very important in the study of nematic liquid crystals. However, there is a paucity of efficient numerical schemes for these equations. Also, traditional finite difference schemes will not yield conservative solutions, but rather dissipative solutions due to the intrinsic numerical diffusion in these methods.

Within the existing literature we can refer to [16], where the authors present some numerical examples to illustrate their theory. In recent years, a semi-discrete finite difference scheme for approximating one-dimensional equation (1.3) was considered in [20]. The authors were even able to prove convergence of the numerical approximation, generated by their scheme, to the *dissipative* solution of (1.3). However, the underlying assumptions on the wave speed $c$ (positivity of the derivative of $c$) precludes consideration of realistic wave speeds given by (1.4). Another recent paper dealing with numerical approximation of (1.3) is [19]. Here, the authors use their analytical construction to define a numerical method that can approximate the *conservative* solution. However, the method is computationally very expensive as there is no time marching. Another recent paper [22] deals with *first order* finite different schemes based on either the conservation or the dissipation of the energy associated with (1.3). In the one-dimensional case, they rewrote the variational wave equation (1.3) in the form of two equivalent first-order systems. Energy conservative as well as energy dissipative schemes approximating both these formulations were derived. Moreover, they also designed an energy conservative scheme based on a Hamiltonian formulation of the variational wave equation.

Furthermore, there are some works on the Ericksen–Leslie (EL) equations [1], a simple set of equations describing the motion of a nematic liquid crystal. In [5], authors have presented a finite element scheme for the EL equations. Their approximations are based on the ideas given in [3] which utilize the Galerkin method with Lagrange finite elements of order 1. Convergence, even convergence to measure-valued solutions, of such schemes is an open problem. In [2], a saddle-point formulation was used to construct finite element approximate solutions to the EL equations.

A penalty method based on well-known penalty formulation for EL equations has been introduced in [23] which uses the *Ginzburg–Landau* function. Convergence of such approximate solutions, based on an energy method and a compactness result, towards measure valued solutions has been proved in [24].

1.4. **Scope and outline of the paper.** In view of the above discussion, there seem to exist no robust and efficient high-order numerical schemes currently available for solving the nonlinear variational wave equation (1.3). Furthermore, one can expect *conservative* as well as *dissipative* solutions of the variational wave equation (1.3) after singularity formation. Hence, there is a need for higher-order schemes (energy conservative and energy dissipative) that approximate these different types of solutions. Typically, energy conservative schemes produce oscillations at shocks. This is expected as energy needs to be dissipated at shocks. A suitable numerical diffusion operator added to energy conservative scheme results in a energy stable scheme. To the best of our knowledge, this is the first attempt to construct high-order conservative and dissipative schemes for (1.3).

We will require our numerical methods to be shock capturing, exhibit high-order accuracy and low numerical dissipation away from shocks. Shock capturing Runge-Kutta Discontinuous Galerkin methods are high-order accurate away from discontinuities, thus they are a candidate method for carrying out such simulations. Discontinuous Galerkin (DG) methods were first introduced by Hill and Reed [18] for the neutron transport equations (linear hyperbolic equations). These methods were then generalized for systems of hyperbolic conservation laws by Cockburn and co-workers [10] and references therein. In space the solution is approximated using piecewise polynomials on each element. Exact or approximate Riemann solvers from finite volume methods are used to compute the numerical fluxes between elements. Limiters or shock capturing operators are used to achieve non-oscillatory approximate solutions, if they contain shocks [8]. For these reasons, DG methods can be seen as generalization of finite volume methods to higher order.

Given this background, we present a class of schemes in this paper that has following properties:

(1) All the schemes are (formally) high-order accurate.
(2) All the designed schemes resolved the solution (including possible singularities in the angle $\psi$) in a stable manner.
(3) The energy conservative schemes converge to a limit solution (as the mesh is refined), whose energy is preserved. This solution is a *conservative* solution of (1.3).
(4) The energy dissipative schemes also converge to a limit solution with energy being dissipated with time. This solution is a *dissipative* solution of the variational wave equation.

The rest of the paper is organized as follows: In Section 2, we present energy conservative and energy dissipative schemes for the one-dimensional equation (1.3). Details of implementation presented in Section 3 and finally numerical experiments illustrating all these designed schemes are presented in Section 4.

## 2. Numerical schemes for the variational wave equation

2.1. **The grid and notation.** We begin by introducing some notation needed to define the DG schemes. Let the domain $\Omega \subset \mathbb{R}$ be decomposed as $\Omega = \cup_j \Omega_j$ where $\Omega_j = [x_{j-1/2}, x_{j+1/2}]$ for $j = 1, \cdots, N$. We denote $\Delta x_j = x_{j+1/2} - x_{j-1/2}$ and $x_j = (x_{j-1/2} + x_{j+1/2})/2$.

Let $u$ be a grid function and denote $u^+_{j+1/2}$ as the function evaluated at the right side of the cell interface at $x_{j+1/2}$ and let $u^-_{j+1/2}$ denote the value at the left side. We can then introduce the jump, and respectively, the average of any grid function $u$ across the interface as

$$\overline{u}_{j+1/2} := \frac{u^+_{j+1/2} + u^-_{j+1/2}}{2},$$
$$[\![u]\!]_{j+1/2} := u^+_{j+1/2} - u^-_{j+1/2}.$$

Now let $v$ be another grid function. The following identity is readily verified:

$$[\![uv]\!]_{j+1/2} = \overline{u}_{j+1/2}[\![v]\!]_{j+1/2} + [\![u]\!]_{j+1/2}\overline{v}_{j+1/2} \tag{2.1}$$

2.2. **A first-order system of Riemann invariants.** It is easy to check that the variational wave equation (1.3) can be rewritten as a first-order system by introducing the Riemann invariants:

$$R := \psi_t + c(\psi)\psi_x$$
$$S := \psi_t - c(\psi)\psi_x$$

For smooth solutions, equation (1.3) is equivalent to the following system in non-conservative form for $(R, S, \psi)$:

$$\begin{cases} R_t - c(\psi)R_x = \frac{c'(\psi)}{4c(\psi)}\left(R^2 - S^2\right) \\ S_t + c(\psi)S_x = -\frac{c'(\psi)}{4c(\psi)}\left(R^2 - S^2\right) \\ \psi_t = \frac{R+S}{2} \end{cases} \tag{2.2}$$

Observe that one can also rewrite the equation (1.3) in conservative form for $(R, S, \psi)$ as

$$\begin{cases} R_t - (c(\psi)R)_x = -\frac{c_x(\psi)}{2}\left(R - S\right), \\ S_t + (c(\psi)S)_x = -\frac{c_x(\psi)}{2}\left(R - S\right), \\ \psi_t = \frac{R+S}{2}. \end{cases} \tag{2.3}$$

The corresponding energy associated with the system (2.2) is

$$\mathcal{E}(t) = \frac{1}{2}\int_{\mathbb{R}} \left(R^2 + S^2\right)\, dx. \tag{2.4}$$

A simple calculation shows that smooth solutions of (2.2) satisfy the energy identity:

$$(R^2 + S^2)_t - \left(c(\psi)(R^2 - S^2)\right)_x = 0. \tag{2.5}$$

Hence, the fact that the total energy (2.4) is conserved follows from integrating the above identity in space and assuming that the functions $R, S$ decay at infinity.

2.3. **Variational formulation.** We seek an approximation $(R, S, \psi)$ of (2.3) such that for each $t \in [0, T]$, $R$, $S$, and $\psi$ belong to finite dimensional space

$$X^p_{\Delta x}(\Omega) = \left\{ u \in L^2(\Omega) : u|_{\Omega_j} \text{ polynomial of degree} \le p \right\}.$$

The variational form is derived by multiplying the strong form (2.3) with test functions $\phi, \eta, \zeta \in X^p_{\Delta x}(\Omega)$ and integrating over each element separately. After integrating by parts we obtain

$$\begin{aligned}
&\sum_{j=1}^{N} \int_{\Omega_j} R_t\, \phi \mathrm{d}x + \sum_{j=1}^{N} \int_{\Omega_j} cR\phi_x \,\mathrm{d}x - \sum_{j=1}^{N} (cR)(\psi(x_{j+1/2}, t))\phi^-_{j+1/2} \\
&\qquad + \sum_{j=1}^{N} (cR)(\psi(x_{j-1/2}, t))\phi^+_{j-1/2} \\
&\quad = \frac{1}{2}\sum_{j=1}^{N} \int_{\Omega_j} c(R\phi)_x \,\mathrm{d}x - \frac{1}{2}\sum_{j=1}^{N} c(\psi(x_{j+1/2}, t))R^-_{j+1/2}\phi^-_{j+1/2} \\
&\qquad + \frac{1}{2}\sum_{j=1}^{N} c(\psi(x_{j-1/2}, t))R^+_{j-1/2}\phi^+_{j-1/2} - \frac{1}{2}\sum_{j=1}^{N} \int_{\Omega_j} c(S\phi)_x \,\mathrm{d}x \\
&\qquad + \frac{1}{2}\sum_{j=1}^{N} c(\psi(x_{j+1/2}, t))S^-_{j+1/2}\phi^-_{j+1/2} - \frac{1}{2}\sum_{j=1}^{N} c(\psi(x_{j-1/2}, t))S^+_{j-1/2}\phi^+_{j-1/2},
\end{aligned} \tag{2.6}$$

$$\begin{aligned}
&\sum_{j=1}^{N} \int_{\Omega_j} S_t\, \eta \mathrm{d}x - \sum_{j=1}^{N} \int_{\Omega_j} cS\eta_x \,\mathrm{d}x + \sum_{j=1}^{N} (cS)(\psi(x_{j+1/2}, t))\eta^-_{j+1/2} \\
&\qquad - \sum_{j=1}^{N} (cS)(\psi(x_{j-1/2}, t))\eta^+_{j-1/2} \\
&\quad = \frac{1}{2}\sum_{j=1}^{N} \int_{\Omega_j} c(R\eta)_x \,\mathrm{d}x - \frac{1}{2}\sum_{j=1}^{N} c(\psi(x_{j+1/2}, t))R^-_{j+1/2}\eta^-_{j+1/2} \\
&\qquad + \frac{1}{2}\sum_{j=1}^{N} c(\psi(x_{j-1/2}, t))R^+_{j-1/2}\eta^+_{j-1/2} - \frac{1}{2}\sum_{j=1}^{N} \int_{\Omega_j} c(S\eta)_x \,\mathrm{d}x \\
&\qquad + \frac{1}{2}\sum_{j=1}^{N} c(\psi(x_{j+1/2}, t))S^-_{j+1/2}\eta^-_{j+1/2} - \frac{1}{2}\sum_{j=1}^{N} c(\psi(x_{j-1/2}, t))S^+_{j-1/2}\eta^+_{j-1/2}
\end{aligned} \tag{2.7}$$

and

$$\sum_{j=1}^{N} \int_{\Omega_j} \psi_t\, \zeta \mathrm{d}x = \sum_{j=1}^{N} \int_{\Omega_j} \frac{R+S}{2}\, \zeta \,\mathrm{d}x. \tag{2.8}$$

To obtain a numerical scheme, the numerical fluxes $(cR)(\psi(x_{j\pm1/2},t))$, $(cS)(\psi(x_{j\pm1/2},t))$ and $(c)(\psi(x_{j\pm1/2},t))$ all need to be determined.

2.4. **Energy Preserving Scheme Based On System of Riemann Invariants.** Our objective is to design a (semi-discrete) DG scheme such that the numerical approximations conserve a discrete version of the energy (2.26). To this end, we suggest the following:

For a conservative scheme, we use the numerical flux

$$(c)(\psi(x_{j\pm1/2},t)) = \overline{c}_{j\pm1/2} \quad \text{and} \quad (cf)(\psi(x_{j\pm1/2},t)) = \overline{c}_{j\pm1/2}\overline{f}_{j\pm1/2}.$$

Thus, for the $RS$-formulation the DG scheme then becomes: Find $R, S, \psi \in X^p_{\Delta x}(\Omega)$ such that

$$\begin{aligned}
&\sum_{j=1}^{N}\int_{\Omega_j} R_t\phi \mathrm{d}x + \sum_{j=1}^{N}\int_{\Omega_j} cR\phi_x \mathrm{d}x - \sum_{j=1}^{N}\overline{c}_{j+1/2}\overline{R}_{j+1/2}\phi^-_{j+1/2} + \sum_{j=1}^{N}\overline{c}_{j-1/2}\overline{R}_{j-1/2}\phi^+_{j-1/2} \\
&\qquad = \frac{1}{2}\sum_{j=1}^{N}\int_{\Omega_j} c\left(R\phi\right)_x \mathrm{d}x - \frac{1}{2}\sum_{j=1}^{N}\overline{c}_{j+1/2}R^-_{j+1/2}\phi^-_{j+1/2} \\
&\qquad\quad + \frac{1}{2}\sum_{j=1}^{N}\overline{c}_{j-1/2}R^+_{j-1/2}\phi^+_{j-1/2} - \frac{1}{2}\sum_{j=1}^{N}\int_{\Omega_j} c\left(S\phi\right)_x \mathrm{d}x \\
&\qquad\quad + \frac{1}{2}\sum_{j=1}^{N}\overline{c}_{j+1/2}S^-_{j+1/2}\phi^-_{j+1/2} - \frac{1}{2}\sum_{j=1}^{N}\overline{c}_{j-1/2}S^+_{j-1/2}\phi^+_{j-1/2}
\end{aligned} \tag{2.9}$$

for all $\phi \in X^p_{\Delta x}(\Omega)$,

$$\begin{aligned}
&\sum_{j=1}^{N}\int_{\Omega_j} S_t\eta \mathrm{d}x - \sum_{j=1}^{N}\int_{\Omega_j} cS\eta_x \mathrm{d}x + \sum_{j=1}^{N}\overline{c}_{j+1/2}\overline{S}_{j+1/2}\eta^-_{j+1/2} - \sum_{j=1}^{N}\overline{c}_{j-1/2}\overline{S}_{j-1/2}\eta^+_{j-1/2} \\
&\qquad = \frac{1}{2}\sum_{j=1}^{N}\int_{\Omega_j} c\left(R\eta\right)_x \mathrm{d}x - \frac{1}{2}\sum_{j=1}^{N}\overline{c}_{j+1/2}R^-_{j+1/2}\eta^-_{j+1/2} \\
&\qquad\quad + \frac{1}{2}\sum_{j=1}^{N}\overline{c}_{j-1/2}R^+_{j-1/2}\eta^+_{j-1/2} - \frac{1}{2}\sum_{j=1}^{N}\int_{\Omega_j} c\left(S\eta\right)_x \mathrm{d}x \\
&\qquad\quad + \frac{1}{2}\sum_{j=1}^{N}\overline{c}_{j+1/2}S^-_{j+1/2}\eta^-_{j+1/2} - \frac{1}{2}\sum_{j=1}^{N}\overline{c}_{j-1/2}S^+_{j-1/2}\eta^+_{j-1/2}
\end{aligned} \tag{2.10}$$

for all $\eta \in X^p_{\Delta x}(\Omega)$ and

$$\sum_{j=1}^{N}\int_{\Omega_j} \psi_t\,\zeta \mathrm{d}x = \sum_{j=1}^{N}\int_{\Omega_j} \frac{R+S}{2}\,\zeta \,\mathrm{d}x, \tag{2.11}$$

for all $\zeta \in X^p_{\Delta x}(\Omega)$.

The energy conservative property of this semi-discrete scheme is presented in the following theorem:

**Proposition 2.1** (Energy conservation)**.** *Let $R, S \in X^p_{\Delta x}(\Omega)$ be a numerical solution of the semi-discrete scheme* (2.9)–(2.11) *with periodic boundary conditions. We then have*

$$\left( \sum_{j=1}^{N} \int_{\Omega_j} \frac{R^2 + S^2}{2} \, \mathrm{d}x \right)_t = 0. \tag{2.12}$$

*Proof.* Since $R$ and $S$ are a numerical solution then (2.9) and (2.10) hold for any functions $\phi, \eta \in X^p_{\Delta x}(\Omega)$. In particular, they hold for the choice $\phi = R$ and $\eta = S$. We can then calculate

$$\begin{aligned} \sum_{j=1}^{N} \int_{\Omega_j} R_t R \mathrm{d}x = &-\frac{1}{2} \sum_{j=1}^{N} \int_{\Omega_j} c \, (SR)_x \, \mathrm{d}x + \frac{1}{2} \sum_{j=1}^{N} \overline{c}_{j+1/2} R^+_{j+1/2} R^-_{j+1/2} \\ &- \frac{1}{2} \sum_{j=1}^{N} \overline{c}_{j-1/2} R^-_{j-1/2} R^+_{j-1/2} + \frac{1}{2} \sum_{j=1}^{N} \overline{c}_{j+1/2} S^-_{j+1/2} R^-_{j+1/2} \\ &- \frac{1}{2} \sum_{j=1}^{N} \overline{c}_{j-1/2} S^+_{j-1/2} R^+_{j-1/2} \end{aligned} \tag{2.13}$$

and

$$\begin{aligned} \sum_{j=1}^{N} \int_{\Omega_j} S_t S \mathrm{d}x = &\frac{1}{2} \sum_{j=1}^{N} \int_{\Omega_j} c \, (SR)_x \, \mathrm{d}x - \frac{1}{2} \sum_{j=1}^{N} \overline{c}_{j+1/2} S^+_{j+1/2} S^-_{j+1/2} \\ &+ \frac{1}{2} \sum_{j=1}^{N} \overline{c}_{j-1/2} S^-_{j-1/2} S^+_{j-1/2} - \frac{1}{2} \sum_{j=1}^{N} \overline{c}_{j+1/2} S^-_{j+1/2} R^-_{j+1/2} \\ &+ \frac{1}{2} \sum_{j=1}^{N} \overline{c}_{j-1/2} S^+_{j-1/2} R^+_{j-1/2}. \end{aligned} \tag{2.14}$$

Putting these together we obtain

$$\begin{aligned}\left(\sum_{j=1}^{N}\int_{\Omega_j}\frac{R^2+S^2}{2}\,\mathrm{d}x\right)_t &= \sum_{j=1}^{N}\int_{\Omega_j}\left(RR_t+SS_t\right)\,\mathrm{d}x\\ &= \frac{1}{2}\sum_{j=1}^{N}\overline{c}_{j+1/2}\left(R^+_{j+1/2}R^-_{j+1/2}-S^+_{j+1/2}S^-_{j+1/2}\right)\\ &\quad-\frac{1}{2}\sum_{j=1}^{N}\overline{c}_{j-1/2}\left(R^-_{j-1/2}R^+_{j-1/2}-S^-_{j-1/2}S^+_{j-1/2}\right)\\ &= \frac{1}{2}\overline{c}_{N+1/2}\left(R^+_{N+1/2}R^-_{N+1/2}-S^+_{N+1/2}S^-_{N+1/2}\right)\\ &\quad-\frac{1}{2}\overline{c}_{1/2}\left(R^-_{1/2}R^+_{1/2}-S^-_{1/2}S^+_{1/2}\right)=0,\end{aligned}\tag{2.15}$$

where we have used the periodic boundary conditions in the last equality. □

**Remark 2.1.** *Proposition* 2.1 *and similar results to follow are presented for periodic boundary conditions. Naturally, these results also hold when the numerical solution decays at the boundary.*

2.5. **Energy dissipating Scheme Based On System of Riemann Invariants.** We expect the above designed energy conservative scheme (2.9)–(2.11) to approximate a conservative solution of the underlying system (1.3). In order to be able to approximate a dissipative solution of (1.3), we add *numerical viscosity* (scaled by the maximum wave speed) as well as a *shock capturing operator* (similar to Barth [4]) to the energy conservative scheme (2.9)–(2.11). We propose the following modification of the energy conservative scheme (2.9)–(2.11):

Denoting

$$s_{j+1/2}=\max\{c^-_{j+1/2},c^+_{j+1/2}\}$$

for the maximal local wave velocity, a dissipative version of the DG scheme is then given by the following: Find $R, S, \psi \in X^p_{\Delta x}(\Omega)$ such that

$$
\begin{aligned}
\sum_{j=1}^{N}\int_{\Omega_j} R_t\phi \mathrm{d}x + \sum_{j=1}^{N}\int_{\Omega_j} cR\phi_x \mathrm{d}x - \sum_{j=1}^{N}\underbrace{\left(\left(\overline{c}_{j+1/2}\overline{R}_{j+1/2} + \frac{1}{2}s_{j+1/2}[\![R]\!]_{j+1/2}\right)\right.}_{\text{Diffusive flux}}\phi^-_{j+1/2} \\
+ \sum_{j=1}^{N}\underbrace{\left.\left(\overline{c}_{j-1/2}\overline{R}_{j-1/2} + \frac{1}{2}s_{j-1/2}[\![R]\!]_{j-1/2}\right)\right)}_{\text{Diffusive flux}}\phi^+_{j-1/2} \\
= \frac{1}{2}\sum_{j=1}^{N}\int_{\Omega_j} c\left(R\phi\right)_x \mathrm{d}x - \frac{1}{2}\sum_{j=1}^{N}\overline{c}_{j+1/2}R^-_{j+1/2}\phi^-_{j+1/2} \\
+ \frac{1}{2}\sum_{j=1}^{N}\overline{c}_{j-1/2}R^+_{j-1/2}\phi^+_{j-1/2} - \frac{1}{2}\sum_{j=1}^{N}\int_{\Omega_j} c\left(S\phi\right)_x \mathrm{d}x \\
+ \frac{1}{2}\sum_{j=1}^{N}\overline{c}_{j+1/2}S^-_{j+1/2}\phi^-_{j+1/2} - \frac{1}{2}\sum_{j=1}^{N}\overline{c}_{j-1/2}S^+_{j-1/2}\phi^+_{j-1/2} \\
\underbrace{- \sum_{j=1}^{N}\varepsilon_j\int_{\Omega_j} R_x\phi_x \mathrm{d}x}_{\text{shock capturing operator}}
\end{aligned}
\tag{2.16}
$$

for all $\phi \in X^p_{\Delta x}(\Omega)$,

$$\begin{aligned}
\sum_{j=1}^{N}\int_{\Omega_j} S_t\eta \mathrm{d}x - \sum_{j=1}^{N}\int_{\Omega_j} cS\eta_x \mathrm{d}x + \sum_{j=1}^{N}\underbrace{\left(\overline{c}_{j+1/2}\overline{S}_{j+1/2} - \frac{1}{2}s_{j+1/2}[\![S]\!]_{j+1/2}\right)}_{\text{Diffusive flux}}\eta^-_{j+1/2} \\
- \sum_{j=1}^{N}\underbrace{\left(\overline{c}_{j-1/2}\overline{S}_{j-1/2} - \frac{1}{2}s_{j-1/2}[\![S]\!]_{j-1/2}\right)}_{\text{Diffusive flux}}\eta^+_{j-1/2} \\
= \frac{1}{2}\sum_{j=1}^{N}\int_{\Omega_j} c\,(R\eta)_x \,\mathrm{d}x - \frac{1}{2}\sum_{j=1}^{N}\overline{c}_{j+1/2}R^-_{j+1/2}\eta^-_{j+1/2} \\
+ \frac{1}{2}\sum_{j=1}^{N}\overline{c}_{j-1/2}R^+_{j-1/2}\eta^+_{j-1/2} - \frac{1}{2}\sum_{j=1}^{N}\int_{\Omega_j} c\,(S\eta)_x \,\mathrm{d}x \\
+ \frac{1}{2}\sum_{j=1}^{N}\overline{c}_{j+1/2}S^-_{j+1/2}\eta^-_{j+1/2} - \frac{1}{2}\sum_{j=1}^{N}\overline{c}_{j-1/2}S^+_{j-1/2}\eta^+_{j-1/2} \\
\underbrace{- \sum_{j=1}^{N}\varepsilon_j\int_{\Omega_j} S_x\eta_x \mathrm{d}x}_{\text{shock capturing operator}}
\end{aligned} \tag{2.17}$$

for all $\eta \in X^p_{\Delta x}(\Omega)$ and

$$\sum_{j=1}^{N}\int_{\Omega_j} \psi_t\,\zeta \mathrm{d}x = \sum_{j=1}^{N}\int_{\Omega_j} \frac{R+S}{2}\,\zeta\,\mathrm{d}x, \tag{2.18}$$

for all $\zeta \in X^p_{\Delta x}(\Omega)$.

The scaling parameter $\varepsilon_j$ in the *shock capturing operator* is given by

$$\varepsilon_j = \frac{\Delta x_j\, C\,\overline{\mathrm{Res}}}{\left(\int_{\Omega_j}(R_x^2 + S_x^2)\mathrm{d}x\right)^{1/2} + \Delta x_j^{\theta}} \tag{2.19}$$

where $C > 0$ is a constant, $\theta \geq 1/2$ and

$$\overline{\mathrm{Res}} = \left(\int_{\Omega_j}(\mathrm{Res})^2 \mathrm{d}x\right)^{1/2} \tag{2.20}$$

with

$$\mathrm{Res} = (R^2+S^2)_t - \left(c(\psi)(R^2-S^2)\right)_x. \tag{2.21}$$

Note that $\varepsilon_j$ vanishes for smooth solutions.

We have the following theorem illustrating the energy dissipation associated with (2.16)–(2.18).

**Proposition 2.2** (Energy stability)**.** *Let $R, S \in X^p_{\Delta x}(\Omega)$ be a numerical solution of the semi-discrete scheme* (2.16)–(2.18) *with periodic boundary conditions. We then have*

$$\left( \sum_{j=1}^{N} \int_{\Omega_j} \frac{R^2 + S^2}{2} \, \mathrm{d}x \right)_t \leq 0. \tag{2.22}$$

*Proof.* First, we calculate

$$\begin{aligned} \frac{1}{2} \sum_{j=1}^{N} s_{j+1/2} [\![R]\!]_{j+1/2} R^-_{j+1/2} - \frac{1}{2} \sum_{j=1}^{N} s_{j-1/2} [\![R]\!]_{j-1/2} R^+_{j-1/2} \\ + \frac{1}{2} \sum_{j=1}^{N} s_{j+1/2} [\![S]\!]_{j+1/2} S^-_{j+1/2} - \frac{1}{2} \sum_{j=1}^{N} s_{j-1/2} [\![S]\!]_{j-1/2} S^+_{j-1/2} \\ = -\frac{1}{2} \sum_{j=1}^{N} s_{j+1/2} \left( [\![R]\!]^2_{j+1/2} + [\![S]\!]^2_{j+1/2} \right) \leq 0, \end{aligned} \tag{2.23}$$

since $s_{j+1/2} \geq 0$ for all $j$. Since $R$ and $S$ are a numerical solution, we can use (2.16)–(2.17) with $\phi = R$ and $\eta = S$, and proceed in a manner similar to the proof of Proposition 2.1 to

estimate

$$\begin{aligned}
\left(\sum_{j=1}^{N}\int_{\Omega_j}\frac{R^2+S^2}{2}\,\mathrm{d}x\right)_t &= \sum_{j=1}^{N}\int_{\Omega_j}\left(RR_t+SS_t\right)\,\mathrm{d}x \\
&= \frac{1}{2}\overline{c}_{N+1/2}\left(R^+_{N+1/2}R^-_{N+1/2}-S^+_{N+1/2}S^-_{N+1/2}\right) \\
&\quad -\frac{1}{2}\overline{c}_{1/2}\left(R^-_{1/2}R^+_{1/2}-S^-_{1/2}S^+_{1/2}\right)+\frac{1}{2}\sum_{j=1}^{N}s_{j+1/2}[\![R]\!]_{j+1/2}R^-_{j+1/2} \\
&\quad -\frac{1}{2}\sum_{j=1}^{N}s_{j-1/2}[\![R]\!]_{j-1/2}R^+_{j-1/2}+\frac{1}{2}\sum_{j=1}^{N}s_{j+1/2}[\![S]\!]_{j+1/2}S^-_{j+1/2} \\
&\quad -\frac{1}{2}\sum_{j=1}^{N}s_{j-1/2}[\![S]\!]_{j-1/2}S^+_{j-1/2}-\sum_{j=1}^{N}\varepsilon_j\int_{\Omega_j}(R_x^2+S_x^2)\,\mathrm{d}x \\
&= \frac{1}{2}\overline{c}_{N+1/2}\left(R^+_{N+1/2}R^-_{N+1/2}-S^+_{N+1/2}S^-_{N+1/2}\right) \\
&\quad -\frac{1}{2}\overline{c}_{1/2}\left(R^-_{1/2}R^+_{1/2}-S^-_{1/2}S^+_{1/2}\right) \\
&\quad -\frac{1}{2}\sum_{j=1}^{N}s_{j+1/2}\left([\![R]\!]^2_{j+1/2}+[\![S]\!]^2_{j+1/2}\right)-\sum_{j=1}^{N}\varepsilon_j\int_{\Omega_j}(R_x^2+S_x^2)\,\mathrm{d}x \\
&\leq 0,
\end{aligned} \tag{2.24}$$

where we have used the compact support in the last inequality. □

Hence, the scheme (2.16)–(2.18) is energy stable (dissipating) and we expect it to converge to a dissipative solution of (1.3) as the mesh is refined. We remark that energy dissipation results from adding *numerical viscosity* (scaled by the maximum wave speed) and a *shock capturing operator* to the energy conservative scheme (2.9)–(2.11).

2.6. **An alternative first-order system.** It is easy to check that the variational wave equation (1.3) can be rewritten as a first-order system by introducing the independent variables:

$$\begin{aligned}
v &:= \psi_t \\
w &:= c(\psi)\psi_x
\end{aligned}$$

Again, for smooth solutions, equation (1.3) is equivalent to the following system for $(v, w, \psi)$:

$$\begin{cases}
v_t-(c(\psi)w)_x=-c_x(\psi)w \\
w_t-(c(\psi)v)_x=0 \\
\psi_t=v
\end{cases} \tag{2.25}$$

Furthermore, the energy associated with the above equation is

$$\mathcal{E}(t) = \int_{\mathbb{R}} \left(v^2 + w^2\right) dx. \tag{2.26}$$

Again, we can check that smooth solutions of (2.25) preserve this energy. Weak solutions can be either energy conservative or energy dissipative.

2.7. **Variational formulation.** As before, we seek an approximation $(v, w, \psi)$ of (2.25) such that for each $t \in [0, T]$, $v$, $w$, and $\psi$ belong to finite dimensional space

$$X^p_{\Delta x}(\Omega) = \left\{ u \in L^2(\Omega) : u|_{\Omega_j} \text{ polynomial of degree} \le p \right\}.$$

The variational form is derived by multiplying the strong form (2.25) with test functions $\phi, \eta, \zeta \in X^p_{\Delta x}(\Omega)$ and integrating over each element separately. After using integration-by-parts, we obtain

$$\begin{aligned}
&\sum_{j=1}^{N} \int_{\Omega_j} v_t\, \phi \mathrm{d}x + \sum_{j=1}^{N} \int_{\Omega_j} c(\psi) w \phi_x \,\mathrm{d}x - \sum_{j=1}^{N} (cw)_{j+1/2} \phi^-_{j+1/2} + \sum_{j=1}^{N} (cw)_{j-1/2} \phi^+_{j-1/2} \\
&\qquad = \sum_{j=1}^{N} \int_{\Omega_j} c(\psi) \left(w\phi\right)_x \mathrm{d}x - \sum_{j=1}^{N} (c)_{j+1/2} w^-_{j+1/2} \phi^-_{j+1/2} + \sum_{j=1}^{N} (c)_{j-1/2} w^+_{j-1/2} \phi^+_{j-1/2}
\end{aligned} \tag{2.27}$$

and

$$\sum_{j=1}^{N} \int_{\Omega_j} w_t\, \eta \mathrm{d}x + \sum_{j=1}^{N} \int_{\Omega_j} c(\psi) v \eta_x \,\mathrm{d}x - \sum_{j=1}^{N} (cv)_{j+1/2} \eta^-_{j+1/2} + \sum_{j=1}^{N} (cv)_{j-1/2} \eta^+_{j-1/2} = 0, \tag{2.28}$$

and

$$\sum_{j=1}^{N} \int_{\Omega_j} \psi_t\, \zeta \mathrm{d}x = \sum_{j=1}^{N} \int_{\Omega_j} v\, \zeta \,\mathrm{d}x. \tag{2.29}$$

As before, the numerical fluxes $(cv)_{j+1/2}$, $(cw)_{j+1/2}$ and $(c)_{j+1/2}$ all need to be determined.

2.8. **Energy Preserving Scheme.** As before, for a conservative scheme, we use the numerical flux

$$(c)_{j\pm1/2} = \overline{c}_{j\pm1/2} \quad \text{and} \quad (cf)_{j\pm1/2} = \overline{c}_{j\pm1/2} \overline{f}_{j\pm1/2}.$$

Then, for the $vw$-formulation the DG scheme becomes: Find $v, w, \psi \in X^p_{\Delta x}(\Omega)$ such that

$$\begin{aligned}
&\sum_{j=1}^{N} \int_{\Omega_j} v_t\, \phi \mathrm{d}x + \sum_{j=1}^{N} \int_{\Omega_j} c(\psi) w \phi_x \,\mathrm{d}x - \sum_{j=1}^{N} \overline{c}_{j+1/2} \overline{w}_{j+1/2} \phi^-_{j+1/2} + \sum_{j=1}^{N} \overline{c}_{j-1/2} \overline{w}_{j-1/2} \phi^+_{j-1/2} \\
&\qquad = \sum_{j=1}^{N} \int_{\Omega_j} c(\psi) \left(w\phi\right)_x \mathrm{d}x - \sum_{j=1}^{N} \overline{c}_{j+1/2} w^-_{j+1/2} \phi^-_{j+1/2} + \sum_{j=1}^{N} \overline{c}_{j-1/2} w^+_{j-1/2} \phi^+_{j-1/2}
\end{aligned} \tag{2.30}$$

and

$$\sum_{j=1}^{N}\int_{\Omega_j} w_t\,\eta \mathrm{d}x+\sum_{j=1}^{N}\int_{\Omega_j} c(\psi)v\eta_x\,\mathrm{d}x-\sum_{j=1}^{N}\overline{c}_{j+1/2}\overline{v}_{j+1/2}\eta^{-}_{j+1/2}+\sum_{j=1}^{N}\overline{c}_{j-1/2}\overline{v}_{j-1/2}\eta^{+}_{j-1/2}=0, \tag{2.31}$$

and

$$\sum_{j=1}^{N}\int_{\Omega_j}\psi_t\,\zeta\mathrm{d}x=\sum_{j=1}^{N}\int_{\Omega_j} v\,\zeta\,\mathrm{d}x, \tag{2.32}$$

for all $\phi,\eta,\zeta\in X^p_{\Delta x}(\Omega)$.

We have the following theorem for the scheme:

**Proposition 2.3** (Energy conservation)**.** *Let $v,w\in X^p_{\Delta x}(\Omega)$ be a numerical solution of the semi-discrete scheme* (2.30)–(2.32) *with periodic boundary conditions. We then have*

$$\left(\sum_{j=1}^{N}\int_{\Omega_j}\left(v^2+w^2\right)\mathrm{d}x\right)_t=0. \tag{2.33}$$

*Proof.* Since $v$ and $w$ are a numerical solution then (2.30) and (2.31) hold for any functions $\phi,\eta\in X^p_{\Delta x}(\Omega)$. In particular, they hold for the choice $\phi=v$ and $\eta=w$. We can then calculate

$$\begin{aligned}\left(\sum_{j=1}^{N}\int_{\Omega_j}\left(v^2+w^2\right)\mathrm{d}x\right)_t &= 2\sum_{j=1}^{N}\int_{\Omega_j}\left(v_tv+w_tw\right)\mathrm{d}t\\ &= 2\sum_{j=1}^{N}\Big(\overline{c}_{j+1/2}\left(\overline{w}_{j+1/2}v^{-}_{j+1/2}-w^{-}_{j+1/2}v^{-}_{j+1/2}+\overline{v}_{j+1/2}w^{-}_{j+1/2}\right)\\ &\quad+\overline{c}_{j-1/2}\left(-\overline{w}_{j-1/2}v^{+}_{j-1/2}+w^{+}_{j-1/2}v^{+}_{j-1/2}-\overline{v}_{j-1/2}w^{+}_{j-1/2}\right)\Big)\\ &= 2\sum_{j=1}^{N}\overline{c}_{j+1/2}\left(-\overline{w}_{j+1/2}[\![v]\!]_{j+1/2}+[\![wv]\!]_{j+1/2}-\overline{v}_{j+1/2}[\![w]\!]_{j+1/2}\right)\\ &= 0,\end{aligned} \tag{2.34}$$

where we have used the periodic boundary conditions and the identity (2.1). □

2.9. **Energy Dissipating Scheme.** In-order to approximate dissipative solutions, we again add some numerical viscosity and a shock capturing operator to the energy conservative scheme (2.30)–(2.32) to obtain the following dissipative scheme: Find $v,w,\psi\in X^p_{\Delta x}(\Omega)$

such that

$$\begin{aligned}\sum_{j=1}^{N}\int_{\Omega_j} v_t\,\phi\mathrm{d}x+\sum_{j=1}^{N}\int_{\Omega_j} c(\psi)w\phi_x\,\mathrm{d}x\\ -\sum_{j=1}^{N}\left(\overline{c}_{j+1/2}\overline{w}_{j+1/2}+\frac{1}{2}s_{j+1/2}[\![v]\!]_{j+1/2}\right)\phi^-_{j+1/2}\\ +\sum_{j=1}^{N}\left(\overline{c}_{j-1/2}\overline{w}_{j-1/2}+\frac{1}{2}s_{j-1/2}[\![v]\!]_{j-1/2}\right)\phi^+_{j-1/2}\\ =\sum_{j=1}^{N}\int_{\Omega_j} c(\psi)\left(w\phi\right)_x\mathrm{d}x-\sum_{j=1}^{N}\overline{c}_{j+1/2}w^-_{j+1/2}\phi^-_{j+1/2}\\ +\sum_{j=1}^{N}\overline{c}_{j-1/2}w^+_{j-1/2}\phi^+_{j-1/2}-\sum_{j=1}^{N}\varepsilon_j\int_{\Omega_j} v_x\phi_x\mathrm{d}x.\end{aligned}\tag{2.35}$$

for all $\phi\in X^p_{\Delta x}(\Omega)$,

$$\begin{aligned}\sum_{j=1}^{N}\int_{\Omega_j} w_t\,\eta\mathrm{d}x+\sum_{j=1}^{N}\int_{\Omega_j} c(\psi)v\eta_x\,\mathrm{d}x\\ -\sum_{j=1}^{N}\left(\overline{c}_{j+1/2}\overline{v}_{j+1/2}+\frac{1}{2}s_{j+1/2}[\![w]\!]_{j+1/2}\right)\eta^-_{j+1/2}\\ +\sum_{j=1}^{N}\left(\overline{c}_{j-1/2}\overline{v}_{j-1/2}+\frac{1}{2}s_{j-1/2}[\![w]\!]_{j-1/2}\right)\eta^+_{j-1/2}=-\sum_{j=1}^{N}\varepsilon_j\int_{\Omega_j} w_x\eta_x\mathrm{d}x,\end{aligned}\tag{2.36}$$

for all $\eta\in X^p_{\Delta x}(\Omega)$ and

$$\sum_{j=1}^{N}\int_{\Omega_j}\psi_t\,\zeta\mathrm{d}x=\sum_{j=1}^{N}\int_{\Omega_j} v\,\zeta\,\mathrm{d}x,\tag{2.37}$$

for all $\zeta\in X^p_{\Delta x}(\Omega)$.

Expressed in $v$ and $w$, the parameter $\varepsilon_j$ is given by

$$\varepsilon_j=\frac{\Delta x_j\,C\,\overline{\mathrm{Res}}}{\left(\int_{\Omega_j}(v_x^2+w_x^2)\mathrm{d}x\right)^{1/2}+\Delta x_j^{\theta}}\tag{2.38}$$

where $C>0$ is a constant, $\theta\geq 1/2$ and

$$\overline{\mathrm{Res}}=\left(\int_{\Omega_j}(\mathrm{Res})^2\mathrm{d}x\right)^{1/2},\quad \mathrm{Res}=\left(v^2+w^2\right)_t-\left(2c(\psi)vw\right)_x.\tag{2.39}$$

We show that the above scheme dissipates energy in the following theorem:

**Proposition 2.4** (Energy stability)**.** *Let $v, w \in X^p_{\Delta x}(\Omega)$ be a numerical solution of the semi-discrete scheme* (2.35)–(2.37) *with periodic boundary conditions. We then have*

$$\left(\sum_{j=1}^{N}\int_{\Omega_j}\frac{v^2+w^2}{2}\,\mathrm{d}x\right)_t \leq 0. \tag{2.40}$$

*Proof.* Since $v$ and $w$ are a numerical solution, we can use (2.35)–(2.36) with $\phi = v$ and $\eta = w$ and estimate

$$\begin{aligned}
\left(\sum_{j=1}^{N}\int_{\Omega_j}\frac{v^2+w^2}{2}\,\mathrm{d}x\right)_t &= \sum_{j=1}^{N}\int_{\Omega_j}(v_t v + w_t w)\,\mathrm{d}x \\
&= \sum_{j=1}^{N}\Big(\overline{c}_{j+1/2}\left(\overline{w}_{j+1/2}v^-_{j+1/2} - w^-_{j+1/2}v^-_{j+1/2} + \overline{v}_{j+1/2}w^-_{j+1/2}\right) \\
&\quad + \overline{c}_{j-1/2}\left(-\overline{w}_{j-1/2}v^+_{j-1/2} + w^+_{j-1/2}v^+_{j-1/2} - \overline{v}_{j-1/2}w^+_{j-1/2}\right)\Big) \\
&\quad + \frac{1}{2}\sum_{j=1}^{N}\Big(s_{j+1/2}\left(\llbracket v\rrbracket_{j+1/2}v^-_{j+1/2} + \llbracket w\rrbracket_{j+1/2}w^-_{j+1/2}\right) \\
&\quad - s_{j-1/2}\left(\llbracket v\rrbracket_{j-1/2}v^+_{j-1/2} + \llbracket w\rrbracket_{j-1/2}w^+_{j-1/2}\right)\Big) \\
&\quad - \sum_{j=1}^{N}\varepsilon_j\int_{\Omega_j}\left(v_x^2 + w_x^2\right)\mathrm{d}x \\
&= \sum_{j=1}^{N}\overline{c}_{j+1/2}\left(-\overline{w}_{j+1/2}\llbracket v\rrbracket_{j+1/2} + \llbracket wv\rrbracket_{j+1/2} - \overline{v}_{j+1/2}\llbracket w\rrbracket_{j+1/2}\right) \\
&\quad + \frac{1}{2}\sum_{j=1}^{N}\Big(s_{j+1/2}\left(\llbracket v\rrbracket_{j+1/2}v^-_{j+1/2} + \llbracket w\rrbracket_{j+1/2}w^-_{j+1/2}\right) \\
&\quad - s_{j-1/2}\left(\llbracket v\rrbracket_{j-1/2}v^+_{j-1/2} + \llbracket w\rrbracket_{j-1/2}w^+_{j-1/2}\right)\Big) \\
&\quad - \sum_{j=1}^{N}\varepsilon_j\int_{\Omega_j}\left(v_x^2 + w_x^2\right)\mathrm{d}x \\
&= -\frac{1}{2}\sum_{j=1}^{N}s_{j+1/2}\left(\llbracket v\rrbracket^2_{j+1/2} + \llbracket w\rrbracket^2_{j+1/2}\right) - \sum_{j=1}^{N}\varepsilon_j\int_{\Omega_j}\left(v_x^2 + w_x^2\right)\mathrm{d}x \\
&\leq 0,
\end{aligned} \tag{2.41}$$

where we have used the identities (2.1) as well as the periodic boundary conditions. □

## 3. Details on the Implementation

All numerical experiments in this article are performed with an uniform grid spacing $\Delta x_j = \Delta x$. The time step is determined according to

$$\Delta t = 0.1 \frac{\Delta x}{\sup\limits_{\psi \in [0,\pi)} c(\psi)}.$$

Furthermore, for the shock capturing operator, we use $C = 0.1$ and $\theta = 1$.

3.1. **Choice of basis.** Let $\tilde{\Omega} = [-1, 1]$ be the usual reference domain. As a basis for $\mathbb{P}^p(\tilde{\Omega})$, the space of polynomials on $\tilde{\Omega}$ of degree at most $p$, we use the Lagrangian interpolants

$$\ell_k(\xi) = \prod_{\substack{0 \le j \le p \\ j \neq k}} \frac{\xi - \xi_j}{\xi_k - \xi_j}, \tag{3.1}$$

where $\xi_j$, $j = 1, \ldots, p$, are the interpolation points. Note that the Lagrangian interpolants satisfy $\ell_i(\xi_\alpha) = \delta_{i\alpha}$ and thus the discrete orthogonality property

$$\int_{\Omega_j} \ell_j(\xi)\ell_k(\xi) \mathrm{d}\xi = \sum_{\alpha=0}^{p} \rho_\alpha \ell_j(\xi_\alpha)\ell_k(\xi_\alpha) = \rho_j \delta_{jk}, \tag{3.2}$$

where $\rho_\alpha$, $\alpha = 0, \ldots, p$, are quadrature weights.

We introduce the necessary notation required for representing grid functions and quadrature formulas in terms of the basis (3.1). Defining the mapping $\eta_j : \Omega_j \to \tilde{\Omega}$ by

$$\eta_j(x) = 2\frac{x - x_j}{\Delta x}, \tag{3.3}$$

a function $f : \Omega \times [0, T] \to \mathbb{R}$ with $f(\cdot, t) \in X^p_{\Delta x}(\Omega)$ can be written as

$$f(x, t) = \sum_{j=1}^{N} \chi_{\Omega_j}(x) \sum_{k=0}^{p} f_j^{(k)}(t)\ell_k(\eta_j(x)), \tag{3.4}$$

in terms of time dependent coefficients $f_j^{(k)}(t)$. Moreover, we can use the shorthand notation

$$\tilde{f}_j(\xi, t) = f(\eta_j^{-1}(\xi), t) \tag{3.5}$$

for evaluating $f$ on the reference domain. In addition, it is convenient to denote

$$c_j(\xi) = c\left(\tilde{\psi}_j(\xi)\right).$$

The integrals appearing in the DG formulation must be approximated using quadrature. Let $f \in X^p_{\Delta x}(\Omega)$ and represented by (3.4). We can then readily calculate the approximations

$$\int_{\Omega_j} f(x, t)_t \ell_i(\eta_j(x))\, \mathrm{d}x = \frac{\Delta x}{2} \int_{\tilde{\Omega}} \left(\tilde{f}_j\right)_t \ell_i(\xi)\, \mathrm{d}\xi = \frac{\Delta x}{2} \sum_{\alpha=0}^{p} \rho_\alpha \left( \sum_{k=0}^{p} \left(f_j^{(k)}\right)_t \ell_k(\xi_\alpha) \right) \ell_i(\xi_\alpha)$$

$$= \frac{\Delta x}{2} \sum_{\alpha=0}^{p} \rho_\alpha \left( \sum_{k=0}^{p} \left( f_j^{(k)} \right)_t \delta_{k\alpha} \right) \delta_{i\alpha} = \frac{\Delta x}{2} \rho_i \left( f_j^{(i)} \right)_t, \tag{3.6}$$

$$\begin{aligned} \int_{\Omega_j} c(\psi) f(x,t) \ell_i(\eta_j(x))_x \, \mathrm{d}x &= \int_{\tilde{\Omega}} c_j(\xi) \tilde{f}_j(\xi,t) \ell_i'(\xi) \, \mathrm{d}\xi \\ &= \sum_{\alpha=0}^{p} \rho_\alpha c_j(\xi_\alpha) \left( \sum_{k=0}^{p} f_j^{(k)} \ell_k(\xi_\alpha) \right) \ell_i'(\xi_\alpha) \\ &= \sum_{\alpha=0}^{p} \rho_\alpha c_j(\xi_\alpha) \left( \sum_{k=0}^{p} f_j^{(k)} \delta_{k\alpha} \right) \ell_i'(\xi_\alpha) \\ &= \sum_{\alpha=0}^{p} \rho_\alpha c_j(\xi_\alpha) f_j^{(\alpha)} D_{\alpha i}, \end{aligned} \tag{3.7}$$

$$\begin{aligned} \int_{\Omega_j} c(\psi) f(x,t)_x \ell_i(\eta_j(x)) \, \mathrm{d}x &= \int_{\tilde{\Omega}} c_j(\xi) \tilde{f}_j(\xi,t)_\xi \ell_i(\xi) \, \mathrm{d}\xi \\ &= \sum_{\alpha=0}^{p} \rho_\alpha c_j(\xi_\alpha) \left( \sum_{k=0}^{p} f_j^{(k)} \ell_k'(\xi_\alpha) \right) \ell_i(\xi_\alpha) \\ &= \sum_{\alpha=0}^{p} \rho_\alpha c_j(\xi_\alpha) \left( \sum_{k=0}^{p} f_j^{(k)} \ell_k'(\xi_\alpha) \right) \delta_{i\alpha} \\ &= \rho_i c_j(\xi_i) \sum_{k=0}^{p} f_j^{(k)} D_{ik}, \end{aligned} \tag{3.8}$$

$$\int_{\Omega_j} f(x,t)_x \ell_i(\eta_j(x))_x \mathrm{d}x = \frac{2}{\Delta x} \int_{\tilde{\Omega}} \tilde{f}(\xi,t)_\xi \ell_i(\xi)_\xi \mathrm{d}\xi = \frac{2}{\Delta x_j} \sum_{\alpha=0}^{p} \sum_{k=0}^{p} \rho_\alpha f_j^{(k)} D_{\alpha k} D_{\alpha i}, \tag{3.9}$$

and

$$\int_{\Omega_j} \left( f(x,t)_x \right)^2 \mathrm{d}x = \frac{2}{\Delta x} \sum_{\alpha=0}^{p} \rho_\alpha \left( \sum_{k=1}^{p} f_j^{(k)} D_{\alpha k} \right)^2, \tag{3.10}$$

where we have introduced the derivative matrix $D_{ij} = \ell_j'(\xi_i)$.

For the interpolation points $\xi_\alpha$ on the reference domain we use the Gauss–Lobatto–Legendre (GLL) points. This is a set of points particularly convenient for the implementation since they contain the end points. In this paper we will present numerical experiments for $p = 0, 1, 2, 3$. The GLL points, weights, Lagrangian interpolants and their corresponding derivative matrices are omitted here, but can be found in Appendix A.

3.2. **Runge–Kutta time discretization.** The schemes derived in this paper are all in a semi-discrete form

$$u_t = f(t, u_{\Delta x}),$$

where $u_{\Delta x}$ is the discrete solution. The RKDG method utilizes the Runge–Kutta (RK) time marching scheme to advance the solution. Herein, the spatial accuracy in the semi-discrete scheme should be matched with an equally accurate RK scheme to obtain the desired order of accuracy for smooth solutions. Therefore, the following fifth-order RK algorithm was used in this work [25]: Let $u^n_{\Delta x}$ be the discrete solution at time $t^n$ and let $\Delta t^n = t^{n+1} - t^n$. The solutions is then advanced according to

$$\begin{aligned}
k_1 &= f(t^n, u^n_{\Delta x}) \\
k_2 &= f\left(t^n + \frac{4\Delta t^n}{11}, u^n_{\Delta x} + \frac{4\Delta t^n}{11} k_1\right) \\
k_3 &= f\left(t^n + \frac{2\Delta t^n}{5}, u^n_{\Delta x} + \frac{\Delta t^n}{50}(9k_1 + 11k_2)\right) \\
k_4 &= f\left(t^n + \Delta t^n, u^n_{\Delta x} + \frac{\Delta t^n}{4}(-11k_2 + 15k_3)\right) \\
k_5 &= f\Bigg(t^n + (6 - \sqrt{6})\frac{\Delta t^n}{10}, u^n_{\Delta x} \\
&\qquad + \frac{\Delta t^n}{600}\left((81 + 9\sqrt{6})k_1 + (255 - 55\sqrt{6})k_3 + (24 - 14\sqrt{6})k_4\right)\Bigg) \\
k_6 &= f\Bigg(t^n + (6 + \sqrt{6})\frac{\Delta t^n}{10}, u^n_{\Delta x} \\
&\qquad + \frac{\Delta t^n}{600}\left((81 - 9\sqrt{6})k_1 + (255 + 55\sqrt{6})k_3 + (24 + 14\sqrt{6})k_4\right)\Bigg) \\
u^{n+1} &= u^n_{\Delta x} + \frac{1}{36}\Delta t^n \left(4k_1 + (16 + \sqrt{6})k_5 + (16 - \sqrt{6})k_6\right).
\end{aligned}$$

## 4. Numerical experiments

In the following, we perform numerical experiments to demonstrate the properties of the present DG schemes for $p = 0, 1, 2, 3$. Henceforth, the schemes (16 in total) will be named according to ⟨formulation⟩⟨p⟩⟨c/d⟩. For example, the piecewise linear conservative scheme using the *RS* formulation will be referred to as RS1c and the piecewise cubic dissipative scheme using the *vw* formulation will be referred to as vw3d.

4.1. **Order of convergence to manufactured solution.** One of the main attractions of the discontinuous Galerkin scheme is the easy construction of high-order methods. In the following, we numerically demonstrate the order of convergence for smooth solutions.

As previously discussed, the non-linear variational wave equation exhibits blow up in finite time and thus no global smooth solutions are known. However, the order of accuracy can be obtained by using the method of manufactured solutions. If we assert that

$$\psi(x,t) = \sin(x-t) \tag{4.1}$$

then we can for the formulation (2.3) calculate the residual

$$\begin{aligned} Q(x,t) &:= R_t - (c(\psi)R)_x + \frac{c_x(\psi)}{2}(R-S) \\ &= S_t + (c(\psi)S)_x + \frac{c_x(\psi)}{2}(R-S) = \sin(x-t)\left(c^2(\psi)-1\right) - c(\psi)c'(\psi)\cos^2(x-t). \end{aligned} \tag{4.2}$$

Also, for the formulation (2.25) we have

$$v_t - c(\psi)w_x = Q(x,t) \tag{4.3}$$

and

$$w_t - (c(\psi)v)_x = 0. \tag{4.4}$$

Thus, (4.1) will be a smooth solution to the problems

$$\begin{aligned} R_t - (c(\psi)R)_x &= -\frac{c_x(\psi)}{2}(R-S) + Q(x,t) \\ S_t + (c(\psi)S)_x &= -\frac{c_x(\psi)}{2}(R-S) + Q(x,t) \end{aligned}$$

and

$$\begin{aligned} v_t - (c(\psi)w)_x &= -c_x(\psi)w + Q(x,t) \\ w_t - (c(\psi)v)_x &= 0, \end{aligned}$$

which differ from the original problems only through the local source terms $Q(x,t)$. The spatial and temporal accuracy of the schemes can then be calculated by solving with the extra source terms, using periodic boundary conditions and approximating the error as

$$e_{L^2}^{\Delta x} = \left( \frac{\Delta x}{2} \sum_{j=1}^{N} \sum_{\alpha=0}^{p} \rho_\alpha \left| \sin(x_j^\alpha, t) - \psi_j^{\Delta x}(x_j^\alpha, t) \right|^2 \right)^{1/2}, \tag{4.5}$$

where $x_j^\alpha = x_0 + \Delta x \left(j + \frac{1}{2}\xi_\alpha\right)$.

Table 4.1 shows the error and the rate of convergence for the $RS$ schemes and Table 4.2 for the $vw$ schemes. The piecewise constant ($p = 0$) schemes demonstrate second order convergence. For odd polynomial orders $p$ the conservative schemes exhibit sub-optimal convergence rates, a type of behavior that has been observed for the discontinuous Galerkin method when using central fluxes [29]. For the other schemes the order of convergence is optimal ($p + 1$).

TABLE 4.1. The order of convergence at $t = 1.0$ for the manufactured sine solution (4.1) for the $RS$ formulation using $N = 20 \times 2^i$.

| | $i$ | 4 | 5 | 6 | 7 | 8 |
|---|---|---|---|---|---|---|
| RS0c | $e_{L^2}^{\Delta x}$ | $2.279 \cdot 10^{-3}$ | $5.698 \cdot 10^{-4}$ | $1.424 \cdot 10^{-4}$ | $3.561 \cdot 10^{-5}$ | $8.901 \cdot 10^{-6}$ |
| | rate | - | 2.000 | 2.000 | 2.000 | 2.000 |
| RS0d | $e_{L^2}^{\Delta x}$ | $4.053 \cdot 10^{-2}$ | $2.063 \cdot 10^{-2}$ | $1.041 \cdot 10^{-2}$ | $5.231 \cdot 10^{-3}$ | $2.622 \cdot 10^{-3}$ |
| | rate | - | 0.974 | 0.986 | 0.993 | 0.996 |
| RS1c | $e_{L^2}^{\Delta x}$ | $3.925 \cdot 10^{-2}$ | $1.962 \cdot 10^{-2}$ | $9.811 \cdot 10^{-3}$ | $4.906 \cdot 10^{-3}$ | $2.453 \cdot 10^{-3}$ |
| | rate | - | 1.000 | 1.000 | 1.000 | 1.000 |
| RS1d | $e_{L^2}^{\Delta x}$ | $3.590 \cdot 10^{-3}$ | $9.068 \cdot 10^{-4}$ | $2.275 \cdot 10^{-4}$ | $5.695 \cdot 10^{-5}$ | $1.425 \cdot 10^{-5}$ |
| | rate | - | 1.985 | 1.995 | 1.998 | 1.999 |
| RS2c | $e_{L^2}^{\Delta x}$ | $1.820 \cdot 10^{-5}$ | $2.255 \cdot 10^{-6}$ | $2.812 \cdot 10^{-7}$ | $3.513 \cdot 10^{-8}$ | $4.390 \cdot 10^{-9}$ |
| | rate | - | 3.013 | 3.003 | 3.001 | 3.000 |
| RS2d | $e_{L^2}^{\Delta x}$ | $2.090 \cdot 10^{-5}$ | $2.594 \cdot 10^{-6}$ | $3.235 \cdot 10^{-7}$ | $4.040 \cdot 10^{-8}$ | $5.049 \cdot 10^{-9}$ |
| | rate | - | 3.010 | 3.003 | 3.001 | 3.001 |
| RS3c | $e_{L^2}^{\Delta x}$ | $2.445 \cdot 10^{-6}$ | $3.058 \cdot 10^{-7}$ | $3.822 \cdot 10^{-8}$ | $4.777 \cdot 10^{-9}$ | $5.971 \cdot 10^{-10}$ |
| | rate | - | 2.999 | 3.000 | 3.000 | 3.000 |
| RS3d | $e_{L^2}^{\Delta x}$ | $2.577 \cdot 10^{-7}$ | $1.609 \cdot 10^{-8}$ | $1.005 \cdot 10^{-9}$ | $6.282 \cdot 10^{-11}$ | $3.926 \cdot 10^{-12}$ |
| | rate | - | 4.001 | 4.001 | 4.000 | 4.000 |

TABLE 4.2. The order of convergence at $t = 1.0$ for the manufactured sine solution (4.1) for the $vw$ formulation using $N = 20 \times 2^i$.

| | $i$ | 4 | 5 | 6 | 7 | 8 |
|---|---|---|---|---|---|---|
| vw0c | $e_{L^2}^{\Delta x}$ | $2.279 \cdot 10^{-3}$ | $5.698 \cdot 10^{-4}$ | $1.424 \cdot 10^{-4}$ | $3.561 \cdot 10^{-5}$ | $8.901 \cdot 10^{-6}$ |
| | rate | - | 2.000 | 2.000 | 2.000 | 2.000 |
| vw0d | $e_{L^2}^{\Delta x}$ | $5.294 \cdot 10^{-2}$ | $2.676 \cdot 10^{-2}$ | $1.345 \cdot 10^{-2}$ | $6.746 \cdot 10^{-3}$ | $3.380 \cdot 10^{-3}$ |
| | rate | - | 0.985 | 0.992 | 0.996 | 0.998 |
| vw1c | $e_{L^2}^{\Delta x}$ | $4.096 \cdot 10^{-2}$ | $2.046 \cdot 10^{-2}$ | $1.022 \cdot 10^{-2}$ | $5.109 \cdot 10^{-3}$ | $2.554 \cdot 10^{-3}$ |
| | rate | - | 1.002 | 1.001 | 1.000 | 1.000 |
| vw1d | $e_{L^2}^{\Delta x}$ | $3.590 \cdot 10^{-3}$ | $9.068 \cdot 10^{-4}$ | $2.275 \cdot 10^{-4}$ | $5.695 \cdot 10^{-5}$ | $1.425 \cdot 10^{-5}$ |
| | rate | - | 1.985 | 1.995 | 1.998 | 1.999 |
| vw2c | $e_{L^2}^{\Delta x}$ | $1.820 \cdot 10^{-5}$ | $2.255 \cdot 10^{-6}$ | $2.812 \cdot 10^{-7}$ | $3.513 \cdot 10^{-8}$ | $4.390 \cdot 10^{-9}$ |
| | rate | - | 3.013 | 3.003 | 3.001 | 3.000 |
| vw2d | $e_{L^2}^{\Delta x}$ | $1.852 \cdot 10^{-5}$ | $2.296 \cdot 10^{-6}$ | $2.863 \cdot 10^{-7}$ | $3.575 \cdot 10^{-8}$ | $4.468 \cdot 10^{-9}$ |
| | rate | - | 3.013 | 3.003 | 3.001 | 3.000 |
| vw3c | $e_{L^2}^{\Delta x}$ | $2.445 \cdot 10^{-6}$ | $3.058 \cdot 10^{-7}$ | $3.822 \cdot 10^{-8}$ | $4.778 \cdot 10^{-9}$ | $5.971 \cdot 10^{-10}$ |
| | rate | - | 2.999 | 3.000 | 3.000 | 3.000 |
| vw3d | $e_{L^2}^{\Delta x}$ | $2.577 \cdot 10^{-7}$ | $1.609 \cdot 10^{-8}$ | $1.005 \cdot 10^{-9}$ | $6.282 \cdot 10^{-11}$ | $3.926 \cdot 10^{-12}$ |
| | rate | - | 4.001 | 4.001 | 4.000 | 4.000 |

4.2. **Gaussian initial data.** A basic test problem for the nonlinear variational wave equation is obtained by considering the smooth initial data

$$\psi(x,0) = \frac{\pi}{4} + \exp\left(-x^2\right), \tag{4.6}$$

$$\psi_t(x,0) = -c(\psi(x,0))\psi_x(x,0), \tag{4.7}$$

for $x \in \mathbb{R}$. This problem has been tested numerically in the literature [16, 20]. It is an example of an initial-value problem with smooth initial data that exhibits blow-up in finite time.

The initial data (4.6)–(4.7) was solved numerically using the $vw$ schemes with $\alpha = 0.5$ and $\beta = 1.5$ for $t \in [0, 10]$ using $N = 1000$. Results for the $RS$ schemes are similar, and are omitted here to avoid unnecessary redundancy. Figure 4.1 shows the results when using the conservative schemes and Figure 4.2 using the dissipative schemes. Also, Figures 4.3 and 4.4 show the evolutions of the auxiliary variables $v = \psi_t$ and $w = c(\psi)\psi_x$ for the conservative and dissipative piecewise cubic schemes, respectively. The results are consistent with those reported by Holden et al. [20]. Despite the initial data being smooth, the solution develops a singularity in $\psi_x$ at around $t = 6$. After this time, spurious oscillations can be observed in the numerical solutions when using the conservative schemes. This effect is not present when using the dissipative schemes.

The schemes derived in this paper have been categorised into conservative and dissipative schemes. Figure 4.5 shows the evolution of the discrete energy

$$E = \sum_{j=1}^{N} \int_{\Omega_j} \frac{R^2 + S^2}{4} \mathrm{d}x = \frac{\Delta x}{8} \sum_{j=1}^{N} \sum_{k=0}^{p} \rho_k \left( \left(R_j^{(k)}\right)^2 + \left(S_j^{(k)}\right)^2 \right), \tag{4.8}$$

or alternatively for the $vw$ formulation

$$E = \sum_{j=1}^{N} \int_{\Omega_j} \frac{v^2 + w^2}{2} \mathrm{d}x = \frac{\Delta x}{4} \sum_{j=1}^{N} \sum_{k=0}^{p} \rho_k \left( \left(v_j^{(k)}\right)^2 + \left(w_j^{(k)}\right)^2 \right), \tag{4.9}$$

for the Gaussian test problem. The results demonstrate clearly the difference between the dissipative and conservative schemes. Indeed, no significant change in the discrete energy can be observed for any of the conservative schemes. Conversely, the dissipative schemes all cause a reduction in the energy.

A key aspect of the nonlinear variational wave equation is the existence of both conservative and dissipative weak solutions. The schemes derived in this paper enables us to investigate this numerically. Figure 4.6 show the numerical solution to the Gaussian test problem with $\alpha = 0.5$ and $\beta = 4.5$ using the conservative (vw3c) and dissipative (vw3d) piecewise cubic schemes. The results clearly indicate that the solution, while initially smooth, develops a singularity at about $t = 5$ (see Fig. 4.6a). After the formation of the singularity we observe that the conservative and dissipative schemes give two distinct solutions, as shown in Figure 4.6b. Table 4.4 shows that the rest of the conservative schemes indeed converge to the conservative reference solution shown in Figure 4.6b. Conversely, the dissipative schemes converge to the dissipative (dashed) solution in Figure 4.6b, as

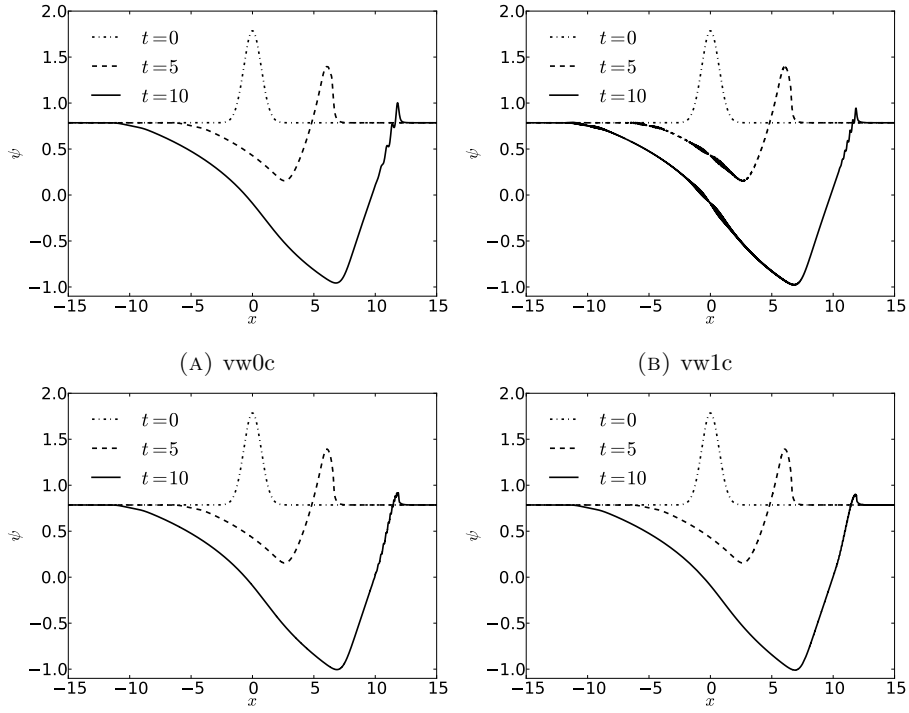


(A) vw0c (B) vw1c

(C) vw2c (D) vw3c

FIGURE 4.1. The numerical solution of the Gaussian test problem with $\alpha = 0.5$ and $\beta = 1.5$ using the conservative schemes based on the $vw$ formulation with $N = 1000$.

shown in Table 4.5. We note that in both cases the convergence is in $N$ as well as in $p$. Also, as can be expected, after the blow up of $\psi_x$ the rate of convergence is slower than for the smooth manufactured solution.

4.3. **Travelling wave.** Glassey et al. [17] discuss weak travelling wave solutions

$$\psi(x,t) = \psi(x - st)$$

for the non-linear variational wave equation. Such a solution must fulfil

$$\psi' \sqrt{|s^2 - \alpha \cos^2(\psi) - \beta \sin^2(\psi)|} = k, \tag{4.10}$$

where $k$ is some integration constant. By choosing $s = \alpha^{1/2}$ we can write

$$\psi' \sin(\psi) = \frac{k}{|\alpha - \beta|^{1/2}}. \tag{4.11}$$

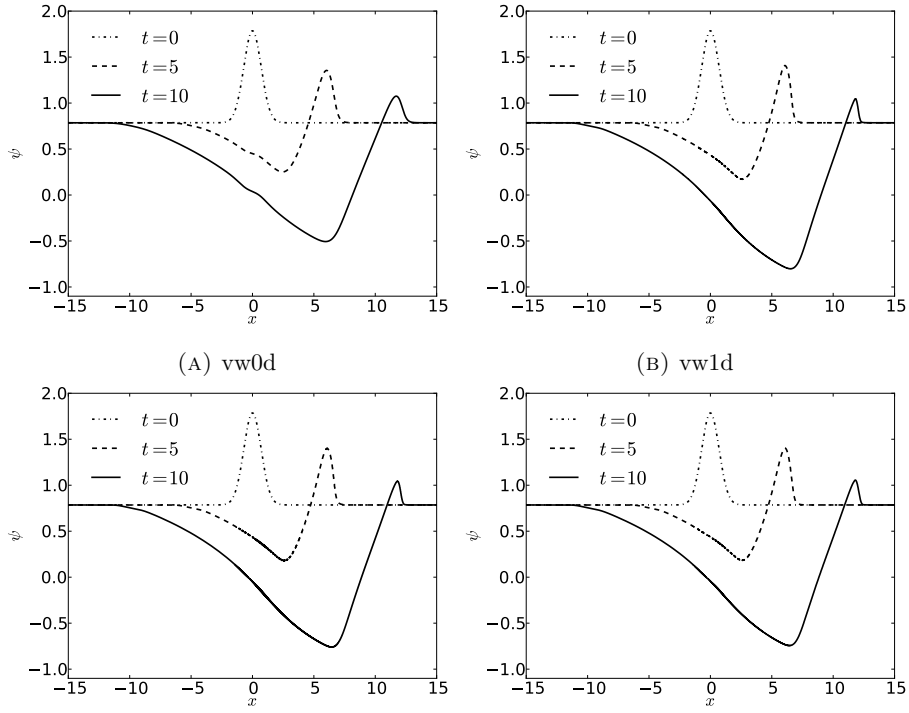


(A) vw0d (B) vw1d

(C) vw2d (D) vw3d

FIGURE 4.2. The numerical solution of the Gaussian test problem with $\alpha = 0.5$ and $\beta = 1.5$ using the dissipative schemes based on the $vw$ formulation with $N = 1000$.

Then by integrating (4.11) with boundary conditions $\psi(0) = 0$ and $\psi(1) = \pi$, we obtain a travelling-wave solution given explicitly as

$$\psi(x,t) = \begin{cases} 0 & x \leq \sqrt{\alpha}t \\ \cos^{-1}\left(-2(x - \sqrt{\alpha}t) + 1\right) & \sqrt{\alpha}t < x < 1 + \sqrt{\alpha}t \\ \pi & x \geq 1 + \sqrt{\alpha}t \end{cases} \tag{4.12}$$

with

$$\psi_x(x,t) = \begin{cases} 0 & x \leq \sqrt{\alpha}t \\ \frac{1}{\sqrt{x - x^2}} & \sqrt{\alpha}t < x < 1 + \sqrt{\alpha}t\,. \\ 0 & x \geq 1 + \sqrt{\alpha}t \end{cases} \tag{4.13}$$

We numerically solve the initial value problem given by the nonlinear variational wave equation and the initial data (4.12)–(4.13) with $\alpha = 0.5$ and $\beta = 1.5$. Figure 4.7 and

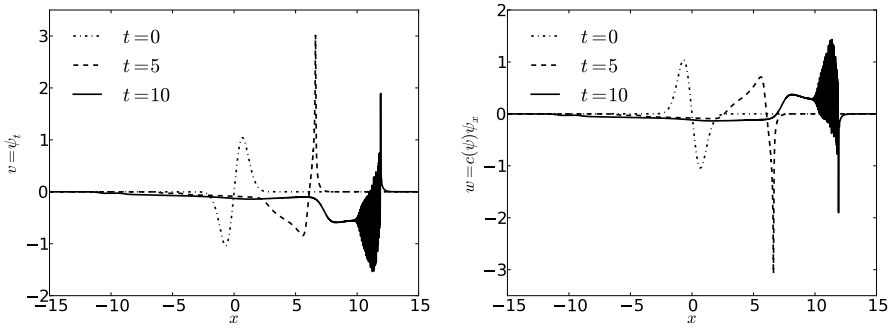


(A) $v$ (B) $w$

FIGURE 4.3. The numerical solution of the Gaussian test problem with $\alpha = 0.5$ and $\beta = 1.5$ using the vw3c scheme with $N = 1000$.

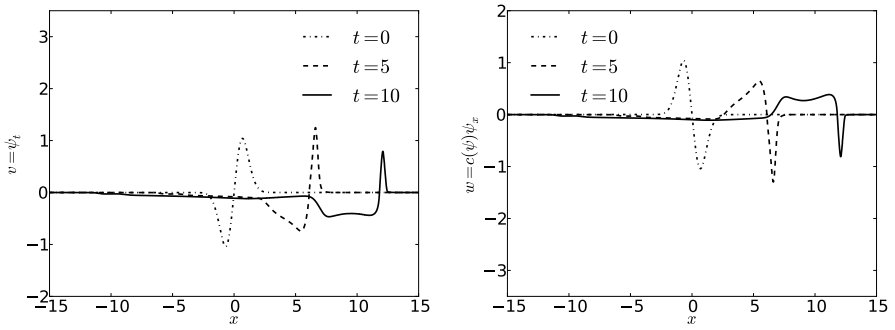


(A) $v$ (B) $w$

FIGURE 4.4. The numerical solution of the Gaussian test problem with $\alpha = 0.5$ and $\beta = 1.5$ using the vw3d scheme with $N = 1000$.

Figure 4.8 show the numerical solution at $t = 1$ with $N = 1000$ using the conservative and dissipative $RS$ schemes, respectively. Results for the $vw$ schemes are similar, and are omitted here to avoid unnecessary redundancy. The numerical solutions are consistent with those reported by Koley et al. [22]. We observe that the strong singularities at the break points cause some numerical irregularities, but overall the schemes are able to capture the travelling wave and become more accurate for higher polynomial order $p$.

## 5. Conclusion

We have considered a nonlinear variational wave equation that models one-dimensional planar waves in nematic liquid crystals. The variational wave equation (1.3) was written

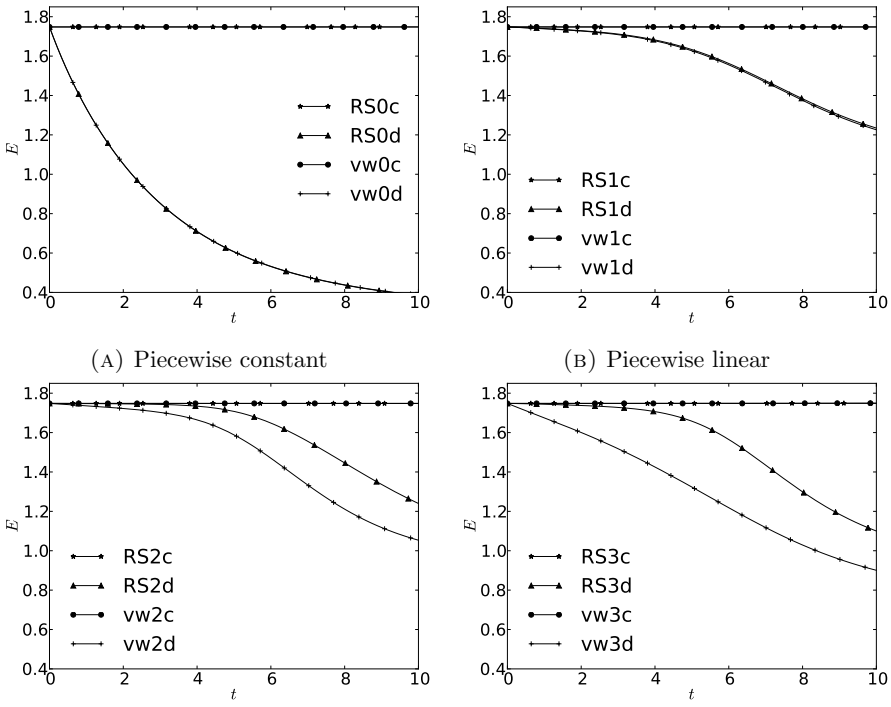


(A) Piecewise constant

(B) Piecewise linear

(C) Piecewise quadratic

(D) Piecewise cubic

FIGURE 4.5. Evolution of the discrete energy (4.8) and (4.9) for the numerical solution of the Gaussian test problem with $\alpha = 0.5$ and $\beta = 1.5$ using $N = 1000$.

TABLE 4.3. The error $\|\psi - \psi_{\text{ref}}\|_2$ for the $vw$ schemes at $t = 1$ for the Gaussian test problem with $\alpha = 0.5$ and $\beta = 1.5$ using $N = 20 \times 2^i$. The reference solution was computed using the vw3c scheme with $N = 25000$.

| $i$ | 3 | 4 | 5 | 6 |
|---|---|---|---|---|
| vw0c | $7.221 \cdot 10^{-2}$ | $3.176 \cdot 10^{-2}$ | $1.528 \cdot 10^{-2}$ | $7.561 \cdot 10^{-3}$ |
| vw0d | $1.902 \cdot 10^{-1}$ | $1.047 \cdot 10^{-1}$ | $5.533 \cdot 10^{-2}$ | $2.851 \cdot 10^{-2}$ |
| vw1c | $8.465 \cdot 10^{-2}$ | $4.180 \cdot 10^{-2}$ | $2.083 \cdot 10^{-2}$ | $1.041 \cdot 10^{-2}$ |
| vw1d | $3.490 \cdot 10^{-2}$ | $9.704 \cdot 10^{-3}$ | $2.523 \cdot 10^{-3}$ | $6.396 \cdot 10^{-4}$ |
| vw2c | $7.566 \cdot 10^{-4}$ | $7.650 \cdot 10^{-5}$ | $9.288 \cdot 10^{-6}$ | $1.151 \cdot 10^{-6}$ |
| vw2d | $7.373 \cdot 10^{-4}$ | $7.770 \cdot 10^{-5}$ | $9.384 \cdot 10^{-6}$ | $1.164 \cdot 10^{-6}$ |
| vw3c | $5.547 \cdot 10^{-5}$ | $6.870 \cdot 10^{-6}$ | $8.568 \cdot 10^{-7}$ | $1.070 \cdot 10^{-7}$ |
| vw3d | $2.612 \cdot 10^{-5}$ | $1.634 \cdot 10^{-6}$ | $1.023 \cdot 10^{-7}$ | $6.397 \cdot 10^{-9}$ |

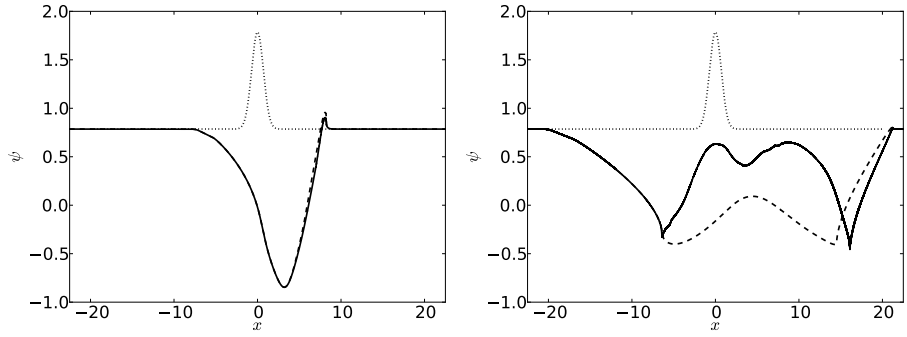


(A) $t = 4$ (B) $t = 12$

FIGURE 4.6. The numerical solution of the Gaussian test problem with $\alpha = 0.5$ and $\beta = 4.5$ using the conservative vw3c (solid) and dissipative vw3d (dashed) schemes using $N = 10000$. The dotted line is the Gaussian initial data.

TABLE 4.4. The error $\|\psi - \psi_{\text{ref}}\|_2$ for the conservative $vw$ schemes at $t = 12$ for the Gaussian initial with $\alpha = 0.5$ and $\beta = 4.5$ with $N = 20 \times 2^i$. The reference solution was computed using the vw3c scheme with $N = 10000$.

| $i$ | 3 | 4 | 5 | 6 | 7 |
|---|---|---|---|---|---|
| vw0c | 2.8578 | 4.5302 | 4.2199 | 3.5382 | 3.0693 |
| vw1c | 4.9764 | 4.3353 | 3.5673 | 3.0770 | 2.8096 |
| vw2c | 2.3927 | 1.3466 | 1.2581 | 1.1201 | 1.0295 |
| vw3c | 1.1941 | 0.7812 | 0.5205 | 0.3233 | 0.1284 |

TABLE 4.5. The error $\|\psi - \psi_{\text{ref}}\|_2$ for the dissipative $vw$ schemes at $t = 12$ for the Gaussian initial with $\alpha = 0.5$ and $\beta = 4.5$ with $N = 20 \times 2^i$. The reference solution was computed using the vw3d scheme with $N = 10000$.

| $i$ | 3 | 4 | 5 | 6 | 7 |
|---|---|---|---|---|---|
| vw0d | 2.1145 | 2.5536 | 2.3978 | 1.9990 | 1.5677 |
| vw1d | 1.7964 | 1.8323 | 1.3663 | 0.8331 | 0.4608 |
| vw2d | 1.5586 | 1.2176 | 0.8640 | 0.4668 | 0.2050 |
| vw3d | 0.6370 | 0.3370 | 0.1764 | 0.0897 | 0.0417 |

in the form of two equivalent first-order systems. An intrinsic property of this equation is the formation of singularities in finite time and the existence of both conservative and dissipative weak solutions. We have constructed robust discontinuous Galerkin schemes for approximating the variational wave equation in one space dimension. The key design

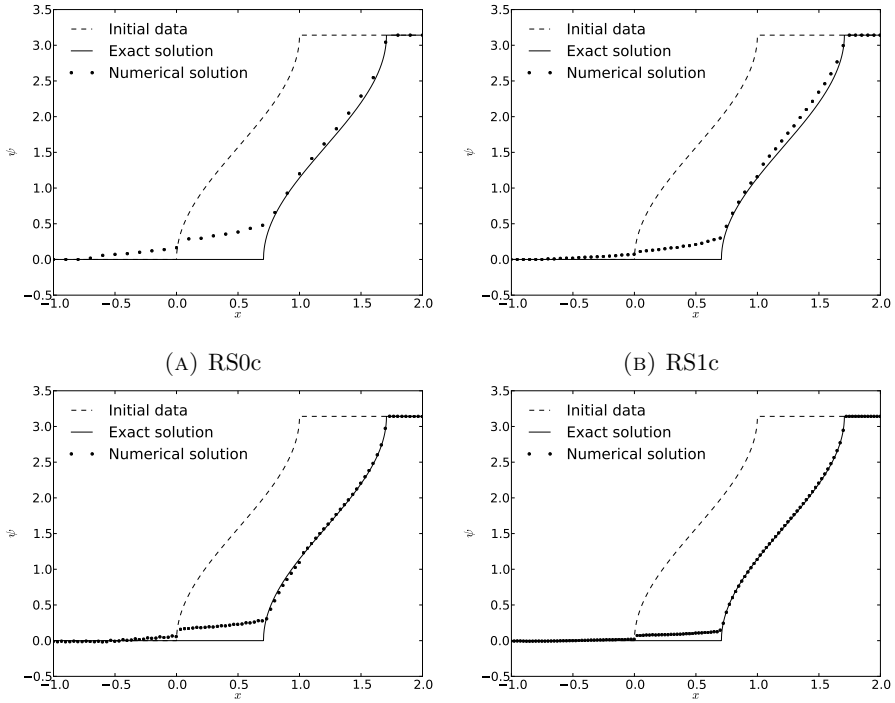


(A) RS0c (B) RS1c

(C) RS2c (D) RS3c

FIGURE 4.7. Numerical solution of the travelling wave initial-value problem with $\alpha = 0.5$ and $\beta = 1.5$ at $t = 1$ using the conservative schemes based on the $RS$ formulation with $N = 1000$.

principle was energy conservation (dissipation), and we have designed high-order semi-discrete schemes that either conserve or dissipate the discrete energy.

Extensive numerical experiments have been presented to illustrate the properties of the DG schemes. The high-order accuracy of the methods was demonstrated using a manufactured smooth solution. It has been shown numerically that the energy conservative and energy dissipative schemes converge to two different solutions when the mesh is refined. To the best of our knowledge, these are the first high-order accurate schemes that can approximate the conservative solutions of the one-dimensional variational wave equation.

There exists a generalization to the current model for 2D. Similar numerical schemes can be developed in this case. Herein, the $vw$ formulation must be used since the Riemann invariants are not defined. This will be the topic of an upcoming paper.

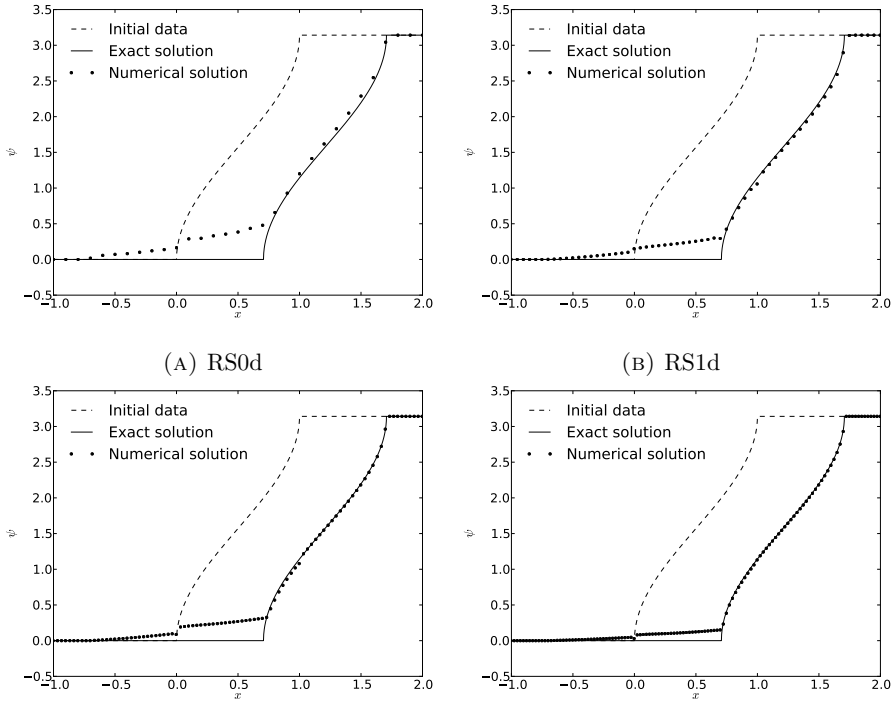


(A) RS0d (B) RS1d

(C) RS2d (D) RS3d

FIGURE 4.8. Numerical solution of the travelling wave initial-value problem with $\alpha = 0.5$ and $\beta = 1.5$ at $t = 1$ using the dissipative schemes based on the $RS$ formulation with $N = 1000$.

## APPENDIX A. GLL POINTS, LAGRANGIAN INTERPOLANTS AND DERIVATIVE MATRICES

A.1. **Piecewise constant** $(p = 0)$**.** For the piecewise constant case the single GLL point is $\xi_0 = 0$ with quadrature weight $\rho_0 = 2$. The derivative matrix is in this case simply given by $D = 0$.

A.2. **Piecewise linear** $(p = 1)$**.** In this case the two GLL points are $\xi_0 = -1$, $\xi_1 = 1$, the weights are $\rho_0 = \rho_1 = 1$.

The Lagrangian interpolants are then given explicitly by

$$\ell_0(\xi) = \frac{1-\xi}{2}, \quad \ell_1(\xi) = \frac{1+\xi}{2}, \tag{A.1}$$

and the derivative matrix is

$$D = \begin{pmatrix} -\frac{1}{2} & \frac{1}{2} \\ -\frac{1}{2} & \frac{1}{2} \end{pmatrix}.$$

A.3. **Piecewise quadratic** ($p = 2$)**.** In the piecewise quadratic case the GLL points are $\xi_0 = -1$, $\xi_1 = 0$ and $\xi_2 = 1$ and the weights are $\rho_0 = 1/3$, $\rho_1 = 4/3$ and $\rho_2 = 1/3$.

The Lagrangian interpolants are then given explicitly by

$$\ell_0(\xi) = \frac{1}{2}\xi(\xi - 1), \quad \ell_1(\xi) = 1 - \xi^2, \quad \ell_2(\xi) = \frac{1}{2}\xi(\xi + 1). \tag{A.2}$$

The derivative matrix then becomes

$$D = \begin{pmatrix} -\frac{3}{2} & 2 & -\frac{1}{2} \\ -\frac{1}{2} & 0 & \frac{1}{2} \\ \frac{1}{2} & -2 & \frac{3}{2} \end{pmatrix}. \tag{A.3}$$

A.4. **Piecewise cubic** ($p = 3$)**.** For a piecewise cubic scheme we use the GLL points $\xi_0 = -1$, $\xi_1 = -\sqrt{1/5}$, $\xi_2 = \sqrt{1/5}$ and $\xi_3 = 1$. The quadrature weights are given by $\rho_0 = \rho_3 = 1/6$ and $\rho_1 = \rho_2 = 5/6$.

The Lagrangian interpolants are given explicitly as

$$\ell_0(\xi) = -\frac{5}{8}(x - 1)\left(x^2 - \frac{1}{5}\right) = -\frac{5}{8}\left(x^3 - x^2 - \frac{1}{5}x + \frac{1}{5}\right), \tag{A.4}$$

$$\ell_1(\xi) = \frac{5}{8}\sqrt{5}\left(x^2 - 1\right)\left(x - \sqrt{\frac{1}{5}}\right) = \frac{5}{8}\sqrt{5}\left(x^3 - \sqrt{\frac{1}{5}}x^2 - x + \sqrt{\frac{1}{5}}\right), \tag{A.5}$$

$$\ell_2(\xi) = -\frac{5}{8}\sqrt{5}\left(x^2 - 1\right)\left(x + \sqrt{\frac{1}{5}}\right) = -\frac{5}{8}\sqrt{5}\left(x^3 + \sqrt{\frac{1}{5}}x^2 - x - \sqrt{\frac{1}{5}}\right), \tag{A.6}$$

$$\ell_3(\xi) = \frac{5}{8}(x + 1)\left(x^2 - \frac{1}{5}\right) = \frac{5}{8}\left(x^3 + x^2 - \frac{1}{5}x - \frac{1}{5}\right), \tag{A.7}$$

which gives the derivative matrix

$$D = \begin{pmatrix} -3 & \frac{10}{8}\sqrt{5}\left(1 + \sqrt{\frac{1}{5}}\right) & -\frac{10}{8}\sqrt{5}\left(1 - \sqrt{\frac{1}{5}}\right) & -\frac{1}{2} \\ -\frac{10}{8}\left(\frac{1}{5} + \sqrt{\frac{1}{5}}\right) & 0 & \frac{4}{8}\sqrt{5} & \frac{10}{8}\left(\frac{1}{5} - \sqrt{\frac{1}{5}}\right) \\ -\frac{10}{8}\left(\frac{1}{5} - \sqrt{\frac{1}{5}}\right) & -\frac{4}{8}\sqrt{5} & 0 & -\frac{10}{8}\left(\frac{1}{5} + \sqrt{\frac{1}{5}}\right) \\ 0.5 & \frac{10}{8}\sqrt{5}\left(1 - \sqrt{\frac{1}{5}}\right) & \frac{10}{8}\sqrt{5}\left(1 + \sqrt{\frac{1}{5}}\right) & 3 \end{pmatrix}. \tag{A.8}$$

## Acknowledgements

The work of Peder Aursand has been funded by the Research Council of Norway (project number 213638). Ujjwal Koley has been supported by a Humboldt Research Fellowship through the Alexander von Humboldt Foundation.

We are grateful to Professor Siddhartha Mishra for his help and advice in the development of these numerical schemes. The authors would also like to thank Professor Nils Henrik Risebro and Professor Helge Holden for fruitful advice in the course of the preparation of this manuscript.

## References

[1] S. Badia, F. Guillén. González and J. V. Gutiérrez–Santacreu. An overview on Numerical Analyses of Nematic Liquid Crystal flows, *Arch. Comput. Methods Eng.*, 18: 285–313 (2011).

[2] S. Badia, F. Guillén. González and J. V. Gutiérrez–Santacreu. Finite element approximation of nematic liquid crystal flows using a saddle-point structure, *J. Comput. Phys.*, 230(4): 1686–1706 (2011).

[3] S. Bartels and A. Prohl. Constraint preserving implicit finite element discretization of harmonic map heat flow into spheres, *Math. Comput.*, 76: 1847–1859 (2007).

[4] T. J. Barth. Numerical methods for gas-dynamics systems on unstructured meshes. In: *An introduction to recent developments in theory and numerics of conservation laws Lecture notes in computational science and engineering*, vol(5), Springer, Berlin. Eds: D Kroner, M. Ohlberger, and C. Rohde, 1999.

[5] R. Becker, X. Feng and A. Prohl. Finite element approximations of the Ericksen–Leslie model for nematic liquid crystal flow, *SIAM J. Numer. Anal.*, 46(4): 1704–1731 (2008).

[6] H. Berestycki, J. M. Coron and I. Ekeland. Variational Methods, Progress in nonlinear differential equations and their applications, *Vol 4*, Birkhäuser, Boston, 1990.

[7] A. Bressan and Y. Zheng. Conservative solutions to a nonlinear variational wave equation, *Commun. Math. Phys.*, 266: 471–497 (2006).

[8] G. Chavent and B. Cockburn. The local projection $p^0p^1$-discontinuous Galerkin finite element methods for scalar conservation law, *Math. Model. Numer. Anal.*, 23: 565–592 (1989).

[9] D. Christodoulou and A. Tahvildar-Zadeh. On the regularity of Spherically symmetric wave maps, *Comm. Pure Appl. Math.*, 46: 1041–1091 (1993).

[10] S. Y. Cockburn, B. Lin and C. W. Shu. TVB Runge-Kutta local projection discontinuous Galerkin finite element methods for conservation laws III: one dimensional systems, *J. Comput. Phys.*, 84: 90–113 (1989).

[11] J. Coron, J. Ghidaglia and F. Hélein. *Nematics*, Kluwer Academic Publishers, Dordrecht, 1991.

[12] R. J. Diperna and A. Majda. Oscillations and Concentrations in weak solutions of the incompressible fluid equations, *Comm. Math. Phys*, 108: 667–689 (1987).

[13] J. L. Ericksen and D. Kinderlehrer. Theory and application of Liquid Crystals, *IMA Volumes in Mathematics and its Applications*, Vol 5, Springer Verlag, New York, 1987.

[14] R. T. Glassey. Finite-time blow-up for solutions of nonlinear wave equations, *Math. Z.*, 177: 1761–1794 (1981).

[15] S. Gottlieb, C.-W. Shu and E. Tadmor. Strong stability preserving high-order time discretization methods, *SIAM Review*, 43(1): 89-112 (2001).

[16] R. Glassey, J. Hunter, and Y. Zheng. Singularities and Oscillations in a nonlinear variational wave equation. In: J. Rauch and M. Taylor, editors, *Singularities and Oscillations*, Volume 91 of the IMA volumes in Mathematics and its Applications, pages 37–60. Springer, New York, 1997.

[17] R. T. Glassey, J. K. Hunter and Yuxi. Zheng. Singularities of a variational wave equation, *J. Diff. Eq.*, 129: 49–78 (1996).

[18] T. R. Hill and W. H. Reed. Triangular mesh methods for neutron transport equation, *Tech. Rep. LA-UR-73-479.*, Los Alamos Scientific Laboratory, 1973.
[19] H. Holden and X. Raynaud. Global semigroup for the nonlinear variational wave equation, *Arch. Rat. Mech. Anal.*, 201(3): 871–964 (2011).
[20] H. Holden, K. H. Karlsen, and N. H. Risebro. A convergent finite-difference method for a nonlinear variational wave equation, *IMA. J. Numer. Anal.*, 29(3): 539–572 (2009).
[21] J. K. Hunter and R. A. Saxton. Dynamics of director fields, *SIAM J. Appl. Math.*, 51: 1498–1521 (1991).
[22] U. Koley, S. Mishra, N. H. Risebro, and F. Weber. Robust finite-difference schemes for a nonlinear variational wave equation modeling liquid crystals, *Submitted.*
[23] F. H. Lin and C. Liu. Non-parabolic dissipative systems modelling the flow of liquid crystals, , *Comm. Pure Appl. Math.*, 48, 501–537 (1995).
[24] F. H. Lin and C. Liu. Existence of solutions for the Ericksen-Leslie system, *Arch. Ration. Mech. Anal.*, 154, 135–156 (2000).
[25] H. A. Luther and H. P. Konen. Some fifth-order classical Runge–Kutta formulas *SIAM Review*, 7(4): 551–558 (1965).
[26] R. A. Saxton. Dynamic instability of the liquid crystal director, *Contemporary Mathematics Vol 100*, Current Progress in Hyperbolic Systems, pages 325–330, ed. W. B. Lindquist, AMS, Providence, 1989.
[27] J. Shatah. Weak solutions and development of singularities in the SU(2) $\sigma$-model, *Comm. Pure Appl. Math.*, 41: 459–469 (1988).
[28] J. Shatah and A. Tahvildar-Zadeh. Regularity of harmonic maps from Minkowski space into rotationally symmetric manifolds, *Comm. Pure Appl. Math*, 45: 947–971 (1992).
[29] C.-W. Shu. Different formulations of the discontinuous Galerkin method for the viscous terms, In: *Conference in Honor of Professor H.-C. Huang on the occasion of his retirement*, Science Press, 14–45, 2000.
[30] P. Zhang and Y. Zheng. On oscillations of an asymptotic equation of a nonlinear variational wave equation, *Asymptot. Anal.*, 18(3): 307–327 (1998).
[31] P. Zhang and Y. Zheng. Singular and rarefactive solutions to a nonlinear variational wave equation, *Chin. Ann. Math.*, 22: 159–170 (2001).
[32] P. Zhang and Y. Zheng. Rarefactive solutions to a nonlinear variational wave equation of liquid crystals, *Commun. Partial Differ. Equ.*, 26: 381–419 (2001).
[33] P. Zhang and Y. Zheng. Weak solutions to a nonlinear variational wave equation, *Arch. Rat. Mech. Anal.*, 166: 303–319 (2003).
[34] P. Zhang and Y. Zheng. Weak solutions to a nonlinear variational wave equation with general data, *Ann. Inst. H. Poincaré Anal. Non Linéaire*, 22: 207–226 (2005).
[35] P. Zhang and Y. Zheng. On the global weak solutions to a nonlinear variational wave equation, *Handbook of Differential Equations. Evolutionary Equations*, ed. C. M. Dafermos and E. Feireisl, vol. 2, pages 561–648, Elsevier, 2006.

(Peder Aursand)
Department of Mathematical Sciences,
Norwegian University of Science and Technology,
NO–7491 Trondheim, Norway.
*E-mail address*: peder.aursand@math.ntnu.no

(Ujjwal Koley)
Institut für Mathematik,
Julius-Maximilians-Universität Würzburg,
Campus Hubland Nord, Emil-Fischer-Strasse 30,
97074, Würzburg, Germany.
*E-mail address*: toujjwal@gmail.com

# Paper D

**High-order energy stable numerical schemes for a nonlinear variational wave equation modeling nematic liquid crystals in two dimensions**

Peder Aursand and Ujjwal Koley

Submitted for publication.

## Preface

The research making up this paper is a continuation of the work in Paper C. We realized that while the 2D variational wave equation can be seen as a natural generalization of the equation considered in Paper C, the mathematical theory for weak solutions to this equation has not been established. Given the promise of the numerical methods developed in the 1D case, we aimed to use similar techniques for the 2D equation to be at the forefront of the analysis.

The method used is essentially the same as for the 1D equation. The extra complexity mostly comes from the added algebra and the implementation becoming more involved. In addition, 2D simulations require more computational work. Ultimately the investigation proved successful. DG schemes could be derived satisfying the same energy respecting properties as in the 1D case, and the results indicate that there might exist different classes of weak solutions.

# HIGH-ORDER ENERGY STABLE NUMERICAL SCHEMES FOR A NONLINEAR VARIATIONAL WAVE EQUATION MODELING NEMATIC LIQUID CRYSTALS IN TWO DIMENSIONS

PEDER AURSAND AND UJJWAL KOLEY

Abstract. We consider a nonlinear variational wave equation that models the dynamics of the director field in nematic liquid crystals with high molecular rotational inertia. Being derived from an energy principle, energy stability is an intrinsic property of solutions to this model. For the two-dimensional case, we design numerical schemes based on the discontinuous Galerkin framework that either conserve or dissipate a discrete version of the energy.

Extensive numerical experiments are performed verifying the scheme's energy stability, order of convergence and computational efficiency. The numerical solutions are compared to those of a simpler first-order Hamiltonian scheme. We provide numerical evidence that solutions of the 2D variational wave equation loose regularity in finite time. After that occurs, dissipative and conservative schemes appear to converge to different solutions.

## 1. Introduction

1.1. **The Equation.** Liquid crystals (LCs) are mesophases, i.e., intermediate states of matter between the liquid and the crystal phase. They possess some of the properties of liquids (e.g. formation, fluidity) as well as some crystalline properties (e.g. electrical, magnetic, etc.) normally associated with solids. The nematic phase is the simplest of the liquid crystal mesophases, and is close to the liquid phase. It is characterized by long-range orientational order, i.e., the long axes of the molecules tend to align along a preferred direction, which can be considered invariant under rotation by an angle of $\pi$. The state of a nematic liquid crystals is usually given by two linearly independent vector fields; one describing the fluid flow and the other describing the dynamics of the preferred axis, which is defined by a vector $\mathbf{n}$ giving its local orientation. Under the assumption of constant degree of orientation, the magnitude of the *director field* $\mathbf{n}$ is usually taken to be unity. In the present work we focus exclusively on the dynamics of the director field (independently of any coupling with the fluid flow), a map

$$\mathbf{n} : \mathbb{R}^3 \times [0, \infty) \to \mathbb{S}^2$$

from the Euclidean space to the unit ball.

*Date*: June 15, 2015.

2010 *Mathematics Subject Classification.* Primary 65M99; Secondary 65M60, 35L60.

*Key words and phrases.* Nonlinear variational wave equation, Energy preserving scheme, Energy stable scheme, Discontinuous Galerkin method, Higher order scheme.

We consider the elastic dynamics of the liquid crystal director field in the inertia-dominated case (zero viscosity). Associated with the director field $\mathbf{n}$, the classical Oseen-Frank elastic energy density $\mathcal{W}$ is given by

$$\mathcal{W}(\mathbf{n}, \nabla\mathbf{n}) = \alpha \left|\mathbf{n} \times (\nabla \times \mathbf{n})\right|^2 + \beta \left(\nabla \cdot \mathbf{n}\right)^2 + \gamma \left(\mathbf{n} \cdot (\nabla \times \mathbf{n})\right)^2. \tag{1.1}$$

The constants $\alpha, \beta$ and $\gamma$ are elastic material constants of the liquid crystal, and are associated with the three basic types of deformations of the medium; bend, splay and twist; respectively. Each of these constants must be positive in order to guarantee the existence of the minimum configuration of the energy $\mathcal{W}$ in the undistorted nematic configuration.

The one constant approximation ($\alpha = \beta = \gamma$) often provides a valuable tool to reach a qualitative insight into distortions of nematic configurations. Observe that, in this case the potential energy density (1.1) reduces to the Dirichlet energy

$$\mathcal{W}(\mathbf{n}, \nabla\mathbf{n}) = \alpha \left|\nabla\mathbf{n}\right|^2.$$

This corresponds to the potential energy density used in harmonic maps into the sphere $\mathbb{S}^2$. The stability of the general Oseen–Frank potential energy equation, derived from the potential (1.1) using a variational principle, is studied by Ericksen and Kinderlehrer [8]. For the parabolic flow associated to (1.1), see [3, 7] and references therein.

In the regime in which inertial effects dominate viscosity, the dynamics of the director $\mathbf{n}$ is governed by the least action principle

$$\mathbb{J}(\mathbf{n}) = \iint \left(\mathbf{n}_t^2 - \mathcal{W}(\mathbf{n}, \nabla\mathbf{n})\right) \, dx\, dt, \qquad \mathbf{n} \cdot \mathbf{n} = 1. \tag{1.2}$$

Standard calculations reveal that the *Euler-Lagrange* equation associated to $\mathbb{J}$ is given by

$$\mathbf{n}_{tt} = \operatorname{div}\left(\mathcal{W}_{\nabla\mathbf{n}}(\mathbf{n}, \nabla\mathbf{n})\right) - \mathcal{W}_{\mathbf{n}}(\mathbf{n}, \nabla\mathbf{n}), \tag{1.3}$$

and is termed the variational wave equation. Introducing the *energy* and *energy density*

$$\mathcal{E}(t) = \int \left(\mathbf{n}_t^2 + \mathcal{W}(\mathbf{n}, \nabla\mathbf{n})\right) \, dx, \qquad \mathbf{E}(t, x) = \mathbf{n}_t^2 + \mathcal{W}(\mathbf{n}, \nabla\mathbf{n}),$$

it is easy to check the identities

$$\mathcal{E}' = 0, \qquad \mathbf{E}_t = \operatorname{div}\left(\mathcal{W}_{\nabla\mathbf{n}}(\mathbf{n}, \nabla\mathbf{n})\mathbf{n}_t\right),$$

in light of (1.3). Given the formidable difficulties in the mathematical analysis of (1.3), it is customary to investigate the particular case of a planar director field configuration.

The physical implications of considering the inertia-dominated regime warrants a comment. Indeed, in many experimental situations the inertial forces acting on the director are orders of magnitude smaller than the dissipative. For this reason, the inertial term is often neglected in modelling [25, 26, 9]. It was however noted early by Leslie [21] that inertial forces might be significant in cases where the director field is subjected to large accelerations. In general, inertia will be more significant in the small time-scale dynamics of the director. For this reason, their inclusion can be warranted in, e.g., liquid crystal acoustics [19], mechanical vibrations [27] and in cases with and external oscillating magnetic field [28].

1.1.1. *One-dimensional planar waves.* Planar deformations are central in the mathematical study of models for nematic liquid crystals. A simple such model can be derived by assuming that the deformation depends on a single space variable $x$ and that the director field $\mathbf{n}$ in confined to the $x$-$y$ plane. In this case we can write the director as

$$\mathbf{n} = (\cos u(x,t),\, \sin u(x,t),\, 0).$$

Geometrically, the molecules are lined up vertically on the $x$-$y$ plane, and at each column (located at $x$) $u(x,t)$ measures the angle of the director field to the $x$-direction. With the above simplifications, the variational principle (1.2) reduces to

$$\begin{cases} u_{tt} - c(u)\,(c(u)u_x)_x = 0, & (x,t) \in \Pi_T, \\ u(x,0) = u_0(x), & x \in \mathbb{R}, \\ u_t(x,0) = u_1(x), & x \in \mathbb{R}, \end{cases} \tag{1.4}$$

where $\Pi_T = \mathbb{R} \times [0,T]$ with fixed $T > 0$ , and the wave speed $c(u)$ given by

$$c^2(u) = \alpha \cos^2 u + \beta \sin^2 u. \tag{1.5}$$

Initially considered by Hunter and Saxton [23, 17], (1.4) is the simplest form of the nonlinear variational wave equation (1.3) studied in the literature.

1.1.2. *Two-dimensional planar waves.* Planar deformations can also be studied in two dimensions. Specifically, if we assume that the deformation depends on two space variables $x, y$, the director can be written in the form

$$\mathbf{n} = (\cos u(x,y,t),\, \sin u(x,y,t),\, 0)$$

with $u$ being the angle to the $x$-$z$ plane. The corresponding variational wave equation is given by

$$\begin{cases} u_{tt} - c(u)\,(c(u)u_x)_x - b(u)\,(b(u)u_y)_y - a'(u)u_x u_y - 2a(u)u_{xy} = 0, & (x,y,t) \in \mathbb{Q}_T, \\ u(x,y,0) = u_0(x,y), & (x,y) \in \mathbb{R}^2, \\ u_t(x,y,0) = u_1(x,y), & (x,y) \in \mathbb{R}^2, \end{cases} \tag{1.6}$$

where $\mathbb{Q}_T = \mathbb{R}^2 \times [0,T]$ with $T > 0$ fixed, $u : \mathbb{Q}_T \to \mathbb{R}$ is the unknown function and $a, b, c$ are given by

$$\begin{aligned} c^2(u) &= \alpha \cos^2 u + \beta \sin^2 u, \\ b^2(u) &= \alpha \sin^2 u + \beta \cos^2 u, \\ a(u) &= \frac{\alpha - \beta}{2} \sin(2u). \end{aligned}$$

In this picture, $c(u)$ is the wave speed in the $x$-direction and $b(u)$ is the wave speed in the $y$-direction.

For smooth solutions of (1.6) it is straightforward to verify that the energy

$$\begin{aligned}\mathcal{E}(t) &= \iint_{\mathbb{R}^2} \left(u_t^2 + c^2(u)u_x^2 + b^2(u)u_y^2 + 2a(u)u_xu_y\right)\,dx\,dy \\ &= \iint_{\mathbb{R}^2} u_t^2 + \left(\alpha(\cos(u)u_x + \sin(u)u_y)\right)^2 + \left(\beta(\sin(u)u_x - \cos(u)u_y)\right)^2\,dx\,dy\end{aligned} \tag{1.7}$$

is conserved, i.e., we have

$$\frac{d\mathcal{E}(t)}{dt} \equiv 0. \tag{1.8}$$

Moreover, for all $t \in [0,T]$ we have

$$\iint_{\mathbb{R}^2} \left(u_t^2 + \min\{\alpha,\beta\}(u_x^2+u_y^2)\right)\,dx\,dy \le \mathcal{E}(t) \le \iint_{\mathbb{R}^2} \left(u_t^2 + \max\{\alpha,\beta\}(u_x^2+u_y^2)\right)\,dx\,dy.$$

In particular, it follows that $\mathcal{E}(t) \ge 0$ for all $t \in [0,T]$. To see this, first we consider $\alpha \ge \beta$ (for $\alpha \le \beta$, we argue in the same way). Then

$$\begin{aligned}&c^2(u)u_x^2 + b^2(u)u_y^2 + 2a(u)u_xu_y \\ &\quad= \left(\alpha\cos^2(u) + \beta\sin^2(u)\right)u_x^2 + \left(\alpha\sin^2 u + \beta\cos^2 u\right)u_y^2 + 2(\alpha-\beta)\sin(u)\cos(u)u_xu_y \\ &\quad\le \left(\alpha\cos^2(u) + \beta\sin^2(u)\right)u_x^2 + \left(\alpha\sin^2 u + \beta\cos^2 u\right)u_y^2 + 2(\alpha-\beta)\left|\sin(u)\cos(u)u_xu_y\right| \\ &\qquad= \alpha\left(\cos^2(u)u_x^2 + \sin^2(u)u_y^2 + 2\left|\sin(u)\cos(u)u_xu_y\right|\right) \\ &\qquad\quad+ \beta\left(\sin^2(u)u_x^2 + \cos^2(u)u_y^2 - 2\left|\sin(u)\cos(u)u_xu_y\right|\right) \\ &\quad= \alpha\left(|\cos(u)u_x| + |\sin(u)u_y|\right)^2 + \beta\left(|\sin(u)u_x| - |\cos(u)u_y|\right)^2 \\ &\quad\le \alpha\Big[\left(|\cos(u)u_x| + |\sin(u)u_y|\right)^2 + \left(|\sin(u)u_x| - |\cos(u)u_y|\right)^2\Big] = \alpha(u_x^2+u_y^2),\end{aligned}$$

and

$$\begin{aligned}&c^2(u)u_x^2 + b^2(u)u_y^2 + 2a(u)u_xu_y \\ &\quad= \left(\alpha\cos^2(u) + \beta\sin^2(u)\right)u_x^2 + \left(\alpha\sin^2 u + \beta\cos^2 u\right)u_y^2 + 2(\alpha-\beta)\sin(u)\cos(u)u_xu_y \\ &\quad\ge \left(\alpha\cos^2(u) + \beta\sin^2(u)\right)u_x^2 + \left(\alpha\sin^2 u + \beta\cos^2 u\right)u_y^2 - 2(\alpha-\beta)\left|\sin(u)\cos(u)u_xu_y\right| \\ &\qquad= \alpha\left(\cos^2(u)u_x^2 + \sin^2(u)u_y^2 - 2\left|\sin(u)\cos(u)u_xu_y\right|\right) \\ &\qquad\quad+ \beta\left(\sin^2(u)u_x^2 + \cos^2(u)u_y^2 + 2\left|\sin(u)\cos(u)u_xu_y\right|\right) \\ &\quad= \alpha\left(|\cos(u)u_x| - |\sin(u)u_y|\right)^2 + \beta\left(|\sin(u)u_x| + |\cos(u)u_y|\right)^2 \\ &\quad\ge \beta\Big[\left(|\cos(u)u_x| - |\sin(u)u_y|\right)^2 + \left(|\sin(u)u_x| + |\cos(u)u_y|\right)^2\Big] = \beta(u_x^2+u_y^2).\end{aligned}$$

1.2. **Mathematical Difficulties.** There exists a fairly satisfactory well posedness theory for the one dimensional equation (1.4). However, despite its apparent simplicity, the mathematical analysis of (1.4) is complicated. Independently of the smoothness of the initial data, due to the nonlinear nature of the equation, singularities may form in the solution [10, 12, 11]. Therefore, solutions of (1.4) should be interpreted in the weak sense:

**Definition 1.1.** *Set* $\Pi_T = \mathbb{R} \times (0,T)$. *A function*

$$u(t,x) \in L^\infty\left([0,T]; W^{1,p}(\mathbb{R})\right) \cap C(\Pi_T), u_t \in L^\infty\left([0,T]; L^p(\mathbb{R})\right),$$

*for all* $p \in [1, 3+q]$, *where* $q$ *is some positive constant, is a weak solution of the initial value problem* (1.4) *if it satisfies:*

***(D.1)*** *For all test functions* $\varphi \in \mathcal{D}(\mathbb{R} \times [0,T))$

$$\iint_{\Pi_T} \left(u_t\varphi_t - c^2(u)u_x\varphi_x - c(u)c'(u)(u_x)^2\varphi\right)\, dx\, dt = 0. \tag{1.9}$$

***(D.2)*** $u(\cdot,t) \to u_0$ *in* $C\left([0,T]; L^2(\mathbb{R})\right)$ *as* $t \to 0^+$.

***(D.3)*** $u_t(\cdot,t) \to u_1$ *as a distribution in* $\Pi_T$ *when* $t \to 0^+$.

In recent years, there has been an increased interest to understand the different classes of weak solutions (conservative and dissipative) of the Cauchy problem (1.4), under the restrictive assumption on the wave speed $c$ (positivity of the derivative of $c$). The literature herein is substantial, and we will here only give a non-exhaustive overview. Within the existing framework, we mention the papers by Zhang and Zheng [29, 30, 31, 32, 33, 34], Bressan and Zheng [4] and Holden and Raynaud [15]. In fact, taking advantage of Young measure theory, existence of a global weak solution with initial data $u_0 \in H^1(\mathbb{R})$ and $u_1 \in L^2(\mathbb{R})$ has been proved in [33]. However, the regularity assumptions on the wave speed $c(u)$ ($c(u)$ is smooth, bounded, positive with derivative that is non-negative and strictly positive on the initial data $u_0$) in the analysis of [29, 30, 31, 32, 33, 34] precludes consideration of the physical wave speed given by (1.5).

A novel approach to the study of (1.4) was taken by Bressan and Zheng [4]. They have constructed the solutions by introducing new variables related to the characteristics, leading to a characterization of singularities in the energy density. The solution $u$, constructed by the above principle, is locally Lipschitz continuous and the map $t \to u(t,\cdot)$ is continuously differentiable with values in $L^p_{\text{loc}}(\mathbb{R})$ for $1 \le p < 2$.

Drawing preliminary motivation from [4], Holden and Raynaud [15] provides a rigorous construction of a semigroup of conservative solutions of (1.4). Since their construction is based on energy measures as independent variables, the formation of singularities is somewhat natural and they were able to overcome the non-physical condition on wave speed ($c'(u) > 0$). Moreover, their analysis can incorporate initial data $u_0, u_1$ that contain measures.

On the other side, the existence of solutions to two dimensional planar waves (1.6) is completely open. Contrary to its one dimensional counterpart, it is not possible to rewrite (1.6) as a system of equations in terms of Riemann invariants (for a brief justification, see Sec 2). Therefore, the same proofs do not apply mutatis mutandis in the two dimensional case. Having said this, one can of course rewrite (1.6) as a first order system using different change of variables (see Sec 2). However, due to lack of "symmetry" of this formulation, it is hard to establish well posedness of such equations using this approach.

1.3. **Numerical Schemes.** Except under very simplifying assumptions, there does not exist elementary and explicit solutions for (1.4). Moreover, the existence of two classes

of weak solutions renders the initial value problem ill-posed after the formation of singularities. Consequently, robust numerical schemes are important in the study of the variational wave equation. Furthermore, capturing conservative solutions numerically is indeed a delicate issue since we expect that traditional finite difference schemes will not yield conservative solutions, due to the intrinsic numerical diffusion in these schemes.

There is a sparsity of efficient numerical schemes for the 1D equation (1.4) available in the literature. We can refer to [11], where the authors present some numerical examples to illustrate their theory. By the way of the theory of Young's measure-valued solutions, Holden et. al. [16] proved convergence of the numerical approximation generated by a semi-discrete finite difference scheme for one-dimensional equation (1.4) to the *dissipative* weak solution of (1.4), under a restrictive assumption on the wave speed ($c'(u) > 0$). To overcome such non-physical assumptions, Holden and Raynaud [15] used their analytical construction, as mentioned earlier, to define a numerical method that can approximate the *conservative* solution. However, the main drawback of this method is that it is computationally very expensive as there is no time marching.

Finally, we mention recent papers [20, 1] which deals with finite difference schemes and discontinuous Galerkin schemes, respectively, for (1.4). Their main idea was to rewrite (1.4) in the form of a first order systems and design numerical schemes for those systems. The key design principle was either energy conservation or energy dissipation. In that context, they have presented schemes that either conserve or dissipate the discrete energy. They also validated the properties of the schemes via extensive numerical experiments.

Numerical results for the two-dimensional variational wave equation (1.6) are even more sparse than for the one-dimensional case. In fact, to the best of the authors' knowledge, the only available numerical experiments are given in the final section of the recent paper by Koley et al. [20].

1.4. **Scope and Outline of the Paper.** The purpose of this paper is to develop efficient high-order schemes for the two-dimensional nonlinear variational wave equation (1.6). By using the Runge–Kutta Discontinuous Galerkin (RK-DG) framework we aim to derive schemes that either *conserve* or *dissipate* a discrete version of the energy inherited from the variational formulation of the problem. Since the behavior of solutions to the 2D equation (1.6) is largely unknown, these schemes will allow us to begin investigate if crucial properties of the 1D equation (1.4) carry over in the two-dimensional case. To the best of our knowledge, this is the first systematic numerical study of the two-dimensional variational wave equation (1.6).

Our approach for constructing high-order schemes is the RK-DG method [13, 6], where the test and trial functions are discontinuous piecewise polynomials. In contrast to high order finite-volume schemes, the high order of accuracy is already built into the finite dimensional spaces and no reconstruction is needed. Exact or approximate Riemann solvers from finite volume methods are used to compute the numerical fluxes between elements. For an energy dissipative scheme we will employ a combination of dissipative fluxes and, in order to control possible spurious oscillations near shocks, shock capturing operators [18, 5, 2]. These methods have recently been shown to be entropy stable for conservation laws

[14]. In contrast to for finite volume methods, entropy stability has gained more attention in finite element methods since one advantage of this method is that the formulation immediately allows the use of general unstructured grids.

The shock capturing DG schemes in this paper have the following properties:

(1) The schemes are arbitrarily high-order accurate.
(2) The schemes are robust and resolved the solution (including possible singularities in the angle $u$) in a stable manner.
(3) The energy conservative scheme preserve the discrete energy at the semi-discrete level. Using a high-order time stepping method, this property also holds in the fully discrete case for all orders of accuracy tested.
(4) The energy dissipative scheme dissipate the discrete energy at the semi-discrete level. Using a high-order time stepping method, this property also holds in the fully discrete case for all orders of accuracy tested.

In the current presentation we consider, for simplicity, a Cartesian grid. The schemes can however be generalized to more general geometries. For such applications, it might be useful to write (1.6) in the form

$$u_{tt} - (T(u)\nabla)\,(T(u)\nabla u) = 0 \tag{1.10}$$

where

$$T(u) = \begin{pmatrix} \sqrt{\alpha}\cos(u) & \sqrt{\alpha}\sin(u) \\ -\sqrt{\beta}\sin(u) & \sqrt{\beta}\cos(u) \end{pmatrix}.$$

The rest of the paper is organized as follows: In Section 2, we present energy conservative and energy dissipative schemes for the one-dimensional equation (1.6). Section 3 concerns a first-order Hamiltonian (energy preserving) scheme for comparison. Section 4 contains numerical experiments verifying the order of convergence, energy stability and efficiency of the schemes.

## 2. Discontinuous Galerkin Schemes in Two-space Dimensions

Drawing primary motivation from the one-dimensional case [1], we aim to design energy conservative and energy dissipative discontinuous Galerkin schemes of the two-dimensional version of the nonlinear variational wave equation (1.6), by rewriting it as a first-order system. First, we briefly mention why formulation based on Riemann invariants does not work in two dimensional case.

### 2.1. **The system of equations.**

We introduce three new independent variables:

$$\begin{aligned} p &:= u_t, \\ v &:= \cos(u)u_x + \sin(u)u_y, \\ w &:= \sin(u)u_x - \cos(u)u_y. \end{aligned}$$

Then, for smooth solutions, we see that

$$\begin{aligned} v_t &= \cos(u)u_{xt} - \sin(u)u_t u_x + \sin(u)u_{yt} + \cos(u)u_t u_y \\ &= (\cos(u)u_t)_x - u_t(\cos(u))_x + (\sin(u)u_t)_y - u_t(\sin(u))_y - u_t\left(\sin(u)u_x - \cos(u)u_y\right), \end{aligned}$$

and

$$\begin{aligned} w_t &= \sin(u)u_{xt} + \cos(u)u_t u_x - \cos(u)u_{yt} + \sin(u)u_t u_y \\ &= (\sin(u)u_t)_x - u_t(\sin(u))_x - (\cos(u)u_t)_y + u_t(\cos(u))_y + u_t\left(\cos(u)u_x + \sin(u)u_y\right). \end{aligned}$$

Moreover, a straightforward calculation using equation (1.6) reveals that

$$\begin{aligned} p_t - (\alpha-\beta)\left(\cos(u)\sin(u)u_x^2 - \cos^2(u)u_x u_y + \sin^2(u)u_x u_y - \cos(u)\sin(u)u_y^2\right) \\ = \alpha\left(\cos(u)(\cos(u)u_x + \sin(u)u_y)\right)_x + \alpha\left(\sin(u)(\cos(u)u_x + \sin(u)u_y)\right)_y \\ + \beta\left(\sin(u)(\sin(u)u_x - \cos(u)u_y)\right)_x - \beta\left(\cos(u)(\sin(u)u_x - \cos(u)u_y)\right)_y. \end{aligned}$$

Hence, for smooth solutions, equation (1.6) is equivalent to the following system for $(p, v, w, u)$,

$$\begin{cases} p_t - \alpha(f(u)v)_x - \alpha(g(u)v)_y - \beta(g(u)w)_x + \beta(f(u)w)_y - \alpha vw + \beta vw = 0, \\ v_t - (f(u)p)_x + pf(u)_x - (g(u)p)_y + pg(u)_y + pw = 0, \\ w_t - (g(u)p)_x + pg(u)_x + (f(u)p)_y - pf(u)_y - pv = 0, \\ u_t = p, \end{cases} \tag{2.1}$$

where $f(u) := \cos(u)$, and $g(u) := \sin(u)$. Furthermore, the corresponding energy associated with the system (2.1) is

$$\mathcal{E}(t) = \iint_{\mathbb{R}^2} \left(p^2 + \alpha\, v^2 + \beta\, w^2\right) \mathrm{d}x\, \mathrm{d}y. \tag{2.2}$$

A simple calculation shows that smooth solutions of (2.1) satisfy the energy identity:

$$\left(p^2 + \alpha\, v^2 + \beta\, w^2\right)_t + 2\left(\alpha\, p\, f(u)\, v + \beta\, p\, g(u)\, w\right)_x + 2\left(\alpha\, p\, g(u)\, v - \beta\, p\, f(u)\, w\right)_y = 0. \tag{2.3}$$

Hence, the fact that the total energy (2.2) is conserved follows from integrating the above identity in space and assuming that the functions $p, u, v$ and $w$ decay at infinity.

2.2. **The grid.** We begin by introducing some notation needed to define the DG schemes. Let the domain $\Omega \subset \mathbb{R}^2$ be decomposed as $\Omega = \cup_{i,j}\Omega_{ij}$ with $\Omega_{ij} := \Omega_i \times \Omega_j$ where $\Omega_i = [x_{i-1/2}, x_{i+1/2}]$ and $\Omega_j = [y_{j-1/2}, y_{j+1/2}]$ for $i, j = 1, \cdots, N$. Moreover, we denote $\Delta x_i = x_{i+1/2} - x_{i-1/2}$ and $\Delta y_j = y_{j+1/2} - y_{j-1/2}$. Furthermore, we also denote $x_i = (x_{i-1/2} + x_{i+1/2})/2$ and $y_j = (y_{j-1/2} + y_{j+1/2})/2$.

Let $u$ be a grid function and denote $u^+_{i+1/2}(y)$ as the function evaluated at the right side of the cell interface at $x_{i+1/2}$ and let $u^-_{i+1/2}(y)$ denote the value at the left side. Similarly, we let $u^+_{j+1/2}(x)$ be the function evaluated at the upper side of the cell interface at $y_{i+1/2}$ and let $u^-_{j+1/2}(x)$ denote the value at the lower side. We can then introduce the jump and, respectively, the average of any grid function $u$ across the interfaces as

$$\begin{aligned} \overline{u}_{i+1/2}(y) &:= \frac{u^+_{i+1/2}(y) + u^-_{i+1/2}(y)}{2}, \quad \overline{u}_{j+1/2}(x) := \frac{u^+_{j+1/2}(x) + u^-_{j+1/2}(x)}{2}, \\ [\![u]\!]_{i+1/2}(y) &:= u^+_{i+1/2}(y) - u^-_{i+1/2}(y), \quad [\![u]\!]_{j+1/2}(x) := u^+_{j+1/2}(x) - u^-_{j+1/2}(x). \end{aligned}$$

Moreover, let $v$ be another grid function. Then the following identities are readily verified:

$$[\![uv]\!]_{i+1/2} = \overline{u}_{i+1/2}[\![v]\!]_{i+1/2} + [\![u]\!]_{i+1/2}\overline{v}_{i+1/2}, \quad [\![uv]\!]_{j+1/2} = \overline{u}_{j+1/2}[\![v]\!]_{j+1/2} + [\![u]\!]_{j+1/2}\overline{v}_{j+1/2} \tag{2.4}$$

2.3. **Variational Formulation.** We seek an approximation $(p, v, w, u)$ of (2.1) such that for each $t \in [0, T]$, $p$, $v$, $w$, and $u$ belong to finite dimensional space

$$X_h^s(\Omega) = \left\{ u \in L^2(\Omega) : u|_{\Omega_{ij}} \text{ polynomial of degree} \le p \right\}.$$

The variational form is derived by multiplying the strong form (2.1) with test functions $\phi, \nu, \psi, \zeta \in X_h^s(\Omega)$ and integrating over each element separately. After using integration-by-parts, we obtain

$$\begin{aligned}
&\sum_{i,j=1}^{N} \int_{\Omega_{ij}} p_t\, \phi \,\mathrm{d}x\,\mathrm{d}y + \alpha \sum_{i,j=1}^{N} \int_{\Omega_{ij}} f(u)\, v\, \phi_x \,\mathrm{d}x\,\mathrm{d}y - \alpha \sum_{i,j=1}^{N} \int_{\Omega_j} (fv)_{i+1/2}\, \phi^-_{i+1/2} \,\mathrm{d}y \\
&+ \alpha \sum_{i,j=1}^{N} \int_{\Omega_j} (fv)_{i-1/2}\, \phi^+_{i-1/2} \,\mathrm{d}y + \alpha \sum_{i,j=1}^{N} \int_{\Omega_{ij}} g(u)\, v\, \phi_y \,\mathrm{d}x\,\mathrm{d}y - \alpha \sum_{i,j=1}^{N} \int_{\Omega_i} (gv)_{j+1/2}\, \phi^-_{j+1/2} \,\mathrm{d}x \\
&+ \alpha \sum_{i,j=1}^{N} \int_{\Omega_i} (gv)_{j-1/2}\, \phi^+_{j-1/2} \,\mathrm{d}x + \beta \sum_{i,j=1}^{N} \int_{\Omega_{ij}} g(u)\, w\, \phi_x \,\mathrm{d}x\,\mathrm{d}y - \beta \sum_{i,j=1}^{N} \int_{\Omega_j} (gw)_{i+1/2}\, \phi^-_{i+1/2} \,\mathrm{d}y \\
&+ \beta \sum_{i,j=1}^{N} \int_{\Omega_j} (gw)_{i-1/2}\, \phi^+_{i-1/2} \,\mathrm{d}y - \beta \sum_{i,j=1}^{N} \int_{\Omega_j} f(u)\, w\, \phi_y \,\mathrm{d}x\,\mathrm{d}y + \beta \sum_{i,j=1}^{N} \int_{\Omega_i} (fw)_{j+1/2}\, \phi^-_{j+1/2} \,\mathrm{d}x \\
&\quad - \beta \sum_{i,j=1}^{N} \int_{\Omega_i} (fw)_{j-1/2}\, \phi^+_{j-1/2} \,\mathrm{d}x - \alpha \sum_{i,j=1}^{N} \int_{\Omega_{ij}} v\, w\, \phi \,\mathrm{d}x\,\mathrm{d}y + \beta \sum_{i,j=1}^{N} \int_{\Omega_{ij}} v\, w\, \phi \,\mathrm{d}x\,\mathrm{d}y = 0,
\end{aligned} \tag{2.5}$$

and

$$\begin{aligned}
&\sum_{i,j=1}^{N} \int_{\Omega_{ij}} v_t\, \nu \,\mathrm{d}x\,\mathrm{d}y + \sum_{i,j=1}^{N} \int_{\Omega_{ij}} f(u)\, p\, \nu_x \,\mathrm{d}x\,\mathrm{d}y - \sum_{i,j=1}^{N} \int_{\Omega_j} (f\, p)_{i+1/2}\, \nu^-_{i+1/2} \,\mathrm{d}y \\
&+ \sum_{i,j=1}^{N} \int_{\Omega_j} (f\, p)_{i-1/2}\, \nu^+_{i-1/2} \,\mathrm{d}y - \sum_{i,j=1}^{N} \int_{\Omega_{ij}} f(u)\, (p\, \nu)_x \,\mathrm{d}x\,\mathrm{d}y + \sum_{i,j=1}^{N} \int_{\Omega_j} (f)_{i+1/2}\, p^-_{i+1/2}\, \nu^-_{i+1/2} \,\mathrm{d}y \\
&- \sum_{i,j=1}^{N} \int_{\Omega_j} (f)_{i-1/2}\, p^+_{i-1/2}\, \nu^+_{i-1/2} \,\mathrm{d}y + \sum_{i,j=1}^{N} \int_{\Omega_{ij}} g(u)\, p\, \nu_y \,\mathrm{d}x\,\mathrm{d}y - \sum_{i,j=1}^{N} \int_{\Omega_i} (g\, p)_{j+1/2}\, \nu^-_{j+1/2} \,\mathrm{d}x \\
&+ \sum_{i,j=1}^{N} \int_{\Omega_i} (g\, p)_{j-1/2}\, \nu^+_{j-1/2} \,\mathrm{d}x - \sum_{i,j=1}^{N} \int_{\Omega_{ij}} g(u)\, (p\, \nu)_y \,\mathrm{d}x\,\mathrm{d}y + \sum_{i,j=1}^{N} \int_{\Omega_i} (g)_{j+1/2}\, p^-_{j+1/2}\, \nu^-_{j+1/2} \,\mathrm{d}x
\end{aligned}$$

$$- \sum_{i,j=1}^{N} \int_{\Omega_i} (g)_{j-1/2}\, p^{+}_{j-1/2}\, \nu^{+}_{j-1/2}\, \mathrm{d}x + \sum_{i,j=1}^{N} \int_{\Omega_{ij}} p\, w\, \nu\, \mathrm{d}x\, \mathrm{d}y = 0, \quad (2.6)$$

and

$$\begin{aligned}
&\sum_{i,j=1}^{N} \int_{\Omega_{ij}} w_t\, \psi\, \mathrm{d}x\, \mathrm{d}y + \sum_{i,j=1}^{N} \int_{\Omega_{ij}} g(u)\, p\, \psi_x\, \mathrm{d}x\, \mathrm{d}y - \sum_{i,j=1}^{N} \int_{\Omega_j} (g\, p)_{i+1/2}\, \psi^{-}_{i+1/2}\, \mathrm{d}y \\
&+ \sum_{i,j=1}^{N} \int_{\Omega_j} (g\, p)_{i-1/2}\, \psi^{+}_{i-1/2}\, \mathrm{d}y - \sum_{i,j=1}^{N} \int_{\Omega_{ij}} g(u)\, (p\, \psi)_x\, \mathrm{d}x\, \mathrm{d}y + \sum_{i,j=1}^{N} \int_{\Omega_j} (g)_{i+1/2}\, p^{-}_{i+1/2}\, \psi^{-}_{i+1/2}\, \mathrm{d}y \\
&- \sum_{i,j=1}^{N} \int_{\Omega_j} (g)_{i-1/2}\, p^{+}_{i-1/2}\, \psi^{+}_{i-1/2}\, \mathrm{d}y - \sum_{i,j=1}^{N} \int_{\Omega_{ij}} f(u)\, p\, \psi_y\, \mathrm{d}x\, \mathrm{d}y + \sum_{i,j=1}^{N} \int_{\Omega_i} (f\, p)_{j+1/2}\, \psi^{-}_{j+1/2}\, \mathrm{d}x \\
&- \sum_{i,j=1}^{N} \int_{\Omega_i} (f\, p)_{j-1/2}\, \psi^{+}_{j-1/2}\, \mathrm{d}x + \sum_{i,j=1}^{N} \int_{\Omega_{ij}} f(u)\, (p\, \psi)_y\, \mathrm{d}x\, \mathrm{d}y - \sum_{i,j=1}^{N} \int_{\Omega_i} (f)_{j+1/2}\, p^{-}_{j+1/2}\, \psi^{-}_{j+1/2}\, \mathrm{d}x \\
&+ \sum_{i,j=1}^{N} \int_{\Omega_i} (f)_{j-1/2}\, p^{+}_{j-1/2}\, \psi^{+}_{j-1/2}\, \mathrm{d}x - \sum_{i,j=1}^{N} \int_{\Omega_{ij}} p\, v\, \psi\, \mathrm{d}x\, \mathrm{d}y = 0, \quad (2.7)
\end{aligned}$$

and

$$\sum_{i,j=1}^{N} \int_{\Omega_{ij}} u_t\, \zeta\, \mathrm{d}x\, \mathrm{d}y = \sum_{i,j=1}^{N} \int_{\Omega_{ij}} p\, \zeta\, \mathrm{d}x\, \mathrm{d}y. \quad (2.8)$$

**Remark 2.1.** *Admittedly, the notation used in* (2.5)–(2.8) *is more cumbersome than the vector notation often seen in the DG literature. The purpose of this is to be able to treat the fluxes in the different equations differently in order to ensure energy conservation.*

In order to complete the description of the above schemes, we need to specify numerical flux functions.

2.4. **Energy Preserving Scheme.** For a conservative scheme, we use the central numerical flux

$$(f)_{k\pm1/2} = \overline{f}_{k\pm1/2} \quad \text{and} \quad (fg)_{k\pm1/2} = \overline{f}_{k\pm1/2}\overline{g}_{k\pm1/2},$$

for any grid functions $f, g \in X^s_h(\Omega)$. An energy preserving RK-DG scheme based on the weak formulation (2.5)–(2.8) becomes: Find $p, v, w, u \in X^s_h(\Omega)$ such that

$$\begin{aligned}
&\sum_{i,j=1}^{N} \int_{\Omega_{ij}} p_t\, \phi\, \mathrm{d}x\, \mathrm{d}y + \alpha \sum_{i,j=1}^{N} \int_{\Omega_{ij}} f(u)\, v\, \phi_x\, \mathrm{d}x\, \mathrm{d}y \\
&\qquad - \alpha \sum_{i,j=1}^{N} \int_{\Omega_j} \overline{f}_{i+1/2}\, \overline{v}_{i+1/2}\, \phi^{-}_{i+1/2}\, \mathrm{d}y + \alpha \sum_{i,j=1}^{N} \int_{\Omega_j} \overline{f}_{i-1/2}\, \overline{v}_{i-1/2}\, \phi^{+}_{i-1/2}\, \mathrm{d}y
\end{aligned}$$

$$
\begin{aligned}
&+\alpha\sum_{i,j=1}^{N}\int_{\Omega_{ij}} g(u)\,v\,\phi_y\,\mathrm{d}x\,\mathrm{d}y-\alpha\sum_{i,j=1}^{N}\int_{\Omega_i}\overline{g}_{j+1/2}\,\overline{v}_{j+1/2}\,\phi^-_{j+1/2}\,\mathrm{d}x\\
&+\alpha\sum_{i,j=1}^{N}\int_{\Omega_i}\overline{g}_{j-1/2}\,\overline{v}_{j-1/2}\,\phi^+_{j-1/2}\,\mathrm{d}x+\beta\sum_{i,j=1}^{N}\int_{\Omega_{ij}} g(u)\,w\,\phi_x\,\mathrm{d}x\,\mathrm{d}y\\
&-\beta\sum_{i,j=1}^{N}\int_{\Omega_j}\overline{g}_{i+1/2}\,\overline{w}_{i+1/2}\,\phi^-_{i+1/2}\,\mathrm{d}y+\beta\sum_{i,j=1}^{N}\int_{\Omega_j}\overline{g}_{i-1/2}\,\overline{w}_{i-1/2}\,\phi^+_{i-1/2}\,\mathrm{d}y\\
&-\beta\sum_{i,j=1}^{N}\int_{\Omega_j} f(u)\,w\,\phi_y\,\mathrm{d}x\,\mathrm{d}y+\beta\sum_{i,j=1}^{N}\int_{\Omega_i}\overline{f}_{j+1/2}\,\overline{w}_{j+1/2}\,\phi^-_{j+1/2}\,\mathrm{d}x\\
&-\beta\sum_{i,j=1}^{N}\int_{\Omega_i}\overline{f}_{j-1/2}\,\overline{w}_{j-1/2}\,\phi^+_{j-1/2}\,\mathrm{d}x-\alpha\sum_{i,j=1}^{N}\int_{\Omega_{ij}} v\,w\,\phi\,\mathrm{d}x\,\mathrm{d}y\\
&+\beta\sum_{i,j=1}^{N}\int_{\Omega_{ij}} v\,w\,\phi\,\mathrm{d}x\,\mathrm{d}y=0, \qquad (2.9)
\end{aligned}
$$

for all $\phi\in X^s_{\Delta x}(\Omega)$,

$$
\begin{aligned}
&\sum_{i,j=1}^{N}\int_{\Omega_{ij}} v_t\,\nu\,\mathrm{d}x\,\mathrm{d}y+\sum_{i,j=1}^{N}\int_{\Omega_{ij}} f(u)\,p\,\nu_x\,\mathrm{d}x\,\mathrm{d}y-\sum_{i,j=1}^{N}\int_{\Omega_j}\overline{f}_{i+1/2}\,\overline{p}_{i+1/2}\,\nu^-_{i+1/2}\,\mathrm{d}y\\
&+\sum_{i,j=1}^{N}\int_{\Omega_j}\overline{f}_{i-1/2}\,\overline{p}_{i-1/2}\,\nu^+_{i-1/2}\,\mathrm{d}y-\sum_{i,j=1}^{N}\int_{\Omega_{ij}} f(u)\,(p\,\nu)_x\,\mathrm{d}x\,\mathrm{d}y\\
&+\sum_{i,j=1}^{N}\int_{\Omega_j}\overline{f}_{i+1/2}\,p^-_{i+1/2}\,\nu^-_{i+1/2}\,\mathrm{d}y-\sum_{i,j=1}^{N}\int_{\Omega_j}\overline{f}_{i-1/2}\,p^+_{i-1/2}\,\nu^+_{i-1/2}\,\mathrm{d}y\\
&+\sum_{i,j=1}^{N}\int_{\Omega_{ij}} g(u)\,p\,\nu_y\,\mathrm{d}x\,\mathrm{d}y-\sum_{i,j=1}^{N}\int_{\Omega_i}\overline{g}_{j+1/2}\,\overline{p}_{j+1/2}\,\nu^-_{j+1/2}\,\mathrm{d}x\\
&+\sum_{i,j=1}^{N}\int_{\Omega_i}\overline{g}_{j-1/2}\,\overline{p}_{j-1/2}\,\nu^+_{j-1/2}\,\mathrm{d}x-\sum_{i,j=1}^{N}\int_{\Omega_{ij}} g(u)\,(p\,\nu)_y\,\mathrm{d}x\,\mathrm{d}y\\
&+\sum_{i,j=1}^{N}\int_{\Omega_i}\overline{g}_{j+1/2}\,p^-_{j+1/2}\,\nu^-_{j+1/2}\,\mathrm{d}x-\sum_{i,j=1}^{N}\int_{\Omega_i}\overline{g}_{j-1/2}\,p^+_{j-1/2}\,\nu^+_{j-1/2}\,\mathrm{d}x\\
&+\sum_{i,j=1}^{N}\int_{\Omega_{ij}} p\,w\,\nu\,\mathrm{d}x\,\mathrm{d}y=0, \qquad (2.10)
\end{aligned}
$$

for all $\nu\in X^s_h(\Omega)$,

$$\sum_{i,j=1}^{N}\int_{\Omega_{ij}} w_t\,\psi\,\mathrm{d}x\,\mathrm{d}y+\sum_{i,j=1}^{N}\int_{\Omega_{ij}} g(u)\,p\,\psi_x\,\mathrm{d}x\,\mathrm{d}y-\sum_{i,j=1}^{N}\int_{\Omega_j}\overline{g}_{i+1/2}\,\overline{p}_{i+1/2}\,\psi^-_{i+1/2}\,\mathrm{d}y$$
$$+\sum_{i,j=1}^{N}\int_{\Omega_j}\overline{g}_{i-1/2}\,\overline{p}_{i-1/2}\,\psi^+_{i-1/2}\,\mathrm{d}y-\sum_{i,j=1}^{N}\int_{\Omega_{ij}} g(u)\,(p\,\psi)_x\,\mathrm{d}x\,\mathrm{d}y$$
$$+\sum_{i,j=1}^{N}\int_{\Omega_j}\overline{g}_{i+1/2}\,p^-_{i+1/2}\,\psi^-_{i+1/2}\,\mathrm{d}y-\sum_{i,j=1}^{N}\int_{\Omega_j}\overline{g}_{i-1/2}\,p^+_{i-1/2}\,\psi^+_{i-1/2}\,\mathrm{d}y$$
$$-\sum_{i,j=1}^{N}\int_{\Omega_{ij}} f(u)\,p\,\psi_y\,\mathrm{d}x\,\mathrm{d}y+\sum_{i,j=1}^{N}\int_{\Omega_i}\overline{f}_{j+1/2}\,\overline{p}_{j+1/2}\,\psi^-_{j+1/2}\,\mathrm{d}x$$
$$-\sum_{i,j=1}^{N}\int_{\Omega_i}\overline{f}_{j-1/2}\,\overline{p}_{j-1/2}\,\psi^+_{j-1/2}\,\mathrm{d}x+\sum_{i,j=1}^{N}\int_{\Omega_{ij}} f(u)\,(p\,\psi)_y\,\mathrm{d}x\,\mathrm{d}y$$
$$-\sum_{i,j=1}^{N}\int_{\Omega_i}\overline{f}_{j+1/2}\,p^-_{j+1/2}\,\psi^-_{j+1/2}\,\mathrm{d}x+\sum_{i,j=1}^{N}\int_{\Omega_i}\overline{f}_{j-1/2}\,p^+_{j-1/2}\,\psi^+_{j-1/2}\,\mathrm{d}x$$
$$-\sum_{i,j=1}^{N}\int_{\Omega_{ij}} p\,v\,\psi\,\mathrm{d}x\,\mathrm{d}y=0, \quad (2.11)$$

for all $\psi\in X_h^s(\Omega)$ and

$$\sum_{i,j=1}^{N}\int_{\Omega_{ij}} u_t\,\zeta\,\mathrm{d}x\,\mathrm{d}y=\sum_{i,j=1}^{N}\int_{\Omega_{ij}} p\,\zeta\,\mathrm{d}x\,\mathrm{d}y. \quad (2.12)$$

for all $\zeta\in X_h^s(\Omega)$.

The above scheme preserves a discrete version of the energy, as shown in the following theorem:

**Theorem 2.1.** *Let $p$, $v$ and $w$ be approximate solutions generated by the scheme* (2.9)–(2.12) *with periodic boundary conditions. Then*

$$\frac{d}{dt}\sum_{i,j=1}^{N}\int_{\Omega_{ij}}\left(p^2(t)+\alpha\,v^2(t)+\beta\,w^2(t)\right)\mathrm{d}x\,\mathrm{d}y=0.$$

*Proof.* Let $p$, $v$ and $w$ be numerical solutions generated by the scheme (2.9)–(2.12). Since those equations hold for any $\phi,\nu,\psi\in X_h^s(\Omega)$, they hold in particular for $\phi=p,\nu=v$ and $\psi=w$. We can then calculate

$$\frac{d}{dt}\sum_{i,j=1}^{N}\int_{\Omega_{ij}}\left(p^2(t)+\alpha\,v^2(t)+\beta\,w^2(t)\right)\mathrm{d}x\,\mathrm{d}y=2\sum_{i,j=1}^{N}\int_{\Omega_{ij}}\left(pp_t+\alpha\,vv_t+\beta\,ww_t\right)\mathrm{d}x\,\mathrm{d}y$$

$$
\begin{aligned}
&= 2\alpha \sum_{i,j=1}^{N} \int_{\Omega_j} \overline{f}_{i+1/2} \left( \overline{v}_{i+1/2} [\![p]\!]_{i+1/2} + \overline{p}_{i+1/2} [\![v]\!]_{i+1/2} - [\![pv]\!]_{i+1/2} \right) \mathrm{d}y \\
&+ 2\alpha \sum_{i,j=1}^{N} \int_{\Omega_i} \overline{g}_{j+1/2} \left( \overline{v}_{j+1/2} [\![p]\!]_{j+1/2} + \overline{p}_{j+1/2} [\![v]\!]_{j+1/2} - [\![pv]\!]_{j+1/2} \right) \mathrm{d}x \\
&+ 2\beta \sum_{i,j=1}^{N} \int_{\Omega_j} \overline{g}_{i+1/2} \left( \overline{v}_{i+1/2} [\![p]\!]_{i+1/2} + \overline{p}_{i+1/2} [\![w]\!]_{i+1/2} - [\![pw]\!]_{i+1/2} \right) \mathrm{d}y \\
&+ 2\alpha \sum_{i,j=1}^{N} \int_{\Omega_i} \overline{f}_{j+1/2} \left( -\overline{w}_{j+1/2} [\![p]\!]_{j+1/2} - \overline{p}_{j+1/2} [\![w]\!]_{j+1/2} + [\![pw]\!]_{j+1/2} \right) \mathrm{d}x = 0,
\end{aligned}
$$

where we have used the periodic boundary conditions and the identities (2.4). □

**Remark 2.2.** *Theorem* 2.1 *and similar results to follow explicitly assume periodic boundary conditions. It is however straightforward to show that these results also hold for certain other situations such as with compactly supported or decaying data.*

2.5. **Energy Dissipating Scheme.** Note that the above designed energy conservative scheme (2.9)–(2.12) is expected to approximate a conservative solution of the underlying system (1.6). To attempt to approximate a dissipative solution of (1.6), one has to add *numerical viscosity*. In this work we propose adding viscosity in the numerical fluxes (scaled by the maximum wave speed) as well as a *shock capturing operator* dissipating energy near shocks or discontinuities. Specifically, we propose the following modification of the energy conservative scheme (2.9)–(2.12):

Denoting

$$
s_{i\pm1/2} = \max\{c^{-}_{i\pm1/2}, c^{+}_{i\pm1/2}\} \text{ and } s_{j\pm1/2} = \max\{b^{-}_{j\pm1/2}, b^{+}_{j\pm1/2}\}
$$

for the maximal local wave velocity, a dissipative version of the DG scheme is then given by the following: Find $p, v, w, u \in X^s_h(\Omega)$ such that

$$
\begin{aligned}
&\sum_{i,j=1}^{N} \int_{\Omega_{ij}} p_t \, \phi \, \mathrm{d}x \, \mathrm{d}y + \alpha \sum_{i,j=1}^{N} \int_{\Omega_{ij}} f(u) \, v \, \phi_x \, \mathrm{d}x \, \mathrm{d}y \\
&\qquad - \alpha \sum_{i,j=1}^{N} \int_{\Omega_j} \underbrace{\left( \overline{f}_{i+1/2} \, \overline{v}_{i+1/2} + \frac{1}{2} s_{i+1/2} [\![p]\!]_{i+1/2} \right)}_{\text{diffusive flux in x-direction}} \phi^{-}_{i+1/2} \, \mathrm{d}y \\
&\qquad + \alpha \sum_{i,j=1}^{N} \int_{\Omega_j} \underbrace{\left( \overline{f}_{i-1/2} \, \overline{v}_{i-1/2} + \frac{1}{2} s_{i-1/2} [\![p]\!]_{i-1/2} \right)}_{\text{diffusive flux in x-direction}} \phi^{+}_{i-1/2} \, \mathrm{d}y
\end{aligned}
$$

$$
\begin{aligned}
&+\alpha\sum_{i,j=1}^{N}\int_{\Omega_{ij}} g(u)\,v\,\phi_y\,\mathrm{d}x\,\mathrm{d}y-\alpha\sum_{i,j=1}^{N}\int_{\Omega_i}\underbrace{\left(\overline{g}_{j+1/2}\,\overline{v}_{j+1/2}+\frac{1}{2}s_{j+1/2}[\![p]\!]_{j+1/2}\right)}_{\text{diffusive flux in y-direction}}\phi^{-}_{j+1/2}\,\mathrm{d}x\\
&+\alpha\sum_{i,j=1}^{N}\int_{\Omega_i}\underbrace{\left(\overline{g}_{j-1/2}\,\overline{v}_{j-1/2}+\frac{1}{2}s_{j-1/2}[\![p]\!]_{j-1/2}\right)}_{\text{diffusive flux in y-direction}}\phi^{+}_{j-1/2}\,\mathrm{d}x+\beta\sum_{i,j=1}^{N}\int_{\Omega_{ij}} g(u)\,w\,\phi_x\,\mathrm{d}x\,\mathrm{d}y\\
&-\beta\sum_{i,j=1}^{N}\int_{\Omega_j}\overline{g}_{i+1/2}\,\overline{w}_{i+1/2}\,\phi^{-}_{i+1/2}\,\mathrm{d}y+\beta\sum_{i,j=1}^{N}\int_{\Omega_j}\overline{g}_{i-1/2}\,\overline{w}_{i-1/2}\,\phi^{+}_{i-1/2}\,\mathrm{d}y\\
&-\beta\sum_{i,j=1}^{N}\int_{\Omega_j} f(u)\,w\,\phi_y\,\mathrm{d}x\,\mathrm{d}y+\beta\sum_{i,j=1}^{N}\int_{\Omega_i}\overline{f}_{j+1/2}\,\overline{w}_{j+1/2}\,\phi^{-}_{j+1/2}\,\mathrm{d}x\\
&-\beta\sum_{i,j=1}^{N}\int_{\Omega_i}\overline{f}_{j-1/2}\,\overline{w}_{j-1/2}\,\phi^{+}_{j-1/2}\,\mathrm{d}x-\alpha\sum_{i,j=1}^{N}\int_{\Omega_{ij}} v\,w\,\phi\,\mathrm{d}x\,\mathrm{d}y\\
&+\beta\sum_{i,j=1}^{N}\int_{\Omega_{ij}} v\,w\,\phi\,\mathrm{d}x\,\mathrm{d}y=\underbrace{-\sum_{i,j=1}^{N}\varepsilon_{ij}\int_{\Omega_{ij}}\left(p_x\,\phi_x+p_y\,\phi_y\right)\,\mathrm{d}x\,\mathrm{d}y}_{\text{shock capturing operator}},
\end{aligned}
\tag{2.13}
$$

for all $\phi\in X_h^s(\Omega)$,

$$
\begin{aligned}
&\sum_{i,j=1}^{N}\int_{\Omega_{ij}} v_t\,\nu\,\mathrm{d}x\,\mathrm{d}y+\sum_{i,j=1}^{N}\int_{\Omega_{ij}} f(u)\,p\,\nu_x\,\mathrm{d}x\,\mathrm{d}y\\
&-\sum_{i,j=1}^{N}\int_{\Omega_j}\underbrace{\left(\overline{f}_{i+1/2}\,\overline{p}_{i+1/2}+\frac{1}{2}s_{i+1/2}[\![v]\!]_{i+1/2}\right)}_{\text{diffusive flux in x-direction}}\nu^{-}_{i+1/2}\,\mathrm{d}y\\
&+\sum_{i,j=1}^{N}\int_{\Omega_j}\underbrace{\left(\overline{f}_{i-1/2}\,\overline{p}_{i-1/2}+\frac{1}{2}s_{i-1/2}[\![v]\!]_{i-1/2}\right)}_{\text{diffusive flux in x-direction}}\nu^{+}_{i-1/2}\,\mathrm{d}y\\
&-\sum_{i,j=1}^{N}\int_{\Omega_{ij}} f(u)\,(p\,\nu)_x\,\mathrm{d}x\,\mathrm{d}y+\sum_{i,j=1}^{N}\int_{\Omega_j}\overline{f}_{i+1/2}\,p^{-}_{i+1/2}\,\nu^{-}_{i+1/2}\,\mathrm{d}y\\
&-\sum_{i,j=1}^{N}\int_{\Omega_j}\overline{f}_{i-1/2}\,p^{+}_{i-1/2}\,\nu^{+}_{i-1/2}\,\mathrm{d}y+\sum_{i,j=1}^{N}\int_{\Omega_{ij}} g(u)\,p\,\nu_y\,\mathrm{d}x\,\mathrm{d}y
\end{aligned}
$$

$$
\begin{aligned}
&- \sum_{i,j=1}^{N} \int_{\Omega_i} \underbrace{\left( \overline{g}_{j+1/2}\, \overline{p}_{j+1/2} + \frac{1}{2} s_{j+1/2} [\![ v ]\!]_{j+1/2} \right)}_{\text{diffusive flux in y-direction}} \nu^{-}_{j+1/2} \, \mathrm{d}x \\
&+ \sum_{i,j=1}^{N} \int_{\Omega_i} \underbrace{\left( \overline{g}_{j-1/2}\, \overline{p}_{j-1/2} + \frac{1}{2} s_{j-1/2} [\![ v ]\!]_{j-1/2} \right)}_{\text{diffusive flux in y-direction}} \nu^{+}_{j-1/2} \, \mathrm{d}x \\
&- \sum_{i,j=1}^{N} \int_{\Omega_{ij}} g(u) \, (p\, \nu)_y \, \mathrm{d}x \, \mathrm{d}y + \sum_{i,j=1}^{N} \int_{\Omega_i} \overline{g}_{j+1/2}\, p^{-}_{j+1/2}\, \nu^{-}_{j+1/2} \, \mathrm{d}x \\
&- \sum_{i,j=1}^{N} \int_{\Omega_i} \overline{g}_{j-1/2}\, p^{+}_{j-1/2}\, \nu^{+}_{j-1/2} \, \mathrm{d}x + \sum_{i,j=1}^{N} \int_{\Omega_{ij}} p\, w\, \nu \, \mathrm{d}x \, \mathrm{d}y \\
&\qquad = \underbrace{- \sum_{i,j=1}^{N} \varepsilon_{ij} \int_{\Omega_{ij}} \left( v_x\, \nu_x + v_y\, \nu_y \right) \, \mathrm{d}x \, \mathrm{d}y}_{\text{shock capturing operator}}, \qquad (2.14)
\end{aligned}
$$

for all $\nu \in X_h^s(\Omega)$,

$$
\begin{aligned}
&\sum_{i,j=1}^{N} \int_{\Omega_{ij}} w_t\, \psi \, \mathrm{d}x \, \mathrm{d}y + \sum_{i,j=1}^{N} \int_{\Omega_{ij}} g(u)\, p\, \psi_x \, \mathrm{d}x \, \mathrm{d}y \\
&\qquad - \sum_{i,j=1}^{N} \int_{\Omega_j} \underbrace{\left( \overline{g}_{i+1/2}\, \overline{p}_{i+1/2} + \frac{1}{2} s_{i+1/2} [\![ w ]\!]_{i+1/2} \right)}_{\text{diffusive flux in x-direction}} \psi^{-}_{i+1/2} \, \mathrm{d}y \\
&\qquad + \sum_{i,j=1}^{N} \int_{\Omega_j} \underbrace{\left( \overline{g}_{i-1/2}\, \overline{p}_{i-1/2} + \frac{1}{2} s_{i-1/2} [\![ w ]\!]_{i-1/2} \right)}_{\text{diffusive flux in x-direction}} \psi^{+}_{i-1/2} \, \mathrm{d}y \\
&\qquad - \sum_{i,j=1}^{N} \int_{\Omega_{ij}} g(u) \, (p\, \psi)_x \, \mathrm{d}x \, \mathrm{d}y + \sum_{i,j=1}^{N} \int_{\Omega_j} \overline{g}_{i+1/2}\, p^{-}_{i+1/2}\, \psi^{-}_{i+1/2} \, \mathrm{d}y \\
&\qquad - \sum_{i,j=1}^{N} \int_{\Omega_j} \overline{g}_{i-1/2}\, p^{+}_{i-1/2}\, \psi^{+}_{i-1/2} \, \mathrm{d}y - \sum_{i,j=1}^{N} \int_{\Omega_{ij}} f(u)\, p\, \psi_y \, \mathrm{d}x \, \mathrm{d}y \\
&\qquad + \sum_{i,j=1}^{N} \int_{\Omega_i} \underbrace{\left( \overline{f}_{j+1/2}\, \overline{p}_{j+1/2} - \frac{1}{2} s_{j+1/2} [\![ w ]\!]_{j+1/2} \right)}_{\text{diffusive flux in y-direction}} \psi^{-}_{j+1/2} \, \mathrm{d}x
\end{aligned}
$$

$$
\begin{aligned}
&- \sum_{i,j=1}^{N} \int_{\Omega_i} \underbrace{\left( \overline{f}_{j-1/2}\, \overline{p}_{j-1/2} - \frac{1}{2} s_{j-1/2} [\![ w ]\!]_{j-1/2} \right)}_{\text{diffusive flux in y-direction}} \psi^{+}_{j-1/2} \,\mathrm{d}x \\
&+ \sum_{i,j=1}^{N} \int_{\Omega_{ij}} f(u)\, (p\,\psi)_y \,\mathrm{d}x\,\mathrm{d}y - \sum_{i,j=1}^{N} \int_{\Omega_i} \overline{f}_{j+1/2}\, p^{-}_{j+1/2}\, \psi^{-}_{j+1/2} \,\mathrm{d}x \\
&+ \sum_{i,j=1}^{N} \int_{\Omega_i} \overline{f}_{j-1/2}\, p^{+}_{j-1/2}\, \psi^{+}_{j-1/2} \,\mathrm{d}x - \sum_{i,j=1}^{N} \int_{\Omega_{ij}} p\, v\, \psi \,\mathrm{d}x\,\mathrm{d}y \\
&= \underbrace{- \sum_{i,j=1}^{N} \varepsilon_{ij} \int_{\Omega_{ij}} (w_x\, \psi_x + w_y\, \psi_y) \,\mathrm{d}x\,\mathrm{d}y}_{\text{shock capturing operator}}, \qquad (2.15)
\end{aligned}
$$

for all $\psi \in X_h^s(\Omega)$,

$$
\sum_{i,j=1}^{N} \int_{\Omega_{ij}} u_t\, \zeta \,\mathrm{d}x\,\mathrm{d}y = \sum_{i,j=1}^{N} \int_{\Omega_{ij}} p\, \zeta \,\mathrm{d}x\,\mathrm{d}y. \qquad (2.16)
$$

for all $\zeta \in X_h^s(\Omega)$.

The scaling parameter $\varepsilon$ in the *shock capturing operator* is given by

$$
\varepsilon_{ij} = \frac{h_{ij}\, C\, \overline{\mathrm{Res}}}{\left( \int_{\Omega_{ij}} (p_x^2 + v_x^2 + w_x^2) \mathrm{d}x\,\mathrm{d}y + \int_{\Omega_{ij}} (p_y^2 + v_y^2 + w_y^2) \mathrm{d}x\,\mathrm{d}y \right)^{1/2} + h_{ij}^{\theta}} \qquad (2.17)
$$

where $C > 0$ is a constant, $\theta \geq 1/2$, $h_{ij} = \max\{\Delta x_{ij}, \Delta y_{ij}\}$ and

$$
\overline{\mathrm{Res}} = \left( \int_{\Omega_{ij}} (\mathrm{Res})^2 \mathrm{d}x\,\mathrm{d}y \right)^{1/2} \qquad (2.18)
$$

with

$$
\mathrm{Res} = \left( p^2 + \alpha\, v^2 + \beta\, w^2 \right)_t + \left( \alpha\, p\, f(u)\, v + \beta\, p\, g(u)\, w \right)_x + \left( \alpha\, p\, g(u)\, v - \beta\, p\, f(u)\, w \right)_y . \qquad (2.19)
$$

The rationale for the scaling parameter is as follows: For smooth solutions of (2.1) the conservation law (2.3) is fulfilled. The numerical solution is then expected to fulfill the same conservation law up to the spatial and temporal accuracy of the scheme. The shock capturing operator will therefore vanish in smooth regions, while introducing added dissipation near shocks and discontinuities.

The above scheme dissipates a discrete version of the energy, as shown in the following theorem:

**Theorem 2.2.** *Let $p$, $v$ and $w$ be approximate solutions generated by the scheme* (2.9)–(2.12) *with periodic boundary conditions. Then*

$$\frac{d}{dt}\sum_{i,j=1}^{N}\int_{\Omega_{ij}}\left(p^2(t)+\alpha\,v^2(t)+\beta\,w^2(t)\right)\right)\,\mathrm{d}x\,\mathrm{d}y\le 0.$$

*Proof.* By using the result from Theorem 2.1, we can write

$$\begin{aligned}
&\frac{d}{dt}\sum_{i,j=1}^{N}\int_{\Omega_{ij}}\left(p^2(t)+\alpha\,v^2(t)+\beta\,w^2(t)\right)\right)\,\mathrm{d}x\,\mathrm{d}y\\
&\qquad=-2\sum_{i,j=1}^{N}\varepsilon_{ij}\int_{\Omega_{ij}}\left(p_x^2+p_y^2+v_x^2+v_y^2+w_x^2+w_y^2\right)\mathrm{d}x\,\mathrm{d}y\\
&\qquad+\alpha\sum_{i,j=1}^{N}\int_{\Omega_j}\left(s_{i+1/2}[\![p]\!]_{i+1/2}p^-_{i+1/2}-s_{i-1/2}[\![p]\!]_{i-1/2}p^+_{i-1/2}\right)\mathrm{d}y\\
&\qquad+\alpha\sum_{i,j=1}^{N}\int_{\Omega_i}\left(s_{j+1/2}[\![p]\!]_{j+1/2}p^-_{j+1/2}-s_{j-1/2}[\![p]\!]_{j-1/2}p^+_{j-1/2}\right)\mathrm{d}x\\
&\qquad+\alpha\sum_{i,j=1}^{N}\int_{\Omega_j}\left(s_{i+1/2}[\![v]\!]_{i+1/2}v^-_{i+1/2}-s_{i-1/2}[\![v]\!]_{i-1/2}v^+_{i-1/2}\right)\mathrm{d}y\\
&\qquad+\alpha\sum_{i,j=1}^{N}\int_{\Omega_i}\left(s_{j+1/2}[\![v]\!]_{j+1/2}v^-_{j+1/2}-s_{j-1/2}[\![v]\!]_{j-1/2}v^+_{j-1/2}\right)\mathrm{d}x\\
&\qquad+\beta\sum_{i,j=1}^{N}\int_{\Omega_j}\left(s_{i+1/2}[\![w]\!]_{i+1/2}w^-_{i+1/2}-s_{i-1/2}[\![w]\!]_{i-1/2}w^+_{i-1/2}\right)\mathrm{d}y\\
&\qquad+\beta\sum_{i,j=1}^{N}\int_{\Omega_i}\left(s_{j+1/2}[\![w]\!]_{j+1/2}w^-_{j+1/2}-s_{j-1/2}[\![w]\!]_{j-1/2}w^+_{j-1/2}\right)\mathrm{d}x
\end{aligned}\tag{2.20}$$

Now, since the periodic boundary condition lends the relation

$$\sum_{i,j=1}^{N}\left(s_{i+1/2}[\![a]\!]_{i+1/2}a^-_{i+1/2}-s_{i-1/2}[\![a]\!]_{i-1/2}a^+_{i-1/2}\right)=-\sum_{i.j=1}^{N}s_{i+1/2}[\![a]\!]^2_{i+1/2},\tag{2.21}$$

we can write

$$\begin{aligned}
&\frac{d}{dt}\sum_{i,j=1}^{N}\int_{\Omega_{ij}}\left(p^2(t)+\alpha\, v^2(t)+\beta\, w^2(t)\right)\right)\,\mathrm{d}x\,\mathrm{d}y \\
&\qquad = -2\sum_{i,j=1}^{N}\varepsilon_{ij}\int_{\Omega_{ij}}\left(p_x^2+p_y^2+v_x^2+v_y^2+w_x^2+w_y^2\right)\mathrm{d}x\,\mathrm{d}y \\
&\qquad -\alpha\sum_{i,j=1}^{N}\int_{\Omega_j} s_{i+1/2}[\![p]\!]^2_{i+1/2}\mathrm{d}y-\alpha\sum_{i,j=1}^{N}\int_{\Omega_i} s_{j+1/2}[\![p]\!]^2_{j+1/2}\mathrm{d}x \\
&\qquad -\alpha\sum_{i,j=1}^{N}\int_{\Omega_j} s_{i+1/2}[\![v]\!]^2_{i+1/2}\mathrm{d}y-\alpha\sum_{i,j=1}^{N}\int_{\Omega_i} s_{j+1/2}[\![v]\!]^2_{j+1/2}\mathrm{d}x \\
&\qquad -\beta\sum_{i,j=1}^{N}\int_{\Omega_j} s_{i+1/2}[\![w]\!]^2_{i+1/2}\mathrm{d}y-\beta\sum_{i,j=1}^{N}\int_{\Omega_i} s_{j+1/2}[\![w]\!]^2_{j+1/2}\mathrm{d}x.
\end{aligned} \tag{2.22}$$

The result then follows from the positivity of $\varepsilon_{ij}$, $s$ and the physical parameters $\alpha$ and $\beta$. □

## 3. Energy Preserving Scheme Based On a Variational Formulation

It is worth noting that all the previous schemes were designed by rewriting the variational wave equation (1.6) as first-order systems and approximating these systems. However, one can also design a scheme for the original variational wave equation (1.6). To achieve this, we design an energy conservative scheme by approximating the nonlinear wave equation (1.6) directly. We proceed by rewriting the nonlinear wave equation (1.6) in the general form:

$$u_{tt} = -\frac{\delta H}{\delta u}, \tag{3.1}$$

with

$$H = H(u,u_x,u_y) := \frac{1}{2}\,c^2(u)\,u_x^2+\frac{1}{2}\,b^2(u)\,u_y^2+a(u)\,u_x\,u_y.$$

Here, $H$ is the "Hamiltonian", and $\frac{\delta H}{\delta u}$ denotes the variational derivative of function $H(u,u_x,u_y)$ with respect to $u$.

A simple calculation, in light of (3.1), reveals that

$$\frac{d}{dt}\int_{\mathbb{R}}\left(\frac{1}{2}u_t^2+H(u,u_x,u_y)\right)\,dx = 0. \tag{3.2}$$

To be more precise, this is a direct consequence of the simple identity:

$$\frac{\delta H}{\delta u} = \frac{\partial H}{\partial u}-\frac{d}{dx}\left(\frac{\partial H}{\partial u_x}\right)-\frac{d}{dy}\left(\frac{\partial H}{\partial u_y}\right). \tag{3.3}$$

We also note that for equation (1.6),

$$\begin{aligned}\frac{\delta H}{\delta u} &= c(u)c'(u)u_x^2 - \left(c^2(u)u_x\right)_x + b(u)b'(u)u_y^2 - \left(b^2(u)u_y\right)_y + a'(u)u_xu_y \\ &\qquad - (a(u)u_y)_x - (a(u)u_x)_y \\ &= -c^2(u)u_{xx} - c(u)c'(u)u_x^2 - b^2(u)u_{yy} - b(u)b'(u)u_y^2 - a'(u)u_xu_y - 2a(u)u_{xy} \\ &= -c(u)\left(c(u)u_x\right)_x - b(u)\left(b(u)u_y\right)_y - a'(u)u_xu_y - 2a(u)u_{xy}.\end{aligned}$$

Based on above observations, we propose the following scheme for (1.6)

$$\begin{aligned}&(u_{ij})_{tt} + c(u_{ij})c'(u_{ij})(D^xu_{ij})^2 - D^x\left(c^2(u_{ij})D^xu_{ij}\right) \\ &\qquad + b(u_{ij})b'(u_{ij})(D^yu_{ij})^2 - D^y\left(b^2(u_{ij})D^yu_{ij}\right) + a'(u_{ij})D^x(u_{ij})D^y(u_{ij}) \\ &\qquad\qquad - D^x\left(a(u_{ij})D^yu_{ij}\right) - D^y\left(a(u_{ij})D^xu_{ij}\right) = 0,\end{aligned} \tag{3.4}$$

where the central differences $D^x$ and $D^y$ are defined by

$$D^xz_{ij} = \frac{z_{i+1,j} - z_{i-1,j}}{2\Delta x}, \text{ and } D^yz_{ij} = \frac{z_{i,j+1} - z_{i,j-1}}{2\Delta y}.$$

This scheme is energy preserving as shown in the following theorem:

**Theorem 3.1.** *Let $u_{ij}(t)$ be an approximate solution generated by the scheme* (3.4) *using periodic boundary conditions. Then we have*

$$\frac{d}{dt}\left(\frac{\Delta x\Delta y}{2}\sum_{i,j}(u_{ij})_t^2 + c^2(u_{ij})\left(D^xu_{ij}\right)^2 + b^2(u_{ij})\left(D^yu_{ij}\right)^2 + 2a(u_{ij})D^x(u_{ij})D^y(u_{ij})\right) = 0.$$

*Proof.* We start by calculating

$$\begin{aligned}&\frac{d}{dt}\left(\frac{\Delta x\Delta y}{2}\sum_{i,j}(u_{ij})_t^2 + c^2(u_{ij})\left(D^xu_{ij}\right)^2 + b^2(u_{ij})\left(D^yu_{ij}\right)^2 + 2a(u_{ij})D^x(u_{ij})D^y(u_{ij})\right) \\ &= \Delta x\Delta y\sum_{i,j}\left((u_{ij})_t(u_{ij})_{tt} + c(u_{ij})c'(u_{ij})\left(D^xu_{ij}\right)^2(u_{ij})_t + c^2(u_{ij})D^xu_{ij}D^x(u_{ij})_t\right) \\ &\quad + \Delta x\Delta y\sum_{i,j}\left(b(u_{ij})b'(u_{ij})\left(D^yu_{ij}\right)^2(u_{ij})_t + b^2(u_{ij})D^yu_{ij}D^y(u_{ij})_t\right) \\ &\quad + \Delta x\Delta y\sum_{i,j}\Big(a'(u_{ij})D^x(u_{ij})D^y(u_{ij})(u_{ij})_t + a(u_{ij})D^x(u_{ij})_tD^yu_{ij} \\ &\qquad\qquad + a(u_{ij})D^xu_{ij}D^y(u_{ij})_t\Big) \\ &= \Delta x\Delta y\sum_{i,j}\left((u_{ij})_t(u_{ij})_{tt} + c(u_{ij})c'(u_{ij})\left(D^xu_{ij}\right)^2(u_{ij})_t - D^x\left(c^2(u_{ij})D^xu_{ij}\right)(u_{ij})_t\right) \\ &\quad + \Delta x\Delta y\sum_{i,j}\left(b(u_{ij})b'(u_{ij})\left(D^yu_{ij}\right)^2(u_{ij})_t - D^y\left(b^2(u_{ij})D^yu_{ij}\right)(u_{ij})_t\right)\end{aligned}$$

$$+ \Delta x \Delta y \sum_{i,j} \Big( a'(u_{ij}) D^x(u_{ij}) D^y(u_{ij}) (u_{ij})_t - D^x \left( a(u_{ij}) D^y u_{ij} \right) (u_{ij})_t - D^y \left( a(u_{ij}) D^x u_{ij} \right) (u_{ij})_t \Big)$$

$= 0.$ (follows from (3.4))

□

## 4. Numerical Experiments

For the numerical experiments, the computational domain is subdivided into $N \times N$ rectangular cells. All cells are of size $\Delta x \times \Delta y$. A uniform time step

$$\Delta t = 0.1 \frac{\min\{\Delta x, \Delta y\}}{\max\{\alpha, \beta\}} \tag{4.1}$$

is used throughout the computation. Moreover, in all experiments the parameters for the shock capturing operator are $C = 0.1$ and $\theta = 1$. To keep focus on the spatial discretization, we will use a fifth-order Runge–Kutta scheme [22] ensuring a satisfactory temporal accuracy. Periodic boundary conditions are used in all experiments.

### 4.1. Gaussian disturbance to homogeneous director state.

In this section we consider the initial value problem (1.6) with the initial data

$$u_0(x, y) = \exp\left(-16\left(x^2 + y^2\right)\right) \tag{4.2a}$$

$$u_1(x, y) = 0 \tag{4.2b}$$

on $(x, y) \in \mathbb{R}^2$. The physical parameters are $\alpha = 1.5$ and $\beta = 0.5$. A numerical solution was computed using $N = 32$ with the dissipative piecewise quadratic ($s = 2$) scheme. Figure 4.1 shows the time evolution of the numerical solution, demonstrating the non-isotropic nature of this model.

A key property of the schemes derived in this paper is that they are designed, at the semi-discrete level, to either conserve or dissipate the energy. Figure 4.2 shows the time evolution of the discrete energy

$$E = \sum_{i,j=1}^{N} \int_{\Omega_{ij}} \frac{p^2 + \alpha v^2 + \beta w^2}{2} \mathrm{d}x = \frac{\Delta x \, \Delta y}{8} \sum_{i,j=1}^{N} \sum_{k,l=0}^{s} \rho_k \rho_l \left( \left( p_{ij}^{(kl)} \right)^2 + \alpha \left( v_{ij}^{(kl)} \right)^2 + \beta \left( w_{ij}^{(kl)} \right)^2 \right), \tag{4.3}$$

for the Gaussian initial value problem using both conservative and dissipative schemes for $s \in \{0, \cdots, 3\}$. The results clearly indicate that the energy preserving (and dissipating) properties carry over to the fully discrete case when using a higher-order time integrator.

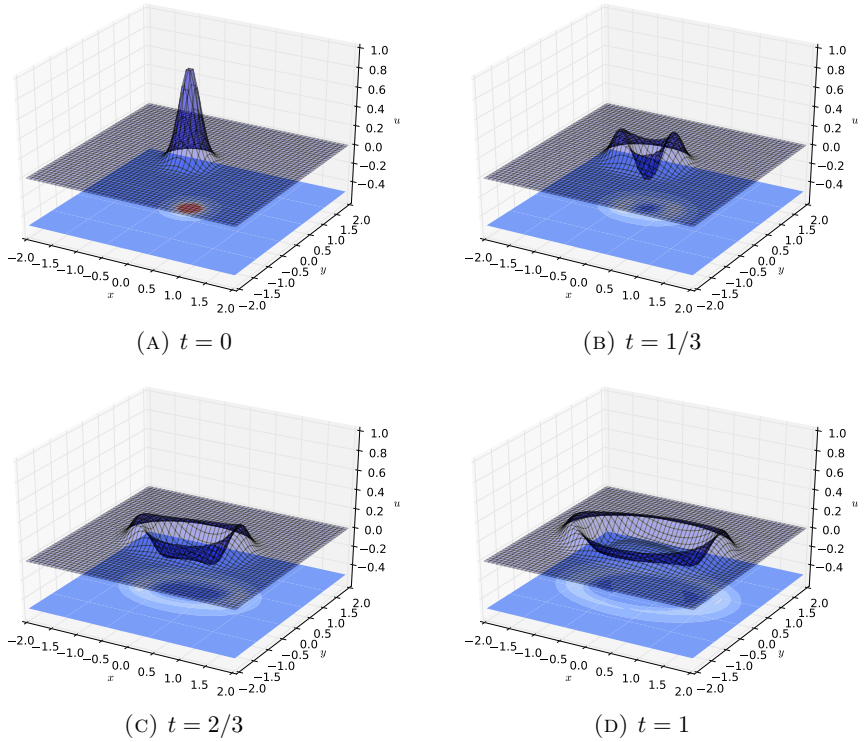

(A) $t = 0$ (B) $t = 1/3$

(C) $t = 2/3$ (D) $t = 1$

FIGURE 4.1. Numerical solution of the initial value problem (1.6) with the initial data (4.2) using the dissipative piecewise quadratic scheme with $N = 32$. The parameters are $\alpha = 1.5$ and $\beta = 0.5$.

4.2. **Loss of regularity.** A crucial property for the 1D variational wave equation is that solutions loose regularity in finite time even for smooth initial data. For the 2D case this is still an open problem. We investigate this numerically by considering the initial value problem (1.6) with data

$$u_0(x, y) = \exp\left(-\left(x^2 + y^2\right)\right) \tag{4.4a}$$

$$u_1(x, y) = -c(u_0(x, y))u_{0,x}(x, y) \tag{4.4b}$$

for $(x, y) \in \mathbb{R}^2$. A numerical experiment was performed using $N = 64$ computational cells with the conservative and dissipative piecewise quadratic schemes. The results, shown in Figure 4.3, indicates a clear steepening of the gradient as the solution evolves.

Smooth solutions of (1.6) satisfies the conservation law (2.19). The root-mean-square of the residual (2.18)can therefore be an indicator function for loss of regularity in the

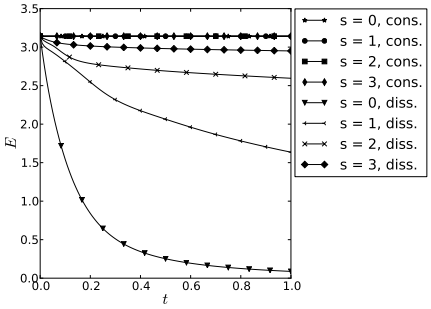


FIGURE 4.2. Evolution of the discrete energy (4.3) for the numerical solutions of the initial value problem (1.6) with the initial data (4.2) using both conservative and dissipative schemes. The parameters were $\alpha = 1.5$ and $\beta = 0.5$ and a $N = 32$ grid size was used.

solution. Figure 4.4 shows the residual at $t = 10$ for both the conservative and dissipative schemes. The results indicate that the solution looses smoothness near the front of the wave propagating in the positive $x$ direction. Moreover, as expected, the dissipative scheme with the shock capturing operator is able to maintain a higher degree of numerical smoothness (as measured by the residual) than the conservative scheme.

4.3. **Bifurcation of solutions.** Another critical feature of the 1D nonlinear variational wave equation (1.4) is the existence of different classes of weak solutions. However, the existence and well-posedness for the initial value problem in the 2D generalization remains an open problem.

In order to investigate this issue numerically, we consider the initial data 4.3 and study the convergence of the three schemes; the conservative DG scheme, the dissipative DG scheme and the Hamiltonian scheme; after the loss of regularity. Figure 4.5 shows the $L^2$ distance between the numerical solutions for different times and under grid refinement. The results indicate that the conservative DG scheme and the Hamiltonian scheme indeed converge to the same solution as the grid is refined. However, the distance between the dissipative and conservative DG schemes seems to converge to a non-zero value that increases as a function of time. This may indicate that the question of well-posedness for the 2D variational wave equation is as delicate as in the 1D case.

4.4. **Order of Convergence and Efficiency.** In the following, we demonstrate the order of convergence and efficiency of both the conservative and dissipative schemes for smooth solutions. As before, we consider the initial value problem (1.6) with the initial data (4.2) with physical parameters $\alpha = 1.5$ and $\beta = 0.5$. A reference solution $u_{\text{ref}}$ was calculated at $t = 0.1$ using the conservative piecewise cubic scheme ($s = 3$) with $N = 1024$. Figure 4.6

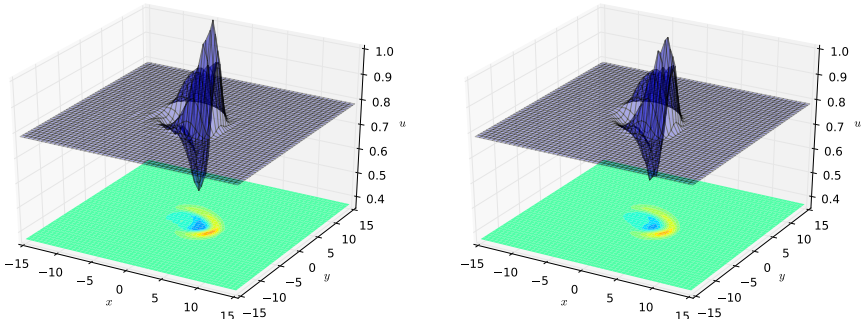


Conservative scheme Dissipative scheme

$t = 3.33$

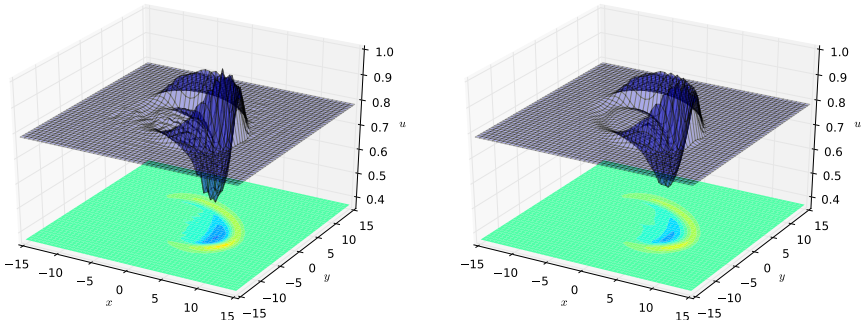


Conservative scheme Dissipative scheme

$t = 6.66$

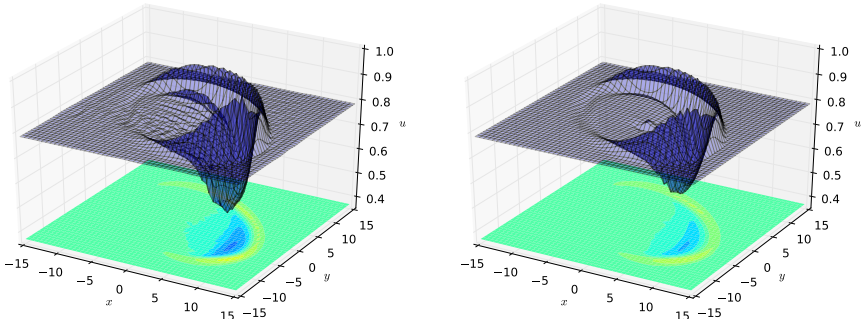


Conservative scheme Dissipative scheme

$t = 10$

FIGURE 4.3. The numerical solution at for left) the piecewise quadratic conservative scheme and right) the piecewise quadratic dissipative scheme of the initial value problem (1.6) with initial data (4.4) with $N = 64$ cells. The physical parameters were $\alpha = 1.5$ and $\beta = 0.5$.

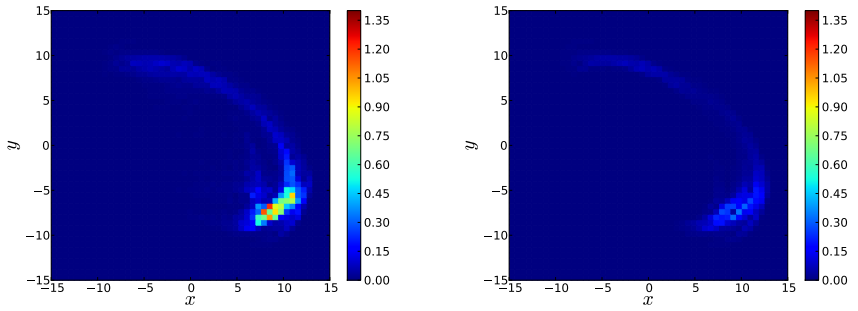


(A) Conservative scheme (B) Dissipative scheme

FIGURE 4.4. The root-mean-square of the residual (2.18) at $t = 10$ for the initial value problem (1.6) with initial data (4.4). At the left: the piecewise quadratic conservative scheme and at the right: the piecewise quadratic dissipative scheme, both with $N = 64$ cells. The physical parameters were $\alpha = 1.5$ and $\beta = 0.5$.

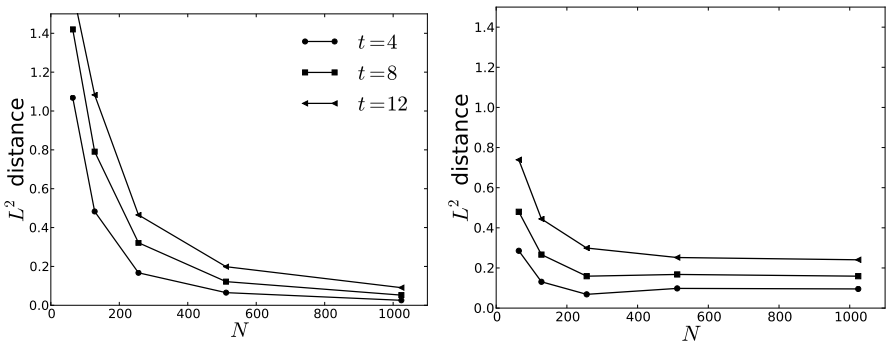


(A) Conservative - Hamiltonian (B) Conservative - dissipative

FIGURE 4.5. The $L^2$ distance between left: the conservative DG scheme and the Hamiltonian scheme and right: the conservative DG scheme and the dissipative DG scheme, for the initial value problem (1.6) with initial data (4.4). The physical parameters were $\alpha = 1.5$ and $\beta = 0.5$.

shows the error

$$e = \|u_N - u_{\text{ref}}\|_2 \tag{4.5}$$

for different grid cell numbers $N = N_x = N_y$. The results indicate a suboptimal order of convergence for odd $s$ when using the conservative numerical flux. For the dissipative

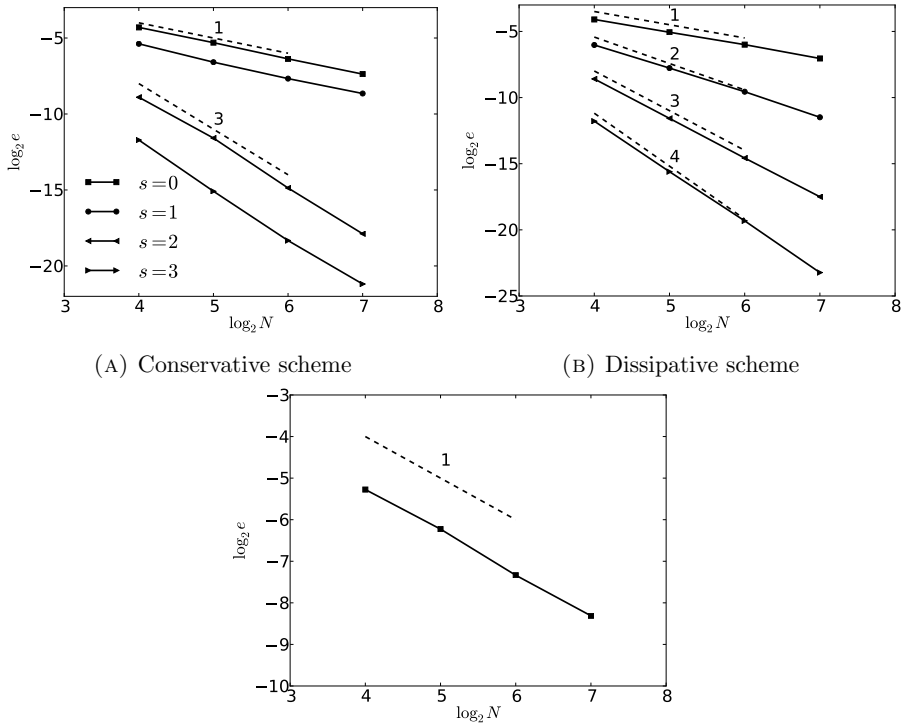


(A) Conservative scheme

(B) Dissipative scheme

(C) Hamiltonian scheme

FIGURE 4.6. The error (4.5) for the numerical solution of the Gaussian initial value problem (4.2) as a function of $N$, using $\alpha = 1.5$ and $\beta = 0.5$. The dashed lines indicate the different orders of convergence.

scheme the order of convergence is optimal. This behavior has been observed also in the 1D case [1], and for certain DG schemes in the literature [24]. The Hamiltonian scheme converges to first order.

Figure 4.7 shows the error (4.5) compared to a a reference solution as a function of computational cost (CPU wall time). The results indicate that the higher-order schemes mostly make up for their increased computational complexity in better accuracy per CPU time. One exception is the conservative piecewise linear scheme, which for this case requires more computational work than the piecewise constant scheme in order to obtain the same accuracy. A possible explanation for this is that enforcing energy preservation using piecewise linear elements results in an un-physically jagged solution in certain regions. This happens despite the fact that the converged solution does not exhibit this behavior.

For the piecewise linear dissipative scheme, this effect is suppressed by the added artificial viscosity.

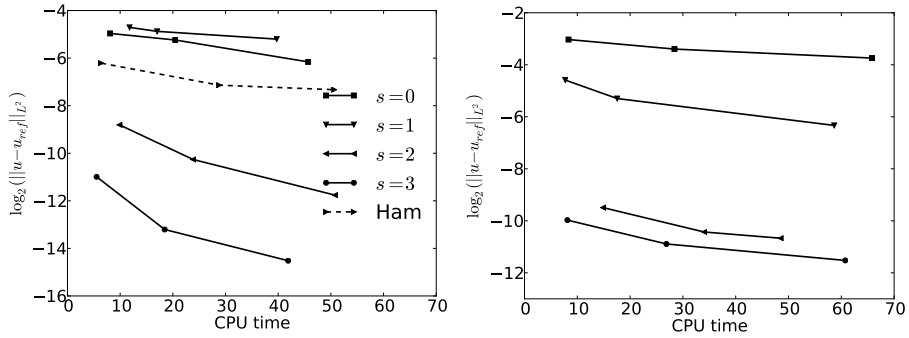


(A) Conservative scheme (B) Dissipative scheme

FIGURE 4.7. The error (4.5) for the numerical solution of the Gaussian initial value problem (4.2) at $t = 0.5$ as a function of CPU time (wall time), using $\alpha = 1.5$ and $\beta = 0.5$. The reference solution was calculated using the piecewise cubic conservative scheme with $N = 1024$ cells.

4.5. **Relaxation from a standing wave.** For this experiment we consider the initial value problem

$$u_0(x, y) = 2\cos(2\pi x)\sin(2\pi x) \tag{4.6a}$$

$$u_1(x, y) = \sin(2\pi(x - y)) \tag{4.6b}$$

on $(x, y) \in [0, 1] \times [0, 1]$ with periodic boundary conditions. The initial value problem can be seen as describing the following: Initially, a standing wave is induced in the director field using e.g. an external electromagnetic field or mechanical vibrations. At $t = 0$, the external influence is removed, and the evolution of the director is purely governed by elastic forces.

Figure 4.8 shows the numerical solution using both conservative and dissipative piecewise quadratic schemes with $N = 64$ cells. For comparison, a numerical solution was also computed using the Hamiltonian scheme derived in Section 3. The physical parameters were, as before, $\alpha = 1.5$ and $\beta = 0.5$. For $t > 0$ the non-isotropic elasticity of the director field deteriorates the initial standing wave and the pattern becomes more complicated. At $t = 2$ the solution given by the dissipative DG scheme is visibly more regular that the solutions given by the conservative schemes (DG and Hamiltonian).

## 5. SUMMARY

Using the Discontinuous Galerkin framework we have derived arbitrarily high-order numerical schemes for the 2D variational wave equation describing the director field in a type

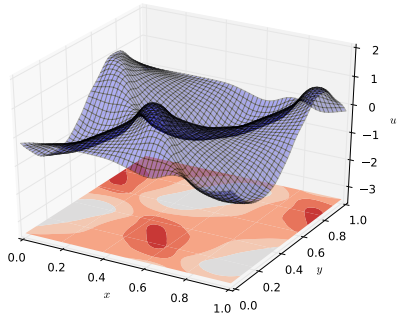


$t = 1$

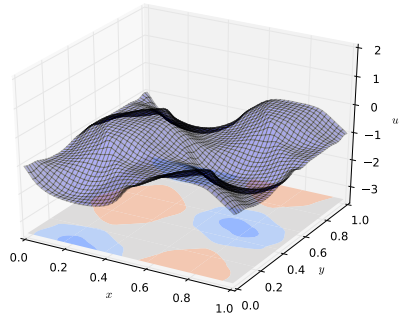


$t = 2$

Dissipative DG scheme

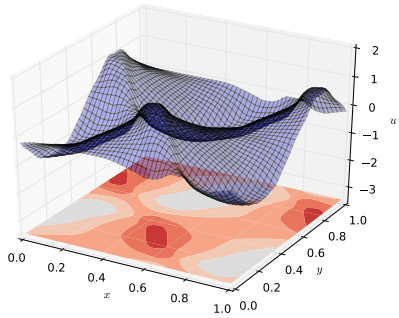


$t = 1$

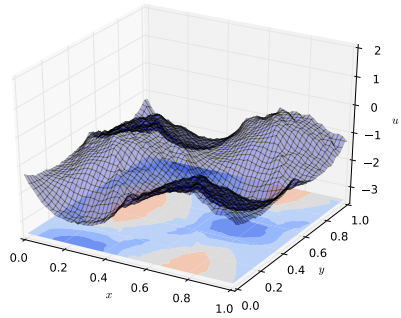


$t = 2$

Conservative DG scheme

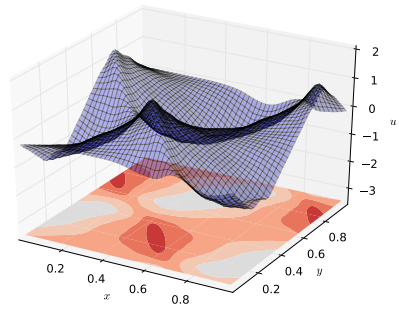


$t = 1$

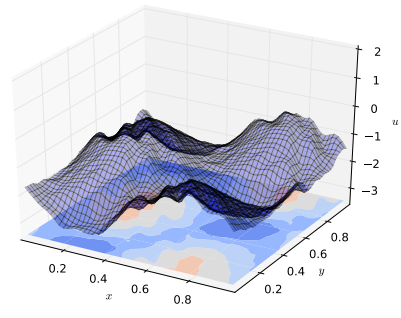


$t = 2$

Hamiltonian scheme

FIGURE 4.8. The numerical solution at left: $t = 1$ and right: $t = 2$ of the initial value problem (1.6) with initial data (4.6) using the conservative and dissipative piecewise quadratic schemes ($s = 3$) with $N = 64$ cells. The bottom row shows the numerical solution using the Hamiltonian scheme. The physical parameters were $\alpha = 1.5$ and $\beta = 0.5$.

of nematic liquid crystals. By design, these schemes either conserve or dissipate the total mechanical energy of the system. The energy conserving scheme is based on a centralized numerical flux, while the dissipative scheme employs a dissipative flux combined with a shock capturing operator.

We have performed extensive numerical experiments both to verify the performance of the schemes and to investigate the behavior of solutions to the variational wave equation. In particular:

- The schemes converge to a high order of accuracy for smooth solutions.
- The high-order schemes outperform low-order scheme in terms of error per CPU time.
- The energy respecting properties (proven at the semi-discrete level) also hold on the fully discrete level when using a high-order numerical integration in time.
- Experiments show that the solution can loose regularity in finite time even for smooth initial data.
- After loss of regularity, results indicate that the conservative and dissipative schemes converge to different solutions as the grid is refined.

To the best of our knowledge, this is the first systematic numerical study of the 2D generalization of the nonlinear variational wave equation (1.4). Indeed, the results here indicate that the mathematical treatment of (1.6) might be as delicate as in the 1D case.

## References

[1] P. Aursand and U. Koley. Local discontinuous Galerkin schemes for a Nonlinear variational wave equation modeling liquid crystals, Preprint 2014

[2] T. J. Barth. Numerical methods for gas-dynamics systems on unstructured meshes. In: *An introduction to recent developments in theory and numerics of conservation laws Lecture notes in computational science and engineering*, vol(5), Springer, Berlin. Eds: D Kroner, M. Ohlberger, and C. Rohde, 1999.

[3] H. Berestycki, J. M. Coron and I. Ekeland. Variational Methods, Progress in nonlinear differential equations and their applications, *Vol 4*, Birkhäuser, Boston, 1990.

[4] A. Bressan and Y. Zheng. Conservative solutions to a nonlinear variational wave equation, *Commun. Math. Phys.*, 266: 471–497 (2006).

[5] G. Chavent and B. Cockburn. The local projection $p^0p^1$-discontinuous Galerkin finite element methods for scalar conservation law, *Math. Model. Numer. Anal.*, 23: 565–592 (1989).

[6] S. Y. Cockburn, B. Lin and C. W. Shu. TVB Runge-Kutta local projection discontinuous Galerkin finite element methods for conservation laws III: one dimensional systems, *J. Comput. Phys.*, 84: 90–113 (1989).

[7] J. Coron, J. Ghidaglia and F. Hélein. *Nematics*, Kluwer Academic Publishers, Dordrecht, 1991.

[8] J. L. Ericksen and D. Kinderlehrer. Theory and application of Liquid Crystals, *IMA Volumes in Mathematics and its Applications*, Vol 5, Springer Verlag, New York, 1987.

[9] X. Gang, S. Chang-Qing, and L. Lei Perturbed solutions in nematic liquid crystals under time-dependent shear. *Phys. Rew. A*, 36(1): 277–284 (1987).

[10] R. T. Glassey. Finite-time blow-up for solutions of nonlinear wave equations, *Math. Z.*, 177: 1761–1794 (1981).

[11] R. Glassey, J. Hunter, and Y. Zheng. Singularities and Oscillations in a nonlinear variational wave equation. In: J. Rauch and M. Taylor, editors, *Singularities and Oscillations*, Volume 91 of the IMA volumes in Mathematics and its Applications, pages 37–60. Springer, New York, 1997.

[12] R. T. Glassey, J. K. Hunter and Yuxi. Zheng. Singularities of a variational wave equation, *J. Diff. Eq.*, 129: 49–78 (1996).
[13] T. R. Hill and W. H. Reed. Triangular mesh methods for neutron transport equation, *Tech. Rep. LA-UR-73-479.*, Los Alamos Scientific Laboratory, 1973.
[14] A. Hiltebrand and S. Mishra. Entropy stable shock capturing space–time discontinuous Galerkin schemes for systems of conservation laws, *Numer. Math.* 126(1): 103–151 (2014).
[15] H. Holden and X. Raynaud. Global semigroup for the nonlinear variational wave equation, *Arch. Rat. Mech. Anal.*, 201(3): 871–964 (2011).
[16] H. Holden, K. H. Karlsen, and N. H. Risebro. A convergent finite-difference method for a nonlinear variational wave equation, *IMA. J. Numer. Anal.*, 29(3): 539–572 (2009).
[17] J. K. Hunter and R. A. Saxton. Dynamics of director fields, *SIAM J. Appl. Math.*, 51: 1498–1521 (1991).
[18] C. Johnson, P. Hansbo and A. Szepessy, On the convergence of shock capturing streamline diffusion methods for hyperbolic conservation laws, *Math. Comput.*, 54(189): 107–129 (1990).
[19] O. A. Kapustina. Liquid crystal acoustics: A modern view of the problem. *Crystallogr. Rep.* 49(4): 680–692 (2004)
[20] U. Koley, S. Mishra, N. H. Risebro, and F. Weber. Robust finite-difference schemes for a nonlinear variational wave equation modeling liquid crystals, *Submitted.*
[21] F. M. Leslie. Theory of flow phenomena in liquid crystals, *Liquid Crystals*, 4, 1–81 (1979).
[22] H. A. Luther and H. P. Konen. Some fifth-order classical Runge–Kutta formulas *SIAM Review*, 7(4): 551–558 (1965).
[23] R. A. Saxton. Dynamic instability of the liquid crystal director, *Contemporary Mathematics Vol 100*, Current Progress in Hyperbolic Systems, pages 325–330, ed. W. B. Lindquist, AMS, Providence, 1989.
[24] C.-W. Shu. Different formulations of the discontinuous Galerkin method for the viscous terms, In: *Conference in Honor of Professor H.-C. Huang on the occasion of his retirement*, Science Press, 14–45, 2000.
[25] I. W. Stewart. *The Static and Dynamic Continuum theory of liquid crystals: a mathematical introduction*, CRC Press, Boca Raton, 2004.
[26] C. Z. van Doorn. Dynamic behavior of twisted nematic liquidcrystal layers in switched fields. *J. Appl. Phys.*, 46: 3738–3745 (1975).
[27] V. A. Vladimirov and M. Y. Zhukov. Vibrational freedericksz transition in liquid crystals. *Phys. Rev. E*, 76:031706 (2007).
[28] C. K. Yun. Inertial coefficient of liquid crystals: A proposal for its measurements. *Phys. Lett. A*, 45(2): 119–120 (1973).
[29] P. Zhang and Y. Zheng. On oscillations of an asymptotic equation of a nonlinear variational wave equation, *Asymptot. Anal.*, 18(3): 307–327 (1998).
[30] P. Zhang and Y. Zheng. Singular and rarefactive solutions to a nonlinear variational wave equation, *Chin. Ann. Math.*, 22: 159–170 (2001).
[31] P. Zhang and Y. Zheng. Rarefactive solutions to a nonlinear variational wave equation of liquid crystals, *Commun. Partial Differ. Equ.*, 26: 381–419 (2001).
[32] P. Zhang and Y. Zheng. Weak solutions to a nonlinear variational wave equation, *Arch. Rat. Mech. Anal.*, 166: 303–319 (2003).
[33] P. Zhang and Y. Zheng. Weak solutions to a nonlinear variational wave equation with general data, *Ann. Inst. H. Poincaré Anal. Non Linéaire*, 22: 207–226 (2005).
[34] P. Zhang and Y. Zheng. On the global weak solutions to a nonlinear variational wave equation, *Handbook of Differential Equations. Evolutionary Equations*, ed. C. M. Dafermos and E. Feireisl, vol. 2, pages 561–648, Elsevier, 2006.

(Peder Aursand)
Department of Mathematical Sciences,
Norwegian University of Science and Technology,
NO–7491 Trondheim, Norway.
*E-mail address*: peder.aursand@math.ntnu.no

(Ujjwal Koley)
Tata Institute of Fundamental Research,
Centre For Applicable Mathematics,
Post Bag No. 6503, GKVK Post Office,
Sharada Nagar, Chikkabommasandra,
Bangalore 560065, India.
*E-mail address*: ujjwal@math.tifrbng.res.in

# Paper E

**Uncertainty quantification for nonlinear waves in liquid crystals using multi-level Monte Carlo**

Peder Aursand and Jonas Šukys

Submitted for publication.

## Preface

This research contained in this paper was performed during my research stay imbedded in Professor Siddhartha Mishra's group at ETH in Zürich. Professor Mishra and his former student Jonas Šukys are experts on applying the multi-level Monte Carlo method to hyperbolic conservation laws. With their help, I proceeded to apply this scheme to the variational wave equations considered in Papers C and D.

For me, the field of uncertainty quantification for PDEs in general and MLMC in particular represented something completely new. During this research I had to both familiarize myself with the theory and the new terminology, as well as to learn how to run simulations on high performance computer clusters. As numerical schemes I opted, for simplicity, to use conservative Hamiltonian methods.

# UNCERTAINTY QUANTIFICATION FOR NONLINEAR WAVES IN LIQUID CRYSTALS USING MULTI-LEVEL MONTE CARLO

PEDER AURSAND AND JONAS ŠUKYS

Abstract. We consider a variational wave equation giving the evolution of the director field of a nematic liquid crystal. The nonlinearity of this wave equation is strongly dependent on the material constants describing the elasticity of the system. Using the multi-level Monte Carlo (MLMC) Finite-Volume sampling method we quantify the influence of uncertain material constants and uncertain initial data on the initial-value problem. The MLMC scheme involves sampling solutions of the Stochastic PDE on a hierarchy of nested meshes. We present results from uncertainty quantification on waves in the director field in both 1D and 2D. Herein, we observe that 5-10 times the computational work is required to achieve a desired accuracy in the estimated mean when using a standard Monte Carlo method compared to when using the MLMC scheme.

## 1. Introduction

The term liquid crystal refers to a state of matter with both crystalline characteristics as well as properties normally associated with liquids. For specific materials, the liquid crystal phase can be observed in certain ranges of temperature, mixture concentrations, or both. Nematic liquid crystals usually consists of elongated molecules for which it is energetically favorable for neighboring molecules to align. Therefore, even though the molecules are free to flow, one can observe macroscopic correlation of the orientation of their long axis. Since the refractive index of the material depends on the molecular orientation, and since the orientation can be influenced by external electromagnetic fields, nematic liquid crystals have seen widespread use in display devices.

Under the assumption of constant local degree of orientation, the state of a nematic liquid crystal is traditionally represented in terms of two linearly independent vector fields: the velocity field and the

*Date*: June 21, 2015.

director field. The latter is a map

$$\mathbf{n} : \mathbb{R}^3 \times [0, \infty) \to \mathbb{S}^2$$

from Euclidean space to the unit ball. In the present work we assume a stationary flow field and will focus on the dynamics of the director field.

The dynamics of the director field can be derived using an energy variational approach. Herein, the elastic energy density associated with distortion of the director field is given by the Oseen–Franck functional

$$\mathcal{W}(\mathbf{n}, \nabla\mathbf{n}) = \alpha \left|\mathbf{n} \times (\nabla \times \mathbf{n})\right|^2 + \beta \left(\nabla \cdot \mathbf{n}\right)^2 + \gamma \left(\mathbf{n} \cdot (\nabla \times \mathbf{n})\right)^2. \quad (1.1)$$

It can be shown that (1.1) is the general form of an energy that is quadratic in $\nabla\mathbf{n}$ and invariant under the transformation $\mathbf{n} \to -\mathbf{n}$ [5]. The constants $\alpha, \beta$ and $\gamma$ are material constants of the liquid crystal, and are associated with the three basic types of deformations of the medium; bend, splay and twist; respectively. Assuming zero dissipation, the evolution of the director $\mathbf{n}$ is then given by the principle of least action

$$\delta \iint \left(\mathbf{n}_t^2 - \mathcal{W}(\mathbf{n}, \nabla\mathbf{n})\right) \mathrm{d}x \, \mathrm{d}t = 0, \qquad \mathbf{n} \cdot \mathbf{n} = 1. \quad (1.2)$$

Standard calculations reveal that the *Euler-Lagrange* equation associated with (1.2) is the *variational wave equation*

$$\mathbf{n}_{tt} = \operatorname{div}\left(\mathcal{W}_{\nabla\mathbf{n}}(\mathbf{n}, \nabla\mathbf{n})\right) - \mathcal{W}_{\mathbf{n}}(\mathbf{n}, \nabla\mathbf{n}).$$

A simple one-dimensional model can be derived by assuming that the director field depends on a single space variable $x$, and, that the director field $\mathbf{n}$ in confined to the $x$-$y$ plane. The director can then be written as

$$\mathbf{n} = (\cos u(x,t),\, \sin u(x,t),\, 0).$$

Here, $u$ denotes the angle between the long axis of the molecules and the $x$-axis. The variational wave equation describing the dynamics of planar waves in 1D is then given by

$$u_{tt} - c(u)\left(c(u)u_x\right)_x = 0, \quad (1.3)$$

where

$$c(u) = \sqrt{\alpha \cos^2(u) + \beta \sin^2(u)}$$

is the nonlinear wave speed. The equation (1.3) was first introduced by Saxton [22], and has since been subject the numerous studies due to its interesting nonlinear properties [13, 9, 12]. Recently, there has also been some effort towards making efficient, stable and convergent numerical schemes for the initial-value problem [11, 15].

A similar model can be derived in 2D by asserting

$$\mathbf{n} = (\cos u(x,y,t),\, \sin u(x,y,t),\, 0)\,.$$

In this case, the variational wave equation takes the form

$$u_{tt} - (T(u)\nabla)\cdot(T(u)\nabla u) = 0 \tag{1.4}$$

with

$$T(u) = \begin{pmatrix} \sqrt{\alpha}\cos(u) & \sqrt{\alpha}\sin(u) \\ \sqrt{\beta}\sin(u) & -\sqrt{\beta}\cos(u) \end{pmatrix}.$$

The material constants $\alpha$ and $\beta$ play a crucial role in the nonlinear dynamics of the planar waves described by (1.3) and (1.4). In the modeling of nematic liquid crystals, the value of these can be subject to uncertainties based on e.g. errors bars in their experimental measurement and simplifications in their dependence on temperature [6]. Moreover, one might wish to study the dynamics of the director field over a range of temperatures. To this end, the problems (1.3) and (1.4) can be recast as the stochastic initial-value problems

$$u_{tt} - c(u,\omega)\left(c(u,\omega)u_x\right)_x = 0, \qquad (x,t)\in\mathbb{R}\times[0,T], \tag{1.5a}$$

$$u(x,0) = u_0(x,\omega), \qquad x\in\mathbb{R}, \tag{1.5b}$$

$$u_t(x,0) = u_1(x,\omega), \qquad x\in\mathbb{R}, \tag{1.5c}$$

and

$$u_{tt} - (T(u,\omega)\nabla)\cdot(T(u,\omega)\nabla u) = 0, \qquad (x,y,t)\in\mathbb{R}^2\times[0,T], \tag{1.6a}$$

$$u(x,y,0) = u_0(x,y,\omega), \qquad (x,y)\in\mathbb{R}^2, \tag{1.6b}$$

$$u_t(x,y,0) = u_1(x,y,\omega), \qquad (x,y)\in\mathbb{R}^2, \tag{1.6c}$$

where $\omega\in\Omega$, for some probability space $(\Omega,\mathcal{F})$.

Uncertainty quantification for solutions of partial differential equations has been an active field of research in recent years [24, 4, 17, 21]. In practical modeling, the physical parameters, initial data, and boundary conditions are often all subject to uncertainty. How to efficiently determine the effect this has on the solutions of nonlinear initial-value problems is a nontrivial issue of great interest in applied sciences and engineering. This is especially true for hyperbolic partial differential equations where solutions might develop shocks and discontinuities [24, 21].

An important class of methods for uncertainty quantification for PDEs is the so-called *non-intrusive* methodology [2]. The main benefit of these types of schemes is that existing code for solving the deterministic problem can be used with few or no changes. Herein, the Monte Carlo sampling method is one of the most notable examples. It relies

on sampling the underlying probability space for the initial-value problem, and in each instance solving the deterministic PDE. The ensemble of solutions can then be used to estimate statistical quantities such as the mean and variance.

While non-intrusive and simple to implement, the Monte Carlo sampling method suffers from a low rate of convergence [18]. This issue can be detrimental to performance, especially for uncertainty quantification for PDEs in high spatial dimensions. Here, obtaining even a single deterministic solution can be computationally expensive. Several techniques have been proposed to assuage the performance issue of Monte Carlo methods. Examples include variance reduction [8] and quasi Monte Carlo methods [7]. In this work we will focus on the *multi-level* Monte Carlo method, first introduced by Heinrich [10] for numerical quadrature. It has since then been successfully applied to hyperbolic conservation laws in conjunction with finite-volume methods [18, 19, 20]. The method relies on performing Monte Carlo sampling on a hierarchy of nested computational grids. By drawing more samples from realizations on coarser grids, where solving the PDE numerically is cheaper, one can efficiently estimate the statistics of the problem.

The asymptotic efficiency of the MLMC method has been rigorously proven for scalar conservation laws, and its performance demonstrated for systems of conservation laws [2]. The potential applicability of this scheme for uncertainty quantification for other nonlinear models in the applied sciences is therefore of great interest. The main purpose of this work is to perform uncertainty quantification for nonlinear waves in liquid crystals in 1D (1.5) and 2D (1.6), using both the MC and MLMC methods. By doing this, we will demonstrate that significant gains in efficiency can be obtained by using MLMC for these variational wave equations. This has, to the best of the authors' knowledge, so far not been the subject of much study.

The paper is organized as follows: Section 2 concerns the deterministic solution of the variational wave equation in 1D and in 2D. Herein, we derive a simple finite-difference scheme that by design preserves the energy stability of the model. In Section 3 we outline how the MC and MLMC methods can used in conjunction with the deterministic solver to perform uncertainty quantification. Section 4 and 5 contains the numerical experiments for 1D and 2D planer waves, respectively. Here, we perform uncertainty quantification using both the basic MC method and the MLMC scheme, and compare their error and efficiency.

## 2. A Hamiltonian finite-difference method

In order to give a deterministic solution of the initial-value problems (1.5) and (1.6), we employ a finite difference scheme based on the Hamiltonian formulation

$$u_{tt} = -\frac{\delta H}{\delta u}. \tag{2.1}$$

This gives an efficient and robust numerical method that, on the semi-discrete level, respects the underlying energy stability of the model. For time integration we will employ the Leapfrog method.

### 2.1. **The 1D model.**

In the 1D case (1.3), we have

$$\frac{\delta H}{\delta u} = -c(u)\left(c(u)u_x\right)_x = c(u)c'(u)u_x^2 - \left(c^2(u)u_x\right)_x. \tag{2.2}$$

For a spatial computational domain $[x_0, x_N]$ we denote $x_i = x_0 + i\Delta x$ for $i \in \{0, \cdots, N\}$. Any grid function $u(x,t)$ can then be written $u_i(t) = u(x_i, t)$. Further, by defining the central difference operator as

$$D_0 u_i := \frac{u_{i+1} - u_{i-1}}{2\Delta x}, \tag{2.3}$$

we can write down the semi-discrete numerical scheme

$$(u_i)_{tt} = c(u_i)c'(u_i)\left(D_0 u_i\right)^2 - D_0\left(c^2(u_i)D_0 u_i\right). \tag{2.4}$$

It is straightforward to show that this scheme preserves a discrete version of the energy [15]. Specifically, at the semi-discrete level, we have

$$\frac{\mathrm{d}}{\mathrm{d}t}\left(\frac{\Delta x}{2}\sum_{i=0}^{N}\left((u_i)_t^2 + c^2(u_i)\left(D_0 u_i\right)^2\right)\right) = 0 \tag{2.5}$$

given periodic boundary conditions or decaying data.

### 2.2. **The 2D model.**

For the 2D equation (1.4), we have,

$$\begin{aligned}\frac{\delta H}{\delta u} &= c(u)c'(u)u_x^2 - \left(c^2(u)u_x\right)_x + b(u)b'(u)u_y^2 - \left(b^2(u)u_y\right)_y + a'(u)u_x u_y \\ &\quad - (a(u)u_y)_x - (a(u)u_x)_y \\ &= -c^2(u)u_{xx} - c(u)c'(u)u_x^2 - b^2(u)u_{yy} - b(u)b'(u)u_y^2 - a'(u)u_x u_y \\ &\quad - 2a(u)u_{xy} \\ &= -c(u)\left(c(u)u_x\right)_x - b(u)\left(b(u)u_y\right)_y - a'(u)u_x u_y - 2a(u)u_{xy}.\end{aligned}$$

Similarly as before, we can for a computational domain $[x_0, x_N] \times [y_0, y_N]$ denote $u_{ij}(t) = u(x_i, y_j, t)$, where $x_i = x_0 + i\Delta x$ and $y_j =$

$y_0 + j\Delta y$. Again, we define central difference operators

$$D_0^x u_{ij} := \frac{u_{i+1,j} - u_{i-1,j}}{2\Delta x} \text{ and } D_0^y u_{ij} = \frac{u_{i,j+1} - u_{i,j-1}}{2\Delta y}. \tag{2.6}$$

This allows us to write down the semi-discrete finite-difference scheme

$$\begin{aligned}(u_{ij})_{tt} + c(u_{ij})c'(u_{ij})(D_0^x u_{ij})^2 - D_0^x\left(c^2(u_{ij})D_0^x u_{ij}\right) + b(u_{ij})b'(u_{ij})(D_0^y u_{ij})^2 \\ - D_0^y\left(b^2(u_{ij})D^y u_{ij}\right) + a'(u_{ij})D_0^x(u_{ij})D_0^y(u_{ij}) \\ - D_0^x\left(a(u_{ij})D_0^y u_{ij}\right) - D_0^y\left(a(u_{ij})D_0^x u_{ij}\right) = 0.\end{aligned} \tag{2.7}$$

Note that in the above we have assumed that the grid parameter $N$ is the same in the $x$ and $y$ dimensions. This is a simplification made for the purpose of this exhibition, and not a limitation inherent to the scheme.

The scheme (2.7) can be shown to preserve a discrete version of the energy of the model [1]. Specifically, solutions fulfill

$$\begin{aligned}\frac{d}{dt}\Bigg(\frac{\Delta x\Delta y}{2}\sum_{i,j}(u_{ij})_t^2 + c^2(u_{ij})\left(D_0^x u_{ij}\right)^2 + b^2(u_{ij})\left(D_0^y u_{ij}\right)^2 \\ + 2a(u_{ij})D_0^x(u_{ij})D_0^y(u_{ij})\Bigg) = 0\end{aligned}$$

given periodic boundary conditions or decaying data.

## 3. Uncertainty quantification using multi-level Monte Carlo

Given a stable and efficient numerical scheme for solving the deterministic initial value problems (1.3) and (1.4), a Monte Carlo (MC) type scheme can be applied to perform uncertainty quantification (for instance, to estimate the mean value and the variance of the solution $u$) for the stochastic initial-value problems (1.5) and (1.6).

### 3.1. **The Monte Carlo Finite-Volume method.**

The Monte Carlo Finite-Volume sampling method can be summed up to three basic steps:

(1) Draw $M$ independent identically distributed samples of $\alpha^k$, $\beta^k$, $u_0^k$ and $u_1^k$ for $k = 1, \ldots, M$.
(2) For each realization $\{\alpha^k, \beta^k, u_0^k, u_1^k\}$ we solve the initial-value problem using the deterministic numerical method with a fixed mesh. The numerical solutions are denoted by $u^k$, $k = 1, \ldots, M$.

(3) Estimate the expectation of the random solution field by calculating the sample mean

$$E_M[u] := \frac{1}{M}\sum_{k=1}^{M} u^k. \tag{3.1}$$

Higher statistical moments such as the variance can also be estimated [23].

Different strategies exist for choosing the number of samples $M$ for a given mesh number $N$ [23]. In this work we will use $M = N$ for all MC calculations.

3.2. **The multi-level Monte Carlo Finite-Volume method.** The deterministic solution of the initial value problem can be expensive, especially in higher dimensions. Indeed, calculating a large number of samples using a very fine mesh can in many cases be computationally infeasible. The *multi-level* Monte Carlo Finite-Volume (MLMC) method is one way of assuaging this concern. It relies on taking Monte Carlo samples on a hierarchy of nested grids. By taking more samples on the coarser grid, where the numerical approximation of the deterministic problem is computationally cheaper, one can obtain the same order of accuracy at a significantly lower cost compared to the MC method.

In this work we use Cartesian grids, and for the level $\ell \in \{0, \cdots, L\}$ we denote

$$\Delta x_\ell = 2^{-\ell}\Delta x_0,$$

for some fixed coarsest mesh size $\Delta x_0$. For simplicity, we assume equal spatial mesh sizes in both dimensions for the 2D model. The MLMC method consists of the three main steps:

(1) For each level $\ell \in \{0, \ldots, L\}$, draw a level-dependent number $M_\ell$ independent identically distributed samples $\alpha_\ell^k$, $\beta_\ell^k$, $u_{0,\ell}^k$ and $u_{1,\ell}^k$ for $k = 1, \ldots, M_\ell$.
(2) For each realization $\{\alpha_\ell^k, \beta_\ell^k, u_{0,\ell}^k, u_{1,\ell}^k\}$ of the parameters solve the deterministic initial value problem. The numerical solutions are denoted by $u_\ell^k$, $k = 1, \ldots, M_\ell$.
(3) Estimate the expectation of the random solution field by using the estimator

$$E^L[u] := E_{M_0}[u_0] + \sum_{\ell=0}^{L} E_{M_\ell}[u_\ell - u_{\ell-1}], \tag{3.2}$$

where $E_M[u]$ denotes the MC estimator (3.1). Higher statistical moments can be calculated in a similar manner [23].

There are different strategies for choosing the level-dependent number of samples $M_\ell$. In this work we will use

$$M_\ell = M_L 2^{2(L-\ell)},$$

a choice designed to equilibrate the error contributions from each successive level, given a first-order deterministic solver [23]. Note, however, that rigorous error estimates for MLMC only exist for scalar conservation laws [16].

For the reader's reference, we emphasize that the MLMC estimates in the rest of this paper are all determined by the following list of parameters:

| | |
|---|---|
| $M_L$ | Number of samples on the finest mesh level |
| $N_L$ | Number of cells in each direction in finest mesh |
| $L$ | Number of levels of refinement |

3.3. **Computation of sample statistics.** When the number of samples is large, storage saving techniques should be used when assembling statistical estimates. For efficient and stable computation of the mean and variance we employ the following on-line algorithm due to Knuth [14]: Let $\bar{u}^0 = 0$ and $\Phi^0 = 0$. Given samples $u^i, i \in \{1, \dots, M\}$ we can proceed iteratively to calculate

$$\bar{u}^i = \sum_{j=1}^{i} \frac{u^j - \bar{u}^{j-1}}{i}, \qquad \Phi^i = \Phi^{i-1} + \left(u^j - \bar{u}^{j-1}\right)\left(u^j - \bar{u}^j\right).$$

Unbiased estimates for the mean and variance of the population are then given by

$$E_M[u] = \bar{u}^M \qquad \text{and} \qquad \mathrm{Var}_M[u] = \frac{\Phi^M}{M-1},$$

respectively. This allows us to update the statistical estimates after calculating each individual samples, eliminating the need for storing all solutions and thereby significantly reducing memory requirements.

Since individual samples only interact when combining the statistical estimates, the MC and MLMC methods are both highly parallelizable. In practice, a parallel implementation will require us to be able to combine statistical estimates from smaller subsets of samples. To this end, the following algorithm proposed by Chan et al. [3] can be used: Let $E_{M_A}[u]$ and $E_{M_B}[u]$ be estimates for the mean for sample sizes $M_A$ and $M_B$, respectively, with $M = M_A + M_B$. The combined mean can then be calculated as

$$E_M[u] = \frac{M_A E_{M_A}[u] + M_B E_{M_B}[u]}{M}$$

and for the variance

$$\Phi_M[u] = \Phi_{M_A}[u] + \Phi_{M_B}[u] + \frac{M_A M_B}{M} \left(E_{M_A}[u] - E_{M_B}[u]\right)^2,$$

with

$$\mathrm{Var}_M[u] = \frac{\Phi_M[u]}{M-1}.$$

3.4. $L^2$ **stability for the MC mean estimator.** The equation (1.3) can be derived from an energy law. Hence, it inherits an $L^2$-stability from the underlying energy functional. It is straightforward to verify that smooth solutions $u(x,t)$ of (1.3) satisfy

$$\frac{\mathrm{d}}{\mathrm{d}t}\mathcal{E}_u(t) = \frac{\mathrm{d}}{\mathrm{d}t}\int \left(u_t^2 + c^2(u)u_x^2\right)\mathrm{d}x = 0.$$

For positive (and nonzero) $\alpha$ and $\beta$ this implies

$$\int \left(u_t^2 + \min\{\alpha,\beta\}u_x^2\right)\mathrm{d}x \le \mathcal{E}_u(t) \le \int \left(u_t^2 + \max\{\alpha,\beta\}u_x^2\right)\mathrm{d}x \quad (3.3)$$

giving a basic stability estimate. In Section 2 we showed that this energy principle is shared by the deterministic solvers at the semi-discrete level.

We can verify that this stability also holds for the MC mean estimator as follows: Assume that $u$ and $v$ are two smooth solutions of (1.3),

thus satisfying (3.3). For the mean $w = (1/2)(u + v)$ we then have

$$\begin{aligned}
\mathcal{E}_w(t) = \int \left(w_t^2 + c^2(w) w_x^2\right) \mathrm{d}x &= \frac{1}{4} \int \left(u_t^2 + c^2(w) u_x^2\right) \mathrm{d}x \\
&\quad + \frac{1}{4} \int \left(v_t^2 + c^2(w) v_x^2\right) \mathrm{d}x \\
&\quad + \frac{1}{2} \int \left(v_t u_t + c^2(w) u_x v_x\right) \mathrm{d}x \\
&\leq \frac{1}{4} \int \left(u_t^2 + \max\{\alpha, \beta\} u_x^2\right) \mathrm{d}x \\
&\quad + \frac{1}{4} \int \left(v_t^2 + \max\{\alpha, \beta\} v_x^2\right) \mathrm{d}x \\
&\quad + \frac{1}{2} \int \left(|v_t u_t| + \max\{\alpha, \beta\} |u_x v_x|\right) \mathrm{d}x \\
&\leq \frac{1}{4} \int \left(u_t^2 + \max\{\alpha, \beta\} u_x^2\right) \mathrm{d}x \\
&\quad + \frac{1}{4} \int \left(v_t^2 + \max\{\alpha, \beta\} v_x^2\right) \mathrm{d}x \\
&\quad + \frac{1}{4} \int \left(u_t^2 + v_t^2 + \max\{\alpha, \beta\} (u_x^2 + v_x^2)\right) \mathrm{d}x \\
&= \frac{1}{2} \int \left(u_t^2 + \max\{\alpha, \beta\} u_x^2\right) \mathrm{d}x \\
&\quad + \frac{1}{2} \int \left(v_t^2 + \max\{\alpha, \beta\} v_x^2\right) \mathrm{d}x.
\end{aligned} \tag{3.4}$$

That the same holds for the MC mean estimator (3.1), i.e.

$$\mathcal{E}_{E_M[u]}(t) \leq \frac{1}{M} \sum_{k=1}^{M} \int \left(\left(u_t^k\right)^2 + \max\{\alpha, \beta\} \left(u_x^k\right)^2\right) \mathrm{d}x,$$

follows by induction.

An analogous result for the 2D equation can be obtained in an analogous way.

## 4. 1D planar waves

In the following, we investigate the propagation of nonlinear 1D planar waves with uncertain, uniformly distributed elastic constants. Specifically, we let the material constants be independent identically distributed variables with

$$\alpha \sim \mathcal{U}(0.3, 0.7), \qquad \beta \sim \mathcal{U}(1.3, 1.7), \tag{4.1}$$

and study the initial value problem (1.5) with

$$u_0(x) = \frac{\pi}{4} + \exp(-x^2) \tag{4.2a}$$

$$u_1(x, \omega) = -c(u_0, \omega) u_{0,x}(x). \tag{4.2b}$$

Notice that this introduces uncertainty in both the flux term as well as in the initial data.

Figure 4.1 shows the estimated mean and standard deviation of the director field using the MC method with $M = N = 512$. Figure 4.2

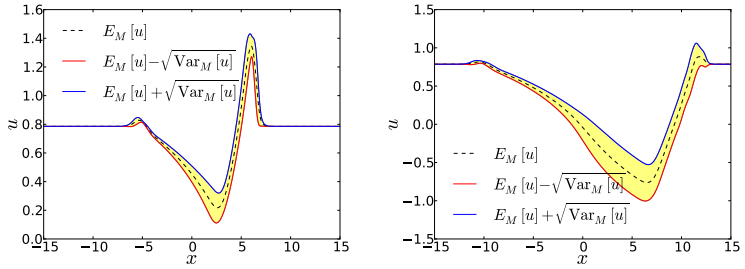


(A) $t = 5$ (B) $t = 10$

FIGURE 4.1. The mean and standard deviation of the director field for the initial value problem (4.2) with $\alpha$ and $\beta$ given by (4.1). Calculated using the MC method with $M = N = 512$.

shows the same estimates, but using the MLMC method with $M_L = 64$, $L = 7$ and $N_L = 8192$. From the results, it is clear that the uncertainty in the elastic constants introduce uncertainties in both the magnitude and position of the propagating disturbance. The error bars for the director field, shown in the filled yellow area, are of the order of $\sim 10\%$.

The MLMC estimates, the variance in particular, are more irregular than their MC counterparts, as can be seen in Figure 4.2. This is not unexpected in regions where the solution may vary greatly between levels of mesh refinement, e.g. near shocks and discontinuities.

4.1. **Convergence and efficiency.** We estimate the order of convergence of the MC and MLMC methods for the initial value problem (4.2).

Since the MC and MLMC estimators are themselves random, the root mean square error estimator is employed to extract statistical convergence rates from the fluctuating error measurements. Let $E_{\mathrm{ref}}[u]$

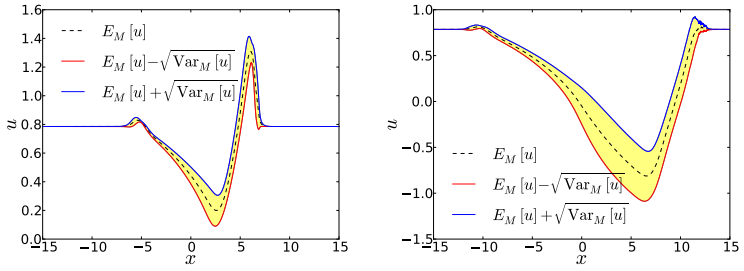


(A) $t = 5$ (B) $t = 10$

FIGURE 4.2. The mean and variance of the director field for the initial value problem (4.2) with $\alpha$ and $\beta$ given by (4.1). Calculated using the MLMC method with $M_L = 64$, $L = 7$ and $N_L = 8192$.

be an accurate reference solution, calculated using the MLMC scheme with a high accuracy. To estimate the error of an MC or MLMC estimator $E_M[u]$ we calculate a sequence of estimates

$$E_M^{(k)}[u], \quad k = 1, \cdots, K$$

for some number $K$. We then define the root-mean-square relative error as

$$\mathcal{E} = \sqrt{\frac{1}{K}\sum_{k}^{K}\left(\mathcal{E}_M^{(k)}\right)^2}, \tag{4.3}$$

where

$$\mathcal{E}_M^{(k)} = \frac{\|E_{\mathrm{ref}}[u] - E_M^{(k)}[u]\|_{L^2}}{\|E_{\mathrm{ref}}[u]\|_{L^2}}.$$

Figure 4.3 shows the error in the mean and the standard deviation for both the MC and MLMC schemes using $K = 20$. For a given mesh refinement $N$, the MC scheme outperforms the MLMC scheme. This is not unexpected, since the MC estimator is a combination of a large number of samples on the finest grid. However, in terms of computational efficiency, we see a clear advantage of using the MLMC scheme. In fact, the results show that obtaining the same accuracy in the mean using the MC scheme requires approximately 8 times the computational effort. For the standard deviation the gain is not as big, but the MLMC scheme is also more efficient in this case.

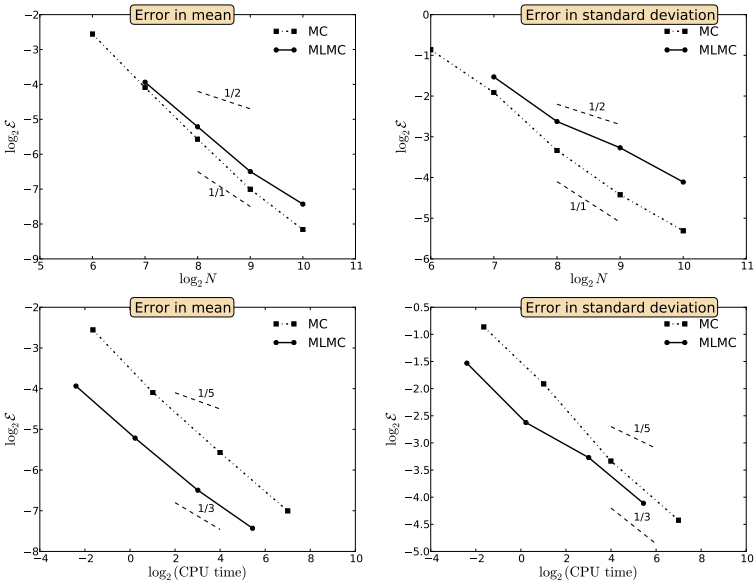


FIGURE 4.3. Error of the mean and standard deviation for the MC and MLMC method for the initial value problem (4.2) at $t = 5$. The reference solution was calculated using $M_L = 64$, $N_L = 8196$ and $L = 7$. The error $\varepsilon$ was calculated using the estimator (4.3) with $K = 20$. Dashed lines indicate expected orders of convergence for scalar conservation laws.

## 5. 2D PLANAR WAVES

In what follows, we investigate the evolution of the 2D variational wave equation given uncertain elastic constants $\alpha$ and $\beta$. For the deterministic numerical solution of the initial value problem (1.6) we use the Hamiltonian scheme described in Section 2.2.

5.1. **Gaussian disturbance.** We consider the following initial data, representing a Gaussian disturbance to an initially homogeneous initial state:

$$u_0(x, y) = \exp\left(-\left(x^2 + y^2\right)\right) \tag{5.1a}$$

$$u_1(x, y, \omega) = -c(u_0, \omega) u_{0,x}(x, y) \tag{5.1b}$$

Furthermore, we let the elastic constants be independent identically distributed random variables given by

$$\alpha \sim \mathcal{U}(0.3, 0.7) \qquad \text{and} \qquad \beta \sim \mathcal{U}(1.3, 1.7). \tag{5.2}$$

Note that this introduces uncertainty in both the governing equation as well as in the initial data.

Figure 5.1 shows the mean and the standard deviation of the director angle and its gradient at $t = 10$, calculated using the Monte Carlo method with $M = N = 512$. Similarly, Figure 5.2 shows the mean

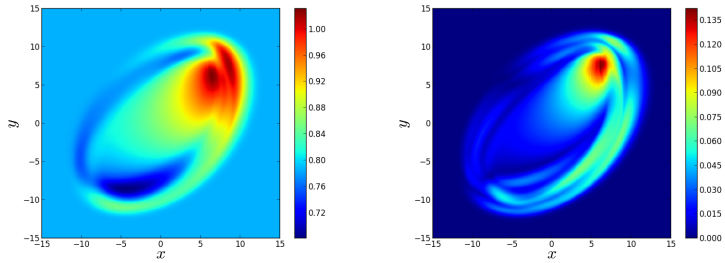


(A) Mean (B) Standard deviation

FIGURE 5.1. The mean and standard deviation of the director field $u$ at $t = 10$ for the initial value problem (5.1). Calculated using the MC method with $M = N = 512$.

and the standard deviation calculated using the MLMC scheme with 6 levels ($L = 5$), $M_L = 8$ samples on the fines level with $2048 \times 2048$ grid cells. The results illustrate the effect of the nonlinearity. There is a clear preferred direction of propagation, and herein a steepening of the slope can be observed. We also observe that the uncertainty is greatest closest to this propagation front, and the relative standard deviation here is about $\sim 10\%$.

5.2. **Convergence and efficiency.** We study the convergence of the MC and MLMC methods using the initial value problem (5.1). As a reference we use the solution displayed in Figure 5.2. Similarly as before, we use a root-mean-square estimate (4.3) for the error.

Figure 5.3 shows the error (4.3) for both the MC and MLMC schemes using $K = 20$. For a fixed grid accuracy $N$ the MC scheme outperforms the MLMC scheme, which is not unexpected. However, as in the 1D case, the efficiency of the MLMC scheme (error per CPU second) is

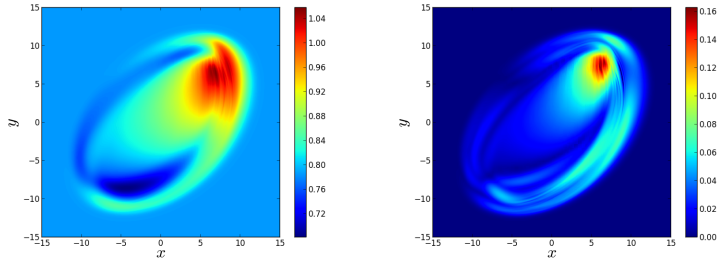


(A) Mean (B) Standard deviation

FIGURE 5.2. The mean and standard deviation of the director field $u$ at $t = 10$ for the initial value problem (5.1). Calculated using the MLMC method with $M_L = 8$, $L = 5$ and $N_L = 2048$.

far superior. In fact, obtaining a lower error in the mean with the MC method requires more than five times the computational efforts. For the standard deviation the difference is not as obvious, but also here the MLMC scheme is superior in terms of efficiency.

5.3. **Relaxation from standing wave.** A second test case is given by the initial data

$$u_0(x, y) = 2\cos(2\pi x)\sin(2\pi x) \tag{5.3a}$$

$$u_1(x, y) = \sin(2\pi(x - y)) \tag{5.3b}$$

on $(x, y) \in [0, 1] \times [0, 1]$ with periodic boundary conditions. Initially, the director field is a standing wave, something that can be caused by the influence of e.g. an electric field or mechanical vibrations. At $t = 0$ the external influence is switched off, and the dynamics of the director field is governed by the elasticity of the liquid crystal.

We consider the stochastic initial value problem consisting of (1.4) with the initial data (5.3). The elastic constants are assumed to be identically uniformly distributed as

$$\alpha \sim \mathcal{U}(0.45, 0.55) \qquad \text{and} \qquad \beta \sim \mathcal{U}(1.45, 1.55). \tag{5.4}$$

Figure 5.4 shows the estimated mean and standard deviation of the director field at $t = 2$ using the MC method with $M = N = 512$. Similarly, Figure 5.5 shows the estimated mean and standard deviation of the director field using the MLMC method with $M_L = 8$, $L = 5$ and $N_L = 2048$. The results show the sinusoidal initial wave deteriorating

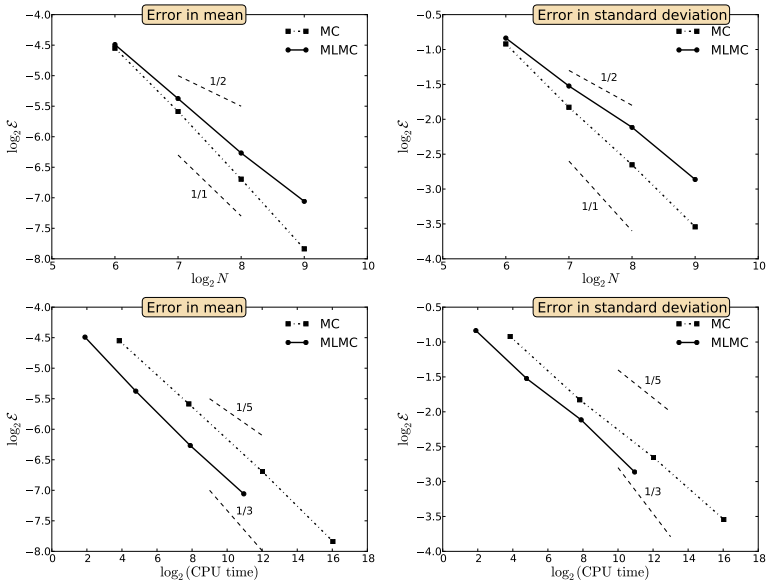


FIGURE 5.3. Error of the mean and standard deviation of the director field $u$ for the MC and MLMC method for the initial value problem (5.1). The reference solution was calculated using $M_L = 8$, $N_L = 2048$ and $L = 6$. The error $\varepsilon$ was calculated using the estimator (4.3) with $K = 20$. Dashed lines indicate expected orders of convergence for scalar conservation laws.

into a more irregular pattern, while the mean still maintains the same periodicity. The variance is clearly largest between the local maxima, indicating that the elastic constants strongly affect both the position and shape of these.

5.4. **Convergence and efficiency.** We can study the convergence of the MC and MLMC methods also for this case. Figure 5.6 shows the RMS error (4.3) at $t = 2$ for both the MC and MLMC schemes using $K = 20$. The results read similar as before. In terms of error per grid size the MC method is superior. However, since most of the sampling in the MLMC method is done on coarse grids, the efficiency of this method is much greater. Specifically, Figure 5.6 shows that obtaining the same error in the mean using the MC method requires more than 10 times the computational effort.

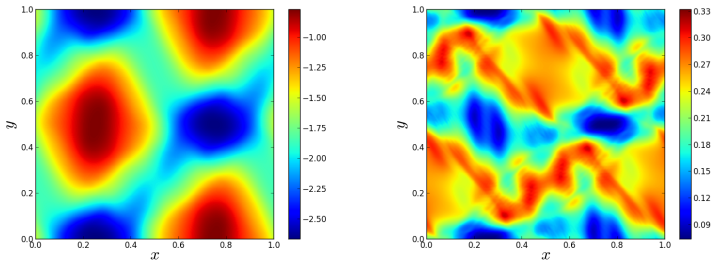


(A) Mean (B) Standard deviation

FIGURE 5.4. The mean and standard deviation of the director field $u$ at $t = 2$ for the initial value problem (5.3). Calculated using the MC method with $M = N = 512$.

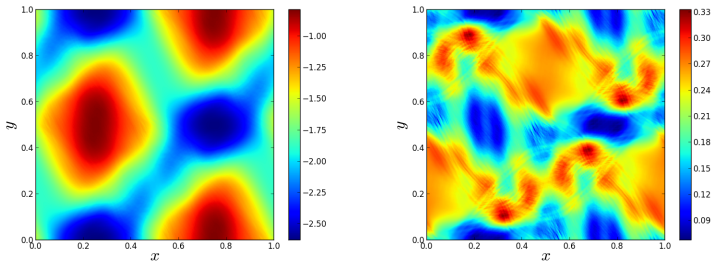


(A) Mean (B) Standard deviation

FIGURE 5.5. The mean and standard deviation of the director field $u$ at $t = 2$ for the initial value problem (5.3). Calculated using the MLMC method with $M_L = 8$, $L = 5$ and $N_L = 2048$.

## 6. SUMMARY

We have studied the evolution of a class of nonlinear waves in the director field of nematic liquid crystals with uncertain elastic constants and uncertain initial data. Herein, we perform uncertainty quantification on the stochastic initial-value problem in 1D and 2D using the Monte Carlo and the multi-level Monte Carlo methods. As the deterministic solver we have used a Hamiltonian finite-difference scheme designed to preserve the energy stability inherent to the model.

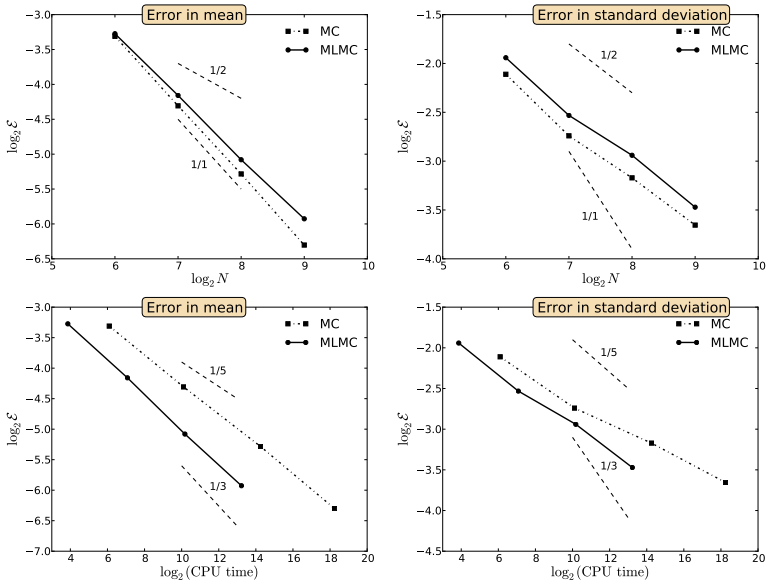


FIGURE 5.6. Error of the mean and standard deviation of the director field $u$ for the MC method with $M = N$ and the MLMC method with $M_L = 8$ and $L = 4$ for the initial value problem (5.3). The reference solution was calculated using $M_L = 32$, $N_L = 2048$ and $L = 6$. The error $\varepsilon$ was calculated using the estimator (4.3) with $K = 20$. Dashed lines indicate expected orders of convergence for scalar conservation laws.

The results, both in 1D and 2D, indicate that the MLMC method can be applied successfully to estimate statistical quantities for models of this kind. In terms of error per computational effort, we observed that the MLMC clearly outperformed the regular MC method. In particular, the results show that in order to obtain the same error in the expectation, the MC method requires 5-10 times the computational work. The efficiency of the MLMC method for the estimation of the variance is lower. However, the obtained numerical results show a clear advantage from using the MLMC scheme also here.

## Acknowledgements

The work of Peder Aursand has been funded by the Research Council of Norway project number 213638. The authors are grateful to professor Siddhartha Mishra for his help and advice in the preparation of this manuscript.

## References

[1] P. Aursand and U. Koley. Higher-order energy stable schemes for a nonlinear variational wave equation modeling nematic liquid crystals in two dimensions. *Preprint*, 2014.

[2] H. Bijl, D. Lucor, S. Mishra, and C. Schwab. *Uncertainty Quantification in Computational Fluid Dynamics*, volume 92. Springer Science & Business Media, 2013.

[3] T. F. Chan, G. H. Golub, and R. J. LeVeque. Updating formulae and a pairwise algorithm for computing sample variances. In *COMPSTAT 1982 5th Symposium held at Toulouse 1982*, pages 30–41. Springer, 1982.

[4] Q.-Y. Chen, D. Gottlieb, and J. S. Hesthaven. Uncertainty analysis for the steady-state flows in a dual throat nozzle. *J. Comput. Phys.*, 204(1):378–398, 2005.

[5] P. G. De Gennes and J. Prost. *The Physics of Liquld Crystals*. Clarendon Press, Oxford, 1993.

[6] W. H. de Jeu, W. A. P. Claassen, and A. M. J. Spruijt. The determination of the elastic constants of nematic liquid crystals. *Mol. Cryst. Liq. Cryst.*, 37(1):269–280, 1976.

[7] J. Dick, F. Y. Kuo, and I. H. Sloan. High-dimensional integration: The quasi Monte-Carlo way. *Acta Numer.*, 22:133–288, 2013.

[8] G. Fishman. *Monte Carlo*. Springer, 1996.

[9] R. T. Glassey, J. K. Hunter, and Y. Zheng. Singularities of a variational wave equation. *J. Diff. Eq.*, 129(1):49–78, 1996.

[10] S. Heinrich. Multilevel monte carlo methods. In *Lecture Notes in Computer Science*, volume 2170 of *Large-scale scientific computing, LSSC 2001, Sozopol, Bulgaria, 2001*, pages 58–67. Springer, 2001.

[11] H. Holden, K. H. Karlsen, and N. H. Risebro. A convergent finite-difference method for a nonlinear variational wave equation. *IMA J. Numer. Anal.*, 29(3):539–572, 2009.

[12] H. Holden and X. Raynaud. Global semigroup of conservative solutions of the nonlinear variational wave equation. *Arch. Rat. Mech. Anal.*, 201(3):871–964, 2011.

[13] J. K. Hunter and R. Saxton. Dynamics of director fields. *SIAM J. Appl. Math.*, 51(6):1498–1521, 1991.

[14] D. Knuth. *The Art of Computer Programming, volume 2: Seminumerical Algorithms*. Addison–Wesley, 1998.

[15] U. Koley, S. Mishra, N. H. Risebro, and F. Weber. Robust finite difference schemes for a nonlinear variational wave equation modeling liquid crystals. *ArXiv e-prints*, 2013.

[16] R. J. LeVeque. *Numerical methods for conservation laws*, volume 132. Springer, 1992.

[17] G Lin, C. H. Su, and G. E. Karniadakis. The stochastic piston problem. *Proceedings of the National Academy of Sciences of the United States of America*, 101(45):15840–15845, 2004.

[18] S. Mishra and C. Schwab. Sparse tensor multi-level Monte Carlo finite volume methods for hyperbolic conservation laws with random initial data. *Math. Comput.*, 81(280):1979–2018, 2012.

[19] S. Mishra, C. Schwab, and J. Šukys. Multi-level Monte Carlo Finite Volume methods for nonlinear systems of conservation laws in multi-dimensions. *J. Comput. Phys.*, 231(8):3365–3388, 2012.

[20] S. Mishra, C. Schwab, and J. Šukys. Multi-level monte carlo finite volume methods for uncertainty quantification of acoustic wave propagation in random heterogeneous layered medium. *Preprint*, 2014.

[21] G. Poëtte, B. Després, and D. Lucor. Uncertainty quantification for systems of conservation laws. *J. Comput. Phys.*, 228(7):2443–2467, 2009.

[22] R. A. Saxton. Dynamic instability of the liquid crystal director. In W. B. Lindquist, editor, *Contemporary Mathematics*, volume 100 of *Current Progress in Hyperbolic Systems, Providence, RI, USA, 1989.*, pages 325–330, 1989.

[23] J. Šukys. *Robust multi-level Monte Carlo Finite Volume methods for systems of hyperbolic conservation laws with random input data.* PhD thesis, Diss., Eidgenössische Technische Hochschule ETH Zürich, Nr. 21990, 2014.

[24] D. Xiu and J. S. Hesthaven. High-order collocation methods for differential equations with random inputs. *SIAM J. Sci. Comput.*, 27(3):1118–1139, 2005.

(Peder Aursand) Department of Mathematical Sciences, Norwegian University of Science and Technology, NO–7491 Trondheim, Norway.

(Jonas Šukys) Computational Science and Engineering Laboratory, ETH Zürich, CH–8092 Zürich, Switzerland.